

Mechanistic Studies of Electron Transfer, Complex Formation,
C-H Bond Activation, and Product Binding in
Soluble Methane Monooxygenase

by

Daniel A. Kopp

B.S. Chemistry and Biology
The College of William and Mary, 1997

SUBMITTED TO THE DEPARTMENT OF CHEMISTRY IN PARTIAL
FULFILLMENT OF THE REQUIREMENTS FOR THE DEGREE OF

DOCTOR OF PHILOSOPHY IN CHEMISTRY

AT THE

MASSACHUSETTS INSTITUTE OF TECHNOLOGY

February 2003

© Massachusetts Institute of Technology, 2003

All rights reserved

Signature of Author: _____

Department of Chemistry
December 16, 2002

Certified by: _____

Stephen J. Lippard
Thesis Supervisor

Accepted by: _____

Robert W. Field
Chairman, Departmental Committee on Graduate Students

This doctoral thesis has been examined by Committee of the Department of Chemistry as follows:

Catherine L. Drennan
Cecil and Ida Green Career Development Assistant Professor of Chemistry
Committee Chair

Stephen J. Lippard
Arthur Amos Noyes Professor of Chemistry
Thesis Supervisor

JoAnne Stubbe
Novartis Professor of Chemistry and Professor of Biology

Mechanistic Studies of Electron Transfer, Complex Formation, C-H Bond
Activation, and Product Binding in Soluble Methane Monooxygenase

by

Daniel A. Kopp

Submitted to the Department of Chemistry on December 16, 2002, in partial
fulfillment of the requirements for the Degree of Doctor of Philosophy

Chapter 1. Soluble Methane Monooxygenase: Activation of Dioxygen and Methane

The mechanisms by which soluble methane monooxygenase uses dioxygen to convert methane selectively to methanol have come into sharp focus. Diverse techniques have clarified subtle details about each step in the reaction, from binding and activating dioxygen, to hydroxylation of alkanes and other substrates, to the electron transfer events required to complete the catalytic cycle.

Chapter 2. Electron Transfer Reactions of the Reductase Component of Soluble Methane Monooxygenase from *Methylococcus capsulatus* (Bath)

Soluble methane monooxygenase (sMMO) catalyzes the hydroxylation of methane by dioxygen to afford methanol and water, the first step of carbon assimilation in methanotrophic bacteria. This enzyme comprises three protein components: a hydroxylase (MMOH) that contains a dinuclear non-heme iron active site, a reductase (MMOR) that facilitates electron transfer from NADH to the diiron site of MMOH, and a coupling protein (MMOB). MMOR uses a non-covalently bound FAD cofactor and a [2Fe-2S] cluster to mediate electron transfer. The gene encoding MMOR was cloned from *Methylococcus capsulatus* (Bath) and expressed in *Escherichia coli* in high yield. Purified recombinant MMOR was indistinguishable from the native protein in all aspects examined, including activity, mass, cofactor content, and EPR spectrum of the [2Fe-2S] cluster. Redox potentials for the FAD and [2Fe-2S] cofactors, determined by reductive titrations in the presence of indicator dyes, are $\text{FAD}_{\text{ox/sq}}$, -176 ± 7 mV; $\text{FAD}_{\text{sq/hq}}$, -266 ± 15 mV; and $[\text{2Fe-2S}]_{\text{ox/red}}$, -209 ± 14 mV. The midpoint potentials of MMOR are not altered by the addition of MMOH, MMOB, or both MMOH and MMOB. The reaction of MMOR with NADH was investigated by stopped-flow UV-visible spectroscopy, and the kinetic and spectral properties of intermediates are described. The effects of pH on the redox properties of MMOR are described and exploited in pH jump kinetic studies to measure the rate constant of 130 ± 17 s⁻¹ for electron transfer between the FAD and [2Fe-2S] cofactors in two-electron reduced MMOR. The thermodynamic and kinetic parameters determined significantly extend our understanding of the sMMO system.

Chapter 3. Structural Features of the MMOH/MMOR Complex as Revealed by Mass Spectrometric Analysis of Covalently Cross-linked Proteins.

Soluble methane monooxygenase requires complexes between its three component proteins for efficient catalytic turnover. The hydroxylase (MMOH) must bind both to the reductase (MMOR) for electron transfer and to the regulatory protein (MMOB) to allow reaction with substrates. Although structures of MMOH, MMOB, and one domain of MMOR have been determined, little is known about structures of the complexes. Proteins cross-linked by a carbodiimide reagent were analyzed by specific proteolysis and capillary HPLC-mass spectrometry. Tandem mass spectra conclusively identified two amine-to-carboxylate cross-linked sites involving the alpha subunit of MMOH and the [2Fe-2S] domain of MMOR (MMOR-Fd). The amino terminus of the MMOH alpha subunit cross-links to the side chains of MMOR-Fd residues Glu56 and Glu91. These Glu residues are close to one another on the surface of MMOR-Fd and far from the [2Fe-2S] cluster. The amino terminus of the alpha subunit of MMOH is disordered in the crystal structure of MMOH, precluding a detailed structural model of the complex based on the cross-link. A proposed binding site for MMOR on MMOH can be ruled out, however. The MMOR Glu56Gln Glu91Gln double mutant retains >80% of its NADH oxidase activity, yet limits maximal sMMO activity to ~65% of the level supported by wild type MMOR. The double mutation diminished but does not abolish cross-linking to MMOH, indicating that other residues of MMOR also form cross-links to MMOH.

Chapter 4. Cationic Species Can Be Produced in Soluble Methane Monooxygenase-Catalyzed Hydroxylation Reactions; Radical Intermediates Are Not Formed

Reactions of methylcubane (**1**) with cytochrome P450 enzymes and with a methane monooxygenase (MMO) system have been studied. Oxidation of **1** by P450 isoenzymes ($\Delta 2B1$, $\Delta 2B4$, $\Delta 2B4$ T302A, $\Delta 2E1$, $\Delta 2E1$ T303A) gave cubylmethanol (**2**), 2-, 3-, and 4-methylcubanol (**3**), and 1-homocubanol (**4**) with different regioselectivities. The soluble methane monooxygenase (MMO) systems from *M. capsulatus* (Bath) and *M. trichosporium* OB3b hydroxylated **1** at all available positions in the ratio 2:3:5 (**2**, **3**, **4** respectively). Product **4**, the major product, derived from a cationic rearrangement of the cubylmethyl system was identified by comparison to an authentic sample. These results suggest that the formation of cationic rearrangement products from both enzymic systems may derive from a solvolysis-type reaction such as first-formed protonated cubylmethanol by the insertion of the elements of OH^+ . The implication of a cationic component also supports some mechanistic similarities between P450 and MMO hydroxylation reactions.

Chapter 5. Evaluation of Norcarane as a Probe for Radicals in Cytochrome P450- and Soluble Methane Monooxygenase-Catalyzed Hydroxylation Reactions

Norcarane was employed as a mechanistic probe in oxidations catalyzed by hepatic cytochrome P450 enzymes and by the soluble methane monooxygenase (sMMO) enzyme from *Methylococcus capsulatus* (Bath). In all cases, the major oxidation products (>75%) were endo- and exo-2-norcaranol. Small amounts of 3-norcaranol, 2-norcaranone, and 3-norcaranone also formed. In addition, the rearrangement products (2-cyclohexenyl)methanol and 3-cycloheptenol were detected in the reactions, the former possibly arising from a radical intermediate and the latter ascribed to a cationic intermediate. The formation of the cation-derived rearrangement product is consistent with one or more reaction pathways and is in accord with the results of previous probe studies with the same enzymes. The appearance of the putative radical-derived rearrangement product is in conflict with other mechanistic probe results with the same enzymes. The unique implication of a discrete radical intermediate in hydroxylations of norcarane may be the consequence of a minor reaction pathway for the enzymes that is not manifest in reactions with other probes. Alternatively, it might reflect a previously unappreciated reactivity of norcaranyl cationic intermediates, which can convert to (2-cyclohexenyl)methanol. We conclude that generalizations regarding the intermediacy of radicals in P450 and sMMO enzyme-catalyzed hydroxylations based on the norcarane results should be considered hypothetical until the origin of the unanticipated results can be determined.

Chapter 6. Product Binding to the Diiron(III) and Mixed-Valence Diiron Centers of Methane Monooxygenase Hydroxylase Studied by ^1H , ^2H and ^{19}F ENDOR Spectroscopy

The binding of ethanol and 1,1,1-trifluoroethanol (TFE) to both the H_{mv} and H_{ox} forms of soluble methane monooxygenase (sMMO) in solution has been studied by Q-band (35 GHz) CW and pulsed ENDOR spectroscopy of ^1H , ^2H and ^{19}F nuclei of exogenous ligands. As part of this investigation we introduce ^{19}F , in this case from bound TFE, as a new probe for the binding of small molecules to a metalloenzyme active site. The H_{mv} form was prepared in solution by chemical reduction of H_{ox} . For study of H_{ox} itself, frozen solutions were subjected to γ -irradiation in the frozen solution state at 77 K, which affords an EPR-visible mixed-valent diiron center, denoted $(\text{H}_{\text{ox}})_{\text{mv}}$, held in the geometry of the diiron(III) state. The ^{19}F and ^2H ENDOR spectra of bound TFE together with ^1H ENDOR spectra of bound ethanol indicate that the alcohols bind close to the Fe(II) ion of the mixed-valence cluster in H_{mv} and in a bridging or semi-bridging fashion to H_{ox} . DMSO does not affect the binding of either of the ethanols or of methanol to H_{ox} , nor of ethanol or methanol to H_{mv} . It does, however, displace TFE from the diiron site in H_{mv} . These results provide the first evidence that

crystal structures of sMMO hydroxylase into which product alcohols were introduced by diffusion represent the structures in solution.

Thesis Supervisor: Stephen J. Lippard

Title: Arthur Amos Noyes Professor of Chemistry

For Karen

I couldn't have done it without you

Acknowledgements

I must first of all thank my thesis advisor, Steve Lippard. He has not only provided a place for me to work and project to work on, but also keeps his lab full of excellent scientists and wonderful people. Steve allowed me the freedom to pursue experiments I chose, and helped keep me on the path to success, even when it seemed out of reach.

In the lab, my coworkers have been a vital source of knowledge and help. George Gassner, my first mentor in the lab here, taught me an enormous amount of practical biochemistry and, by his example, what it means to be a good scientist. All the MMO students and postdocs here have played a part in helping me – Ann Valentine, Dave Coufal, Shannon Stahl, and Doug Whittington in my early days here especially. Maarten Merkx and Jens Müller, who put the Europe in the European bay, were fun labmates and coworkers. Jessica Blazyk, whose cloning efforts made Chapter 2 possible, has always been ready to offer her opinions. Her meticulous nature has helped me learn to pay attention to details. Without Matt Sazinsky, the SSRL trips would have been pure torture, instead of mostly torture with some laughs thrown in for good measure.

Edna Ambundo has always been ready with a laugh or to tell a funny story. I'm glad I won't be in the lab after she leaves – it will be an emptier and quieter place without her. Liz Cadieux helped me learn some molecular biology in the waning months of my research, helping speed me along toward graduation. The newer additions to the lab – Joey Bautista, Lisa Chatwood, and Laurance Beauvais have all been great labmates. Good luck to you!

One of the real benefits of working in Steve's lab is the access to top-notch collaborators. The mass spectrometry work in Chapter 3 relied on the expertise of Prof. Cathy Costello and her postdoc Eric Berg. They graciously allowed me into their lab and stayed motivated through numerous disappointments. Prof. Brian Hoffman, Stoyan Smoukov and Roman Davydov at Northwestern have always been willing to discuss results, patiently answer questions and instruct me on what it was that they were doing. Prof. Martin Newcomb has been a very energetic and thoughtful collaborator, and without his assistance the probe substrate experiments would have been beyond my skills to achieve.

I owe a particular debt of gratitude to my family. My parents, Jane and Harry have supported me in every way possible. At the risk of stating the obvious, I wouldn't be here today if it wasn't for them. My sister Sarah has also stood by me, when she wasn't busy teasing me. Of course my wife Karen has been closest to me through it all. I hope I can offer her as much as she has given to me.

Table of Contents

Abstract.....	3
Dedication.....	7
Acknowledgments.....	8
Table of Contents.....	9
List of Tables.....	14
List of Figures.....	15
Chapter One: Soluble Methane Monooxygenase: Activation of Dioxygen and Methane.....	19
Introduction.....	20
Dioxygen Activation.....	22
Early Steps of Dioxygen Activation: Conversion of MMOH _{red} to MMOH _{peroxo}	22
Conversion of MMOH _{peroxo} to MMOH _Q	23
C-H Bond Activation.....	24
Alkane Substrates.....	24
Kinetic Isotope Effects.....	25
Probe Substrates.....	28
Theoretical investigations of alkane hydroxylation by MMOH _Q	31
Other sMMO research frontiers.....	33
Conclusion.....	35
References.....	37
Chapter Two: Electron Transfer Reactions of the Reductase Component of Soluble Methane Monooxygenase from <i>Methylococcus capsulatus</i> (Bath).....	47
Introduction.....	48
Methods and Materials.....	50
Materials and General Methods.....	50
Expression and Purification of Recombinant MMOR.....	50

Redox Potential Determination.....	51
Stopped-Flow Experiments.....	54
Analysis of Diode Array Spectra.....	54
Procedures for Variable-pH Experiments.....	55
Results.....	56
Characterization of Recombinant MMOR.....	56
Redox Potentials of MMOR.....	57
Kinetic Behavior of MMOR Reduction by NADH.....	57
Complexes of MMOR with NAD(H).....	58
Effect of pH on the Reaction of MMOR with NADH.....	59
Effect of pH on Relative Redox Potentials.....	60
Measurement of Electron Transfer by pH Jump.....	61
Discussion.....	62
Recombinant MMOR.....	62
Redox Potentials of MMOR Cofactors.....	63
Electron Transfer Properties.....	64
Influence of pH on the Redox Properties of MMOR.....	66
Intramolecular Electron Transfer.....	70
Conclusion.....	71
References.....	72
Chapter 3. Structural Features of the MMOH/MMOR Complex as Revealed by Mass Spectrometric Analysis of Covalently Cross-linked Proteins.....	90
Introduction.....	91
Methods and Materials.....	93
Protein Purification.....	94
EDC Cross-linking Reactions.....	94
SVSB Cross-linking Reactions.....	94
In-gel Proteolytic Digestion.....	94
MALDI-TOF Mass Spectrometry.....	96

Capillary LC-MS.....	96
Data Analysis.....	97
Site-Directed Mutagenesis.....	97
NADH Consumption Assays.....	97
Results.....	98
Chemical Cross-linking of sMMO Complexes.....	98
In-gel Digestion and MALDI-TOF Analysis of Isolated sMMO Proteins.....	100
In-gel Digestion and MALDI-TOF Analysis of MMOH _α :MMOR-Fd.....	100
Analysis of the SVSB-Promoted MMOH:MMOB Cross-link.....	101
Other Approaches to Sample Preparation.....	102
Solution Digestion and Off-Line HPLC.....	102
SDS-PAGE and Electroelution of Cross-linked Bands.....	103
Affinity Tags.....	104
LC-QoTOF Analysis of MMOH _α :MMOR-Fd.....	104
Rationale.....	104
LC-QoTOF and Tandem MS Data.....	105
Identification of Two MMOH _α :MMOR-Fd Cross-Links.....	107
The MMOR EQ2 Mutant.....	108
Discussion.....	109
Cross-linking Reactions of sMMO Proteins.....	109
Digestion and Mass Spectrometric Analysis of Unmodified sMMO Proteins.....	110
MALDI-TOF Analysis of Cross-Linked sMMO Proteins.....	110
Solution Digestion and Other Methods of Sample Preparation.....	111
LC-QoTOF Analysis of MMOH _α :MMOR-Fd.....	113
Implications for the MMOH/MMOR Complex.....	114
Structural Implications of the Identified Cross-links.....	115
Other Approaches to Understanding Structures of sMMO Protein	

Complexes.....	117
Conclusion.....	117
References.....	119
Chapter Four: Cationic Species Can Be Produced in Soluble Methane Monooxygenase-Catalyzed Hydroxylation Reactions; Radical Species Are Not Formed.....	147
Introduction.....	148
Experimental Section.....	150
Protein Purification.....	150
Preparation of Substrates and Authentic Product Standards.....	151
Substrate Hydroxylation and Product Analysis.....	151
Results and Discussion.....	151
Conclusion.....	156
References.....	157
Chapter Five: Evaluation of Norcarane as a Probe for Radicals in Cytochrome P450- and Soluble Methane Monooxygenase-Catalyzed Hydroxylation Reactions.....	166
Introduction.....	167
Experimental Section.....	170
Solvolysis Reactions.....	170
P450-Catalyzed Oxidations.....	171
sMMO-Catalyzed Oxidations.....	172
Results.....	172
Enzyme-Catalyzed Oxidations.....	172
Solvolysis Studies.....	175
Discussion.....	176
Cationic Rearrangement Product.....	179
Radical Rearrangement Product.....	181
Conclusion.....	189

References.....	191
Chapter Six: Product Binding to the Diiron(III) and Mixed-Valence Diiron Centers of Methane Monooxygenase Hydroxylase Studied by ^1H and ^{19}F ENDOR Spectroscopy.....	203
Introduction.....	204
Experimental Section.....	206
Protein Purification and Sample Preparation.....	206
ENDOR Spectroscopy.....	207
Results and Discussion.....	210
EPR.....	210
^1H ENDOR of Exchangeable Protons of H_{mv}	211
ENDOR of Nonexchangeable ^1H of Alcohols Bound to H_{mv}	214
ENDOR of Nonexchangeable ^1H of Alcohols Bound to $(\text{H}_{\text{ox}})_{\text{mv}}$	215
^{19}F ENDOR.....	216
^{19}F ENDOR of $(\text{H}_{\text{ox}} + \text{TFE})_{\text{mv}}$	217
^{19}F ENDOR of $\text{H}_{\text{mv}} + \text{TFE}$	218
DMSO Binding to H_{mv} (+ Alcohols).....	219
Conclusion.....	220
References.....	222
Appendix: Single Turnover Hydroxylations of Norcarane.....	237
Introduction.....	238
Experimental.....	238
Results.....	239
Single-Turnover Oxidation of Norcarane: Single Mixing.....	239
Single-Turnover Oxidation of Norcarane: Double Mixing.....	240
Discussion.....	241
Conclusion.....	242
References.....	243
Biographical Note.....	251

List of Tables

Table 2.1. Properties of Native and Recombinant MMOR.....	76
Table 2.2. Midpoint Potentials at 25 °C and pH 7.0 of MMOR Alone and in Complexes with Other sMMO Proteins.....	77
Table 2.3. pH-dependent Distribution of Electrons in MMOR _{2e}	78
Table 3.1. Peptides Observed in MALDI-TOF Spectrum of MMOH _α In-Gel Digest.....	123
Table 3.2. Sequence Coverage of Unmodified sMMO Proteins Following In-Gel Digestion.....	125
Table 3.3. Peptides Observed in MALDI-TOF Spectrum of MMOH _α :MMOR-Fd Cross-Link.....	126
Table 3.4. Tandem MS Data for Peptide with Cross-Link between MMOR-Fd Glu56 and MMOH _α N-terminus.....	130
Table 3.5. Tandem MS Data for Peptide with Cross-Link between Fd Glu91 and MMOH _α N-terminus.....	131
Table 3.6. NADH Oxidation Activity of sMMO with MMOR or MMOR EQ2...	132
Table 5.1. Results of Enzyme-Catalyzed Oxidations of Norcarane.....	196
Table 5.2. Results of Stability Control Studies.....	197
Table 5.3. Products from Enzyme-Catalyzed Oxidations of Norcarane.....	198
Table A1. Rate Constants for Single Turnover of MMOH in the Presence or Absence of Norcarane, Measured by Single Mixing Stopped-Flow Spectroscopy.....	244
Table A2. Summary of Rate Constants Observed for Reaction of Norcarane with H _{peroxo} and Q Monitored by Double Mixing Stopped-Flow.	245

List of Figures

Figure 1.1. Protein components of sMMO from <i>Methylococcus capsulatus</i> (Bath). (A) X-ray structure of MMOH. (B) NMR structure of MMOB. (C) NMR structure of MMOR-Fd with cartoon depiction of the C-terminal domains of MMOR.....	43
Figure 1.2. (A) Active site structure of MMOH _{ox} . (B) Active site structure of MMOH _{red}	44
Figure 1.3. The catalytic cycle of sMMO.....	45
Figure 1.4. Rearrangement mechanisms of norcarane.	46
Figure 2.1. Simplified view of the sMMO catalytic cycle.....	79
Figure 2.2. Difference spectra recorded during reductive titration of MMOR with the redox dyes phenosafranine and anthraquinone-2,6-disulfonate...	80
Figure 2.3. Reaction of MMOR _{ox} with NADH. (A) Single wavelength stopped-flow traces recorded at 458, 625, and 725 nm. (B) Derived spectra of species observed during the reaction. (C) Dependence of k_1 on the concentration of NADH.....	81
Figure 2.4. Interactions of MMOR with NADH.....	82
Figure 2.5. Product inhibition of the reaction of MMOR _{ox} with NADH. (A) Traces recorded at 458 nm. (B) Traces recorded at 625 nm. (C) Traces recorded at 725 nm.....	83
Figure 2.6. Effect of pH on the reduction of MMOR _{ox} by NADH.....	84
Figure 2.7. Effect of pH on the reduction of MMOR _{ox} by NADH as revealed by diode array stopped-flow.....	85
Figure 2.8. Spectra of FAD _{ox} and FAD _{hq} at pH 5.47 and 8.01.....	86
Figure 2.9. Differences between the redox potentials of MMOR at varying pH...	87
Figure 2.10. Equilibration of electrons in MMOR _{2e-} following a pH jump.....	88
Figure 2.11. Protonation states of fully reduced FAD.....	89
Figure 3.1. Structures of sMMO component proteins.	133

Figure 3.2. (A) Mechanism of EDC-promoted protein cross-linking. (B) EDC cross-linking of MMOH and MMOR-Fd. (C) EDC cross-linking of MMOH and MMOB.....	134
Figure 3.3. (A) Mechanism of SVSB-promoted protein cross-linking.(B) Cross-linking of MMOB to MMOH _α by SVSB (C) Densitometer trace indicating MMOH _α :MMOB cross-link.....	135
Figure 3.4. Structures of cross-linking reagents that failed to cross-link sMMO complexes.....	136
Figure 3.5. MALDI-TOF spectrum of MMOH _α tryptic peptides.....	137
Figure 3.6. Sequence of MMOH _α and the tryptic peptides observed by MALDI-TOF following SDS-PAGE and in-gel digestion.....	138
Figure 3.7. Recovery of gel purified MMOH _α :MMOR-Fd by electroelution.....	139
Figure 3.8. (A) Inability of N-terminally His-tagged MMOR-Fd to cross-link to MMOH. (B) Inability of C-terminally His-tagged MMOR-Fd to cross-link to MMOH.....	140
Figure 3.9. Nomenclature of peptide fragment ions.....	141
Figure 3.10. Total ion chromatogram from LC-QoTOF analysis of a tryptic digest of MMOH _α :MMOR-Fd.....	142
Figure 3.11. Mass spectrum of MMOH _α N-terminus:MMOR-Fd Glu56 cross-link.....	143
Figure 3.12. Structure (A) and tandem mass spectrum (B) of cross-link between MMOH _α N-terminus and MMOR-Fd Glu56.....	144
Figure 3.13. Structure (A) and tandem mass spectrum (B) of cross-link between MMOH _α N-terminus and MMOR-Fd Glu91.....	145
Figure 3.14. Locations of cross-linking residues on (A) MMOR-Fd and (B) MMOH.....	146
Figure 3.15. EDC cross-linking of MMOH to MMOR EQ2.....	147
Figure 4.1. Structures of methylcubane and its MMO hydroxylation products..	160

Figure 4.2. GC traces of products from reactions of methylcubane with (A) <i>M. c.</i> (Bath) sMMO, (B) <i>M. t.</i> OB3b sMMO, (C) the P450 CYP2B1, and (D) of authentic product standards.....	161
Figure 4.3. Mass spectra of (A) major product of sMMO-catalyzed methylcubane oxidation and (B) of authentic 1-homocubanol.....	162
Figure 4.4. Structures of radical probe substrate 5 and its MMO hydroxylation products.....	163
Figure 4.5. Possible analogous intermediates produced in cytochrome P450- and MMOH-catalyzed oxidations.....	164
Figure 4.6. Formation of cation-derived products by loss of H ₂ O from protonated alcohols.....	165
Figure 5.1. Norcarane and products observed from its enzyme-catalyzed hydroxylation reactions.....	199
Figure 5.2. Iron–oxygen intermediates produced in P450 and sMMO oxidations.....	200
Figure 5.3. Other probe substrates that can distinguish between radical and cationic rearrangements.....	201
Figure 5.4. Representative GC-MS trace from oxidation of norcarane by sMMO.....	202
Figure 6.1. Crystal-structure based representation of the MMOH _{mv} active site.....	226
Figure 6.2. MMOH _{mv} EPR spectra in the presence and absence of substrates...	227
Figure 6.3. ¹ H ENDOR spectra of H _{mv} and H _{mv} in the presence of TFE, ethanol, or methanol.....	228
Figure 6.4. Field dependence of ² H ReMims spectra of H _{mv} + TFE in D ₂ O.....	229
Figure 6.5. ² H 35 GHz Mims ENDOR of H _{mv} to which CD ₃ OH, CD ₃ CD ₂ OH, or CF ₃ CD ₂ OH have been added, and of (H _{ox} + CF ₃ CD ₂ OH) _{mv}	230
Figure 6.6. Field dependence of ² H Mims spectra of H _{mv} + CD ₃ CD ₂ OH in H ₂ O.....	231

Figure 6.7. Field dependence of ^2H Mims spectra of $(\text{H}_{\text{ox}} + \text{CF}_3\text{CD}_2\text{OH})_{\text{mv}}$ in H_2O	232
Figure 6.8. Typical CW vs. pulsed $^1\text{H}/^{19}\text{F}$ ENDOR of $\text{H}_{\text{mv}} + \text{TFE}$	233
Figure 6.9. τ Dependence of the $^1\text{H}/^{19}\text{F}$ ENDOR signal.....	234
Figure 6.10. Field dependence of ^{19}F Mims spectra of $(\text{H}_{\text{ox}} + \text{CF}_3\text{CD}_2\text{OH})_{\text{mv}}$ in H_2O	235
Figure 6.11. τ Dependence of the $^1\text{H}/^{19}\text{F}$ ENDOR signal for $\text{H}_{\text{mv}} + \text{TFE}$	236
Figure A1. Single turnover reactions of $\text{MMOH}_{\text{red}}/2\text{MMOB}$ with or without norcarane, recorded in sigle mixing mode.....	246
Figure A2. Simulations of single mixing data in the absence of substrate.....	247
Figure A3. Simulations of single mixing data in the presence of norcarane, assuming norcarane reacts only with Q.....	248
Figure A4. Simulations of single mixing data in the presence of norcarane, assuming norcarane reacts with H_{peroxo} and Q.....	249
Figure A5. Double mixing stopped flow reaction of $\text{MMOH}_{\text{red}}/2\text{MMOB}$ with and with norcarane.....	250

Chapter One:

Soluble Methane Monooxygenase: Activation of Dioxygen and Methane

Introduction^{1,2}

It looks so simple on paper. The conversion of methane to methanol (Equation 1) appears to be a straightforward reaction:



In practice, however, it is very difficult to prevent the reaction of methane with dioxygen from proceeding rather vigorously or even explosively to afford carbon dioxide and water, as happens with a gas stove. Although reagents have been developed that can convert methane to a methanol derivative in good yield, even using dioxygen as oxidant, most catalysts that activate alkanes still suffer serious drawbacks such as the requirement of high pressures and temperatures.³ On the other hand, nature's own catalyst, methane monooxygenase (MMO), operates in neutral aqueous solution at moderate temperatures and atmospheric pressure. The selective conversion to methanol is achieved by reductive activation of dioxygen, as illustrated in Equation 2:



MMOs occur in bacteria that obtain all the energy and carbon needed for life from methane. MMO carries out the first step of carbon metabolism by such organisms, conversion of methane to methanol. The methanol is further oxidized by a dehydrogenase to formaldehyde, which can either be incorporated into biomass or oxidized to CO₂ to provide energy for the cell.⁴ Two varieties of MMO have been discovered in methanotrophic bacteria. The first is a copper-containing, membrane-bound enzyme known as pMMO, for particulate MMO.⁵

A soluble, iron-containing MMO (sMMO) has been characterized more thoroughly and is the focus of this chapter.^{6,7} In particular, sMMOs from the species *Methylosinus trichosporium* OB3b and *Methylococcus capsulatus* (Bath), referred to hereafter as *Mt* and *Mc*, respectively, have been studied extensively.

The sMMO system requires three proteins to achieve catalysis (Figure 1.1). The active site (Figure 1.2) for dioxygen activation and methane hydroxylation is located within a four-helix bundle in the α subunits of the $\alpha_2\beta_2\gamma_2$ hydroxylase (MMOH). The catalytic cycle shown in Figure 1.3 illustrates the roles of the three proteins. In the presence of the regulatory protein MMOB, MMOH_{red} binds and reductively activates dioxygen, proceeding through putative superoxo and peroxo intermediates before converting it to the strongly oxidizing MMOH_Q intermediate. MMOH_Q is the species that hydroxylates methane, leaving MMOH in the resting diiron(III) form called MMOH_{ox}. The iron-sulfur flavoprotein MMOR uses two electrons derived from NADH to return MMOH_{ox} to its reduced state, completing the catalytic cycle.

Although the gross features have been understood for some time, recent experiments have uncovered increasingly subtle aspects of the sMMO mechanism. The earliest steps of dioxygen activation are being elucidated, and probe substrates continue to provide information on the nature of the C–H bond activation step. Site-directed mutagenesis has suggested how MMOB might alter the behavior of MMOH. Other features of the sMMO system are coming under scrutiny. Included are aspects of electron transfer, binding of substrate analogues and

products to the active site, the nature of binding interactions between the protein components, and the existence of a fourth protein (MMOD) that interacts with MMOH. The function of MMOD remains to be determined.

Dioxygen activation

As is the case for cytochrome P450 enzymes (P450s), the ability of sMMO to hydroxylate unactivated hydrocarbon substrates derives from a high-valent iron(IV) intermediate. Consequently, much effort has been devoted to understanding the nature of this intermediate and how it is formed. The following sections detail the early part of the catalytic cycle, in which the $\text{MMOH}_{\text{red}}/2\text{MMOB}$ complex reacts with dioxygen to produce intermediates capable of hydroxylating a variety of substrates.

Early Steps of Dioxygen Activation: Conversion of MMOH_{red} to $\text{MMOH}_{\text{peroxo}}$. The existence of a Michaelis complex between dioxygen and MMOH_{red} was inferred from the lack of an O_2 concentration dependence on the kinetics of disappearance of the characteristic $g = 16$ EPR signal of MMOH_{red} ,⁸ depicted as $\text{O}_2 \cdot \text{MMOH}_{\text{red}}$ in Figure 1.3. Although $\text{MMOH}_{\text{peroxo}}$ is the first spectroscopically observable intermediate that occurs after mixing of $\text{MMOH}_{\text{red}}/2\text{MMOB}$ with dioxygen, conversion of $\text{O}_2 \cdot \text{MMOH}_{\text{red}}$ to $\text{MMOH}_{\text{superoxo}}$ is supported by three lines of evidence. Results from both density functional theory (DFT) and ^{18}O isotope effect studies point to the existence of a superoxo

complex occurring before formation of $\text{MMOH}_{\text{peroxo}}$.^{9,10} The $^{18}(\text{V}/\text{K})$ values of 1.0167 ± 0.0010 (no substrate) and 1.0152 ± 0.0007 (acetonitrile) are consistent with a reduction in O-O bond order of 0.5, as would be expected for a one-electron reduction of dioxygen with concomitant iron binding.¹¹ DFT calculations revealed a $\text{Fe(II)Fe(III)(O}_2^-)$ species of intermediate energy between MMOH_{red} and $\text{MMOH}_{\text{peroxo}}$.⁹ Characteristic Mössbauer and optical spectroscopic features identify the $\text{MMOH}_{\text{peroxo}}$ intermediate, which occurs after mixing of $\text{MMOH}_{\text{red}}/2\text{MMOB}$ with dioxygen.¹² Stopped-flow kinetic experiments with *Mt* MMOH also indicate that a species forms after $\text{O}_2 \cdot \text{MMOH}_{\text{red}}$ but before $\text{MMOH}_{\text{peroxo}}$.^{13,14}

Conversion of $\text{MMOH}_{\text{superoxo}}$ to $\text{MMOH}_{\text{peroxo}}$ has been reported to have a significant pH dependence for *Mt* sMMO. A $\text{p}K_{\text{a}}$ of 7.6 was determined for a functional group relevant to this process, with a rate constant approaching zero at pH 8.6.¹⁴ No such effect has been observed with *Mc* sMMO, however.¹² Mutation of a conserved histidine to alanine in the N-terminal region of MMOB (His33Ala of *Mt* MMOB) leads to a >50-fold decrease in the rate constant for formation of $\text{MMOH}_{\text{peroxo}}$, while having only a small effect on steady-state activity.¹⁵ This effect was assigned to the step in which $\text{MMOH}_{\text{peroxo}}$ is formed from its immediate precursor, not a prior event such as binding of dioxygen to MMOH_{red} .

Conversion of $\text{MMOH}_{\text{peroxo}}$ to MMOH_{Q} . The formation of MMOH_{Q} is retarded at high pH for *Mt* MMOH, like formation of $\text{MMOH}_{\text{peroxo}}$. A functional

group involved in this process also had a pK_a of 7.6. Proton inventory plots derived from kinetic solvent isotope effect studies indicate that a single proton is involved in each step.¹³ A histidine to alanine site-directed mutant (*Mt* MMOB His5Ala) had a decreased rate constant for formation of MMOH_Q .¹⁵ On the other hand, both DFT^{9,16} and experimental¹² data for *Mc* MMOH indicate that $\text{MMOH}_{\text{peroxo}}$ can convert to MMOH_Q in a proton-independent manner. This conversion traverses an (η_2, η_2) peroxodiiron(III) species that homolyzes to form the di(μ -oxo)diiron(IV) unit in MMOH_Q .

C-H Bond Activation

The ability of sMMO to hydroxylate unactivated C-H bonds has led to many comparisons with cytochrome P450. In particular, it has been assumed that sMMO operates analogously to the radical rebound mechanism proposed for P450.¹⁷ Compared with the large number of P450s described, sMMO is unique in its ability to hydroxylate the simplest and least reactive of saturated hydrocarbons, methane. Recent studies aimed at understanding the C-H activation chemistry of sMMO are described in this section.

Alkane Substrates. The discovery of non-linear Eyring or Arrhenius plots for the reaction of MMOH_Q with methane^{14,18} was a major surprise. Other steps in the catalytic cycle including formation of $\text{MMOH}_{\text{peroxo}}$ and its conversion to MMOH_Q do not show such non-linear temperature-dependent behavior. A change in the rate-determining step as a function of temperature has been as-

signed as the cause of the non-linear effect.^{14,18} In a recent sequential mixing experiment in which MMOH_Q is allowed to accumulate before addition of methane, the non-linear effect is abrogated (Ambundo EA and Lippard SJ, unpublished observations), conflicting with an earlier report.¹⁴ The Arrhenius plot derived from sequential mixing data reported¹⁴ are, in our hands, equally well reproduced by linear and non-linear fits (Ambundo EA and Lippard SJ, unpublished observations). The measured activation energies also provide a means to evaluate the validity of theoretical calculations of sMMO-catalyzed alkane hydroxylation (see below).

The effect of an MMOB variant containing four point mutations (MMOB_{quad})¹⁵ on single turnover reactions revealed no changes in kinetic properties of MMOH_{peroxo} or MMOH_Q formation, but there was a significant increase in the rate constant of MMOH_Q decay in the presence of furan or nitrobenzene. Steady-state turnover for these substrates is also accelerated compared with that for wild-type MMOB. When methane is the substrate, the MMOB_{quad} mutant reduces the rate constant for MMOH_Q decay. It was proposed that MMOB_{quad} facilitates access of the larger substrates to the MMOH active site.¹⁵

Kinetic Isotope Effects. The reaction of MMOH_Q with methane shows a remarkable kinetic isotope effect (KIE) of 23 or more when comparing CH₄ to CD₄.¹⁸⁻²⁰ This value greatly exceeds the maximum KIE of 7 for a classical, primary ¹H/²H isotope effect. A combination of primary and secondary isotope effects may contribute to this value. Hydrogen tunneling has also been suggested

as a reason for the large magnitude of the KIE for methane. A combination of kinetic and thermodynamic isotope effects is yet another possibility.

In view of the large value of the KIE for methane, the result obtained when ethane is investigated is even more remarkable. The $k_{\text{H}}/k_{\text{D}}$ for reaction of C_2H_6 vs. C_2D_6 with MMOH_Q is exactly 1.^{20,21} This result clearly indicates that the rate-limiting step for ethane hydroxylation does not involve C-H bond breaking, in sharp contrast to the corresponding methane reaction.

An isotope effect of 2 for ethane is observed, however, when the $\text{MMOB}_{\text{quad}}$ mutant is substituted for wild type MMOB .²¹ The KIE for ethane reflects a twofold increase in the rate constant for decay of MMOH_Q . Under the same conditions, the rate constant for decay of MMOH_Q decreases sevenfold when methane is the substrate, such that the $k_{\text{H}}/k_{\text{D}}$ is 6 for $\text{MMOB}_{\text{quad}}$. Rate constants for reaction with the deuterated alkanes were unchanged when the MMOB mutant was used.

The KIE results were interpreted in terms of the model depicted in eq 3:



In the case of methane, k_{CH} is rate determining, and so decay of MMOH_Q displays an isotope effect. For ethane, substrate binding (k_{sb}) must be rate determining to explain the lack of an isotope effect. It was proposed that MMOH can discriminate between the two hydrocarbons by virtue of their size. The absence of any isotope effect for propane (C_3H_8 vs. C_3D_8) is consistent with this interpreta-

tion.²¹ Additional evidence for a substrate-binding step occurring before C-H bond activation comes from the observation that the rate constant for decay of MMOH_Q can be saturated at high concentrations of the substrates nitromethane and acetonitrile.²⁰

Alteration of the kinetic rate constants by use of MMOB_{quad} was proposed to diminish the size discrimination effect, increasing k_{sb} for ethane such that k_{CH} becomes at least partially rate-limiting, revealing an isotope effect. The decreased value of k_{CH} for methane with the MMOB mutant was postulated to be a consequence of changes in MMOH protein dynamics, removing any tunneling contributions from the C-H bond activation step. The resulting measured k_H/k_D value of 6 is consistent with classical transition state theory.²¹ The suggested ability of the MMOH active site to discriminate between methane and ethane based upon size seems somewhat remarkable, especially in view of its ability to hydroxylate bulky substrates, such as octane,²² adamantane²³ and methylcubane.²⁴⁻²⁶

A somewhat different interpretation of these effects is suggested by studies with substituted methanes CH₃X, where X = CN, NO₂ and OH.²⁰ This alternative model also explains why a substrate such as acetonitrile has a much lower rate constant for reaction with MMOH_Q than does methane or ethane, despite having a significantly weaker (~10 kcal mol⁻¹) C-H bond. Based on the size discrimination argument, acetonitrile should not display a KIE, because it is similar to ethane. The KIE for acetonitrile was determined to be 46, indicating that k_{CH} is rate-limiting for this substrate.²⁰ The rate-limiting step for any particular sub-

strate, k_{sb} or k_{CH} , depends on both the C-H bond energy and the energy required to translocate the solvated substrate into the hydrophobic cavity at the active site.²⁷ Ethane lacks a KIE because its C-H bond energy is sufficiently low to drop the value of k_{CH} below that of k_{sb} . Desolvation of polar substrates like acetonitrile is unfavorable, increasing the total activation energy, thus reducing the rate constant for MMOHQ decay.

Probe Substrates. A new catalytic reaction, desaturation of alkanes to afford olefins, was added to the list of known activities of sMMO.^{28,29} Oxidation of ethylbenzene afforded a mixture of phenylethanol, ethylphenol, styrene and styrene epoxide. Styrene is the desaturation product, and styrene epoxide is the consequence of further oxidation of styrene. Cyclohexadienes were converted to mixtures of epoxides, alcohols and benzene. No desaturation products were detected in oxidations of ethane, ethylene, or cyclohexane. The desaturation products are thought to arise by loss of H^+ from a cationic intermediate, which could form by one-electron oxidation of a radical precursor,²⁹ or by loss of water from a protonated alcohol.²⁶ Substrates that yielded desaturated products all contain an activated C-H bond, such that any radical or cation that might lie on the reaction coordinate would be stabilized by conjugation to a benzylic or allylic π system.²⁹

Substrates that can undergo rearrangements of their carbon skeleton to inform on the mechanism of activation continue to be used in the study of sMMO. Early work suggested the involvement of cationic and radical species,³⁰ but later

experiments were inconsistent with long-lived radical intermediates.³¹⁻³³ Substrates that can distinguish between radical and cationic mechanisms, such as methylcubane²⁴⁻²⁶ and norcarane, have been the subjects of recent attention.^{34,35}

The reaction of sMMO with methylcyclopropanes³⁶ was reinvestigated in experiments in which 1,1,2,2-tetramethylcyclopropane and 1,1-dimethylcyclopropane, both of which are hydroxylated α to a quaternary carbon, yielded rearranged products. Methylcyclopropanes lacking a quaternary carbon, such as cis- and trans-1,2-dimethylcyclopropane and trans-2-phenylmethylcyclopropane, did not afford rearranged products. The failure to observe rearrangements of products deriving from the phenylmethylcyclopropane radical is surprising in view of its fast ring-opening chemistry, which is three orders of magnitude greater than the corresponding radicals of the methylcyclopropanes.³⁵ It was suggested that steric factors cause bulky substrates to react via a radical intermediate, whereas less hindered substrates may approach the activated oxygen atom of MMOH_Q more closely, allowing the hydroxylation to proceed too quickly for carbon skeletal rearrangement. It could be interesting to see whether the MMOB_{quad} mutant, proposed to increase access of large substrates to the active site,¹⁵ would alter the relative yield of rearranged products from such cyclopropanes.

Norcarane (**1**) is one of several probe substrates that can undergo different rearrangements depending on the mechanism of C-H bond activation (Figure 1.4).^{24,29,34,35} The major products of norcarane oxidation are the two diastereomers of 2-norcaranol, accounting for ~80% of the products; only small

amounts of the radical- and cation-derived products were observed. Because the norcaran-2-yl radical (**2**) has a comparatively slow rate constant for rearrangement,^{37,38} even the small amount of cyclohexenylmethanol (**3**) observed indicates a relatively long lifetime for the radical intermediate, on the order of 20–150 ps.^{34,35}

At first glance, the results suggest that both radical and cationic species are involved in the formation of products from norcarane. Yet the broader picture is confusing. Considering the several probe substrates that have been applied to investigate sMMO hydroxylation chemistry, there is no clear correlation between yield of rearranged product and the rearrangement rate constant.^{34,35} In the case of *Mc* sMMO, norcarane is the only probe substrate to provide evidence for a radical intermediate with a significant (> 1 ps) lifetime, despite having a rearrangement rate constant 2–3 orders of magnitude slower than probes that do not rearrange.^{33,39} Further complicating the norcarane analysis, cationic species **4** rearranges to give mostly 3-cycloheptenol (**5**), but also some of the ‘radical-derived’ product **3**.⁴⁰ The formation of a ‘radical-derived’ product from a cationic reaction manifold was not considered in the analysis of norcarane hydroxylation results from *Mt* sMMO.³⁴

The conclusion from the probe substrate work is that different substrates are almost certainly hydroxylated by different mechanisms. For instance, propylene is converted to its epoxide whereas propane is converted to an alcohol.²² New information is making it clear that a single substrate, such as norcarane,

may react by different mechanisms. Clues to this behavior were available in earlier studies. *cis*-2-Butene is oxidized to afford a ~1:1 mixture of the epoxide and alcohol.²³ High-level theoretical calculations find that methane and ethane partition between concerted and bound-radical pathways upon reaction with MMOH_Q (see below).

Theoretical Investigations of Alkane Hydroxylation by MMOH_Q. Quantum chemical investigations are of increasing importance for achieving mechanistic understanding of metalloenzymes, and sMMO is no exception.^{41,42} Several theoretical studies concur that methane hydroxylation by MMOH_Q begins with a nearly linear approach of a C-H bond to a bridging oxo group of the di(μ -oxo)diiron(IV) core in this intermediate.⁴²⁻⁴⁴ The transition state found for this geometry features a nearly linear O-H-C arrangement with the O-H distance slightly shorter (0.02-0.06 Å) than the C-H distance, the C...O distance being about 2.5 Å.

Calculations based on a model of the sMMO active site consisting of two iron atoms ligated by formates, imidazoles and solvent-derived ligands, were used to create models of the various species in the catalytic cycle.¹⁶ Using this model, activation of methane was found to proceed by conversion of MMOH_Q from a diiron(IV) singlet to an Fe(III)Fe(IV)O[•] state. The oxygen radical form of MMOH_Q can abstract a hydrogen atom from CH₄ through the linear transition state described above. The reaction then proceeds by a radical recoil/rebound

mechanism, where a methyl radical first recoils away from the oxo group of MMOH_Q, then rebounds to form the new C–O bond of the product.

In another study that used a large (~100 atom) model of the sMMO active site,⁹ two alternative pathways from transition state to product were identified.⁴⁴ The first resembles a radical recoil/rebound mechanism. The second pathway features a non-linear O–H–C geometry; the H atom rotates up out of the O–C axis and the C–O distance contracts to form the new bond.

This latter work was extended by applying molecular dynamics to probe the partitioning of alkane substrates between these two reaction channels.⁴⁵ Ethane was chosen as the substrate to determine whether the calculations could reproduce and explain a well-known result. Oxidation of chiral ethane, CH₃CHDT, by sMMO gave the surprising result of partial (72%) retention and 28% inversion of stereochemistry.^{31,32} A radical mechanism would be expected to give complete scrambling and afford a racemic mixture of products; a fully concerted mechanism would be expected to yield products of a single configuration.

The theoretical result (69–84% retention of configuration) matches the experimental number closely, validating the approach and providing a framework for understanding the chiral ethane result. Depending on whether or not tunneling effects are included in the calculations, 12–16.5% of the products are formed from the concerted reaction channel. The remaining products derive from a bound radical, with a mean lifetime of 320–400 fs. This lifetime agrees with the majority of the probe substrate results, with some notable exceptions.^{33–35}

Similar studies could shed light on the behavior of the larger probe substrates such as norcarane. For instance, a series of transition states for activation of methylcyclopropane has been computed. Like methane, a linear C-H-O geometry was found for the H atom abstraction transition state. In contrast to methane, the transition state for the rebound step featured little spin density and high charge on the methyl carbon, indicating considerable cationic character.¹⁶

Other sMMO Research Frontiers

In addition to the mechanistic studies that focused on the reactivity of the diiron site, other aspects of sMMO are actively being investigated. Structural studies continue to describe the various redox states and complexes with products and substrate analogues of the hydroxylase.^{27,46,47} Advanced EPR methodologies have measured the interaction of products and product analogues with the diiron site in the solution phase, complementing and supporting the results obtained from X-ray crystallography.⁴⁸ Calculations are also being extended to include effects of the protein environment.⁴⁹⁻⁵¹ Component interactions have been investigated by covalent modification of positively charged residues on MMOH, interfering with protein complex formation, but not with hydrogen-peroxide-mediated catalysis.⁵²

The interaction of MMOB with MMOH has been probed by extending the NMR studies carried out in pursuit of the MMOB solution structure.^{53,54} The binding surface of MMOB has been described by examination of the location of

those residues that have the greatest line broadening upon formation of an MMOH/MMOB complex.^{53,55} Target residues for site-directed mutagenesis were selected on the basis of such information, and some of the effects of those mutations were described above.^{15,21} Mutants with successive deletions from the N-terminus of *Mc* MMOB have pinpointed the region Ser4–Tyr7 as critical for full sMMO activity and MMOB autocatalytic degradation,⁵⁶ complementing the *Mt* MMOB mutation studies.¹⁵

The diiron center of MMOH is ~15 Å from a spin-label positioned on the native Cys89 of *Mc* MMOB, as determined in a saturation recovery EPR study.⁵⁷ This distance constrains MMOB to bind in the canyon region of MMOH. MMOB most likely contacts a single helix, E or F, of the α subunit that contains iron-ligating Glu residues.

The solution structure of the [2Fe-2S] domain of MMOR has been solved,⁵⁸ and that of the C-terminal domains including the FAD and NAD(H) binding sites is underway. These structures will allow detailed analysis of the electron-transfer and redox properties of MMOR, which have recently been scrutinized.⁵⁹

Crystallization of an MMOH/MMOB complex, as was recently reported, could provide an atomic resolution structure of the MMOH_{red} active site as it exists in a complex with MMOB.⁶⁰ Such a structure might illuminate the changes in the active site that allow productive reaction with dioxygen.

Development of techniques for recombinant expression of MMOH raises the possibility of mechanistic studies on site-directed mutants of MMOH.^{61,62} Very recently, expression and purification of site-directed mutants of MMOH has been achieved.^{63,64} Alterations in the vicinity of the active site of the α subunit could not only reveal the roles of individual residues, but also provide new tools for understanding the chemistry of the active site, as has occurred in the P450 field.^{65,66}

A fourth protein, MMOD, has been identified in *Mc* cells expressing the sMMO proteins. The 'extra' gene in the *mmo* operon, *orfY*, that encodes MMOD was previously thought not to be expressed *in vivo*.⁵ Addition of recombinant MMOD inhibits sMMO activity *in vitro* and alters the spectroscopic properties of the diiron centre of MMOH.⁶⁷ The functional role of this protein *in vivo* remains obscure, and for this reason MMOD is certain to be the subject of further scrutiny.

Conclusion

The sMMO system represents a paradigm for dioxygen activation by non-heme diiron proteins. It also represents one extreme of reactivity in this class. Diiron sites in biology achieve a variety of reactions ranging from O₂ transport in hemerythrin, to desaturation of alkyl chains in stearoyl-ACP 9 desaturase, one-electron oxidation of tyrosine in the R2 protein of ribonucleotide reductase, and hydrocarbon hydroxylation by MMO.⁶⁸

A broad arsenal of techniques has been applied to study the mechanism of sMMO. Kinetic and spectroscopic methods, site-directed mutagenesis, isotope effect experiments, use of probe substrates, X-ray, NMR and EPR structural methods, and quantum mechanics have all made important contributions to our knowledge about sMMO. The future holds the promise of an even more intimate understanding, as results of structural studies of protein complexes, further calculational work, and advances in the molecular biology of sMMO become available.

References

- 1) This work has been published in slightly different form. See reference 2.
- 2) Kopp, D. A.; Lippard, S. J. *Curr. Opin. Chem. Biol.* **2002**, *6*, 568-576.
- 3) Labinger, J. A.; Bercaw, J. E. *Nature* **2002**, *417*, 507-514.
- 4) Anthony, C. *The Biochemistry of Methylotrophs*; Academic Press: London, 1982.
- 5) Murrell, J. C.; Gilbert, B.; McDonald, I. R. *Arch. Microbiol.* **2000**, *173*, 325-332.
- 6) Wallar, B. J.; Lipscomb, J. D. *Chem. Rev.* **1996**, *96*, 2625-2657.
- 7) Merkx, M.; Kopp, D. A.; Sazinsky, M. H.; Blazyk, J. L.; Muller, J.; Lippard, S. J. *Angew. Chem.* **2001**, *40*, 2782-2807.
- 8) Liu, Y.; Nesheim, J. C.; Lee, S. K.; Lipscomb, J. D. *J. Biol. Chem.* **1995**, *270*, 24662-24665.
- 9) Dunietz, B. D.; Beachy, M. D.; Cao, Y. X.; Whittington, D. A.; Lippard, S. J.; Friesner, R. A. *J. Am. Chem. Soc.* **2000**, *122*, 2828-2839.
- 10) Stahl, S. S.; Francisco, W. A.; Merkx, M.; Klinman, J. P.; Lippard, S. J. *J. Biol. Chem.* **2001**, *276*, 4549-4553.
- 11) Tian, G. C.; Klinman, J. P. *J. Am. Chem. Soc.* **1993**, *115*, 8891-8897.
- 12) Liu, K. E.; Valentine, A. M.; Wang, D. L.; Huynh, B. H.; Edmondson, D. E.; Salifoglou, A.; Lippard, S. J. *J. Am. Chem. Soc.* **1995**, *117*, 10174-10185.
- 13) Lee, S.-K.; Lipscomb, J. D. *Biochemistry* **1999**, *38*, 4423-4432.
- 14) Brazeau, B. J.; Lipscomb, J. D. *Biochemistry* **2000**, *39*, 13503-13515.

- 15) Wallar, B. J.; Lipscomb, J. D. *Biochemistry* **2001**, *40*, 2220-2233.
- 16) Siegbahn, P. E. M. *J. Biol. Inorg. Chem.* **2001**, *6*, 27-45.
- 17) Stahl, S. S.; Lippard, S. J. ; Ferreira, G. C., Moura, J. J. G. and Franco, R., Ed.; Wiley-VCH: Weinheim, 1999, pp 303-321.
- 18) Valentine, A. M.; Stahl, S. S.; Lippard, S. J. *J. Am. Chem. Soc.* **1999**, *121*, 3876-3887.
- 19) Nesheim, J. C.; Lipscomb, J. D. *Biochemistry* **1996**, *35*, 10240-10247.
- 20) Ambundo, E. A.; Friesner, R. A.; Lippard, S. J. *J. Am. Chem. Soc.* **2002**, *124*, 8770-8771.
- 21) Brazeau, B. J.; Wallar, B. J.; Lipscomb, J. D. *J. Am. Chem. Soc.* **2001**, *123*, 10421-10422.
- 22) Colby, J.; Stirling, D. I.; Dalton, H. *Biochem. J.* **1977**, *165*, 395-402.
- 23) Green, J.; Dalton, H. *J. Biol. Chem.* **1989**, *264*, 17698-17703.
- 24) Choi, S. Y.; Eaton, P. E.; Hollenberg, P. F.; Liu, K. E.; Lippard, S. J.; Newcomb, M.; Putt, D. A.; Upadhyaya, S. P.; Xiong, Y. S. *J. Am. Chem. Soc.* **1996**, *118*, 6547-6555.
- 25) Jin, Y.; Lipscomb, J. D. *Biochemistry* **1999**, *38*, 6178-6186.
- 26) Choi, S. Y.; Eaton, P. E.; Kopp, D. A.; Lippard, S. J.; Newcomb, M.; Shen, R. *N. J. Am. Chem. Soc.* **1999**, *121*, 12198-12199.
- 27) Whittington, D. A.; Rosenzweig, A. C.; Frederick, C. A.; Lippard, S. J. *Biochemistry* **2001**, *40*, 3476-3482.
- 28) Gassner, G. T.; Lippard, S. J. *Biochemistry* **1999**, *38*, 12768-12785.

- 29) Jin, Y.; Lipscomb, J. D. *J. Biol. Inorg. Chem.* **2001**, *6*, 717-725.
- 30) Ruzicka, F.; Huang, D. S.; Donnelly, M. I.; Frey, P. A. *Biochemistry* **1990**, *29*, 1696-1700.
- 31) Priestley, N. D.; Floss, H. G.; Froland, W. A.; Lipscomb, J. D.; Williams, P. G.; Morimoto, H. *J. Am. Chem. Soc.* **1992**, *114*, 7561-7562.
- 32) Valentine, A. M.; Wilkinson, B.; Liu, K. E.; Komar-Panicucci, S.; Priestley, N. D.; Williams, P. G.; Morimoto, H.; Floss, H. G.; Lippard, S. J. *J. Am. Chem. Soc.* **1997**, *119*, 1818-1827.
- 33) Liu, K. E.; Johnson, C. C.; Newcomb, M.; Lippard, S. J. *J. Am. Chem. Soc.* **1993**, *115*, 939-947.
- 34) Brazeau, B. J.; Austin, R. N.; Tarr, C.; Groves, J. T.; Lipscomb, J. D. *J. Am. Chem. Soc.* **2001**, *123*, 11831-11837.
- 35) Newcomb, M.; Shen, R. N.; Lu, Y.; Coon, M. J.; Hollenberg, P. F.; Kopp, D. A.; Lippard, S. J. *J. Am. Chem. Soc.* **2002**, *124*, 6879-6886.
- 36) Jin, Y.; Lipscomb, J. D. *Biochim. Biophys. Acta-Protein Struct. Molec. Enzym.* **2000**, *1543*, 47-59.
- 37) Friedrich, E. C.; Holmstead, R. L. *J. Org. Chem.* **1972**, *37*, 2550-4.
- 38) Austin, R. N.; Chang, H.-K.; Zylstra, G. J.; Groves, J. T. *J. Am. Chem. Soc.* **2000**, *122*, 11747-11748.
- 39) Valentine, A. M.; LeTadic-Biadatti, M. H.; Toy, P. H.; Newcomb, M.; Lippard, S. J. *J. Biol. Chem.* **1999**, *274*, 10771-10776.
- 40) Friedrich, E. C.; Jassawalla, J. D. C. *Tetrahedron Lett.* **1978**, 953-956.

- 41) Shaik, S.; de Visser, S. P.; Ogliaro, F.; Schwarz, H.; Schroder, D. *Curr. Opin. Chem. Biol.* **2002**, *6*.
- 42) Guallar, V.; Gherman, B. F.; Lippard, S. J.; Friesner, R. A. *Curr. Opin. Chem. Biol.* **2002**, *6*, 236-242.
- 43) Basch, H.; Mogi, K.; Musaev, D. G.; Morokuma, K. *J. Am. Chem. Soc.* **1999**, *121*, 7249-7256.
- 44) Gherman, B. F.; Dunietz, B. D.; Whittington, D. A.; Lippard, S. J.; Friesner, R. A. *J. Am. Chem. Soc.* **2001**, *123*, 3836-3837.
- 45) Guallar, V.; Gherman, B. F.; Miller, W. H.; Lippard, S. J.; Friesner, R. A. *J. Am. Chem. Soc.* **2002**, *124*, 3377-3384.
- 46) Whittington, D. A.; Sazinsky, M. H.; Lippard, S. J. *J. Am. Chem. Soc.* **2001**, *123*, 1794-1795.
- 47) Whittington, D. A.; Lippard, S. J. *J. Am. Chem. Soc.* **2001**, *123*, 827-838.
- 48) Smoukov, S. K.; Kopp, D. A.; Valentine, A. M.; Davydov, R.; Lippard, S. J.; Hoffman, B. M. *J. Am. Chem. Soc.* **2002**, *124*, 2657-2663.
- 49) Lovell, T.; Han, W. G.; Liu, T. Q.; Noodleman, L. *J. Am. Chem. Soc.* **2002**, *124*, 5890-5894.
- 50) Lovell, T.; Li, J.; Noodleman, L. *Inorg. Chem.* **2001**, *40*, 5251-5266.
- 51) Lovell, T.; Li, J.; Noodleman, L. *Inorg. Chem.* **2001**, *40*, 5267-5278.
- 52) Balendra, S.; Lesieur, C.; Smith, T. J.; Dalton, H. *Biochemistry* **2002**, *41*, 2571-2579.

- 53) Walters, K. J.; Gassner, G. T.; Lippard, S. J.; Wagner, G. *Proc. Natl. Acad. Sci. U. S. A.* **1999**, *96*, 7877-7882.
- 54) Chang, S. L.; Wallar, B. J.; Lipscomb, J. D.; Mayo, K. H. *Biochemistry* **1999**, *38*, 5799-5812.
- 55) Chang, S. L.; Wallar, B. J.; Lipscomb, J. D.; Mayo, K. H. *Biochemistry* **2001**, *40*, 9539-9551.
- 56) Callaghan, A. J.; Smith, T. J.; Slade, S. E.; Dalton, H. *Eur. J. Biochem.* **2002**, *269*, 1835-1843.
- 57) MacArthur, R.; Sazinsky, M. H.; Kuhne, H.; Whittington, D. A.; Lippard, S. J.; Brudvig, G. W. *J. Am. Chem. Soc.* **2002**, *124*, 13392-13393.
- 58) Müller, J.; Lugovskoy, A. A.; Wagner, G.; Lippard, S. J. *Biochemistry* **2002**, *41*, 42-51.
- 59) Kopp, D. A.; Gassner, G. T.; Blazyk, J. L.; Lippard, S. J. *Biochemistry* **2001**, *40*, 14932-14941.
- 60) Kochkina, V. M.; Morozov, I. A.; Harutyunyan, E. G. *Mol. Biol.* **2001**, *35*, 730-731.
- 61) Lloyd, J. S.; De Marco, P.; Dalton, H.; Murrell, J. C. *Arch. Microbiol.* **1999**, *171*, 364-370.
- 62) Lloyd, J. S.; Finch, R.; Dalton, H.; Murrell, J. C. *Microbiology-(UK)* **1999**, *145*, 461-470.
- 63) Smith, T. J.; Slade, S. E.; Burton, N. P.; Murrell, J. C.; Dalton, H. *Appl. Environ. Microbiol.* **2002**, *68*, 5265-5273.

- 64) Murrell, J. C. *Microbiology* **2002**, *148*, 3329-3330.
- 65) Raag, R.; Martinis, S. A.; Sligar, S. G.; Poulos, T. L. *Biochemistry* **1991**, *30*, 11420-11429.
- 66) Vidakovic, M.; Sligar, S. G.; Li, H. Y.; Poulos, T. L. *Biochemistry* **1998**, *37*, 9211-9219.
- 67) Merkx, M.; Lippard, S. J. *J. Biol. Chem.* **2002**, *277*, 5858-5865.
- 68) Solomon, E. I.; Brunold, T. C.; Davis, M. I.; Kemsley, J. N.; Lee, S. K.; Lehnert, N.; Neese, F.; Skulan, A. J.; Yang, Y. S.; Zhou, J. *Chem. Rev.* **2000**, *100*, 235-349.
- 69) Rosenzweig, A. C.; Nordlund, P.; Takahara, P. M.; Frederick, C. A.; Lippard, S. J. *Chem. Biol.* **1995**, *2*, 409-418.
- 70) Elango, N.; Radhakrishnan, R.; Froland, W. A.; Wallar, B. J.; Earhart, C. A.; Lipscomb, J. D.; Ohlendorf, D. H. *Protein Sci.* **1997**, *6*, 556-568.
- 71) Koradi, R.; Billeter, M.; Wuthrich, K. *J. Mol. Graph.* **1996**, *14*, 51-55.

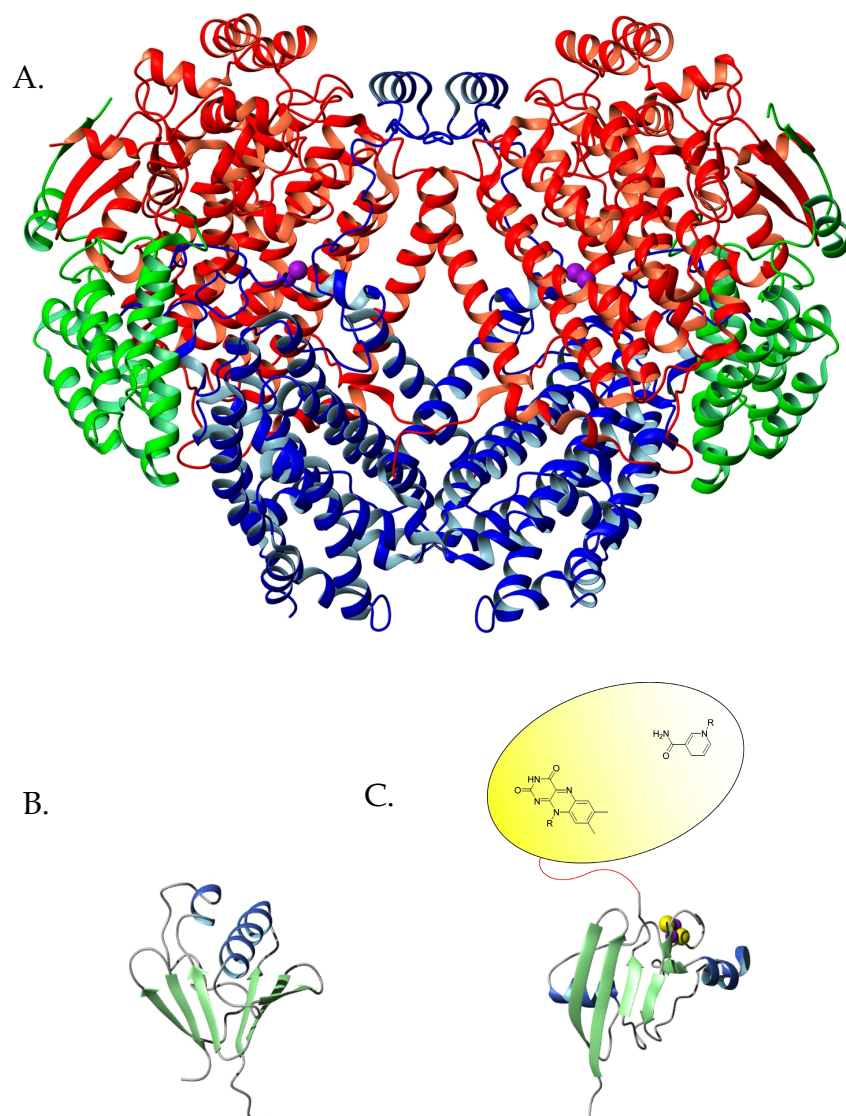
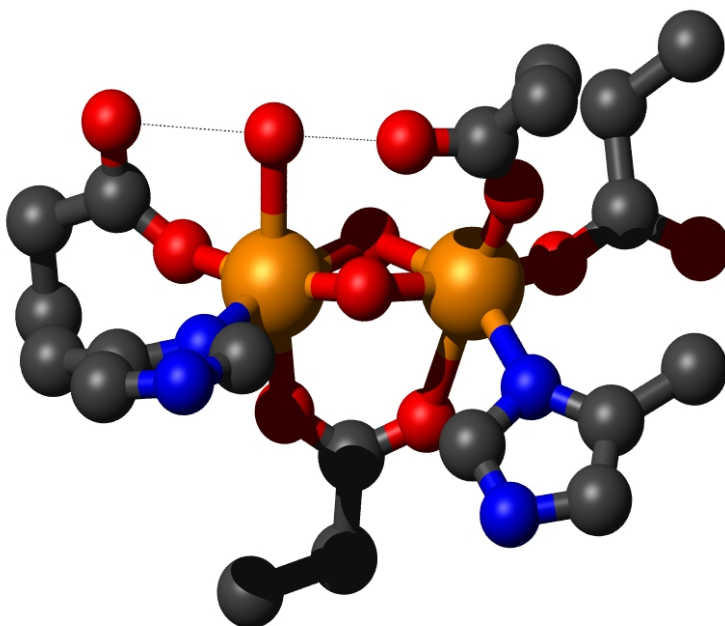


Figure 1.1. Protein components of sMMO *Mc*. (A) X-ray crystal structure of MMOH.⁶⁹ The α subunit is colored red, the β subunit blue, and the γ subunit green. Iron atoms are shown as purple spheres. (B) Solution structure of MMOB. Flexible regions of N- and C- termini are not shown.⁵³ (C) Structure of MMOR. The solution structure of the [2Fe-2S] domain of MMOR,⁵⁸ is shown with a cartoon representing the FAD and NAD(H) binding domains. The Fe and S atoms of the [2Fe-2S] cluster are shown as purple and yellow spheres, respectively. The structures of MMOH and MMOB from *Mt* have also been solved.^{54,70} Figures prepared from PDB coordinates using MOLMOL.⁷¹

A.



B.

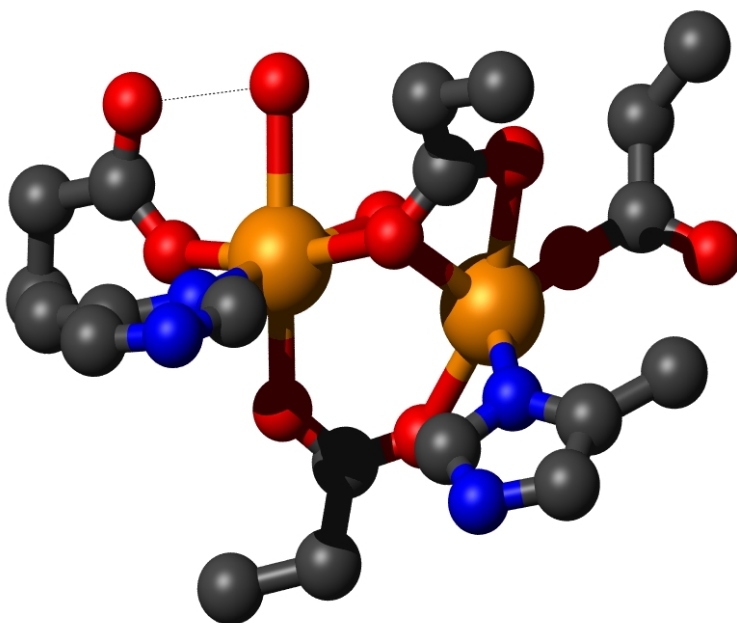


Figure 1.2. Active site structures of (A) MMOH_{ox} and (B) MMOH_{red} .⁶⁹ Colors: grey, carbon; red, oxygen; blue, nitrogen; orange, iron.

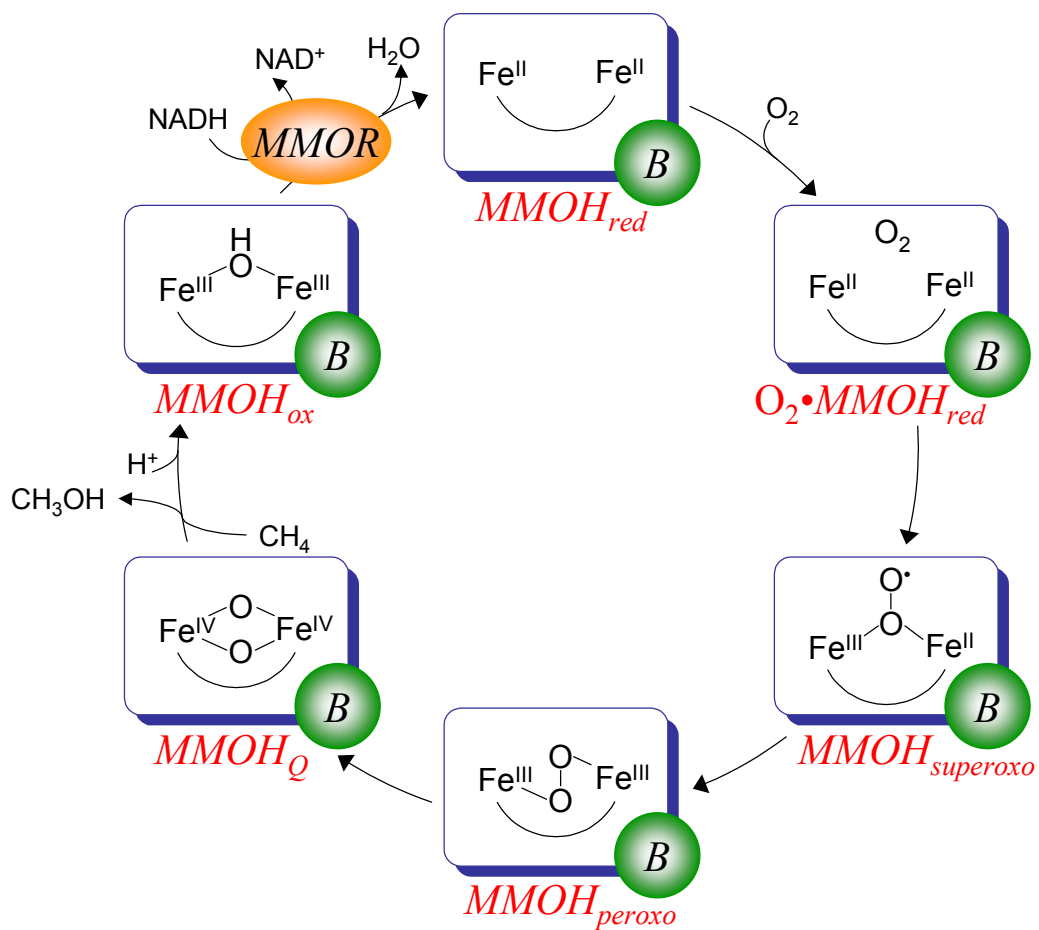


Figure 1.3. The catalytic cycle of sMMO. See text for details.

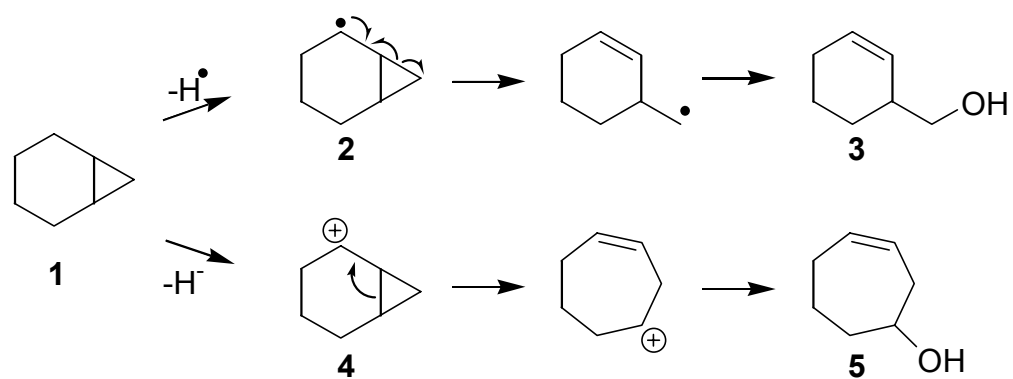


Figure 1.4. Rearrangement mechanisms of norcarane (1).

Chapter Two:**Electron Transfer Reactions of the Reductase Component of Soluble Methane
Monooxygenase from *Methylococcus capsulatus* (Bath)**

Introduction^{1,2}

Methanotrophic bacteria use methane as their sole source of carbon and energy. These organisms are of interest for their role in regulating atmospheric concentrations of methane, a potent greenhouse gas,³ and for environmental bioremediation applications.^{4,5} Chemists are intrigued by the ability of methanotrophs to oxidize methane selectively to methanol in buffered aqueous solution, using dioxygen as the oxidant at ambient pressure and temperature. Methane monooxygenase, the enzyme system that catalyzes this remarkable transformation, has been scrutinized for over two decades.⁶⁻¹⁰

Two classes of MMO have been identified, a copper-containing, membrane-bound (particulate) form referred to as pMMO¹¹ and a soluble form, sMMO, that contains non-heme iron. The sMMO from *Methylococcus capsulatus* (Bath) uses three proteins to carry out the reaction in eq. 1. MMOH is a 251 kDa



multimeric hydroxylase that houses a carboxylate-bridged diiron active site in each of its two α subunits. Reducing equivalents are delivered to the active sites of MMOH by MMOR, a 38.5 kDa protein with FAD and [2Fe-2S] cofactors. A 15.9 kDa coupling protein termed MMOB serves to couple oxidation of NADH to methane hydroxylation.^{9,10,12}

The catalytic cycle of sMMO is illustrated in Figure 2.1. A complex of the reduced, diiron(II) MMOH and MMOB reacts with dioxygen, proceeding through a series of spectroscopically characterized, transient intermediates.^{13,14}

A diiron(IV) species is believed to be responsible for the hydroxylation of methane.^{13,15} In the final stages of the reaction cycle, the diiron(III) centers of MMOH are reduced by intermolecular electron transfer from MMOR, and methanol is discharged from the active site. The methane and dioxygen activation steps of the sMMO reaction have been extensively studied, but until now the electron transfer reactions required for catalysis have received little attention.

MMOR has been grouped with other electron transfer proteins, including Fd and FNR, PDR, E₃, nitrate reductase, cytochrome *b*₅ reductase, and cytochrome P450 reductase, on the basis of function and sequence homology.^{16,17} Other bacterial mono- and dioxygenases have related systems, including alkene monooxygenase and phenol hydroxylase.¹⁸⁻²¹ These proteins all use a flavin to convert reducing equivalents between the two-electron currency of NAD(P)H and the single-electron units required by metal centers.

This chapter reports thermodynamic and kinetic investigations of the interaction of MMOR with NADH. The distribution of electrons between FAD and [2Fe-2S] cofactors in MMOR_{2e-} was also examined, as was the effect of pH on this distribution. The redox potentials of the MMOR cofactors were determined relative to one another as a function of pH. By pH jump methodology, we determined the rate constant for electron transfer between the FAD and [2Fe-2S] cofactors, providing the first direct measurement of an isolated electron transfer step in the sMMO reaction cycle. The results of these studies are described herein.

Materials and Methods

Materials and General Methods. *Taq* DNA polymerase was obtained from Gibco BRL (Gaithersburg, MD), restriction enzymes *Eco*RI and *Hind*III from New England Biolabs (Beverly, MA), plasmid pKK223-3 from Amersham Pharmacia Biotech, (Piscataway, NJ), and alkaline phosphatase from Boehringer Mannheim (Indianapolis, IN).

The FAD content of MMOR was determined by boiling a sample of the protein for 3 min, centrifuging for 5 min at 10,000*g* to pellet the denatured protein, and measuring the optical spectrum of the supernatant using $\epsilon_{450}^{\text{FAD}} = 11,300 \text{ M}^{-1} \text{ cm}^{-1}$. Iron determinations were made by the ferrozine method.^{22,23} EPR spectra were recorded with a Bruker EMX spectrometer fitted with an Oxford ESR 900 liquid helium cryostat. UV-visible spectra were obtained with an HP 8453 diode array spectrophotometer.

Expression and Purification of Recombinant MMOR. The expression plasmid pRED-K2² was transformed into *E. coli* JM105 cells. Cells were grown to saturation at 37 °C and with 200 rpm shaking in 100 mL of LB-Ap (100 µg/mL) medium. The saturated culture was diluted 100-fold into six 1 L quantities of LB-Ap (100 µg/mL). When the culture reached an OD₆₀₀ of 0.4, 1.0 mL of a freshly prepared and filter-sterilized 100 mM solution of Fe(NH₄)₂(SO₄)₂·6H₂O was added to each liter of medium. MMOR expression was induced at OD₆₀₀ of 0.6 by adding IPTG to a final concentration of 1 mM. Expression was continued for an additional 3.5 h before the cells were harvested. The cells were disrupted by

sonication, and insoluble debris was removed by centrifugation at 100,000g for 35 min. After passage through 0.2 μm membranes, the soluble fraction was applied to a DEAE-Sepharose CL6B (Amersham Pharmacia) column (2.6×15 cm) equilibrated in buffer A (20 mM Tris, pH 7.0, 8 mM sodium thioglycolate, and 50 mM NaCl). Proteins were eluted with an 800 mL gradient of buffer A to buffer B (20 mM Tris, pH 7.0, 8 mM sodium thioglycolate, and 500 mM NaCl). MMOR eluted at approximately 380 mM NaCl. Fractions containing MMOR, as determined by their optical spectra and SDS-PAGE analysis, were pooled and concentrated by ultrafiltration. Further purification was carried out by affinity chromatography on a 5'-AMP Sepharose (Sigma) column (2.6×11 cm). After applying MMOR to this column, contaminating proteins were washed off with 100 mL of buffer A. Most of this fraction (~80-90%) consisted of MMOR lacking FAD but containing an intact [2Fe-2S] cluster. Elution with buffer B containing 1 mM NADH afforded > 95% pure MMOR, as judged by SDS-PAGE, containing both FAD and [2Fe-2S] cofactors. Pure protein was exchanged into 25 mM MOPS, pH 7.0, 1 mM DTT buffer with a Biogel P6 desalting column. A typical preparation yielded 15 mg of pure MMOR per L of starting *E. coli* culture. Samples for mass spectrometry were prepared as previously reported.²⁴

Redox Potential Determination. The midpoint potentials of the $\text{FAD}_{\text{ox/sq}}$, $\text{FAD}_{\text{sq/hq}}$, and $[\text{2Fe-2S}]_{\text{ox/red}}$ couples of MMOR were determined with a series of reductive titration experiments in the presence of redox indicator dyes. Each titration included approximately 30 μM MMOR and dye in 1 mL of 50 mM potas-

sium phosphate buffer, pH 7.0, at 25 °C. The indicators were phenosafranine ($E^{\circ} = -252$ mV), anthraquinone-2-sulfonate ($E^{\circ} = -226$ mV), anthraquinone-2,6-disulfonate ($E^{\circ} = -184$ mV) and anthraquinone-1,5-disulfonate ($E^{\circ} = -174$ mV). Titrations with the high potential anthraquinone disulfonate dyes were very slow to reach equilibrium. In order to circumvent this problem, titrations with high potential dyes were performed with a small concentration (~10% relative to the anthraquinone dye) of phenosafranine.

Aliquots of 1-2 mM sodium dithionite were added by means of a gas-tight Hamilton syringe equipped with a repeating dispenser. Titrations were carried out in a sealed quartz cuvette under an anaerobic nitrogen atmosphere. UV-visible spectra were recorded after each addition, allowing 3-10 min for equilibration.

Data were processed by first correcting the spectra for dilution and then subtracting the starting (oxidized) spectrum from each spectrum of the titration. Each difference spectrum was then fit as a linear combination of component spectra (KaleidaGraph 3.0, Synergy Software, Reading, PA), as shown in eq. 2. The component spectra, represented by $\Delta\epsilon_i(\lambda)$ in eq. 2, correspond to the

$$\Delta A(\lambda) = \sum \Delta\epsilon_i(\lambda) \Delta c_i \quad (2)$$

absorption spectral differences for the reduced minus the oxidized states of each chromophore for $380 < \lambda < 800$ nm.

Initial protein and dye concentrations were determined by fitting the starting spectrum to a linear combination of oxidized protein and dye spectra to

make the analysis internally consistent and eliminate any errors due to inaccurate extinction coefficients. The chromophores considered were FAD_{ox} , FAD_{sq} , FAD_{hq} , $[2Fe-2S]_{ox}$, $[2Fe-2S]_{red}$, dye_{ox} , and dye_{red} . The dye and $[2Fe-2S]$ spectra were determined experimentally by titrating the dyes or the MMOR-Fd domain with dithionite; component spectra of the MMOR-FAD domain were determined by evolving factor analysis (Specfit, Spectrum Software Associates, Marlborough, MA) of a reductive titration.²⁵

Concentration differences were converted to ratios of reduced/oxidized chromophores according to eq. 3. The solution potential was calculated from the

$$\frac{c_{i,red}}{c_{i,ox}} = \frac{\Delta c_i}{c_{i,total} - \Delta c_i} \quad (3)$$

ratio of reduced to oxidized dye and related to the midpoint potential of one of the MMOR cofactors by the Nernst relationship, eq. 4. In principle, each

$$E = E^{\circ}_{dye} - \frac{RT}{n_{dye}F} \ln\left(\frac{[dye_{red}]}{[dye_{ox}]}\right) = E^{\circ}_i - \frac{RT}{n_iF} \ln\left(\frac{[i_{red}]}{[i_{ox}]}\right) \quad (4)$$

spectrum of a titration provides a measurement of the midpoint potential for each redox couple of MMOR. In practice, only those spectra for which the solution potential, dye midpoint potential, and estimated MMOR potential fell within 40 mV of one another were used in calculating the midpoint potentials of the cofactors.

Relative redox potentials at various pH values were determined as above, except that no indicator dyes were included. The difference spectra were fit with

component spectra that had been determined at the relevant pH.²⁵ Without indicator dye, the solution potential is unknown; thus, the redox potential of each couple was determined relative to the other redox couples of MMOR. The pK_a values determined from these data were obtained by fitting to equations following the form of eq. 6 (see below).

Stopped-Flow Experiments. A Hi-Tech model SF-61 DX2 was used for all experiments, equipped with either a photomultiplier and a tungsten lamp for single wavelength mode, or a diode array detector using a 75 W xenon arc lamp for multiwavelength illumination. The flow system was first made anaerobic by flushing with a solution of sodium dithionite; alternatively, glucose oxidase, catalase, and 1 mM glucose were employed. Anaerobic buffer was then used to rinse the flow system. MMOR was made anaerobic by 8-10 cycles of vacuum gas exchange with O₂-free N₂. NADH solutions were made anaerobic by purging with N₂ for at least 20 min. Experiments were thermostatted at 4 °C. Concentrations of MMOR were in the 10-25 μM range and NADH concentrations were ~10 times that of MMOR, except when otherwise specified. Where MMOB was included, it was loaded in the syringe with NADH. Data were fit (eq. 5) to a sum of

$$\text{Abs}_\lambda(t) = \sum A_i \exp(-k_i t) + C \quad (5)$$

three or four exponential decays, as appropriate.

Analysis of Diode Array Spectra. Diode array spectra of MMOR_{2e-}, recorded between 1 and 2 s after mixing MMOR and NADH as described above, were fit as a sum of component spectra, with the following additional con-

straints. The concentration of FAD_{sq} was equal to the concentration of $[\text{2Fe-2S}]_{\text{red}}$, and the total concentration of $[\text{2Fe-2S}]$ was equal to the total concentration of FAD. Because equilibration between molecules of MMOR is slow on the time scales used in kinetic experiments (up to 2 s), the two electrons of $\text{MMOR}_{2\text{e-}}$ can reside either both on FAD (FAD_{hq}) or one on FAD and one on the $[\text{2Fe-2S}]$ cluster. Thus, the concentrations of FAD_{sq} and $[\text{2Fe-2S}]_{\text{red}}$ must in principle always be equal in $\text{MMOR}_{2\text{e-}}$.

Procedures for Variable-pH Experiments. For experiments in which the pH was varied, MMOR was prepared in 1 mM MOPS, pH 7.0 and mixed with strongly buffered solutions at the desired pH. Buffers used were 50 mM MES for $5.27 \leq \text{pH} \leq 6.30$; 50 mM MOPS for $6.31 \leq \text{pH} \leq 7.50$; and 50 mM TAPS for $7.51 \leq \text{pH} \leq 8.50$. Constant ionic strength of 100 mM was maintained in all solutions by addition of NaCl.

To determine the $\text{p}K_a$ associated with pH-dependent effects on the reaction of MMOR with NADH, the change in absorbance at 625 nm over 1 s was recorded with the stopped-flow instrument. The data were fit to a sum of three exponentials, and the fit parameters were used to calculate A_{625} at $t = 0$ s and $t = 1$ s. The difference between these two values was computed and plotted as a function of pH. The relationship defined in eq. 6 was used to fit these data and determine

$$\Delta A = \Delta A_{\text{max}} - \frac{\Delta A_{\text{max}} - \Delta A_{\text{min}}}{1 + 10^{(\text{pH} - \text{p}K_a)}} \quad (6)$$

the pK_a , where ΔA_{\max} and ΔA_{\min} are the maximum and minimum values of ΔA_{625} , respectively.

A double-mixing pH jump experiment was carried out by first mixing 160 μM MMOR with 160 μM NADH to generate MMOR_{2e-}, followed by mixing with a buffer of different pH after a 1 s delay. To jump to a higher pH value, MMOR and NADH were prepared in 50 mM MES (pH 5.79) and mixed with 50 mM TAPS (pH 9.68). The final pH of the mixture was 8.10. To jump to a lower pH, MMOR and NADH were prepared in 50 mM TAPS (pH 8.02) and mixed with 50 mM MES (pH 4.82). The final mixture had a pH of 5.78.

Results

Characterization of Recombinant MMOR. Several experimental results establish the identity of recombinant MMOR with that isolated from the native *M. capsulatus* (Bath) bacteria. Table 2.1 compares important parameters for native and recombinant MMOR. The cofactor content of recombinant MMOR was determined to be 1.1 ± 0.1 FAD and 2.06 ± 0.05 Fe per mole protein, respectively, in agreement with literature values.²⁶ The UV-visible spectrum was the same as that of native MMOR. Substituting recombinant MMOR for native MMOR in sMMO activity assays afforded identical results. Mass spectrometric analysis gave a molecular weight within experimental error of the computed value for the apoprotein with the N-terminal methionine intact.²⁴ In addition, the EPR spectrum of fully reduced recombinant MMOR shows a rhombic signal characteristic

of a mixed valence $[2\text{Fe-2S}]^+$ cluster with g values very close to those observed for native MMOR.²⁷

Redox Potentials of MMOR. Selected difference spectra obtained from a reductive titration of MMOR in the presence of the indicators phenosafranine and anthraquinone-2,6-disulfonate are shown in Figure 2.2. For a titration with a single dye, fitting to the difference spectra required fewer independent variables (four) than for fits to the raw spectra (seven). The calculated midpoint potentials for the three redox couples are displayed in Table 2.2.

Redox potentials of MMOR were also measured in the presence of the other two sMMO components (Table 2.2). Complexes of the type MMOH/2MMOR and MMOH/2MMOR/2MMOB were examined, as was an equimolar mixture of MMOR and MMOB. The potentials of MMOR in the complexes do not change from those of free MMOR, within the error of the measurements. Although MMOH forms complexes with MMOR and MMOB, the latter two do not interact with one another.^{12,28}

Kinetic Behavior of MMOR Reduction by NADH. The reaction of oxidized MMOR with NADH was investigated by stopped-flow optical spectroscopy. Preliminary studies of this reaction were reported previously,^{12,29,30} and spectra of intermediates in the reaction were derived from fits to the diode array kinetic traces.¹² Figure 2.3A shows the time-dependent changes in absorbance at three wavelengths, 458, 625, and 740 nm. Fits to these changes are superimposed on the data, reflecting the steps outlined in Figure 2.4. The reduction chemistry

begins with NADH binding to MMOR to produce a species with a charge-transfer interaction between the nicotinamide ring of NADH and the flavin isoalloxazine. The charge-transfer intermediate, termed CT1, has a visible band centered at about 575 nm (Figure 2.3B). Transfer of hydride produces NAD⁺ and the reduced flavin (FAD_{hq}). The resulting species, CT2, has a more intense charge-transfer band that is red-shifted ($\lambda_{\text{max}} \sim 740$ nm) relative to that of CT1 (Figure 2.3B). Formation of CT2 is apparent in Figure 2.3A as an increase in A_{740} at $t < 8$ ms. Release of NAD⁺ is observed by the disappearance of the CT2 band, which occurs simultaneously with electron transfer from FAD_{hq} to [2Fe-2S]_{ox}. The NAD⁺ release phase appears in Figure 2.3A as a decrease in A_{740} for $t > 10$ ms, due to loss of the charge-transfer interaction between NAD⁺ and FAD_{hq}, and the continuing increase in A_{625} arising from the increasing concentration of FAD_{sq}. The final species, SQ, has a spectrum characteristic of FAD_{sq} and [2Fe-2S]_{red} (Figure 2.3B).

The reduction kinetics of MMOR were also measured in the presence of MMOB. Addition of 1 to 5 equivalents of MMOB to the reaction of MMOR with NADH had no effect on the reaction rates or spectra of the intermediates.

Complexes of MMOR with NAD(H). The binding that was observed upon mixing MMOR with NADH was originally modeled as a single step with an observed rate constant.¹² Investigation of the NADH concentration dependence of this reaction, however, reveals that binding occurs in more than one step. Specifically, the rate constant for the formation of the first observed intermediate,

CT1, can be saturated (Figure 2.3C). This result implies the existence of a spectroscopically silent species that forms prior to CT1. This species is termed MC1 for Michaelis complex 1 (Figure 2.4). A fit to the data reveals a K_d value of 3.8 μM for NADH binding to oxidized MMOR.

In order to investigate the binding of NAD^+ to oxidized MMOR, the kinetics of the reaction of MMOR with NADH were studied in the presence of varying concentrations of NAD^+ and at three different wavelengths (Figure 2.5). As expected, the reaction is inhibited by NAD^+ . The data were modeled according to Figure 2.2 with HopKINSIM.^{31,32} The K_d value for NAD^+ binding to MMOR_{ox} was estimated to be $\sim 5 \mu\text{M}$. In addition, the K_d value for NAD^+ binding to two-electron reduced MMOR was estimated from the absorbance changes at 725 nm at 1 s after mixing (Figure 2.5C) to be $70 \pm 24 \mu\text{M}$. Increased absorbance at 725 nm at 1 s is due to the formation of a CT2-type charge-transfer complex between MMOR_{2e^-} and excess NAD^+ .

Effect of pH on the Reaction of MMOR and NADH. This reaction was also examined in buffers at twelve different pH values in the range 5.3 to 8.3. Below pH 5.0, MMOR precipitates from solution; thus, the pH was kept above this value to ensure that no protein precipitated in the stopped-flow spectrometer. Figure 2.6A shows that, at high pH, the final value of A_{625} is significantly larger than at low pH. It is also evident that the maximum value of A_{725} is reduced at low pH values. The rates of the processes described in Figure 2.4 are unchanged.

The net change in absorbance at 625 nm between 0 and 1 s as a function of pH reflects a process having a pK_a of 6.2 ± 0.1 (Figure 2.6B).

Figures 2.7A and 2.7B display the effect of pH on the reaction of MMOR with NADH as monitored spectrophotometrically from 400 to 700 nm. Differences in the initial spectra recorded after mixing reveal pH effects on the absorbance of MMOR_{ox} , which arise mainly from changes in the spectrum of FAD.²⁵ Comparison of spectra recorded at 1.5 s after mixing at pH 5.27 and 8.01 illustrates the different distribution of the two electrons among the FAD and [2Fe-2S] cofactors (Figure 2.7C). To quantify this electron distribution, the spectra were fit as a sum of the component spectra, and the results of the fit are shown in Table 2.3. The component spectra used in the fitting were determined at the appropriate pH. Of the five redox states accessible to the two cofactors ($\text{FAD}_{\text{ox, sq, hq}}$ and $[\text{2Fe-2S}]_{\text{ox, red}}$), only the spectra of FAD_{ox} and FAD_{hq} undergo significant pH-dependent changes (Figure 2.8).

Effect of pH on Relative Redox Potentials. The observed effect of pH on electron distribution in the kinetically generated $\text{MMOR}_{2\text{e-}}$ led us to investigate the effect of pH on the thermodynamic redox potentials of MMOR. Reductive titrations of MMOR_{ox} were performed at varying pH values, and difference spectra were fit as sums of component difference spectra recorded at the appropriate pH. Since no redox indicator dye was included, the solution potential was unknown, and the redox potential of a particular couple was determined relative to the other redox couples of MMOR. These results are presented in Figure 2.9. The

difference between the potentials of the [2Fe-2S] cluster and the FAD_{sq/hq} couple ($E_{\text{FeS}} - E_{\text{FAD2}}$) varies from 2.8 ± 6.3 mV at pH 5.62 to 83.9 ± 11.7 mV at pH 8.01. Fitting the data to eq. 6 reveals a pK_a of 6.3 ± 0.2 . The value of $E_{\text{FeS}} - E_{\text{FAD1}}$ changes from -45.6 ± 3.5 mV to 31.1 ± 3.7 mV over the same pH range, and the corresponding pK_a value is 7.3 ± 0.1 mV. The pH-dependent difference between the two FAD couples, $E_{\text{FAD2}} - E_{\text{FAD1}}$, has an inverted bell-shaped profile with a minimum value of -93.5 ± 3.9 mV at pH 7.00, and approaches a value of ~ -50 mV at the extremes of the pH range examined. The two pK_a values derived from fits of the data are 6.6 ± 0.5 and 7.6 ± 0.9 for the low and high pH ranges, respectively (Figure 2.9).

Measurement of Electron Transfer by pH Jump. The pH dependence of the electron distribution among cofactors in MMOR makes possible the measurement of electron transfer rates in the absence of other complicating factors, such as the presence of excess quantities of NAD(H). By preparing MMOR_{2e-} at one pH value, it is possible to follow the redistribution of electrons following a rapid change in solution pH. Such an experiment was carried out by using the double-mixing stopped-flow method. In the first mixing event, MMOR was mixed with an equimolar amount of NADH. Following a 1-s delay, a second mixing event changed the pH. The absorbance at 625 nm was followed as a function of time after the pH change, as shown in Figure 2.10. The traces were readily fit to a single exponential function and the computed rate constants were 126 ± 22 s⁻¹ for jumping to a higher pH and 134 ± 5 s⁻¹ for jumping to a lower pH. The

rate constant determined using data for both the forward and reverse reactions is $130 \pm 17 \text{ s}^{-1}$. In both directions, the electron transfer between FAD and [2Fe-2S] occurred with a greater rate constant than observed upon mixing MMOR with NADH ($k_3 = 90 \text{ s}^{-1}$, Figure 2.2), where electron transfer is accompanied by release of NAD^+ .

Discussion

Recombinant MMOR. The first high-yield recombinant system for expression of MMOR has been achieved. Good yields of pure protein with a full complement of cofactors can be obtained in a few days. A previous account detailing the expression of *M. capsulatus* (Bath) MMOR in *E. coli* demonstrated the reconstitution of MMOR activity in *E. coli* cell extracts, but the yield was no greater than that from the native organism, and no purification of the MMOR protein was reported.³³ Development of a high-yielding recombinant system has made feasible the kinetic and thermodynamic studies in the present work. The amount of MMOR in *Methylosinus trichosporium* OB3b cells is ~10% of the amount of MMOH,³⁴ and only small quantities of MMOR (~ 5-10 mg) can be purified from 100 g of *M. capsulatus* (Bath) cell paste in a routine preparation. With the recombinant system, we can easily obtain the 100 mg quantities required for extensive kinetic and thermodynamic characterization.

In addition, the purification of MMOR from the present recombinant system is more convenient than from the native organism. The protocol has fewer

steps, and *E. coli* are simpler to grow than *M. capsulatus* (Bath), because the latter requires methane for growth and, even under optimal conditions, grows slowly by comparison with *E. coli*. The recombinant system also makes possible mutagenesis studies.

Redox Potentials of MMOR Cofactors. The reduction potentials of the MMOR cofactors determined here are more accurate than those reported previously.²⁷ The $\text{FAD}_{\text{ox/sq}}$ potential we measured is 26 mV more negative than the published value,²⁷ although the two are within experimental error of one another, given the larger error in the latter. The method used here has the advantage of treating data from many wavelengths simultaneously and generates multiple measurements of the redox potential per experiment. In addition, fitting of difference spectra allows the use of fewer parameters than would otherwise be necessary. Having fewer parameters improves the chance of finding a unique solution for the fit. Our study has also measured the potentials in the presence of several redox dyes, covering a range of 78 mV, thereby decreasing the possibility that systematic errors are introduced by a non-ideal dye-protein combination.

Addition of MMOB does not affect these potentials within experimental error, consistent with other observations indicating that no complex is formed between MMOB and MMOR.¹² The midpoint potentials for the MMOR cofactors are also unaltered in complexes with MMOH and MMOH/2MMOB. Previous studies have revealed that, for the sMMO of *Methylosinus trichosporium* (OB3b), binding of MMOR to MMOH alters the potentials of the non-heme diiron active

site of MMOH.^{35,36} We show here for the first time that the reverse is not true; the potentials of MMOR are unchanged in the MMOH/MMOR complex.

Electron Transfer Properties. Electron transfer reactions involving NAD(P)H, flavin, and [2Fe-2S] cofactors have been studied in detail for other enzymes. Phthalate dioxygenase reductase³⁷ and E₃³⁸ in particular have been well characterized. MMOR, PDR, and E₃ share similar mechanisms in their reactions with NADH. Each binds NADH, proceeds through two charge-transfer intermediates, and finally passes one electron to a [2Fe-2S] center. The existence of an MC1-type pre-complex has been established for PDR but not for E₃.^{37,38}

Based on the stopped-flow optical experiments, we propose the following model for the reduction of MMOR by NADH (Figure 2.2). The initial step is rapid binding of NADH to MMOR to produce a Michaelis complex, MC1. The K_d value for this interaction is calculated to be 3.8 μM (Figure 2.4). Formation of MC1 does not alter the spectrum of MMOR; its existence is inferred from the kinetic behavior of the enzyme. In an earlier kinetic study of the interaction of NADH with MMOR,²⁹ a precomplex of this sort was proposed on the basis of a linear double-reciprocal plot. A subsequent investigation³⁰ reported that such a complex did not exist; rather, MMOR and NADH reacted with a second order rate constant of $2.9 \times 10^6 \text{ M}^{-1} \text{ s}^{-1}$. These studies were carried out at 18 °C; at this temperature, the early phases of the reaction (including CT1 formation) occur largely or completely during the dead time of the instrument, making their true rate constants difficult to determine. At 4 °C, the temperature used in this study,

we find the value of CT1 formation to be 350 s^{-1} with saturating NADH. With the 2 ms dead time of our instrument approximately 50% of the optical change will be observed, enough to make an accurate determination of the rate constant. For these reasons, we stand by our proposed mechanism for MMOR reduction (Figure 2.4) involving a pre-complex of NADH with MMOR prior to the first observed intermediate.

Next, a conformational change is presumed to occur, with an observed rate constant of 350 s^{-1} , that gives rise to the charge-transfer interaction of CT1. Transfer of hydride from NADH to FAD ensues with a rate constant of 190 s^{-1} , yielding the CT2 species. CT2 has a more intense, lower energy charge-transfer band than CT1. The breakdown of CT2 occurs with a rate constant of 90 s^{-1} . Since this process is slower than the rate at which it is formed, CT2 builds up to appreciable concentrations under the conditions examined.

Electron transfer and release of NAD^+ are observed to occur simultaneously, affording the SQ species with reduced $[\text{2Fe-2S}]$ and FAD_{sq} . A more complete description of the SQ state is that of an equilibrium between $\text{FAD}_{\text{sq}}/[\text{2Fe-2S}]_{\text{red}}$ and $\text{FAD}_{\text{hq}}/[\text{2Fe-2S}]_{\text{ox}}$. The spectrum of SQ shows maxima at approximately 600 and 650 nm, consistent with a neutral flavin semiquinone. This information alone does not distinguish between the possibilities that (i) the electron transfer and NAD^+ release steps are independent and coincidentally occur at similar rates, (ii) the two steps are truly coupled, or (iii) that one event

triggers the rapid execution of the other. Similar behavior was also observed for PDR and E₃.^{37,38}

Influence of pH on Redox Properties of MMOR. Figure 2.6A shows the effect of pH on the reaction of MMOR with NADH. From single wavelength stopped-flow data, it can be concluded that the kinetics of MMOR reduction by NADH are not altered as a function of pH (Figure 2.6A). Thus, the reduced A₇₂₅ values at low pH measured ~ 10 ms after mixing (Figure 2.6A) are due to a lower value of ϵ_{725} for CT2, not decreased concentrations of CT2. Although the kinetics of the reaction do not change with pH, the distribution of electrons between FAD and [2Fe-2S] in MMOR_{2e-} is affected by changes in pH. The pK_a for the process affecting the final value of A₆₂₅ is 6.2 ± 0.1 (Figure 2.6B).

From the data collected with the diode array, it is apparent that the spectrum of MMOR_{ox} is altered by pH (initial spectra, Figures 2.7A and 2.7B). In Figure 2.7C, the changes in electron distribution are demonstrated in the final spectra. The pH effect on electron distribution is quantified in Table 2.3. At pH 5.27, nearly all of the MMOR is in the FAD_{hq}/[2Fe-2S]_{ox} state. At pH 8.01, there is a mixture of FAD_{hq}/[2Fe-2S]_{ox} and FAD_{sq}/[2Fe-2S]_{red}. This observation suggests that the difference between the [2Fe-2S]_{ox/red} and FAD_{sq/hq} couples ($E_{\text{FeS}} - E_{\text{FAD2}}$) within a given molecule is diminished at low pH. This pH-dependent change in potential need not be reflected in the true thermodynamic potentials for the protein co-factors, since interprotein electron transfer reactions cannot occur to establish equilibrium on this time scale (vide infra). Only this ΔE needs to be con-

sidered for the stopped-flow reaction, because the FAD_{ox} redox state is also inaccessible on the time scale studied.

Equilibrium titrations of MMOR at varying pH reveal that the true $E_{\text{FeS}} - E_{\text{FAD2}}$ difference is also diminished at low pH (Figure 2.9). At pH 8.0 the value of $E_{\text{FeS}} - E_{\text{FAD2}}$ is 83.9 mV, meaning that electron transfer from FAD_{hq} to $[\text{2Fe-2S}]_{\text{ox}}$ is favorable. At pH 5.6 this value is only 2.8 mV and there is little driving force for the same electron transfer. The $\text{p}K_a$ values for $E_{\text{FAD2}} - E_{\text{FAD1}}$ (6.6 ± 0.5 and 7.6 ± 0.9) coincide with those found for $E_{\text{FeS}} - E_{\text{FAD2}}$ (6.3 ± 0.2) and $E_{\text{FeS}} - E_{\text{FAD1}}$ (7.3 ± 0.1), respectively. The agreement of these values is consistent with the titratable group(s) being associated with the flavin moiety. In addition, the $\text{p}K_a$ calculated for changes in $E_{\text{FeS}} - E_{\text{FAD2}}$ compares well with the $\text{p}K_a$ of 6.2 ± 0.1 determined in stopped-flow studies.

An artificial value for $E_{\text{FeS}} - E_{\text{FAD2}}$ under the conditions employed in the stopped-flow experiment can be calculated from the species distribution by using the Nernst equation (Table 2.3). Doing so reveals that $E_{\text{FeS}} - E_{\text{FAD2}}$ increases with increasing pH, consistent with the thermodynamic experiment (Fig. 7). In fact, the $\text{p}K_a$ measured in both the titration and stopped-flow experiments is identical within error (~ 6.3). It is not surprising, however, that the $E_{\text{FeS}} - E_{\text{FAD2}}$ values determined in titration experiments, 2.8 and 83.9 mV at low and high pH, respectively, are significantly different from those calculated from the stopped-flow data. At least three differences between the kinetic and thermodynamic experiments may contribute to this discrepancy. The major reason is that the titration

experiments measure true equilibrium differences in potential; several minutes were allowed to elapse between the addition of reducing agent and the recording of a spectrum to assure that equilibrium was attained. Spectra from the diode-array during the stopped-flow experiment were recorded 1.5 s after mixing MMOR_{ox} and NADH. On this time scale, disproportionation between molecules of $\text{MMOR}_{2\text{e}^-}$ is slow, and the reaction does not reach thermodynamic equilibrium. Moreover, the stopped-flow experiments were conducted at 4 °C, whereas the titrations were performed at 25 °C. In addition, MMOR_{ox} was allowed to react in the stopped-flow experiment with 10 equiv of NADH to ensure pseudo-first-order behavior. As a consequence, the derived ΔE values are measured for a mixture of species in which NAD(H) is bound to the protein. The titrations were performed in the absence of any such pyridine nucleotide.

The increase of $E_{\text{FeS}} - E_{\text{FAD2}}$ with increasing pH must arise from an increase in E_{FAD2} , a decrease in E_{FeS} , or a combination of both effects. The evidence suggests that the majority of the effect arises from an increase in E_{FAD2} . There is no pH effect on the optical spectrum of the [2Fe-2S] cluster in either redox state, whereas the spectra of FAD_{ox} and FAD_{hq} are pH-dependent (Figure 2.8).²⁵ In addition, the pH dependence of $E_{\text{FAD2}} - E_{\text{FAD1}}$ shows two $\text{p}K_a$ values (6.6 ± 0.5 and 7.6 ± 0.9), each of which is very close to a $\text{p}K_a$ determined for one of the other ΔE values (Figure 2.9). It appears that there is one $\text{p}K_a$ associated with E_{FAD2} , measured as 6.6 ± 0.5 and again as 6.3 ± 0.2 ; and a second $\text{p}K_a$ associated with E_{FAD1} , measured as 7.6 ± 0.9 and a second time as 7.3 ± 0.1 . By this reasoning, there is a

pK_a of ~ 7.3 affecting the value of E_{FAD1} , and pK_a of ~ 6.3 for E_{FAD2} , which is consistent with the value of 6.2 determined in the stopped-flow experiment. Furthermore, it appears that there is no macroscopic pK_a associated with E_{FeS} . After correcting for the pH effect on proton-coupled redox reactions, an additional protein-centered pK_a of 6.5 ± 0.2 is revealed.²⁵

Presumably, protonation of some group(s) on, or hydrogen bonded to, the FAD isoalloxazine ring increases the $\text{FAD}_{\text{sq/hq}}$ reduction potential relative to that of the [2Fe-2S] cluster. Specifically, we propose that the N1 position of the flavin is a likely site of protonation (Figure 2.11). In the hydroquinone state, N1 is typically deprotonated at pH 7 and bears substantial negative charge, as judged by ^{15}N and ^{13}C NMR spectral studies for all flavoproteins that have been investigated.³⁹ One-electron transfer from FAD_{hq} (FADH^\cdot) to $[\text{2Fe-2S}]_{\text{ox}}$ removes this negative charge from the flavin, affording the neutral semiquinone. Protonation of N1 affords a neutral FAD_{hq} (FADH_2), thereby rendering electron transfer to [2Fe-2S] less favorable. Mutagenesis studies of flavodoxins also reveal that removing acidic residues in the vicinity of N1 increases the semiquinone/hydroquinone reduction potential.⁴⁰⁻⁴² Protonation of the N1 site is also consistent with the observation of lower ϵ_{725} for CT2 at low pH. The charge-transfer interaction between the pyridine moiety of NAD^+ and FADH_2 will be much weaker than between NAD^+ and FADH^\cdot . The measured pK_a of 6.2 for FAD_{hq} is within the range of values measured for the N1 position of other flavoproteins.⁴³ More extensive studies could further our understanding of the mo-

lecular basis of the pH effects described above. Without more information, however, we cannot completely rule out the possibility that pH effects occur at both FAD and [2Fe-2S] cofactors.

Intramolecular Electron Transfer. Electron transfer between FAD and [2Fe-2S], as measured by the pH jump method, occurs with a rate constant of $130 \pm 17 \text{ s}^{-1}$. This value probably does not reflect the true rate of electron transfer. Calculations indicate that electron transfer between redox centers located 14 \AA or less apart typically occurs at rates in the 10^7 - 10^{13} s^{-1} range.⁴⁴ The X-ray structure of PDR reveals the 8-CH₃ group of the flavin and Fe1 of the [2Fe-2S] cluster to be separated by 7.2 \AA .¹⁷ This distance is well within the 14 \AA range predicted to allow very rapid electron transfer, independent of other factors such as pathway or the packing density of the intervening protein. MMOR is expected to have a similar structure, and although the flavin-to-[2Fe-2S] distance may be greater in MMOR than in PDR, it is likely to be less than 14 \AA . We therefore conclude that the relatively slow rate constant for electron transfer in MMOR reflects a rate-limiting, preceding step such as a conformational change of the protein, perhaps one that is coupled with proton transfer. The link between the FAD and [2Fe-2S] domains of MMOR may be sufficiently flexible to allow these two cofactors to be positioned such that rapid tunneling cannot occur in all conformations.

The greater electron transfer rate constant measured in the pH jump, compared to the constant pH (90 s^{-1} , k_3 in Figure 2.2), experiments suggests that NAD⁺ release is rate-limiting in the latter case. In the pH jump experiment, a mi-

nority fraction of MMOR_{2e-} has bound NAD⁺, owing to the weak binding constant ($K_d \sim 70 \mu\text{M}$) and the use of equimolar concentrations of MMOR_{2e-} and NAD⁺.

Conclusion

The studies of intramolecular electron transfer in the sMMO system described here, coupled with forthcoming structural information about the [2Fe-2S] domain of MMOR,^{25,45} will provide a detailed understanding of intermolecular electron transfer in the sMMO system.¹² Electron transfer steps in the overall catalytic cycle of sMMO have been the subject of little work until now. With the availability of large quantities of recombinant MMOR, this previously neglected aspect of the sMMO system can now be investigated. For not only is the hydroxylation of the C-H bond in methane a remarkable feat of chemistry, but the carefully orchestrated intra- and interprotein electron transfer steps are as well. Knowledge of these processes will not only enrich our understanding of the sMMO system, but will also contribute to the general field of electron transfer in biology.

References

- 1) This work has been published in slightly different form. See reference 2.
- 2) Kopp, D. A.; Gassner, G. T.; Blazyk, J. L.; Lippard, S. J. *Biochemistry* **2001**, *40*, 14932-14941.
- 3) Mancinelli, R. L. *Annu. Rev. Microbiol.* **1995**, *49*, 581-605.
- 4) Tsien, H. C.; Brusseau, G. A.; Hanson, R. S.; Wackett, L. P. *Appl. Environ. Microbiol.* **1989**, *55*, 3155-3161.
- 5) Brockman, F. J.; Payne, W.; Workman, D. J.; Soong, A.; Manley, S.; Hazen, T. C. *J. Hazard. Mater.* **1995**, *41*, 287-298.
- 6) Colby, J.; Dalton, H. *Biochem. J.* **1978**, *171*, 461-468.
- 7) Feig, A. L.; Lippard, S. J. *Chem. Rev.* **1994**, *94*, 759-805.
- 8) Wallar, B. J.; Lipscomb, J. D. *Chem. Rev.* **1996**, *96*, 2625-2657.
- 9) Valentine, A. M.; Lippard, S. J. *J. Chem. Soc. Dalton* **1997**, 3925-3931.
- 10) Merkx, M.; Kopp, D. A.; Sazinsky, M. H.; Blazyk, J. L.; Muller, J.; Lippard, S. J. *Angew. Chem. Int. Edit.* **2001**, *40*, 2782-2807.
- 11) Nguyen, H. H. T.; Elliott, S. J.; Yip, J. H. K.; Chan, S. I. *J. Biol. Chem.* **1998**, *273*, 7957-7966.
- 12) Gassner, G. T.; Lippard, S. J. *Biochemistry* **1999**, *38*, 12768-12785.
- 13) Liu, K. E.; Valentine, A. M.; Wang, D. L.; Huynh, B. H.; Edmondson, D. E.; Salifoglou, A.; Lippard, S. J. *J. Am. Chem. Soc.* **1995**, *117*, 10174-10185.
- 14) Valentine, A. M.; Stahl, S. S.; Lippard, S. J. *J. Am. Chem. Soc.* **1999**, *121*, 3876-3887.

- 15) Shu, L. J.; Nesheim, J. C.; Kauffmann, K.; Munck, E.; Lipscomb, J. D.; Que, L. *Science* **1997**, *275*, 515-518.
- 16) Miller, V. P.; Thorson, J. S.; Ploux, O.; Lo, S. F.; Liu, H. W. *Biochemistry* **1993**, *32*, 11934-11942.
- 17) Correll, C. C.; Batie, C. J.; Ballou, D. P.; Ludwig, M. L. *Science* **1992**, *258*, 1604-1610.
- 18) Zhou, N. Y.; Jenkins, A.; Chion, C.; Leak, D. J. *FEBS Lett.* **1998**, *430*, 181-185.
- 19) Nordlund, I.; Powlowski, J.; Shingler, V. *J. Bacteriol.* **1990**, *172*, 6826-6833.
- 20) Mason, J. R.; Cammack, R. *Annu. Rev. Microbiol.* **1992**, *46*, 277-305.
- 21) Butler, C. S.; Mason, J. R. *Advances in Microbial Physiology*, 1997; Vol. 38, pp 47-84.
- 22) Massey, V. *J. Biol. Chem.* **1957**, *229*, 763-70.
- 23) Stookey, L. L. *Anal. Chem.* **1970**, *42*, 779-81.
- 24) Coufal, D. E.; Blazyk, J. L.; Whittington, D. A.; Wu, W. W.; Rosenzweig, A. C.; Lippard, S. J. *Eur. J. Biochem.* **2000**, *267*, 2174-2185.
- 25) Blazyk, J. L.; Lippard, S. J. *Biochemistry* **2002**, in press.
- 26) Colby, J.; Dalton, H. *Biochem. J.* **1979**, *177*, 903-908.
- 27) Lund, J.; Dalton, H. *Eur. J. Biochem.* **1985**, *147*, 291-296.
- 28) Walters, K. J.; Gassner, G. T.; Lippard, S. J.; Wagner, G. *Proc. Natl. Acad. Sci. U. S. A.* **1999**, *96*, 7877-7882.
- 29) Lund, J.; Woodland, M. P.; Dalton, H. *Eur. J. Biochem.* **1985**, *147*, 297-305.

- 30) Green, J.; Dalton, H. *Biochem. J.* **1989**, *259*, 167-172.
- 31) Barshop, B. A.; Wrenn, R. F.; Frieden, C. *Anal. Biochem.* **1983**, *130*, 134-145.
- 32) Wachsstock, D. H.; Pollard, T. D. *Biophys. J.* **1994**, *67*, 1260-1273.
- 33) West, C. A.; Salmond, G. P. C.; Dalton, H.; Murrell, J. C. *J. Gen. Microbiol.* **1992**, *138*, 1301-1307.
- 34) Fox, B. G.; Froland, W. A.; Dege, J. E.; Lipscomb, J. D. *J. Biol. Chem.* **1989**, *264*, 10023-10033.
- 35) Paulsen, K. E.; Liu, Y.; Fox, B. G.; Lipscomb, J. D.; Munck, E.; Stankovich, M. T. *Biochemistry* **1994**, *33*, 713-722.
- 36) Liu, Y.; Nesheim, J. C.; Paulsen, K. E.; Stankovich, M. T.; Lipscomb, J. D. *Biochemistry* **1997**, *36*, 5223-5233.
- 37) Gassner, G.; Wang, L. H.; Batie, C.; Ballou, D. P. *Biochemistry* **1994**, *33*, 12184-12193.
- 38) Gassner, G. T.; Johnson, D. A.; Liu, H. W.; Ballou, D. P. *Biochemistry* **1996**, *35*, 7752-7761.
- 39) Müller, F. ; Müller, F., Ed.; CRC Press: Boca Raton, FL, 1992, pp 557-595.
- 40) Geoghegan, S. M.; Mayhew, S. G.; Yalloway, G. N.; Butler, G. *Eur. J. Biochem.* **2000**, *267*, 4434-4444.
- 41) Hoover, D. M.; Drennan, C. L.; Metzger, A. L.; Osborne, C.; Weber, C. H.; Pattridge, K. A.; Ludwig, M. L. *J. Mol. Biol.* **1999**, *294*, 725-743.
- 42) Zhou, Z. M.; Swenson, R. P. *Biochemistry* **1996**, *35*, 15980-15988.
- 43) Franken, H. D.; Ruterjans, H.; Muller, F. *Eur. J. Biochem.* **1984**, *138*, 481-489.

- 44) Page, C. C.; Moser, C. C.; Chen, X. X.; Dutton, P. L. *Nature* **1999**, *402*, 47-52.
- 45) Müller, J.; Lugovskoy, A. A.; Wagner, G.; Lippard, S. J. *Biochemistry* **2002**, *41*, 42-51.

Table 2.1. Properties of Native and Recombinant MMOR

	native MMOR	recombinant MMOR
MW measured ^a (Da)	38,545.6 ^b ± 3.9	38,546.9 ± 3.9
Fe content (mol/mol protein)	1.92 ^c	2.06 ± 0.05
FAD content (mol/mol protein)	1.00 ^c	1.1 ± 0.1
λ_{\max} (nm), pH 7.0, 25 °C	334, 394, 458	334, 394, 458
<i>g</i> values (fully reduced)	2.047, 1.960, 1.864 ^c	2.047, 1.958, 1.871 ^d

^aExpected 38,542.6 Da for apoprotein with N-terminal methionine intact. ^bAs reported.²⁴ ^cAs reported.²⁶ ^dEPR recorded at 10 K, 50 μ W, modulation amplitude 25.7 G.

Table 2.2. Midpoint Potentials at 25 °C and pH 7.0 of MMOR Alone and in Complexes with Other sMMO Proteins.

	FAD _{ox/sq} (mV)	[2Fe-2S] _{ox/red} (mV)	FAD _{sq/hq} (mV)
MMOR native ^a	-150 ± 20	-220 ± 20	-260 ± 5
MMOR recombinant	-176 ± 7	-209 ± 14	-266 ± 15
MMOR + MMOB	-178 ± 1	-200 ± 6	-255 ± 4
MMOH/2MMOR	-167 ± 14	-207 ± 5	-260 ± 9
MMOH/2MMOB/2MMOR	-160 ± 2	-208 ± 6	-258 ± 8

^a As reported.²⁷

Table 2.3. pH-Dependent Distribution of Electrons in MMOR_{2e-}

Species	% of total cofactor	
	pH 5.27	pH 8.01
[2Fe-2S] _{ox}	99.5	67.4
[2Fe-2S] _{red}	0.5	32.6
FAD _{ox}	0.3	0.3
FAD _{sq}	0.5	32.6
FAD _{hq}	99.2	67.1
$E_{\text{FeS}} - E_{\text{FAD}2}^a$	-244 mV	-35 mV

^aArtificial difference in redox potential between the [2Fe-2S] and FAD cofactors computed from the species distribution given in this table by application of the Nernst equation.

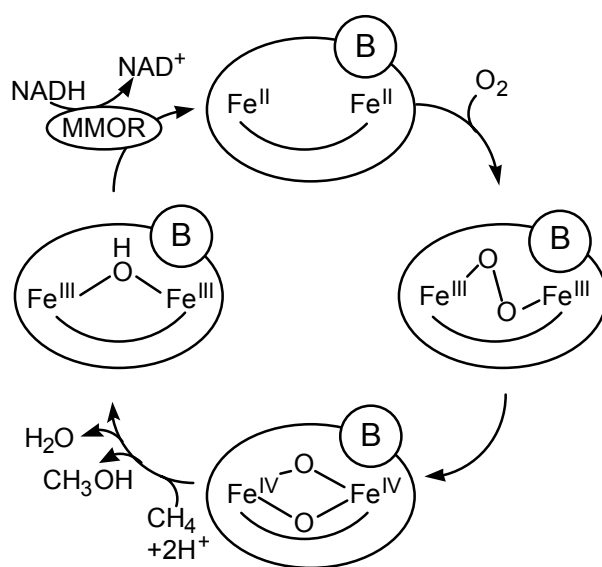


Figure 2.1. Simplified view of the sMMO catalytic cycle.

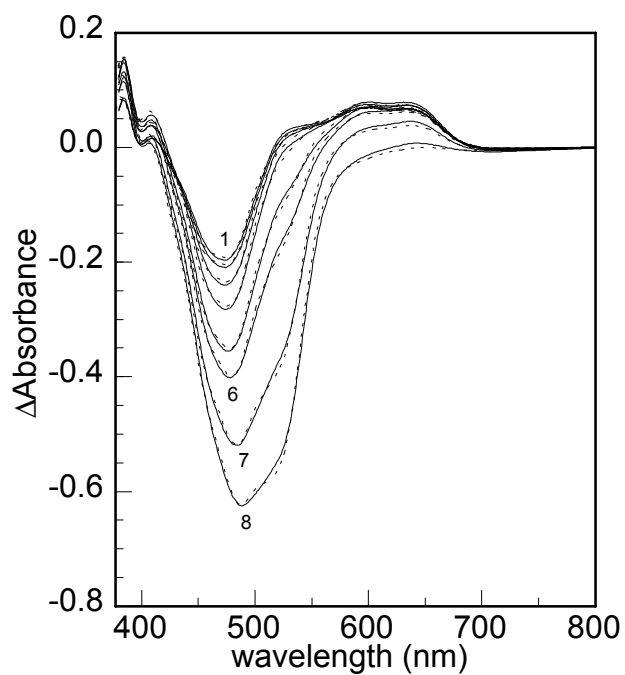


Figure 2.2. Difference spectra for the reductive titration of a 1 mL mixture of 29 μ M MMOR, 3.8 μ M phenosafranin, and 39 μ M anthraquinone-2,6-disulfonate by dithionite. Spectra 1-8 correspond to the addition of 110, 130, 150, 170, 190, 210, 220, and 240 μ L, respectively, of a solution of \sim 1 mM sodium dithionite. Fits (dashed lines) are superimposed on the data over the wavelength range 380-800 nm.

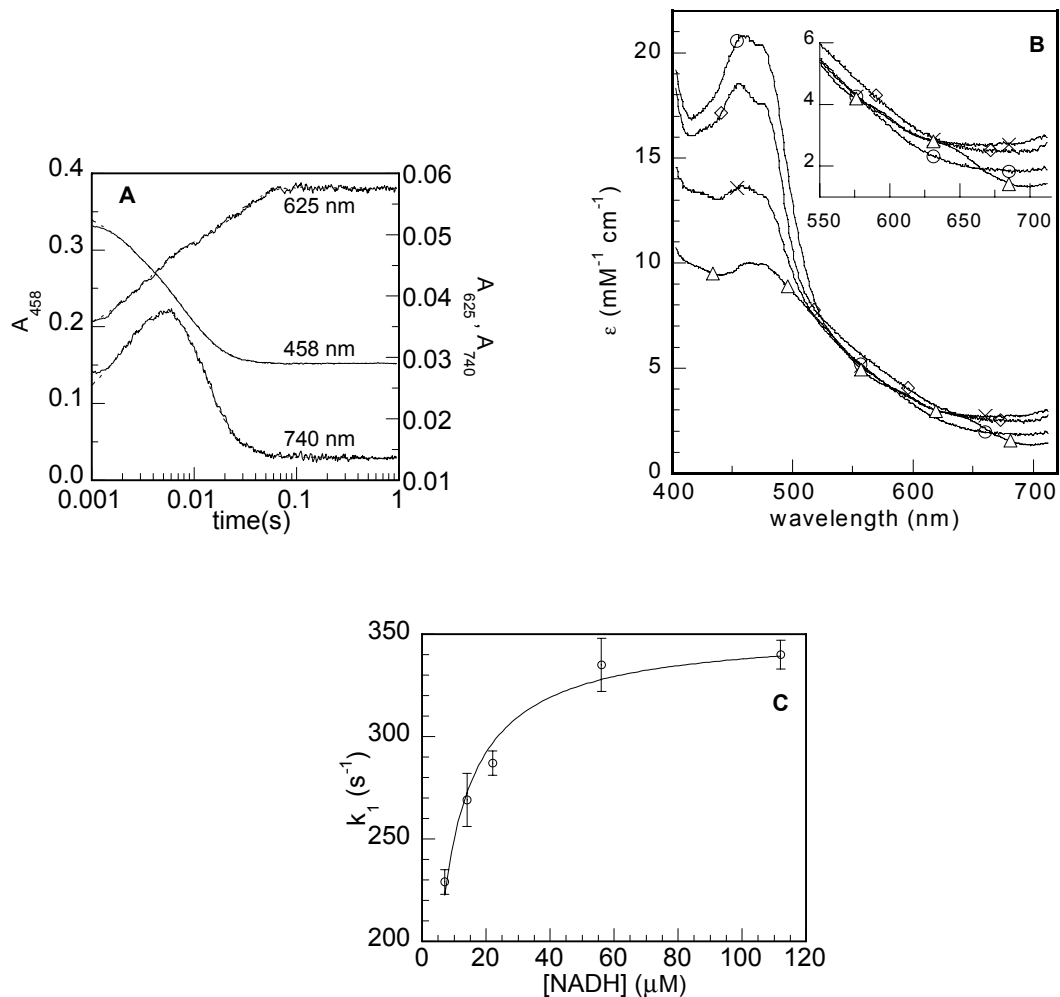


Figure 2.3. Reaction of MMOR_{ox} with NADH studied by stopped-flow UV-visible spectroscopy. (A) Time-dependent absorbance changes at 458, 625, and 725 nm during the reaction of 20 μM MMOR_{ox} with 200 μM NADH at 4 °C. Dashed lines are fits to eq. 5. (B) Derived spectra of species (circles, MMOR_{ox} ; diamonds, CT1; crosses, CT2; triangles, SQ) observed in the reaction. Species MMOR_{ox} , CT1, CT2, and SQ are defined in Figure 2.2. Inset - enlargement of long-wavelength region. (C) Dependence of k_1 (Figure 2.2) on the concentration of NADH.

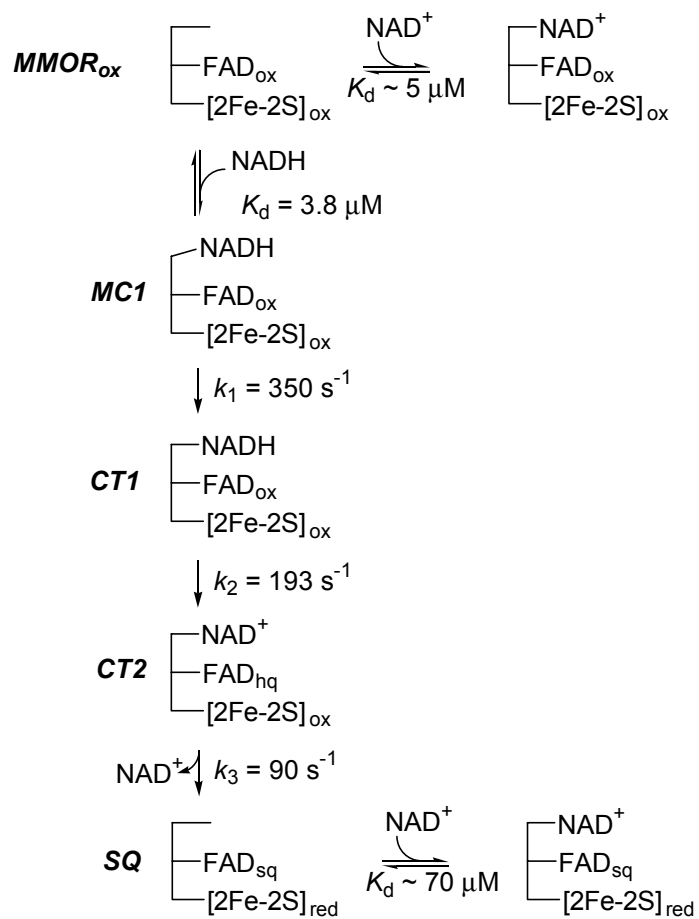


Figure 2.4. Reaction of MMOR_{ox} with NADH.

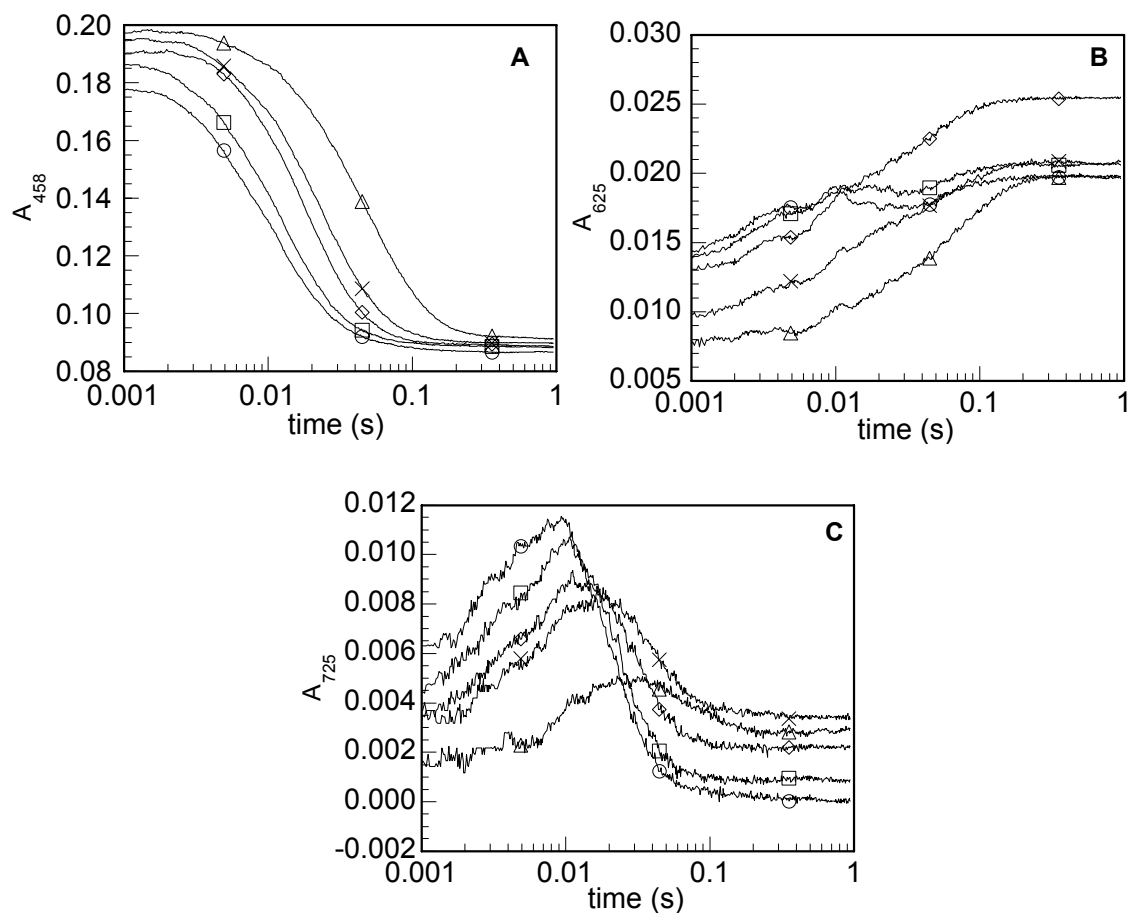


Figure 2.5. Product inhibition of reaction of MMOR_{ox} and NADH. Time-dependent absorbance changes were recorded at 458 nm (A), 625 nm (B), and 725 nm (C) by allowing a 22.4 μ M MMOR_{ox} solution to react with 224 μ M NADH in the presence of varying concentrations (circles, 0 μ M; squares, 62.5 μ M; diamonds, 250 μ M; crosses, 500 μ M; triangles 1.5 mM) of NAD^+ .

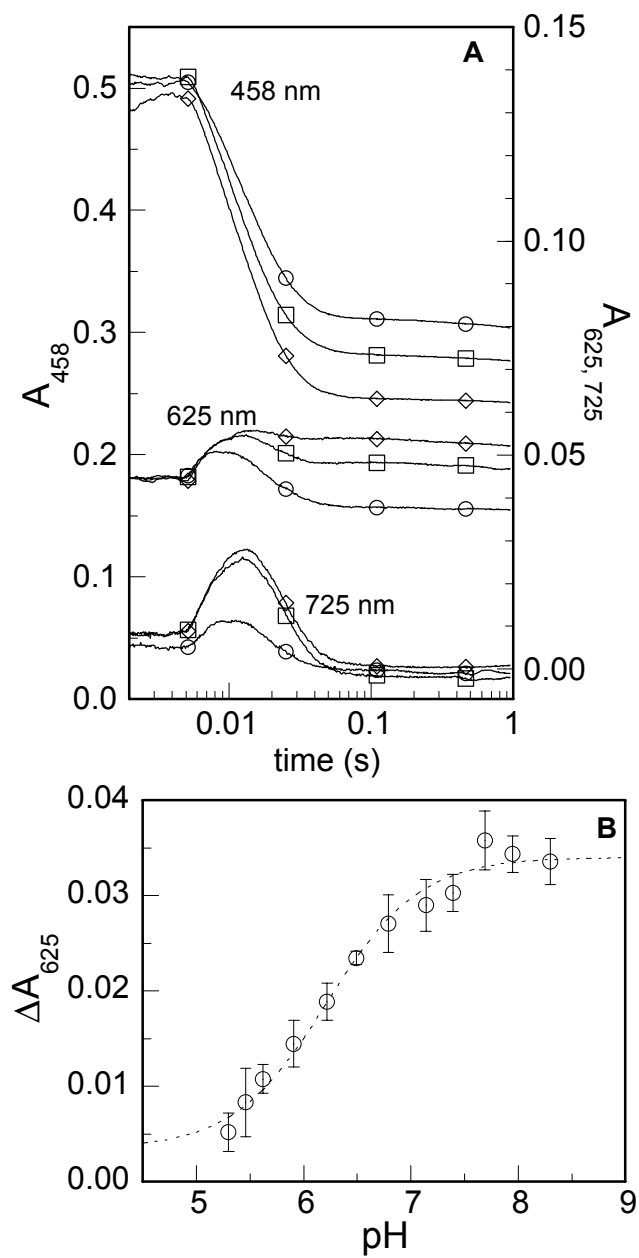


Figure 2.6. Effect of pH on the reduction of MMOR_{ox} by NADH. (A) 25 μ M MMOR_{ox} was allowed to react with 250 μ M NADH at 4 °C. Traces recorded at 458, 625, and 725 nm are shown for pH values of 5.35 (circles), 7.10 (squares), and 8.50 (diamonds). (B) Net change in absorbance at 625 nm as a function of pH. Dashed line is a fit to eq. 6.

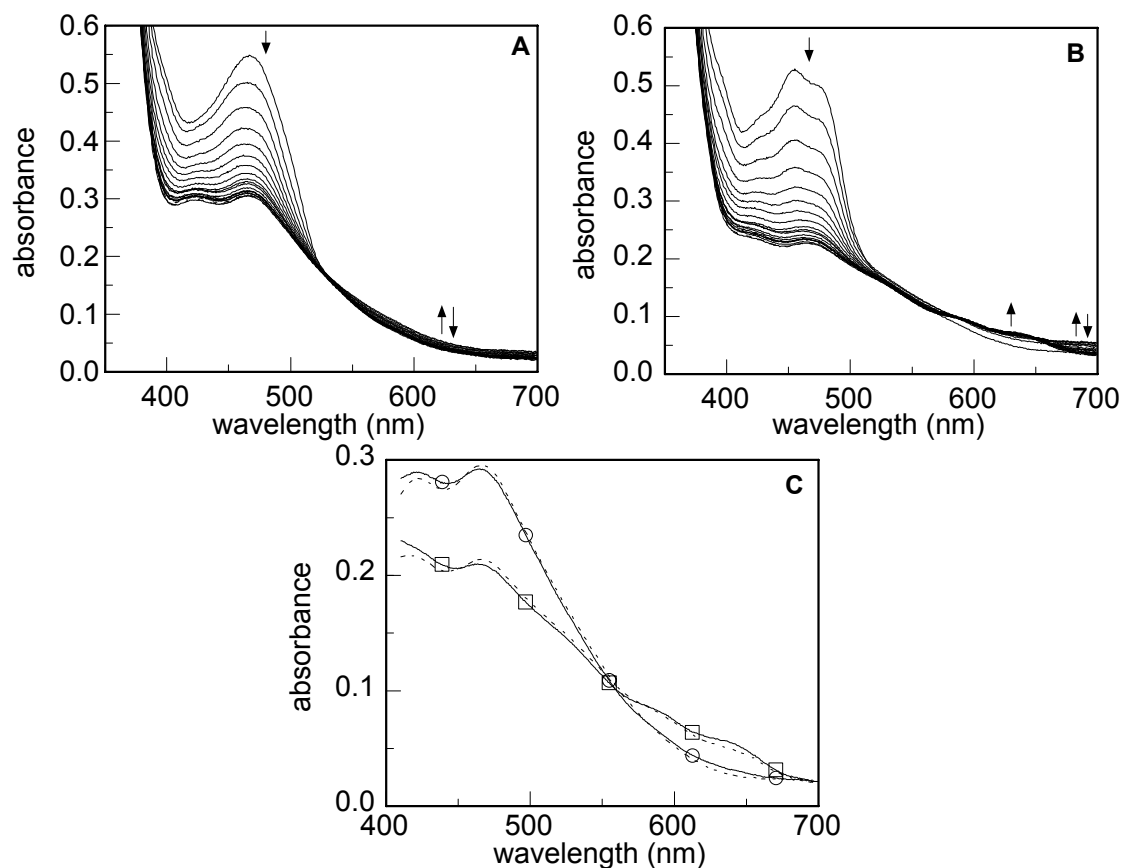


Figure 2.7. (A) Spectra recorded at ~3 ms intervals by diode array stopped-flow spectrophotometry in the first 68 ms after mixing MMOR_{ox} with a ten-fold excess of NADH at pH 5.27. (B) As in (A), but at pH 8.01. (C) Spectra recorded 1.5 s after mixing. Circles, pH 5.27; squares, pH 8.01. Dashed lines are fits to sums of component spectra.

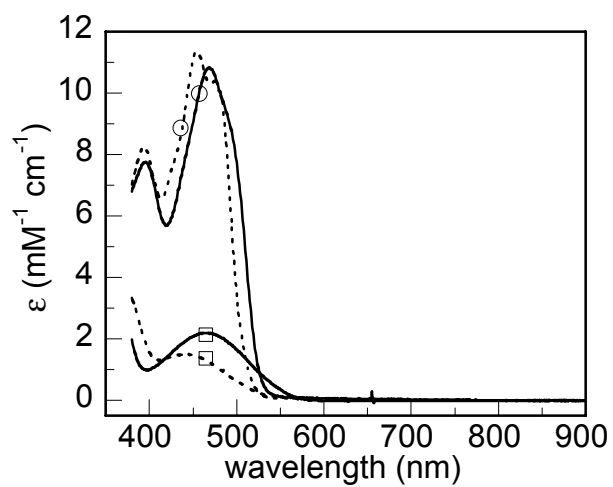


Figure 2.8. Spectra of FAD_{ox} (circles) and FAD_{hq} (squares) at pH 5.47 (solid lines) and pH 8.01 (dashed lines).²⁵

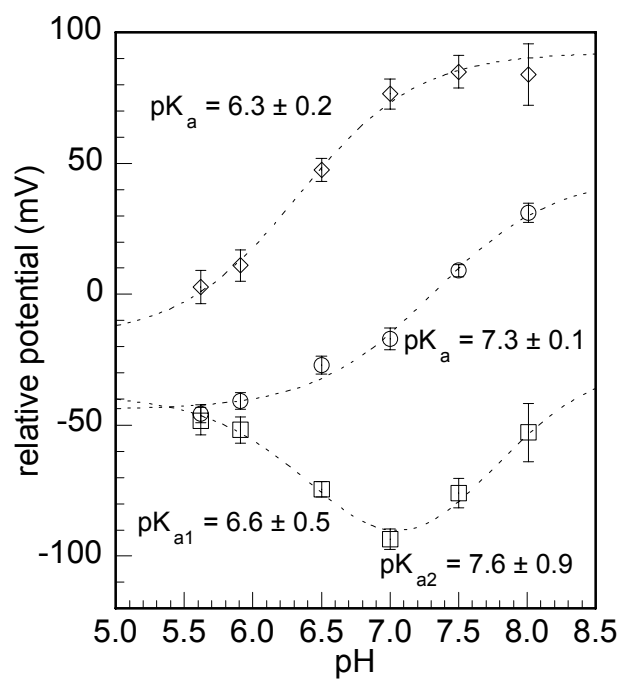


Figure 2.9. Differences between the redox potentials of MMOR at varying pH.

Circles, $E_{FeS} - E_{FAD1}$; squares, $E_{FAD2} - E_{FAD1}$; diamonds, $E_{FeS} - E_{FAD2}$. Dashed lines are fits of the same form as eq. 6.

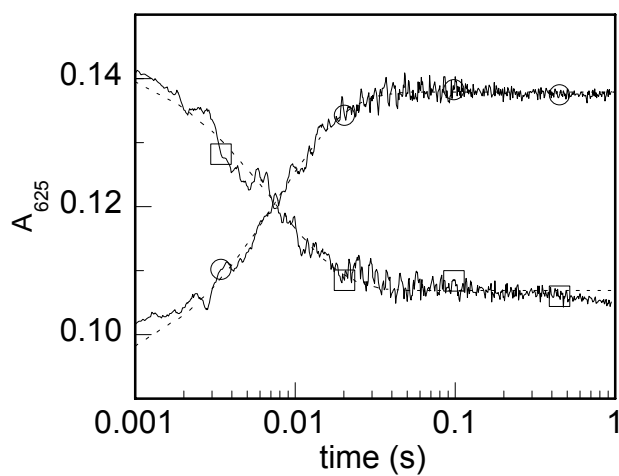


Figure 2.10. Equilibration of electrons in MMOR_{2e^-} following a pH jump. Absorbance at 625 nm is shown as a function of time; circles, after jump from pH 5.79 to 8.10; squares, after jump from pH 8.02 to 5.78. Dashed lines are single exponential fits.

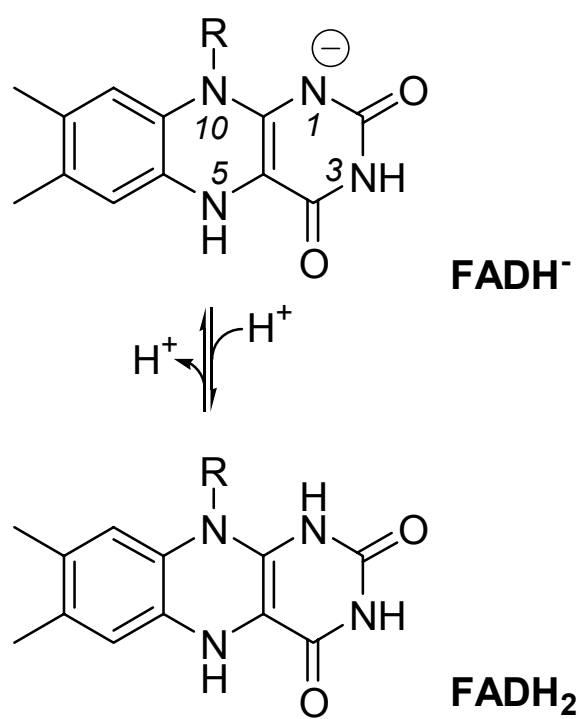


Figure 2.11. Protonation states of fully reduced FAD.

Chapter Three:

**Structural Features of the MMOH/MMOR Complex as Revealed by Mass
Spectrometric Analysis of Covalently Cross-linked Proteins**

Introduction

Methanotrophic bacteria rely on metalloenzymes to catalyze methane hydroxylation (eq 1), the first step in the metabolic pathway that



supplies all the carbon and energy required by the cells. In the presence of sufficient concentrations of copper, *Methylococcus capsulatus* (Bath) produces a membrane-bound copper enzyme, particulate methane monooxygenase (pMMO), to convert methane to methanol. When copper is unavailable, an iron-containing soluble methane monooxygenase (sMMO) is employed.¹

The sMMO system comprises three proteins. A hydroxylase (MMOH) contains the carboxylate-bridged diiron active site for oxygen and methane activation; a reductase (MMOR) is responsible for electron transfer from NADH to the active site of MMOH; and a regulatory protein (MMOB) is required for full activity. A fourth protein (MMOD) encoded within the *mmo* operon binds to the hydroxylase and inhibits catalysis *in vitro*, but the function of MMOD *in vivo* has yet to be determined.²

Complex formation between MMOH, MMOR, and MMOB is required for sMMO catalysis.³ MMOH itself is composed of three polypeptides with $\alpha_2\beta_2\gamma_2$ stoichiometry. Each alpha subunit houses a dinuclear iron active site. The catalytic cycle begins with the Fe_2^{III} resting state. MMOR binds to MMOH in order to transfer two electrons (derived from NADH) to the active site, affording the Fe_2^{II} state of MMOH. In the presence of MMOB, the Fe_2^{II} active site can react with O_2

to produce a series of intermediates that hydroxylate substrates. Turnover is very low in the absence of MMOB.^{3,4} An MMOB:MMOH ratio of 2 produces maximal activity, and increasing additional amounts of MMOB inhibit activity. Binding of MMOB to MMOH not only changes its reactivity toward dioxygen, but the redox potentials and spectroscopic properties of the diiron center are altered and electron transfer from MMOR is accelerated.^{1,3}

Three-dimensional structures of MMOH, MMOB and the [2Fe-2S] domain of MMOR (termed MMOR-Fd), depicted in Figure 3.1, have provided much useful information about sMMO catalysis.⁵⁻⁷ Despite the importance of protein-protein interactions in the catalytic cycle, only limited structural information is available for the complexes between the three components. The sMMO proteins can be covalently cross-linked by the reagent 1-ethyl-3-(3-dimethylaminopropyl)-carbodiimide (EDC).⁸ SDS-PAGE analysis of the cross-linked reaction products allowed identification of the polypeptides involved in the interaction. These early cross-linking studies also correctly identified some, but not all of the polypeptides in close proximity in the MMOH holoprotein before its crystal structure was determined.^{9,10} From small-angle X-ray scattering studies it was concluded that, in a ternary MMOH-MMOB-MMOR complex, the hydroxylase component undergoes a large structural rearrangement.¹¹ NMR titrations with MMOH have indicated residues on MMOB and MMOR-Fd that interact with MMOH (Figure 3.1).^{6,7,12} Modification of positively charged residues on the surface of MMOH inhibits the binding of MMOB and electron transfer from MMOR.¹³ Measure-

ments of the distance between the diiron site and a site-specific spin label on MMOB have provided information about where MMOB must contact MMOH.¹⁴

Mass spectrometric analysis of proteins has matured in recent years into a powerful technique, capable of studying protein complexes.^{15,16} The components of a protein complex can be identified by peptide mapping, whereby the mass spectrum recorded of peptides resulting from proteolytic digestion is matched to a sequence database.^{17,18} In some cases, mass spectrometry has located the sites of chemical cross-linking within such a protein complex.^{19,20} Interaction sites of protein complexes involved in vision,^{21,22} DNA replication,²³⁻²⁵ and interprotein electron transfer^{20,26} have all been elucidated in this manner.

In the present chapter we report the results of cross-linking reactions involving the components of sMMO. LC-MS analysis of peptides derived from in-gel digestion led to the identification of two EDC-promoted cross-links between MMOR-Fd and MMOH_α. The structures implied by these cross-link sites are described, and the resulting functional implications for sMMO complexes are discussed.

Methods and Materials

Cross-linking reagents EDC, *N*-succinimidyl(4-vinylsulfonyl)benzoate (SVSB), *N*-succinimidyl-3-(2-pyridylthio)propionate (SPDP), and *N*-5-azido-2-nitrobenzoyl-oxysuccinimide (ANB-NOS) were from Pierce (Rockford, IL) Di-

bromobimane was purchased from Calbiochem (La Jolla, CA). Other biochemicals were from Sigma (St. Louis, MO).

Protein Purification. MMOH was isolated from cultures of *Methylococcus capsulatus* (Bath), as previously described.³ Conditions for purification of recombinant MMOB, MMOR, MMOR-FAD, and MMOR-Fd from *E. coli* have also been reported.^{3,27,28}

EDC Cross-linking reactions. Typically, solutions of 10-20 μ M protein in 25 mM MOPS (pH 7.0) were allowed to react with 25 or 50 mM EDC for 5 min at ambient temperature. Reactions were quenched by addition of an equal volume of 2x SDS loading buffer, or an equal volume of 100 mM Tris pH 7.2, 200 mM DTT.

SVSB Cross-linking Reactions. A 2.4 μ L aliquot of 0.5 M SVSB freshly prepared in DMSO was added to a 120 μ L portion of a 60 μ M solution of MMOB in 25 mM MOPS at pH 7.0. After a 1.5 h incubation at ambient temperature, MMOB was separated from excess SVSB by gel filtration and concentrated. Approximately 2 equiv of MMOH were added to modified MMOB and allowed to react for an additional 30 min.

In-gel Proteolytic Digestion. Samples of the cross-linking reactions were separated by SDS-PAGE, using either 7.5% or 4-20% Ready Gels (Bio-Rad, Hercules, CA). Gels were stained either with Coomassie Blue or with a negative zinc stain. Zinc staining was carried out by soaking the gel in 0.2 M imidazole for 10 min, then rinsing briefly with water and incubating in 0.2 M ZnSO₄. When the

desired degree of opacity was reached, the zinc solution was removed and the gel stored in water.

Bands of interest were excised from the gel and cut with a clean razor blade into pieces approximately 1×1×1 mm, and placed in a clean 1.5 mL centrifuge tube. The gel pieces were washed 3× with 100 µL of 100 mM ammonium bicarbonate, pH 8.5, 50% acetonitrile, and finally once with 100 µL of acetonitrile.

After drying for 15 min in a centrifugal evaporator, the gel pieces were treated with 30 µL of 20 mM DTT in 100 mM ammonium bicarbonate in 5% acetonitrile and incubated for 1 hr at 55 °C. DTT was removed by washing with 100 µL of 100 mM ammonium bicarbonate, then with 100 µL of acetonitrile. Cysteine alkylation was then accomplished by addition of 30 µL of 100 mM iodoacetamide in 100 mM ammonium bicarbonate, followed by incubation for 30 min at room temperature in the dark. Gel pieces were washed twice with 100 mM ammonium bicarbonate and acetonitrile before drying in a centrifugal evaporator.

Gel pieces were rehydrated with 20 µL of 50 mM ammonium bicarbonate. Sequencing grade trypsin (Sigma, St. Louis MO or Promega, Madison WI) was added to give an enzyme:substrate ratio of approximately 1:100 by weight. Digestion was allowed to proceed overnight at 37 °C.

Peptides were extracted from the gel pieces with 100 µL of 20 mM ammonium bicarbonate; then twice with 100 µL of 1:1 water:acetonitrile plus 1% TFA; then once with 100 µL of acetonitrile. All extracts were combined in a fresh tube,

flash frozen and dried in a centrifugal evaporator. Dried extracts were stored at -20 °C until analyzed.

MALDI-TOF Mass Spectrometry. Dried samples were resuspended in 10 μ L of water with 0.1% TFA added and desalted with C18 ZipTips (Millipore, Bedford MA) according to the manufacturer's instructions. Spots were prepared on a stainless steel target by combining 0.5 μ L matrix solution with 0.5 μ L of sample and allowing the solvent to evaporate. The matrix solution was either 2,5-dihydroxybenzoic acid or α -cyano-4-hydroxycinnamic acid at a concentration of 10 mg/mL in 30% acetonitrile. Mass spectra of positive ions were recorded in linear mode on a Finnegan MAT Vision 2000 or in reflectron mode on a Bruker ReflexIV, both with delayed extraction. A total of 50-100 shots from a UV nitrogen laser were summed for each spectrum. All mass spectra were recorded in the Mass Spectrometry Resource at the Boston University School of Medicine.

Capillary LC-MS. Samples were analyzed with an LC Packings capillary LC coupled to an Applied Biosystems Inc. (Foster City, CA) Sciex QSTAR quadrupole orthogonal time-of-flight (QoTOF) mass spectrometer using information dependent acquisition. Peptide separation was achieved by using a 256 μ m ID \times 20 cm homemade capillary column packed with Michrom (Auburn, CA) Magic C₁₈ stationary phase. A 100 min gradient from 95:5 CH₃CN:H₂O with 0.1% formic acid to 85:10:5 CH₃CN:iPrOH:H₂O with 0.1% formic acid was run at 1 μ L/min. Eluent was sprayed at 4500 V and tandem MS data were generated with collision energies of 18, 24, and 36V for each selected peptide.

Data Analysis. Amino acid sequences of sMMO proteins²⁹ (derived from the DNA sequence) were used to calculate masses of tryptic peptides, employing the programs PEPTIDEMASS³⁰ or GPMAW.³¹ Observed masses were manually matched to calculated values to make assignments.

Site-Directed Mutagenesis. The MMOR variant carrying Glu56Gln and Glu91Gln mutations was prepared from pRED21 according to the QuikChange method (Stratagene, La Jolla, CA). pRED21 contains the *M. capsulatus* (Bath) *mmoC* gene in a pET21 vector.⁷ The Glu56Gln mutation was introduced first with the primer 5'-GCAAGGCCTTGTGCAGCCAAAGGGACTACGACC-3' and its reverse complement. Positive clones for the Glu56Gln mutation were selected and sequenced at the MIT Biopolymers Lab using a ABI 3730 sequencer. The Glu91Gln mutation was introduced in the Glu56Gln background using the primer 5'-CCGAAGACCGACCCTGCAAATCGAACTGCCCTATAC-3' and its reverse complement. The DNA sequence of the double mutant was similarly verified, and the plasmid pRED21 E56Q E91Q was transformed into *E. coli* BL21(DE3). Expression of MMOR Glu56Gln Glu91Gln, referred to hereafter as MMOR EQ2, was similar to that of wild type MMOR, except that an IPTG concentration of 0.1 mM, rather than 1.0 mM, was used for induction. Purification was performed in the same manner as for MMOR.

NADH Consumption Assays. The activity of sMMO was measured by combining 1 μ M MMOH and 2 μ M MMOB with varying amounts of MMOR or MMOR EQ2.³ Propylene saturated buffer (25 mM MOPS, pH 7.0) was added to

give a final propylene concentration of 0.8 mM. Reactions, thermostatted at 25 °C, were initiated by addition of NADH to a final concentration of 160 μ M, in a total volume of 400 μ L in a quartz cuvette. The absorbance at 340 nm was measured for 2 min, and the rate of NADH consumption calculated as a linear fit of ΔA_{340} vs. time.

Results

Chemical Cross-linking of sMMO Complexes. EDC reacts to facilitate amide bond formation between amine and carboxylate groups, forming intra- or intermolecular cross-links on proteins, as illustrated in Figure 3.2A. Products resulting from EDC cross-linking of MMOH alone and in complex with MMOR-Fd are shown in Figure 3.2B. MMOH forms several intramolecular cross-links, including $\text{MMOH}_{\alpha}:\text{MMOH}_{\beta}$, $\text{MMOH}_{\beta}:\text{MMOH}_{\beta}$, and with extended reaction times, $\text{MMOH}_{\alpha}:\text{MMOH}_{\beta}:\text{MMOH}_{\gamma}$. The band arising from cross-linking between MMOH and MMOR-Fd, assigned as $\text{MMOH}_{\alpha}:\text{MMOR-Fd}$ based on its mobility, and confirmed by proteolytic digestion and mass spectrometry (see below). Full-length MMOR was also found to cross-link to the alpha subunit of MMOH, in contrast to previous findings for sMMO from *M. trichosporium* OB3b.⁸ Incubation of MMOH and MMOR-FAD with EDC did not produce a cross-link, indicating that the site for cross-linking to MMOH_{α} lies within the [2Fe-2S] domain of MMOR. A mixture of MMOR-Fd and MMOR-FAD did not form a cross-link upon reaction with EDC, suggesting that surfaces of these domains may not be in

close contact in the full-length protein. Electron transfer kinetic and ITC experiments also support this conclusion.²⁸ Figure 3.2C displays the EDC-promoted cross-link between MMOH and MMOB, in which the alpha subunit participates. MMOH will also cross-link to MMOD.²

The reagent SVSB facilitates cross-link formation between MMOB and MMOH _{α} , as well as between the MMOH subunits. The structure of SVSB and evidence of its ability to cross-link MMOH and MMOB are presented in Figure 3.3. SVSB was unable, however, to cross-link MMOR-Fd to MMOH.

Other cross-linking reagents, shown in Figure 3.4, were allowed to react with MMO complexes but did not produce cross-links. The amine-to-thiol cross-linker SPDP has the capability to react with the same residues as SVSB, but it does not produce a cross-link between MMOH and MMOB. Presumably, the reactivity of the dithiopyridyl moiety is less than that of the vinyl sulfone of SVSB, or the residues involved in the SVSB cross-link cannot accommodate the shorter spacer arm of SPDP (6.8 Å vs. 8.3 Å). The photoactivatable reagent ANB-NOS, like SVSB, has a succinimidyl ester to react with amines. If a protein amine reacts with that succinimidyl ester, a cross-link can be made by photolysis of the aryl azide, producing a highly reactive nitrene. Attempts to cross-link sMMO components with this reagent were unsuccessful. The fluorogenic cross-linker dibromobimane can react with two cysteine thiols. Peptides containing this cross-linker are fluorescent, providing a convenient means to detect them. It was able to modify, but

not cross-link, MMOH $_{\alpha}$ and MMOR-Fd. Other sMMO proteins did not react with dibromobimane.

In-gel Digestion and MALDI-TOF Analysis of Unmodified sMMO Proteins. The isolated MMO proteins were subjected to in-gel proteolysis and mass spectrometric analysis. Figure 3.5 shows a MALDI-TOF spectrum of tryptic peptides of MMOH $_{\alpha}$, and the data are also presented in Table 3.1. A summary of the sequence coverage observed for the MMO proteins is displayed in Table 3.2.

Figure 3.6 reveals the locations of the peptides listed in Table 3.1 in the MMOH $_{\alpha}$ sequence. A difficulty of the in-gel digestion approach is apparent from this plot, namely, the presence of many overlapping peptides that provide redundant information. Peptides containing a missed trypsin cleavage site, or a modification such as methionine oxidation or sodium ionization, further complicate the spectra but frequently without providing additional information about the protein. For example, the sequence LWTLLDDIKR, corresponding to residues 506-514 of MMOH $_{\alpha}$, occurs in three different peptides due to missed cleavage sites (Figure 3.6). As a result, the abundance and therefore signal intensity of each of those peptides is less than if complete proteolysis had occurred, making it more difficult to detect them.

In-gel Digestion and MALDI-TOF Analysis of MMOH $_{\alpha}$:MMOR-Fd. The major cross-linked product resulting from treatment of the MMOH/MMOR-Fd complex with EDC is the 71.5 kDa H $_{\alpha}$:MMOR-Fd band shown in Figure 3.2B. This material was subjected to in-gel digestion and the resulting peptides ana-

lyzed by MALDI-TOF mass spectrometry. Table 3.3 lists the peptides observed and their assignments. The sequence coverage was 76% and 77% for MMOH_α and MMOR-Fd, respectively.

The remaining, unidentified peptide masses were then compared to a list of hypothetical cross-linked peptide masses, the latter generated by calculating tryptic digests of MMOH_α and MMOR-Fd. The mass of a cross-linked peptide is taken to be equal to the sum of the masses of a peptide derived from MMOH_α and the mass of a peptide derived from MMOR-Fd, minus 18.01 Da to account for the loss of water upon formation the peptide bond (Figure 3.2A). A hypothetical cross-link was scored as chemically reasonable only if one peptide contains an internal lysine residue or a native protein amino terminus, and the other peptide contains an aspartate or glutamate residue or native protein carboxyl terminus. Several unassigned masses did match hypothetical cross-links, but upon further inspection, most were not chemically reasonable.

Analysis of the SVSB-Promoted MMOH:MMOB Cross-link. Digestion and analysis of MMOB proved to be somewhat difficult. Samples of MMOB and MMOB_{SVSB} contained many more peptides than would be expected, the majority of the peptides could not be assigned. These samples were prepared from gels having a 4-20% polyacrylamide gradient, and the MMOB was excised from a high percentage polyacrylamide region of the gel. It is possible that the high polyacrylamide percentage interfered with digestion and/or sample recovery. Nonetheless, several unassigned peptides were observed in the MMOB_{SVSB} sam-

ple that were not present in the unmodified MMOB sample. These were analyzed as being potential intramolecular cross-links. Three close mass matches were found, but none made chemical sense based on the expected reactivity of SVSB. Examination of unassigned peptides from MMOH:MMOB_{SVSB} revealed four peptides that matched in mass, but again, none made chemical sense.

Other Approaches to Sample Preparation.

In response to the concern that the in-gel digestion procedure might inhibit recovery of large peptides from the gel matrix after proteolysis, a number of other sample preparation methods were investigated.

Solution Digestion and Off-Line HPLC. A 2 nmol EDC cross-linking reaction of MMOH and MMOR-Fd was carried out and quenched with sodium acetate. Following buffer exchange and lyophilization, the protein mixture was dissolved in 8M urea, reduced and alkylated. After dilution to reduce the urea concentration, trypsin was added and digestion allowed to proceed overnight at 37 °C. The resulting peptide mixture was separated by RP-HPLC and the fractions collected. The fractions in turn were lyophilized, dissolved in an appropriate solvent, and spotted on a MALDI target with α -cyano-4-hydroxycinnamic acid as the matrix.

In total, 1,000 peptides were detected. Many of these, however, represented the same peptide in multiple fractions, collected on a simple time-window basis. Sequence coverage was 79% for MMOH _{α} , 84% for MMOH _{β} , 100% for

MMOH_γ, and 97% for MMOR-Fd (Table 3.2). A total of 450 peptides remained unidentified. This method provided a great deal of information, but without a separation step prior to proteolytic digestion, identification of a cross-linked peptide against a background of an excess of unmodified peptides is impossible. Based on the success of the solution digest to produce good sequence coverage, other methods were sought to allow solution digestion on cross-linked material previously separated from unmodified proteins.

SDS-PAGE and Electroelution of Cross-linked Bands. An MMOH_α:MMOR-Fd EDC cross-linking reaction was performed and the quenched reaction mixture was separated by SDS-PAGE. The cross-linked band was excised and loaded in an electroelution apparatus that uses an applied electric field to move proteins across a barrier and trap them with a low molecular-weight cutoff dialysis membrane. Following electroelution, SDS was removed by precipitation. Figure 3.7 shows recovery of purified MMOH_α:MMOR-Fd by this procedure. The proteins were then treated with DTT and iodoacetamide to alkylate cysteine residues, and digested with trypsin. The MALDI-TOF spectrum of the resulting peptides was very poor, due to the presence of residual SDS. Attempts to carry out electroelution with SDS-free buffer failed to return protein. Neither dialysis, gel filtration, nor ultrafiltration of electroeluted proteins could remove SDS to sufficiently low levels that good MALDI-TOF spectra could be obtained.

Affinity Tags. Both MMOB and MMOR-Fd can be expressed in *E. coli*, and so the potential exists to engineer affinity tags as part of their amino acid sequence. An MMOB expression system prepared using pET32 produces an amino-terminal fusion of thioredoxin, a His₆ tag, a thrombin cleavage site, an S-tag, and a Factor X_a site at the native N-terminus (Trx-MMOB). Affinity purification might facilitate isolation of cross-linked products and allow their digestion in solution. S-tag MMOB, prepared by thrombin treatment of Trx-MMOB, failed to cross-link to MMOH upon reaction with EDC, however.

Both N- and C- terminal His₆ fusions of MMOR-Fd were next prepared. The N-terminal His₆ fusion was created by cloning MMOR-Fd into pET15b, which installs a 20 amino acid N-terminal fusion peptide of the sequence MGSSHHHHHSSGLVPRGSH. A C-terminal His₆ tag was added to MMOR-Fd by cloning into pET24b, adding the sequence KLAAALEHHHHHHH. Both His-tagged constructs were expressed in *E. coli* and purified by Ni²⁺ affinity chromatography. Neither was able to form cross-links to MMOH in the presence of EDC (Figure 3.8).

LC-QoTOF MS Analysis of MMOH_α:MMOR-Fd.

Rationale. The in-gel digestion method, while imperfect, offers the advantage of separating cross-linked from unreacted proteins prior to proteolysis. In order to avoid some of the drawbacks of MALDI-TOF, the peptide mixture was analyzed by LC-QoTOF MS. Coupling a chromatographic separation to mass

spectrometry results in simpler spectra. The QoTOF spectrometer also has excellent mass accuracy and the ability to acquire tandem mass spectra automatically during the LC run. The tandem MS capability offers a solution to another problem of MALDI-TOF analysis, providing means to confirm that a putative cross-link actually has the proposed composition.

LC-QoTOF and Tandem MS Data. A sample of the MMOH $_{\alpha}$:MMOR-Fd EDC cross-link was subjected to LC-MS analysis on a QoTOF instrument. Data were recorded by using information dependent acquisition (IDA). Under IDA, the spectrometer selects ions for tandem mass spectra on the fly. Under the conditions used for tandem mass spectrometry of peptides, fragmentation occurs most commonly on the peptide backbone. Figure 3.9 illustrates the naming scheme used for the peptide fragment ions. Differences between prominent fragment ions are compared to a list of exact residue masses for each of the 20 amino acids.³² Consequently, accurate masses and sequence information are available for many major components of the peptide mixture. Unmodified peptides were assigned on the basis of exact mass, and tandem mass spectra were used (when available) to help identify any remaining peptides.

The total ion chromatogram is shown in Figure 3.10, and sequence coverage statistics are presented in Table 3.2. In all, 177 unique peptide masses were observed, and 88 of them were identified. Of those that were identified, 34 unique peptides were from MMOH $_{\alpha}$, 12 from MMOH $_{\beta}$, 10 from MMOR-Fd, and 2 contained cross-links. The remainder of the identified peptides involved simple

modifications of observed peptides. For instance, a peptide might appear in both its $[M+2H]^{2+}$ and $[M+H+Na]^{2+}$ states. The intensities of the unidentified peptides were generally lower than those of identified peptides.

Nearly all the residues of MMOR-Fd were observed, as was the majority of $MMOH_{\alpha}$ sequence. The presence of $MMOH_{\beta}$ in the sample is most likely due to imperfect resolution of proteins during SDS-PAGE. Intensities of $MMOH_{\beta}$ peptides were low compared to those of the $MMOH_{\alpha}$ or MMOR-Fd peptides. Four major gaps in the $MMOH_{\alpha}$ sequence accounted for the most of its missing residues. Those gaps involved residues 95-134, 183-245, 331-360, and 392-419. The large size of these tryptic peptides most likely limited the efficiency of their extraction from the gel, and thus they were not observed by LC-MS.

The mass spectrum of peptides eluting at 33.5 min is presented in Figure 3.11. The electrospray ionization method frequently generates ions in more than one charge state. Both 2^{+} and 3^{+} ions of a peptide with mass 1942.15 Da can be seen in Figure 3.11. In such a case, mass measurements can be made from the isotopic series of each charge state, allowing multiple measurements from a single spectrum. As shown in the inset of Figure 3.11, the resolving power, defined as $M/\Delta m$ measured full width at half maximum, of the QSTAR exceeds 5,000. At this resolving power, the isotopic distribution is clearly discernable for typical tryptic peptides. The peak at lowest m/z is the monoisotopic peak, containing only ^{12}C , 1H , ^{14}N , ^{16}O and ^{32}S . Each successive peak contains one more atom of a heavy isotope than the previous peak. The relative height of each isotopic peak

can be calculated based on the known natural abundances of the isotopes. The occurrence of ^{13}C dominates the shape of the isotopic distribution of peptides.

Identification of Two MMOH_α :MMOR-Fd Cross-links. Peaks marked with an asterisk in Figure 3.10 are branched peptides resulting from EDC cross-linking. The mass spectrum of one of these is depicted in Figure 3.11. The observed mass, 1942.15 Da, closely matches that calculated, 1941.93 Da, for a cross-link between MMOR-Fd 52-62 (sequence: ALCSEGDYDLK) and MMOH_α 2-8 (sequence: ALSTATK). At first glance, this pair does not appear chemically reasonable. The MMOR-Fd derived peptide contains three carboxylate side chains, but the MMOH_α derived peptide lacks the required internal Lys residue. MMOH_α 2-8 has the N-terminal amine of native MMOH_α , however. Numbering of MMOH_α begins at the initial Met, even though it is missing from the mature protein as expressed in *M. capsulatus* (Bath).³³ Thus, the N-terminal Ala residue is given the number 2. This numbering scheme is used in order to remain consistent with that used in X-ray crystallographic studies.

The tandem mass spectrum of precursor ion 648.4³⁺ (Figure 3.12) confirms the assignment. The entire y-ion series is present, and it demonstrates unambiguously that Glu56 is the only one of the three carboxylates on MMOR-Fd 52-62 involved in a cross-link. Table 3.4 lists the ions observed in the tandem spectrum and shows their assignments.

A second cross-linked peptide, consisting of MMOR-Fd 88-98 (sequence: TDLEIELPYTH) and MMOH_α 2-8 was also identified. The calculated mass of the

peptide, 2002.03 Da, matches that observed for a peptide eluting at 42.5 min, 2002.23 Da. The tandem data recorded for this peptide are shown in Figure 3.13 and presented in Table 3.5. The tandem data locate the cross-link at Glu91 of MMOR-Fd, and rule out Asp89 and Glu93 as possible sites of cross-linking.

MMOR-Fd 52-62 and 88-98 were also observed in the LC-MS data as unmodified peptides. The residues of MMOH_α 2-8, however, were only identified as part of a cross-link to MMOR-Fd. These observations are consistent with MMOH_α having a single site of cross-linking at the N-terminus, which can react with either MMOR-Fd Glu56 or Glu91.

Examination of the solution structure of MMOR-Fd⁷ reveals that Glu56 and Glu91 are well exposed to solvent and quite close to one another (Figure 3.14A). The carboxylate oxygen atoms of the two side chains are ~ 6 Å apart. In the crystal structure of MMOH, the most N-terminal residue is Ala15.³⁴ The remainder of the N-terminal polypeptide is disordered. Figure 3.14B depicts the structure of MMOH with the position of Ala15 highlighted.

A previous mass spectrometric investigation of MMOH reported N-terminal variants of MMOH_α. In addition to the native protein, with Ala2 at the N-terminus, two truncated forms were discovered. Lys8 was at the N-terminus of one truncate, Ala10 at the other.³³ No cross-links to MMOR-Fd involving these truncates were detected in our study, nor were they found in unmodified form.

The MMOR EQ2 Mutant. In order to confirm that the EDC-promoted cross-links between MMOH_α and MMOR(-Fd) involve the site identified, the

double mutant MMOR Glu56Gln Glu91Gln (MMOR EQ2) was prepared. MMOR EQ2 was expected to be similar to MMOR in most respects, but to lack the ability to form the identified cross-links. Indeed, the UV-visible spectrum of purified MMOR EQ2 is identical to that of MMOR. Similar levels of NADH oxidase activity (Table 3.6) in the two variants indicate that binding of NADH, reduction and re-oxidation of cofactors is not seriously affected by the mutations. Steady-state activity of the sMMO system, however, is impaired with MMOR EQ2.

A comparison of EDC cross-linking of MMOR and MMOR EQ2 to MMOH is made in Figure 3.15. MMOR EQ2 still forms cross-links to MMOH_α, although the yield of cross-linked material is lower than for MMOR.

Discussion

Recently, mass spectrometric analyses of protein cross-linking reactions have identified protein components of a complex,^{17,18} or the precise residues involved in chemical cross-links.^{19-22,35} The high sensitivity and suitability to automation of mass spectrometry allow it to identify proteins and protein complexes on a proteome-wide scale.^{36,37} Since for sMMO, crystals of MMOH-MMOB and MMOH-MMOD complexes as yet have not yielded X-ray diffraction patterns suitable for structure determination, cross-linking presents an alternative method to investigate the structures of sMMO complexes.

Cross-linking Reactions of sMMO Proteins. The zero-length cross-linker EDC reacts with sMMO proteins to produce several different products.⁸ The pre-

sent work confirms most of these earlier results. The subunits of MMOH cross-link to afford $\text{MMOH}_\alpha:\text{MMOH}_\beta$ and $\text{MMOH}_\beta:\text{MMOH}_\beta$ products. The regulatory protein MMOB cross-links to MMOH_α , consistent with its ability to influence the reactivity of the diiron active site located within this polypeptide.¹ In contrast to previous work, however, we find that MMOR (and MMOR-Fd) cross-links to MMOH_α , not MMOH_β .⁸ This and other structural considerations are discussed below.

Thiol-to-amine cross-linking between MMOB and MMOH was achieved with SVSB. MMOB has only one cysteine residue, and it reacts slowly with thiol-modifying reagents.³⁸ Thus, the $\text{MMOH}_\alpha:\text{MMOB}$ SVSB cross-link most likely involves a lysine from MMOB and a cysteine from MMOH_α .

Digestion and Mass Spectrometric Analysis of Unmodified sMMO Proteins. In-gel digestion followed by MALDI-TOF analysis of the individual proteins of sMMO resulted in good sequence coverage of each protein (Table 3.2). Generally, more complete sequence coverage is associated with smaller proteins. Regions of a protein may not be observed either because the peptides were not present in the sample or because they failed to ionize in the mass spectrometer. Certain peptides might remain in the gel pieces during extraction. In a complex mixture, some species may become ionized preferentially to others, leading to the loss of signal for some components.

MALDI-TOF Analysis of Cross-linked sMMO Proteins. In the MALDI-TOF spectrum of $\text{MMOH}_\alpha:\text{Fd}$, there were 21 peptides observed that were candi-

date cross-links. Thirteen of these had masses that matched (within 0.1%) one or more hypothetical cross-link masses, but most were not chemically reasonable. One particular mass (2240 Da) matched seven different hypothetical cross-links, though only two were reasonable.

A sample of $\text{MMOH}_\alpha:\text{MMOB}_{\text{SVSB}}$ was similarly analyzed. Sequence coverage was lower than for the $\text{MMOH}_\alpha:\text{MMOR-Fd}$ cross-link, and the MALDI-TOF mass spectrum contained a large number of unassigned masses. Those unassigned masses were compared to a list of hypothetical masses calculated for cross-links between amines and thiols, and accounting for the additional mass introduced by the cross-linker. No chemically reasonable matches between observed and hypothetical masses were found.

Considering the number of unassigned masses that were observed in these spectra, another method of sample preparation was sought. Concerns about in-gel digestion followed by MALDI-TOF included the possibility that cross-linked peptides would not be observed in the mass spectrum. Such peptides might be too large to be extracted from the gel, and/or the complexity of the peptide mixture might give rise to ion suppression effects that preclude measurement of the desired peptides. Initial attempts to avoid these problems focused on digestion of the cross-linked mixture in solution.

Solution Digestion and Other Methods of Sample Preparation. Digestion in solution, rather than in the gel, and HPLC were applied to address the concerns described above. Solution digestion omits the need for extraction; all

peptides resulting from digestion are certain to be present in the mixture. The mixture itself was separated by reverse-phase HPLC to reduce the number of peptides present in a particular MALDI sample, and thereby lessen concerns related to ion suppression. Unlike the in-gel digestion method, the solution digest approach does not separate cross-linked material from other proteins present in the sample. The digest contains peptides derived from unmodified MMOH $_{\alpha}$, MMOH $_{\beta}$, MMOH $_{\gamma}$, and MMOR-Fd; cross-links between MMOH subunits; and the cross-link of interest, between MMOH $_{\alpha}$ and MMOR-Fd. The amount of MMOH $_{\alpha}$:MMOR-Fd cross-link is ~10% that of other proteins in the sample, so detection becomes challenging. Sequence coverage was improved relative to the in-gel method, but no cross-links were identified.

It was then clear that separation of cross-linked proteins prior to digestion in solution would be the preferred method of sample preparation. Unfortunately, the only separation method that worked well was SDS-PAGE. Attempts to purify and recover by electroelution cross-linked protein for solution digestion were problematic, failing to remove SDS to low enough levels for mass spectrometry. Affinity tags, intended to allow a simple chromatographic purification, interfered with cross-linking.

Thus, although the in-gel digestion method has drawbacks, it did produce a useful quantity of sufficiently pure material for MS analysis. We therefore abandoned efforts to modify the sample preparation steps and focused instead on different MS techniques. LC-MS was selected because it can separate peptides

prior to their introduction into the mass spectrometer. The QoTOF instrument used also has tandem MS capability, offering a means to gain more detailed structural information about the peptides analyzed than is available from mass alone.

LC-QoTOF Analysis of MMOH_α:MMOR-Fd. The LC-QoTOF analysis of in-gel tryptic digests of MMOH_α:MMOR-Fd provided similar sequence coverage to MALDI-TOF analysis of the same material. Unlike MALDI-TOF, the separation of peptides, greater mass accuracy and tandem MS capability of LC-QoTOF allowed the positive identification of cross-links between MMOH_α and MMOR-Fd.

The identities of two EDC-promoted cross-links between MMOH_α and MMOR-Fd involve an amide bond between the N-terminal amino group of MMOH_α and the Glu56 or Glu91 side chain of MMOR-Fd. The close proximity of Glu56 and Glu91 in the solution structure of MMOR-Fd (Figure 3.14) suggests that the two cross-links represent only a single interaction between the two proteins. That interaction presumably involves electrostatic attraction between the positively charged N-terminus of MMOH_α and a negatively charged region containing Glu56 and Glu91 of MMOR or MMOR-Fd.

Based on their intensity in the LC-MS data, we conclude that the MMOH_α Ala2:MMOR Glu56/Glu91 cross-links account for a significant fraction of total cross-linking, but cross-links between other residues are also present. Figure 3.15 reveals that MMOR EQ2, lacking carboxylates at positions 56 and 91, still forms

cross-links to MMOH_α . The sites of these cross-links are as yet unidentified, but determination of their nature will be facilitated by use of the MMOR EQ2 mutant or a similar double mutation of MMOR-Fd.

Implications Regarding the MMOH/MMOR Complex. Although the occurrence of the identified cross-links is not in doubt, we must consider two issues. Does MMOR-Fd faithfully model of the interactions of MMOR with MMOH and, if so, does the cross-link represent a real interaction in the MMOH/MMOR-Fd complex?

We have several lines of evidence to support the conclusion that MMOR-Fd recapitulates the important features of the MMOH/MMOR complex. Dissociation constants for binding of MMOR and MMOR-Fd to MMOH, measured by isothermal titration calorimetry, are within an order of magnitude of one another.^{3,28} Chemically reduced MMOR-Fd transfers electrons efficiently to the diiron center of MMOH.²⁸ Finally, the FAD domain of MMOR (MMOR-FAD) does not cross-link to MMOH, suggesting that it interacts weakly or not at all with MMOH (data not shown).

Among MMOR proteins from several species, only Glu or Asp residues occur at position 56, and only Glu or His at position 91.⁷ MMOH_α protein sequences are highly conserved along the entire polypeptide, including the N-terminus.²⁹ It is possible that the cross-link does not reflect a functionally important protein complex, but rather reflects the greater reactivity of these groups on the protein surfaces. Such is unlikely, however, since we have identified only two

specific cross-links, and those represent only a single interaction. There are many of surface-accessible carboxylates and amines on both MMOR-Fd and MMOH_α. Protein pairs that do not form tight complexes (MMOH and MMOR-FAD; MMOB and MMOR) do not cross-link under the same conditions.

Structural Implications of the Identified Cross-links. Because MMOR must deliver electrons to the diiron site of MMOH_α, it is likely that the MMOH-MMOR complex brings the [2Fe-2S] cluster of MMOR within about 14 Å of the diiron site to allow efficient electron transfer.³⁹ The canyon region of MMOH_α is the only protein surface within such a distance of the diiron site, and that region has been proposed as a binding site for both MMOR and MMOB.^{9,14} An examination of crystal packing interactions led to a model where MMOR could bind in the vicinity of MMOH_α, namely, Lys385. In MMOH_α, Lys385 is more than 75 Å from Ala15.³⁴ If the 14 residues between the N-terminus and Ala15 were adopted a fully extended conformation, then Ala2 could be at most 54 Å from Ala15. The cross-linking results rule out MMOR binding in the vicinity of MMOH_α Lys385. Thus, the canyon does appear to be a likely site for MMOR binding to MMOH, a conclusion similarly reached for MMOB binding to MMOH.¹⁴ From an analysis of steady state kinetic behavior, MMOB and MMOR do not appear to compete for the same binding sites on MMOH.³

The disorder of the N-terminus of the α subunit in the MMOH crystal structure may suggest that it is unstructured. If so, then cross-linking to a specific

location on MMOR-Fd might reflect only those carboxylate residues that are accessible to it upon complex formation. We must consider the possibility that the crystal structure might not reflect the structure of the components in complex with other proteins. It has been proposed on the basis of small-angle X-ray scattering experiments that MMOH undergoes a large structural change upon formation of a ternary MMOH/MMOB/MMOR complex.¹¹

M. capsulatus (Bath) MMOR forms cross-links to MMOH_α whereas *M. trichosporium* OB3b MMOR apparently cross-links to MMOH_β.⁸ This alternative cross-linking behavior, if real, may be a reflection of differences in the location of reactive residues on the surfaces of the proteins from the two species. The structures of the two MMOH proteins are quite similar,^{9,40} and sequence identities for MMOH_α, MMOH_β, and MMOR proteins are 81, 59, and 42 percent, respectively.²⁹ These facts suggest that MMOR binds to a location on MMOH where the α and β subunits are in close proximity to one another.

NMR binding studies of MMOR-Fd and MMOH revealed the residues on MMOR-Fd that comprise the binding surface. The residues are on the same face of the protein as the [2Fe-2S] cluster, consistent with a model in which the two proteins bind in a manner to bring the redox active [2Fe-2S] and carboxylate-bridged diiron centers close to one another. The residues of the MMOR-Fd β-sheet, including Glu56 and Glu91, experience the least change in backbone ¹⁵N line width upon binding to MMOH.⁷ It is not clear why Glu56 and Glu91, residues that form cross-links and thus presumed to be involved in the binding in-

teraction, as supported by the diminution of sMMO activity in the MMOR EQ2 mutant, should appear from the NMR experiment not to be a part of the binding face of MMOR-Fd.

Other Approaches to Understanding Structures of sMMO Protein Complexes. Besides chemical cross-linking, other methods to elucidate the binding modes of sMMO complexes have been attempted. Analysis of inter-protein packing interactions in crystals of MMOH led to a model for binding of MMOR to MMOH, although the results of the present cross-linking studies seem to rule out this model.³⁴ Solution structures of MMOB and MMOR-Fd have been determined by NMR spectroscopy, and line-broadening experiments have provided information about the surfaces of those proteins that contact MMOH upon binding.^{6,7} Saturation-recovery EPR experiments can measure distances between the diiron active site and a spin label site-specifically attached to MMOB. This method has determined that MMOB Cys 89 is ~ 15 Å from the diiron active site.¹⁴ This information, coupled with structural information about MMOH, suggest that MMOB binds with Cys 89 approaching helices E and F of MMOH _{α} , in the canyon region of MMOH.

Conclusion

Two EDC-promoted cross-links between MMOR-Fd and MMOH _{α} , N-terminus of MMOH _{α} to MMOR-Fd Glu56 and Glu91, were identified through the use of LC-QoTOF mass spectrometry. Accurate masses combined with tandem

mass spectra confirmed the structures of the cross-links. The locations of Glu56 and Glu91 on MMOR-Fd, close to each other on strands β_4 and β_6 , suggest that the two cross-links represent only a single interaction between the N-terminus of MMOH $_{\alpha}$ and the negatively charged region formed by those two carboxylates.

Mutation of full length MMOR Glu56 and Glu91 both to Gln reduces sMMO activity without seriously curtailing the NADH oxidase activity of isolated MMOR. This result suggests that the interaction identified by the cross-linking study is relevant to the formation of the MMOH/MMOR complex. The double mutant still forms cross-links to MMOH, indicating that other sites of cross-link formation exist and remain to be identified.

References

- 1) Merkx, M.; Kopp, D. A.; Sazinsky, M. H.; Blazyk, J. L.; Muller, J.; Lippard, S. J. *Angew. Chem. Int. Ed.* **2001**, *40*, 2782-2807.
- 2) Merkx, M.; Lippard, S. J. *J. Biol. Chem.* **2002**, *277*, 5858-5865.
- 3) Gassner, G. T.; Lippard, S. J. *Biochemistry* **1999**, *38*, 12768-12785.
- 4) Liu, K. E.; Valentine, A. M.; Wang, D. L.; Huynh, B. H.; Edmondson, D. E.; Salifoglou, A.; Lippard, S. J. *J. Am. Chem. Soc.* **1995**, *117*, 10174-10185.
- 5) Rosenzweig, A. C.; Nordlund, P.; Takahara, P. M.; Frederick, C. A.; Lippard, S. J. *Chem. Biol.* **1995**, *2*, 409-418.
- 6) Walters, K. J.; Gassner, G. T.; Lippard, S. J.; Wagner, G. *Proc. Natl. Acad. Sci. U. S. A.* **1999**, *96*, 7877-7882.
- 7) Müller, J.; Lugovskoy, A. A.; Wagner, G.; Lippard, S. J. *Biochemistry* **2002**, *41*, 42-51.
- 8) Fox, B. G.; Liu, Y.; Dege, J. E.; Lipscomb, J. D. *J. Biol. Chem.* **1991**, *266*, 540-550.
- 9) Rosenzweig, A. C.; Frederick, C. A.; Lippard, S. J.; Nordlund, P. *Nature* **1993**, *366*, 537-543.
- 10) Rosenzweig, A. C.; Lippard, S. J. *Acc. Chem. Res.* **1994**, *27*, 229-236.
- 11) Gallagher, S. C.; Callaghan, A. J.; Zhao, J. K.; Dalton, H.; Trewhella, J. *Biochemistry* **1999**, *38*, 6752-6760.
- 12) Chang, S. L.; Wallar, B. J.; Lipscomb, J. D.; Mayo, K. H. *Biochemistry* **2001**, *40*, 9539-9551.

- 13) Balendra, S.; Lesieur, C.; Smith, T. J.; Dalton, H. *Biochemistry* **2002**, *41*, 2571-9.
- 14) MacArthur, R.; Sazinsky, M. H.; Kuhne, H.; Whittington, D. A.; Lippard, S. J.; Brudvig, G. W. *J. Am. Chem. Soc.* **2002**, *124*, 13392-13393.
- 15) Mann, M.; Hendrickson, R. C.; Pandey, A. *Annu. Rev. Biochem.* **2001**, *70*, 437-473.
- 16) Wilm, M.; Shevchenko, A.; Houthaeve, T.; Breit, S.; Schweigerer, L.; Fotsis, T.; Mann, M. *Nature* **1996**, *379*, 466-469.
- 17) Rappsilber, J.; Siniosoglou, S.; Hurt, E. C.; Mann, M. *Anal. Chem.* **2000**, *72*, 267-275.
- 18) Figeys, D.; McBroom, L. D.; Moran, M. F. *Methods* **2001**, *24*, 230-239.
- 19) Lacroix, M.; Rossi, V.; Gaboriaud, C.; Chevallier, S.; Jaquinod, M.; Thielen, N. M.; Gagnon, J.; Arlaud, G. J. *Biochemistry* **1997**, *36*, 6270-6282.
- 20) Müller, E. C.; Lapko, A.; Otto, A.; Müller, J. J.; Ruckpaul, K.; Heinemann, U. *Eur. J. Biochem.* **2001**, *268*, 1837-1843.
- 21) Cai, K.; Itoh, Y.; Khorana, F. C. *Proc. Natl. Acad. Sci. U. S. A.* **2001**, *98*, 4877-4882.
- 22) Itoh, Y.; Cai, K.; Khorana, H. G. *Proc. Natl. Acad. Sci. U. S. A.* **2001**, *98*, 4883-4887.
- 23) Alley, S. C.; Trakselis, M. A.; Mayer, M. U.; Ishmael, F. T.; Jones, A. D.; Benkovic, S. J. *J. Biol. Chem.* **2001**, *276*, 39340-39349.

- 24) Ishmael, F. T.; Alley, S. C.; Benkovic, S. J. *J. Biol. Chem.* **2001**, *276*, 25236-25242.
- 25) Ishmael, F. T.; Alley, S. C.; Benkovic, S. J. *J. Biol. Chem.* **2002**, *277*, 20555-20562.
- 26) Furukawa, Y.; Matsuda, F.; Ishimori, K.; Morishima, I. *J. Am. Chem. Soc.* **2002**, *124*, 4008-4019.
- 27) Kopp, D. A.; Gassner, G. T.; Blazyk, J. L.; Lippard, S. J. *Biochemistry* **2001**, *40*, 14932-14941.
- 28) Blazyk, J. L.; Lippard, S. J. *Biochemistry* **2002**, in press.
- 29) Coufal, D. E.; Blazyk, J. L.; Whittington, D. A.; Wu, W. W.; Rosenzweig, A. C.; Lippard, S. J. *Eur. J. Biochem.* **2000**, *267*, 2174-2185.
- 30) Wilkins, M. R.; Lindskog, I.; Gasteiger, E.; Bairoch, A.; Sanchez, J. C.; Hochstrasser, D. F.; Appel, R. D. *Electrophoresis* **1997**, *18*, 403-408.
- 31) Peri, S.; Steen, H.; Pandey, A. *Trends Biochem. Sci.* **2001**, *26*, 687-689.
- 32) Papayannopoulos, I. A. *Mass. Spectrom. Rev.* **1995**, *14*, 49-73.
- 33) Buzy, A.; Millar, A. L.; Legros, V.; Wilkins, P. C.; Dalton, H.; Jennings, K. R. *Eur. J. Biochem.* **1998**, *254*, 602-609.
- 34) Rosenzweig, A. C.; Brandstetter, H.; Whittington, D. A.; Nordlund, P.; Lippard, S. J.; Frederick, C. A. *Proteins* **1997**, *29*, 141-152.
- 35) Sinz, A.; Wang, K. *Biochemistry* **2001**, *40*, 7903-7913.
- 36) Aebersold, R.; Goodlett, D. R. *Chem. Rev.* **2001**, *101*, 269-295.

- 37) Ho, Y.; Gruhler, A.; Heilbut, A.; Bader, G. D.; Moore, L.; Adams, S. L.; Millar, A.; Taylor, P.; Bennett, K.; Boutilier, K.; Yang, L. Y.; Wolting, C.; Donaldson, I.; Schandorff, S.; Shewnarane, J.; Vo, M.; Taggart, J.; Goudreault, M.; Muskat, B.; Alfarano, C.; Dewar, D.; Lin, Z.; Michalickova, K.; Willems, A. R.; Sassi, H.; Nielsen, P. A.; Rasmussen, K. J.; Andersen, J. R.; Johansen, L. E.; Hansen, L. H.; Jespersen, H.; Podtelejnikov, A.; Nielsen, E.; Crawford, J.; Poulsen, V.; Sorensen, B. D.; Matthiesen, J.; Hendrickson, R. C.; Gleeson, F.; Pawson, T.; Moran, M. F.; Durocher, D.; Mann, M.; Hogue, C. W. V.; Figeys, D.; Tyers, M. *Nature* **2002**, *415*, 180-183.
- 38) Brandstetter, H.; Whittington, D. A.; Lippard, S. J.; Frederick, C. A. *Chem. Biol.* **1999**, *6*, 441-9.
- 39) Page, C. C.; Moser, C. C.; Chen, X. X.; Dutton, P. L. *Nature* **1999**, *402*, 47-52.
- 40) Elango, N.; Radhakrishnan, R.; Froland, W. A.; Wallar, B. J.; Earhart, C. A.; Lipscomb, J. D.; Ohlendorf, D. H. *Protein Sci.* **1997**, *6*, 556-568.

Table 3.1. Peptides Observed in the MALDI-TOF Spectrum of MMOH_α In-Gel Digest.

observed MH ⁺ (Da) ^a	range	Calcd. MH ⁺ (Da) ^a	MMOH _α sequence	MC ^b	rel. area	Δ (Da)	% error	modification
550.2						3.7		
575.8						2.8		
628.3						1.3		
807.2	324-330	807.88	YGVESPR	0	16.3	-0.68	0.084	
814.0	176-182	815	TIGPLWK	0	8.5	-1	0.123	
830.1						1.6		
836.0						4.5		
895.2	386-391	895.99	IYEEWR	0	28	-0.79	0.088	
917.0						2.3		
973.7	9-18	974.06	AATDALAANR	0	3.3	-0.36	0.037	
1034.5	494-502	1035.23	TLIAQPHVR	0	23.7	-0.73	0.071	
1056.7						3.2		
1079.1						2.1		
1094.8	41-49	1096.23	NNRTKYATK	2	100	-1.43	0.130	
1116.8	41-49	1118.22	NNRTKYATK	2	4.5	-1.42	0.127	Na ⁺ adduct
1139.0						3.5		
1160.0	506-514	1160.36	LWTLDDIKR	1	7	-0.36	0.031	
1219.3	515-524	1219.49	LNCVFNPK	1	20.9	-0.19	0.016	
1236.3	78-88	1236.37	QFGSLQDALTR	0	51.5	-0.07	0.006	
1257.9	78-88	1258.36	QFGSLQDALTR	0	3.7	-0.46	0.037	Na ⁺ adduct
1309.5	19-30	1309.42	APTSVNAQEVHR	0	9.9	0.08	0.006	
1333.7	420-431	1333.59	VSQVPFCPSLAK	0	5.6	0.11	0.008	
1347.4						3.2		
1355.7H _β	123-134	1355.49	FLQGYSADGQIR	0	2.3	0.21	0.015	beta contaminant
1371.9	31-40	1371.54	WLQSFNWDK	0	23.2	0.36	0.026	
1392.7	135-146	1391.57	NGYLAQVLDEIR	0	45.9	1.13	0.081	
1414.7	135-146	1413.56	NGYLAQVLDEIR	0	7.1	1.14	0.081	Na ⁺ adduct
1461.1	503-514	1460.67	GDKLWTLDDIKR	2	13.5	0.43	0.029	

-cont'd-

Table 3.1., cont'd. Peptides Observed in the MALDI-TOF Spectrum of MMOH_α In-Gel Digest.

observed MH ⁺ (Da) ^a	range	Calcd. MH ⁺ (Da) ^a	MMOH _α sequence	MC ^b	rel. area	Δ (Da)	% error	modification
1467.0	477-489	1466.68	ELSEVIAELHGLR	0	46	0.32	0.022	
1482.9	477-489	1482.68	ELSEVIAELHGLR	0	2.4	0.22	0.015	oxidized +16
1489.5					6.8			
1532.0	50-61	1533.75	YKMANETKEQFK	2	4.7	-1.75	0.114	
1556.5					5.5			
1638.5	308-320	1637.84	WVYEDWGGIWIGR	0	23.4	0.66	0.040	
1756.2	31-43	1755.93	WLQSFNWFDFKNNR	1	27.9	0.27	0.015	
1858.5	266-280	1857.03	YLNIDLNNAFWTQQK	0	29.9	1.47	0.079	
1880.8	89-104	1881.21	LNAGVRVHPKWNEMTK	2	10.3	-0.41	0.022	
2077.9	246-265	2075.31	HMANGYQTVVSIANDPASAK	0	13.9	2.59	0.125	
2098.9	246-265	2097.3	HMANGYQTVVSIANDPASAK	0	3.2	1.6	0.076	Na ⁺ adduct
2225.2	438-455	2223.35	VHEYNGEMHTFSDQWGER	0	83.3	1.85	0.083	
2243.2	75-94	2247.48	DERQFGSLQDALTRLNAGVR	2	18.1	-4.28	0.190	
2266.7	9-30	2264.46	AATDALAANRAPTSVNAQEVHR	1	8.1	2.24	0.099	
2287.3	9-30	2286.45	AATDALAANRAPTSVNAQEVHR	1	1.4	0.85	0.037	Na ⁺ adduct
2695.1	506-527	2693.19	LWTLDDIKRLNCVFNPKAFN	4	4.8	1.91	0.071	
2752.7	456-476	2750.04	MWLAEPERYECQNIFEQYEGR	1	31.2	2.66	0.097	
2767.4	281-303	2767.31	YFTPVLGMLFEYGSFKVPEPWVK	2	17.5	0.09	0.003	
2958.6	337-360	2956.33	QDAYWAHHDLYLLAYALWPTGFFR	0	4.3	2.27	0.077	
3094.4	78-104	3098.56	QFGSLQDALTRLNAGVRVHPKWNEMTK	3	39.1	-4.16	0.134	
3094.4	361-385	3090.36	LALPDQEEMEWFEANYPGWYDHYGK	0	39.1	4.04	0.131	ambiguous
3113.1	394-419	3109.51	GCEDPSSGFIPLMWFIENNHPIYIDR	0	11.4	3.59	0.115	
3127.1	394-419	3125.51	GCEDPSSGFIPLMWFIENNHPIYIDR	0	8.4	1.59	0.051	oxidized +16
3144.1	62-88	3140.59	LIAKEYARMEAVKDERQFGSLQDALTR	4	4.5	3.51	0.112	
3219.1	105-134	3214.58	VVSNFLEVGEYNAIAATGMLWDSAQAAEQK	0	14.8	4.52	0.141	
3236.2	438-463	3236.53	VHEYNGEMHTFSDQWGERMWLAEPER	1	7.4	-0.33	0.010	

^aObserved and calculated are average masses. ^bMC reports the number of missed trypsin cleavage sites in the peptide.

Table 3.2. Sequence coverage of unmodified sMMO proteins following in-gel digestion.

Sample	MS method	Protein	Residues	
			observed (total)	% coverage
MMOH _α	MALDI-TOF	MMOH _α	361 (526)	69
MMOH _β	MALDI-TOF	MMOH _β	270 (388)	70
MMOH _γ	MALDI-TOF	MMOH _γ	154 (169)	91
MMOB	MALDI-TOF	MMOB	141 (141)	100
MMOR-Fd	MALDI-TOF	MMOR-Fd	95 (98)	97
MMOB _{S_VS_B}	MALDI-TOF	MMOB	112 (141)	80
MMOH _α :MMOB _{S_VS_B}	MALDI-TOF	MMOH _α	208 (526)	40
		MMOB	66 (141)	47
MMOH _α :MMOR-Fd	MALDI-TOF	MMOH _α	402 (526)	76
		MMOR-Fd	76 (98)	78
MMOH:MMOR-Fd	Off-line HPLC/ MALDI-TOF	MMOH _α	416 (526)	79
		MMOH _β	326 (388)	84
		MMOH _γ	169 (169)	100
		MMOR-Fd	95 (98)	97
MMOH _α :MMOR-Fd	LC-QoTOF	MMOH _α	359 (526)	68
		MMOH _β	126 (388)	32
		MMOR-Fd	90 (98)	92

Table 3.3. Peptides Observed in MALDI-TOF Spectrum of MMOH_α:MMOR-Fd Cross-Link.

observed MH ⁺ (Da)	pro- tein	range	calculated MH ⁺ (Da)	sequence	MC	Δ (Da)	rel. area.	% error	modification
807.4	H _α	324-330	807.88	YGVESPR	0	0.48	3.4	0.059	
814.0	H _α	176-182	815	TIGPLWK	0	1	15.9	0.123	
829.5							2		
836.4							1.7		
845.5							0.2		
864.6							0.3		
869.9							0.5		
882.0	Fd	44- 51	882.99	EGGCATCK	0	0.99	1.4	0.112	
888.6							3.7		
895.0	H _α	386-391	895.99	IYEEWR	0	0.99	13.9	0.110	
910.5							0.6		
916.8							0.7		
926.9							1.5		
969.8							1.5		
977.0	H _α	58- 65	977.19	EQFKLIAK	1	0.19	0.7	0.019	
979.9	H _α	70- 77	978.11	MEAVKDER	1	-1.79	0.9	-0.183	
985.8	H _α	50- 57	985.15	YKMANETK	1	-0.65	0.4	-0.066	
997.5							1.4		
1003.6	H _α	44- 51	1003.19	TKYATKYK	2	-0.41	0.6	-0.041	
1033.5	H _α	296-303	1033.26	FKVEPWVK	1	-0.24	19.5	-0.023	
1041.1							0.4		
1049.1							1.1		
1056.4							0.7		
1095.0	H _α	41- 49	1096.23	NNRTKYATK	2	1.23	18.7	0.112	
1105.3	H _α	321-330	1106.27	LGKYGVESPR	1	0.97	0.6	0.088	
1111.1							2.3		

-cont'd-

Table 3.3., cont'd. Peptides Observed in MALDI-TOF Spectrum of MMOH_α:MMOR-Fd Cross-Link.

observed MH ⁺ (Da)	pro- tein	range	calculated MH ⁺ (Da)	sequence	MC	Δ (Da)	rel. area. %	error	modification
1130.0	H _α	176-185	1131.43	TIGPLWKGMK	1	1.43	0.7	0.126	
1146.1							0.5		
1154.9							0.5		
1159.7	H _α	506-514	1160.36	LWTLDDIKR	1	0.66	2	0.057	
1172.3							2.3		
1190.1	Fd	23- 33	1190.3	SDEDVITAALR	0	0.2	1.2	0.017	
1219.3	H _α	515-524	1219.49	LNCVFKNPVK	1	0.19	19.8	0.016	
1226.0	H _α	52- 61	1226.4	MANETKEQFK	1	0.4	1.7	0.033	
1236.4	H _α	78- 88	1236.37	QFGSLQDALTR	0	-0.03	34.2	-0.002	
1256.7	Fd	34- 43	1256.49	QNIFLMSSCR	0	-0.21	3.8	-0.017	
1270.9	Fd	52- 62	1271.39	ALCSEGDYDLK	0	0.49	1.5	0.039	ambiguous
1270.9	H _α	95-104	1270.5	VHPKWNETMK	1	-0.4	1.5	-0.031	assignment
1286.1	H _α	176-186	1287.62	TIGPLWKGMKR	2	1.52	1.2	0.118	
1304.3	H _α	503-513	1304.49	GDKLWTLDDIK	1	0.19	4.1	0.015	
1322.5							0.8		
1333.1	H _α	420-431	1333.59	VSQVPFCPSLAK	0	0.49	9.5	0.037	
1344.5							1.2		
1357.2	H _α	494-505	1357.54	TLIAQPHVRGDK	1	0.34	4.5	0.025	Na ⁺ adduct
1372.1	H _α	31- 40	1371.54	WLQSFNWDFK	0	-0.56	27.5	-0.041	
1392.5	H _α	135-146	1391.57	NGYLAQVLDEIR	0	-0.93	17.4	-0.067	
1460.9	H _α	503-514	1460.67	GDKLWTLDDIKR	2	-0.23	21.1	-0.016	
1467.1	H _α	477-489	1466.68	ELSEVIAELHGLR	0	-0.42	21	-0.029	
1638.7	H _α	308-320	1637.84	WVYEDWGGIWIGR	0	-0.86	24.3	-0.053	
1653.1	H _α	52- 65	1651.97	MANETKEQFKLIAK	2	-1.13	6.8	-0.068	
1669.9							2.4		
1706.7	H _α	514-527	1708.04	RLNCVFKNPVKAFN	3	1.34	0.6	0.078	

-cont'd-

Table 3.3., cont'd. Peptides Observed in MALDI-TOF Spectrum of MMOH_α:MMOR-Fd Cross-Link.

observed MH ⁺ (Da)	pro- tein	calculated range MH ⁺ (Da)	sequence	MC	Δ (Da)	rel. area. %	error	modification
1712.9						1.4		
1756.7	H _α	31- 43	1755.93 WLQSFNWDFKNNR	1	-0.77	73.6	-0.044	
1771.2						8.9		
1788.1						0.6		
1804.0	H _α	147-160	1803.01 HTHQCAVYVNYFFAK	0	-0.99	7.1	-0.055	
1822.3	Fd	84- 98	1821.04 TYPKTDLEIELPYTH	1	-1.26	3	-0.069	
1846.0	H _α	78- 94	1847.08 QFGSLQDALTRLNAGVR	1	1.08	1.5	0.058	
1858.4	H _α	266-280	1857.03 YLNTDLNNAFWTQQK	0	-1.37	79.6	-0.074	
1880.6	H _α	89-104	1881.21 LNAGVRVHPKWNEMTK	2	0.61	3.7	0.032	
1892.8						3.7		
1922.9	H _α	62- 77	1923.24 LIAKEYARMEAVKDER	3	0.34	1.7	0.018	
2006.8						1.5		
2078.1	H _α	246-265	2075.31 HMANGYQTVVSIANDPASAK	0	-2.79	9.6	-0.134	
2132.8	Fd	44- 62	2135.36 EGGCATCKALCSEG DYDLK	1	2.56	2.4	0.120	
2166.8						2.3		
2196.8	H _α	70- 88	2195.46 MEAVKDERQFGSLQDALTR	2	-1.34	2.1	-0.061	
2225.6	H _α	438-455	2223.35 VHEYNGEMHTFSDQWGER	0	-2.25	100	-0.101	
2241.0						16.3		
2266.4	H _α	9- 30	2264.46 AATDALAANRAPTSVNAQEVHR	1	-1.94	3.9	-0.086	
2278.4	H _α	9- 30	2280.46 AATDALAANRAPTSVNAQEVHR	1	2.06	4.5	0.090	oxidized +16
2344.6	H _α	494-513	2342.69 TLIAQPHVRGDKLWTLDDIK	2	-1.91	1.5	-0.082	Na ⁺ adduct
2468.0						2.4		
2481.9						2.2		
	tryp-							
2555.8	sin	100-125	2552.25 VASISLPTSCASAGTQCLISGWGNTK	0	3.5	2.2	0.137	
2662.3	H _α	19- 40	2661.94 APTSVNAQEVHRWLQSFNWDFK	1	-0.36	3.7	-0.014	

-cont'd-

Table 3.3., cont'd. Peptides Observed in MALDI-TOF Spectrum of MMOH_α:MMOR-Fd Cross-Link.

observed MH ⁺ (Da)	pro- tein	range	calculated MH ⁺ (Da)	sequence	MC	Δ (Da)	rel. area. %	error	modification
2754.5	H _α	456-476	2750.04	MWLAEPERYECQNIFEQYEGR	1	-4.46	6.4	-0.162	
2814.8							0.7		
2874.6	Fd	63- 87	2876.28	GCSVQALPPEEEEEGLVLLCRTPK	1	1.68	3.2	0.058	
3042.9	H _α	19- 43	3046.33	APTSVNAQEVHRWLQSFNWDFKNNR	2	3.43	1.9	0.113	
3095.2	H _α	78-104	3098.56	QFGSLQDALTRLNAGVRVHPKWNEMTK	3	3.36	12	0.108	
3111.8	H _α	394-419	3109.51	GCEDPSSGFIPLMWFIEENHPYIDR	0	-2.29	2.6	-0.074	
3220.3	H _α	105-134	3214.58	VVSNFLEVGEYNAIAATGMLWDSAQAAEQK	0	-5.72	15.4	-0.178	
3235.4	H _α	494-520	3238.83	TLIAQPHVRGDKLWTLDDIKRLNCFVK	4	3.43	1.7	0.106	
3985.2	H _α	361-391	3983.32	LALPDQEEMEWFEANYPGWYDHYGKIYEEWR	1	-1.88	4.8	-0.047	oxidized +16
4096.1							2		
4605	H _α	266-303	4605.32	YLNTDLNNAFWTQQKYFTPVLGMLFEYGSKFKVEPWVK	3	0.32	3.4	0.007	

Table 3.4. Tandem MS Data for Peptide with Cross-Link between MMOR-Fd Glu56 and MMOH_α N-terminus.

Mass (mono.)	Mass (calc.)	Difference (Da)	error (ppm)	structure	ion type
1942.144	1941.935	0.208	107	ALCSE(ALSTATK)GDYDLK	precursor
1871.028	1870.898	0.130	70	LCSE(ALSTATK)GDYDLK	y ₁₀
1833.131				?	
1758.013	1757.814	0.199	113	CSE(ALSTATK)GDYDLK	y ₉
1739.973	1739.804	0.168	97	CSE(ALSTATK)GDYDLK	y ₉ -H ₂ O
1682.905	1682.754	0.151	89	ALCSE(ALSTATK)GDYD	b ₉
1597.954	1597.784	0.170	107	SE(ALSTATK)GDYDLK	y ₈
1510.896	1510.752	0.144	95	E(ALSTATK)GDYDLK	y ₇
1498.777				?	
1322.718	1322.589	0.129	98	ALCSE(A)GDYDLK	b ₁ ^α
1232.722	1232.615	0.107	87	ALCSE(ALSTATK)	b ₅
1214.729	1214.615	0.114	94	ALCSE(ALSTATK)	b ₅ -H ₂ O
1048.584	1048.490	0.094	90	CSE(ALSTATK)	y ₉ b ₅
1030.560	1030.480	0.080	77	CSE(ALSTATK)	y ₉ b ₅ -H ₂ O
709.400	709.328	0.072	101	GDYDLK	y ₆
690.456	690.399	0.057	82	ALSTATK	y ₇ ^α
652.380	652.307	0.073	111	DYDLK	y ₅
619.423	619.354	0.069	111	LSTATK	y ₆ ^α
537.335	537.280	0.055	102	YDLK	y ₄
506.325	506.270	0.055	108	STATK	y ₅ ^α
450.192				?	
419.292	419.238	0.053	128	TATK	y ₄ ^α
393.154				?	
374.261	374.217	0.044	118	DLK	y ₃
344.193	344.160	0.033	97	ALC	b ₃
318.240	318.190	0.050	156	ATK	y ₃ ^α
278.127				?	
259.220	259.190	0.030	117	LK	y ₂
247.170	247.153	0.017	67	TK	y ₂ ^α
241.181				?	
184.147	184.129	0.018	95	AL	b ₂
156.145	156.134	0.011	73	AL	a ₂
146.126	146.106	0.020	140	K	y ₁ ^(α)
135.085	135.030	0.055	409	Y	immonium
132.056	132.030	0.026	198	C	immonium
128.114				?	
85.104	85.080	0.024	286	L	immonium

Table 3.5. Tandem MS Data for Peptide with Cross-Link between Fd Glu91 and MMOH_α N-terminus.

Mass (mono.)	Mass (calc.)	diff	error (ppm)	structure	ion
2002.249	2002.030	0.219	109	TDLE(ALSTATK)IELPYTH	precursor
1786.114	1785.950	0.164	92	LE(ALSTATK)IELPYTH	y ₉
1673.039	1672.870	0.169	101	E(ALSTATK)IELPYTH	y ₈
1485.983	1485.800	0.183	123	TDLE(ALSTATK)IEL	b ₇
1372.880	1372.716	0.164	119	TDLE(ALSTATK)IE	b ₆
1243.803	1243.674	0.129	103	TDLE(ALSTATK)I	b ₅
1215.806	1215.679	0.127	105	TDLE(ALSTATK)I	a ₅
1130.708	1130.590	0.118	104	TDLE(ALSTATK)	b ₄
914.593	914.520	0.073	80	LE(ALSTATK)	y ₉ b ₄
886.575				?	
871.531	871.440	0.091	104	IELPYTH	y ₇
773.505				?	
758.440	758.360	0.080	106	ELPYTH	y ₆
756.480				?	
740.414	740.350	0.064	86	ELPYTH	y ₆ -H ₂ O
690.491	690.390	0.101	147	ALSTATK	y ₇ ^α
629.395	629.320	0.075	120	LPYTH	y ₅
624.385				?	
619.426	619.350	0.076	123	LSTATK	y ₆ ^α
516.295	516.233	0.062	120	PYTH	y ₄
506.342	506.270	0.072	142	STATK	y ₅ ^α
498.302				?	
491.296	491.260	0.036	74	LSTAT	y ₆ ^α b ₁ ^α
419.278	419.238	0.040	96	TATK	y ₄ ^α
419.278	419.180	0.098	234	YTH	y ₃
402.227				?	
361.203				?	
329.204	329.167	0.037	112	TDL	b ₃
318.228	318.190	0.038	119	ATK	y ₃ ^α
301.207	301.172	0.035	115	TDL	a ₃
256.147	256.117	0.030	118	TH	y ₂
247.186	247.153	0.033	133	TK	y ₂ ^α
238.146				?	
232.159				?	
216.104	216.082	0.022	103	TD	b ₂
194.116				?	
188.118	188.089	0.029	152	TD	a ₂
170.106				?	
155.094	155.070	0.024	155	H	y ₁
128.095				?	
85.103	85.080	0.023	270	I/L	immonium
73.064	73.047	0.017	226	T	immonium

Table 3.6. NADH Oxidation Activity of sMMO with MMOR or MMOR EQ2.

MMOH:MMOB:MMOR (μM)	NADH oxidation activity (turnover number, s^{-1})		Ratio
	MMOR	MMOR EQ2	
0:0:1	0.187	0.161	86%
1:2:1	0.679	0.425	63%
1:2:2	0.814	0.517	64%

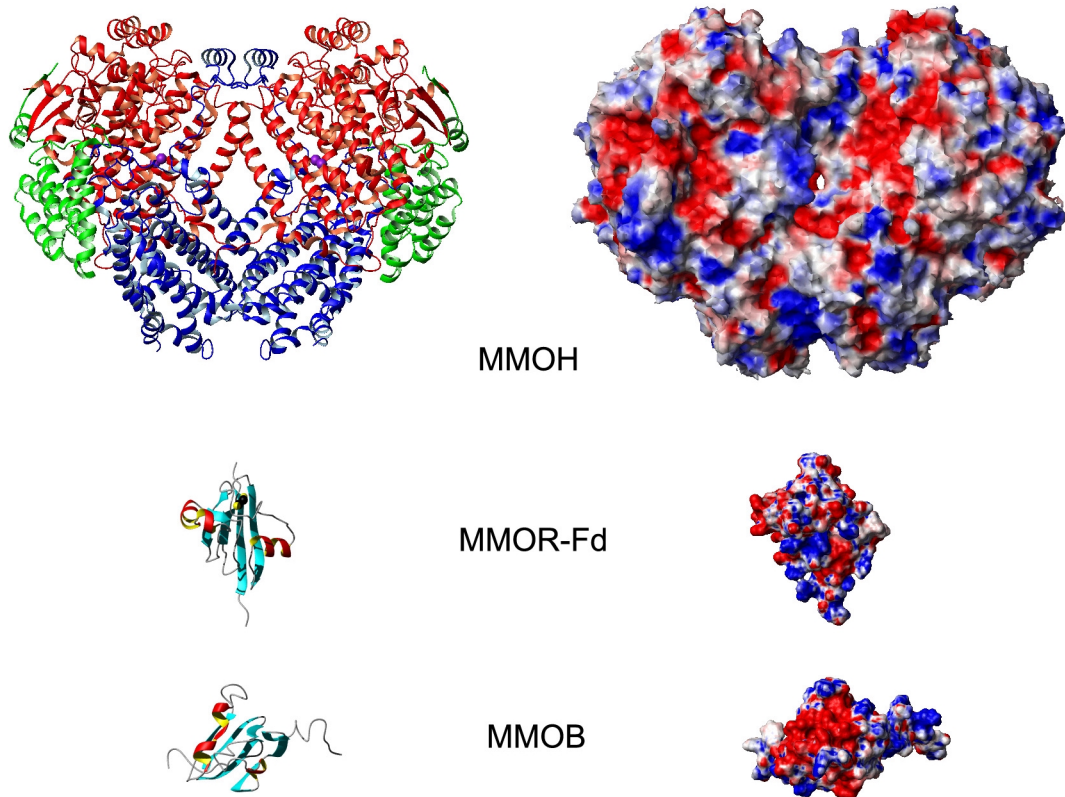


Figure 3.1. 3-D Structures of sMMO component proteins. Ribbon diagrams of MMOH, MMOR-Fd and MMOB are shown on the left. For MMOH, the alpha subunits are red, beta subunits blue, and the gamma subunits green. On the right, in the same orientation, are presented electrostatic surfaces of the proteins. Red and blue regions represent areas of negative and positive charge, respectively. Structures are drawn to the same scale. MMOR-Fd and MMOB are oriented to reveal the faces predicted by NMR studies to contact MMOH.^{6,7}

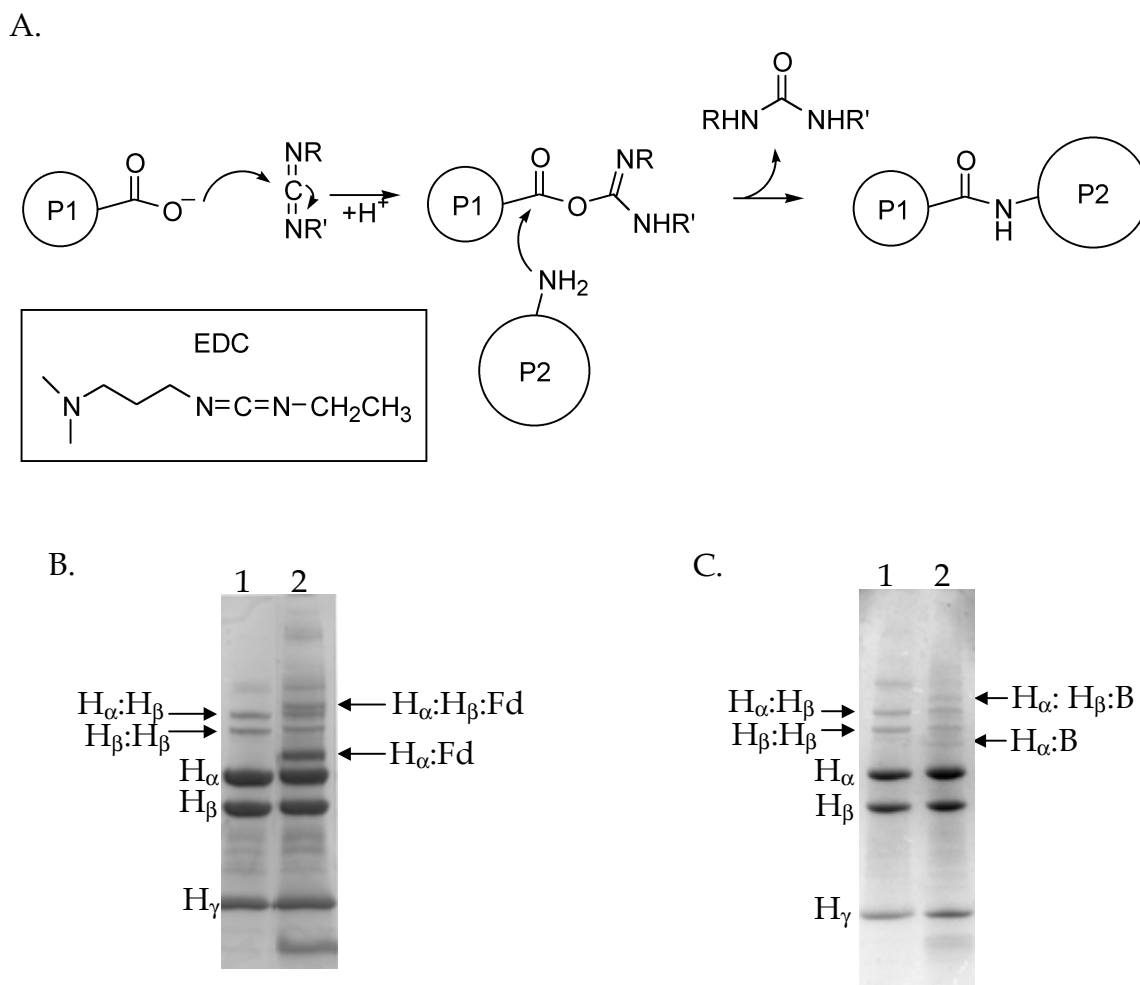
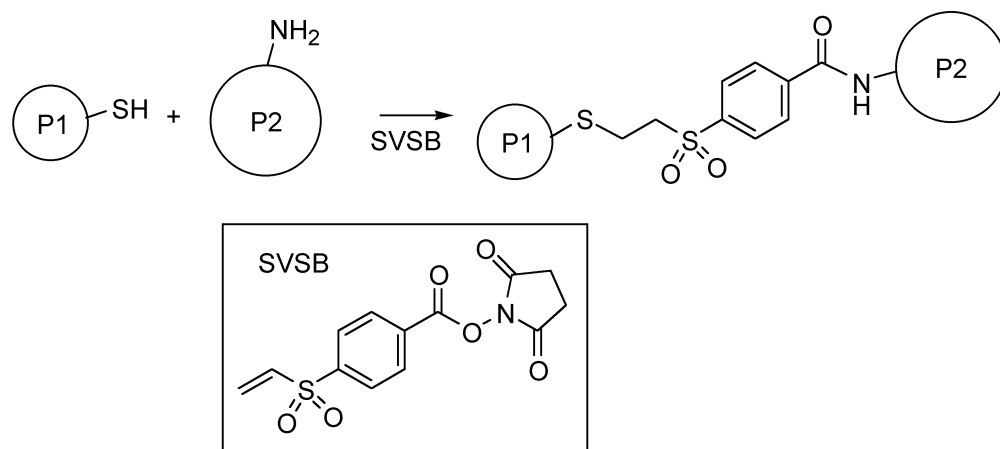
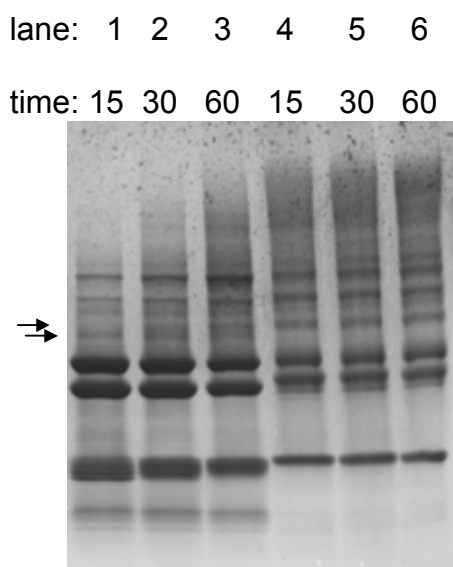


Figure 3.2. (A) Structure of EDC and mechanism of EDC-promoted crosslinking between carboxylate and amine functional groups of proteins P1 and P2. EDC is considered a zero-length cross-linker because the new bond formed includes no atoms of the cross-linker. (B) SDS-PAGE analysis of EDC-promoted crosslinking of MMOH (lane 1) and the MMOH/MMOR-Fd complex (lane 2). Subunits of MMOH are indicated as H_α , H_β , and H_γ . Crosslinked bands are indicated with arrows. (C) SDS-PAGE analysis of EDC-promoted crosslinking of MMOH (lane 1) and the MMOH/MMOB complex (lane 2). Labels as in (B).

A.



B.



C.

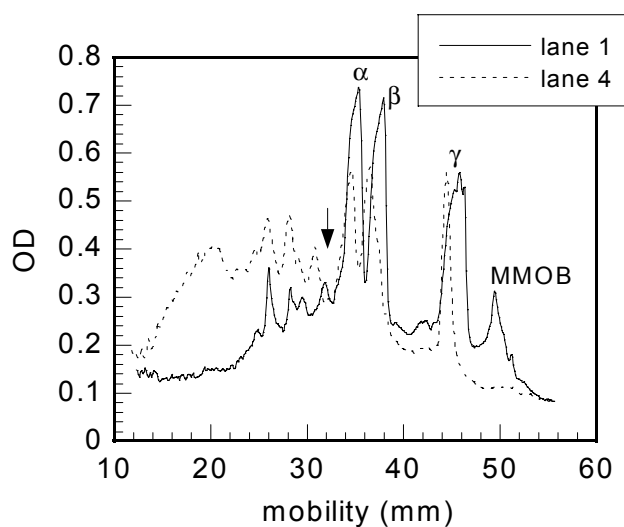


Figure 3.3. (A) Structure of SVSB and its means of protein cross-linking. (B) Time-dependent cross-linking of MMOB to MMOH with SVSB. MMOB was incubated with 10 mM SVSB for 2 hr at room temperature prior to addition of MMOH for up to 1 h (lanes 1-3). In lanes 4-6, no MMOB was present. Arrows indicate bands formed differentially in presence or absence of MMOB. (C) Deniso-tometry traces of lanes 1 and 4; the arrow indicates the band arising from cross-linking between MMOH and MMOB.

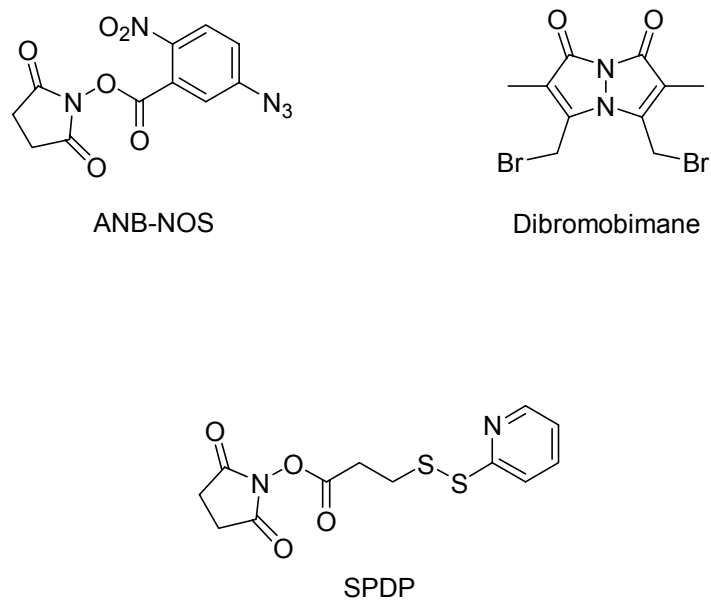


Figure 3.4. Structures of cross-linking reagents that failed to facilitate cross-link formation of complexes between sMMO components.

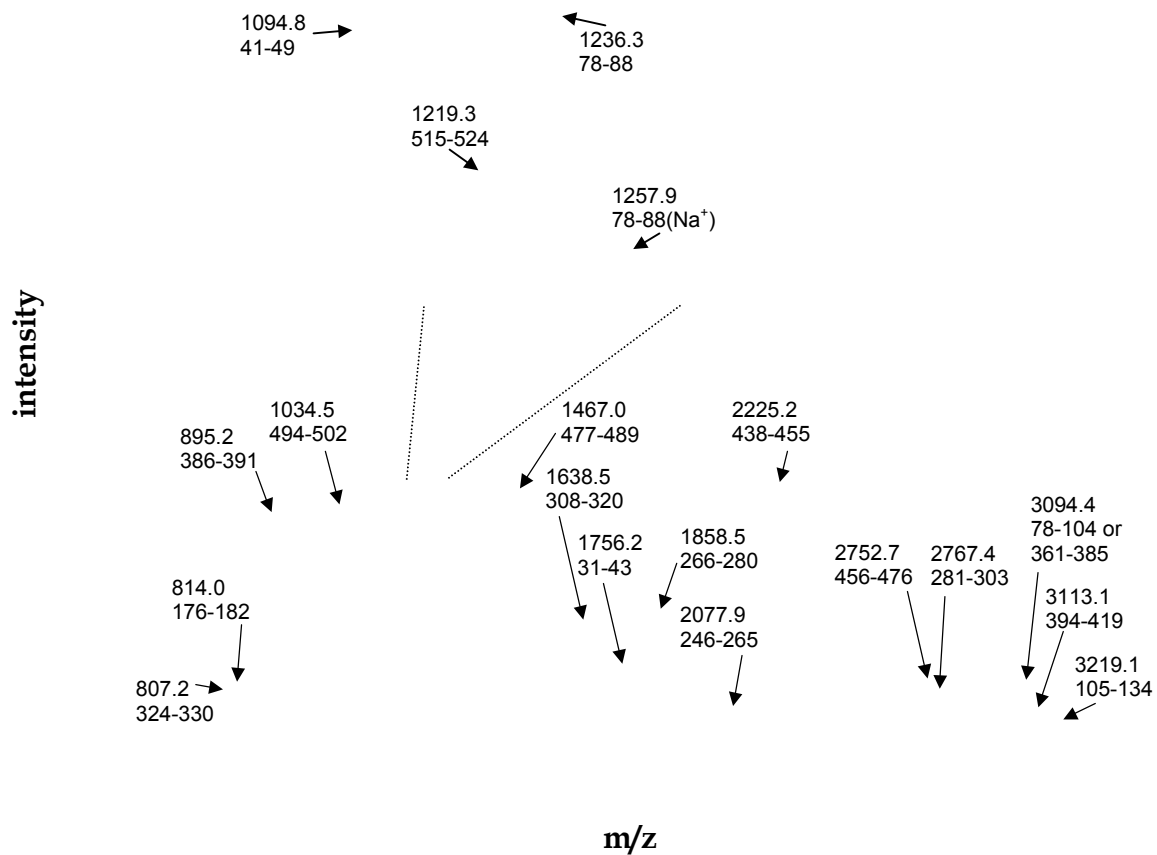


Figure 3.5. MALDI-TOF spectrum of in-gel tryptic digest of MMOH_α. Peaks are labelled with measured m/z (MH⁺) and the assigned residues of MMOH_α. See also Table 3.1 and Figure 3.6.

```

1  -ALSTATKAATDALAANRAPTSVNAQEVHRLQSFNWDFKNNRTKYATKYKMANETKEQF
    <-----><-----> <----->
    <-----Na+><-----><----->
    <-----><----->

61  KLI AKEYARMEAVKDERQFGSLQDALTRLNAGVRVHPKWNETMKVVSNFLEVGEYNAIAA
    <-----><-----><----->
    <----->
    <-----Na+>

121  TGMLWDSAQA AEQNGYLAQVLDEIRHTHQCAYVNYFFAKNGQDPAGHNDARTRTIGPL
    -----><-----> <----->
    <-----Na+>

181  WKG MKRVFSDGFISGDAVECSLNLQLVGEACFTNPLIVAVTEWAAANGDEITPTVFLSIE
    ->

241  TDEL RHMANGYQTVVSIANDPASAKYLN TDLNNAFWTQQKYFTPVLGMLFEYGSKFKEP
    <-----><-----><----->

301  WVKTWDRWVYEDWGGIWIWIRLGLGKYGVESPRSLKDAQDAYWAHHDLYLLAYALWPTGFFR
    --> <-----> <-----> <----->

361  LALPDQEEMEWFEANYPGWYDHYGKIYEEWRARGCEDPSSGFIPLMWFIENNHPIYIDRV
    <-----> <-----><-----><----->
    <-----Na+>

421  SQVPFCPSLAKGASTLRVHEYNGEMHTFSDQWGERMWLAEPERYEQNIFEQYEGRELSE
    -----> <-----> <----->
    <-----><-----><-----><----->

481  VIAELHGLRSDGKTLIAQPHVRGDKLWTLDDIKRLNLCVFKNPVKAFN
    -----> <-----> <----->
    -----OX> <-----><----->
    <----->

```

Figure 3.6. Sequence of MMOH_α and tryptic digest peptides observed by MALDI-TOF following SDS-PAGE and in-gel digestion. See also Figure 3.5 and Table 3.1.

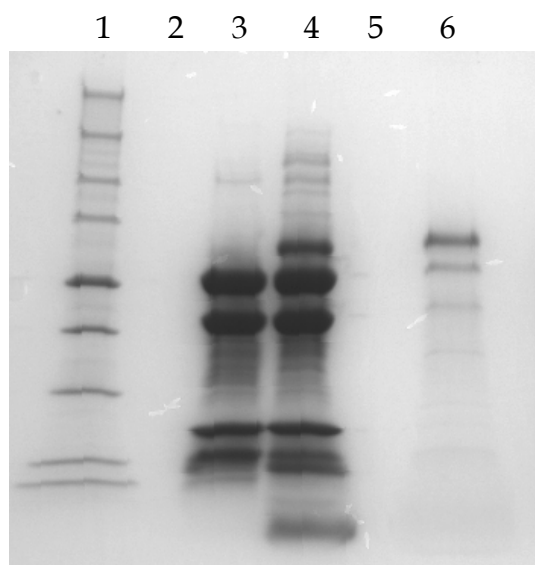


Figure 3.7. Recovery of gel purified MMOH_{α} :MMOR-Fd by electroelution. Lane 1, molecular weight markers; lane 2, empty; lane 3, MMOH/MMOR-Fd mixture; lane 4, MMOH:MMOR-Fd cross-linking reaction; lane 5, empty; lane 6, MMOH_{α} :MMOR-Fd after electroelution.

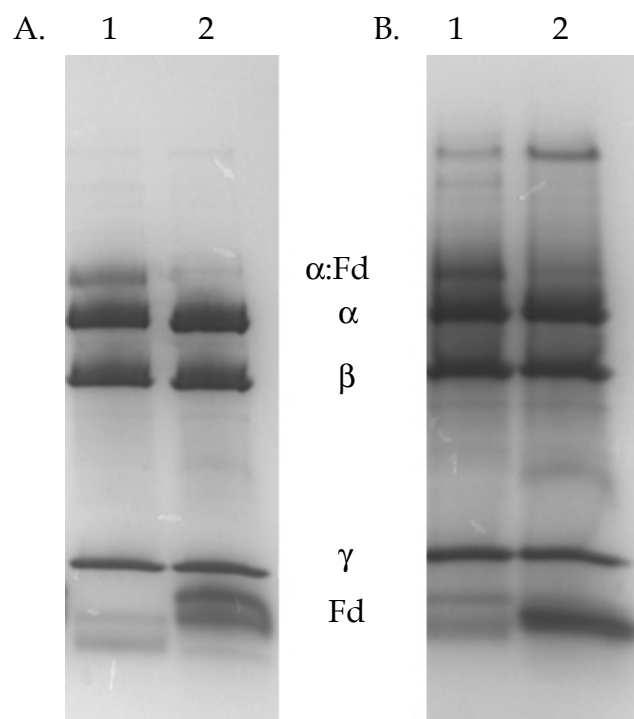


Figure 3.8. Inability of MMOR-Fd His₆ fusion constructs to cross-link to MMOH.

(A) Lane 1, Products of EDC reaction with MMOH and MMOR-Fd. Lane 2, Products of EDC reaction with MMOH and N-terminally His-tagged MMOR-Fd.

(B). As in (A), but lane 2 contains C-terminally His-tagged MMOR-Fd.

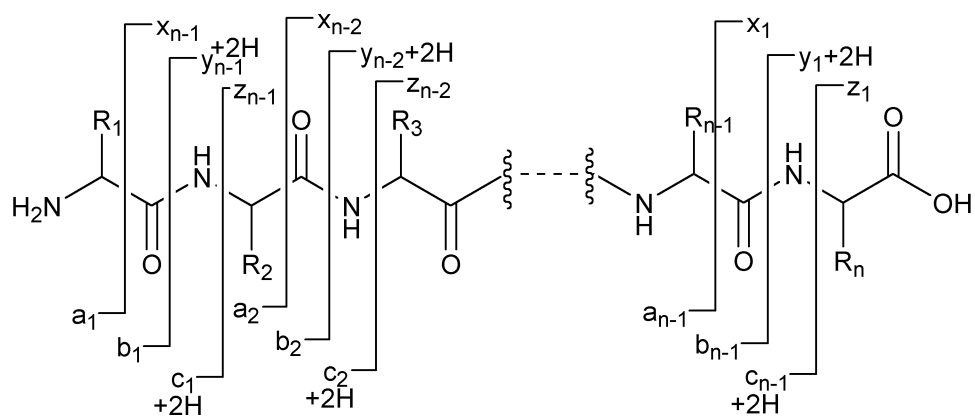


Figure 3.9. Nomenclature of peptide fragment ions.³²

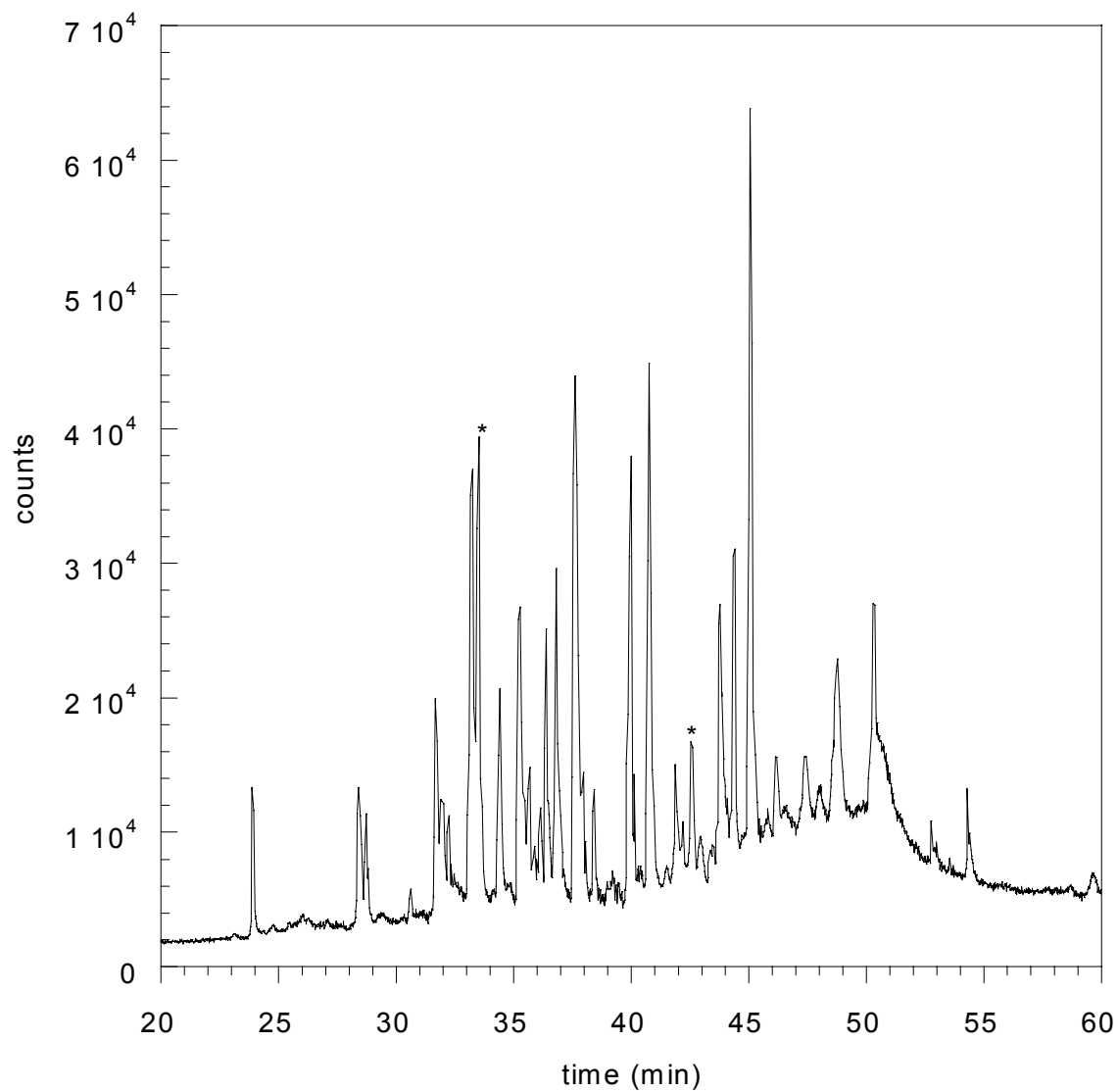


Figure 3.10. Total ion chromatogram from LC-QoTOF analysis of a tryptic digest of MMOH_α;MMOR-Fd. Peak marked with * are cross-linked peptides, as described in the text.

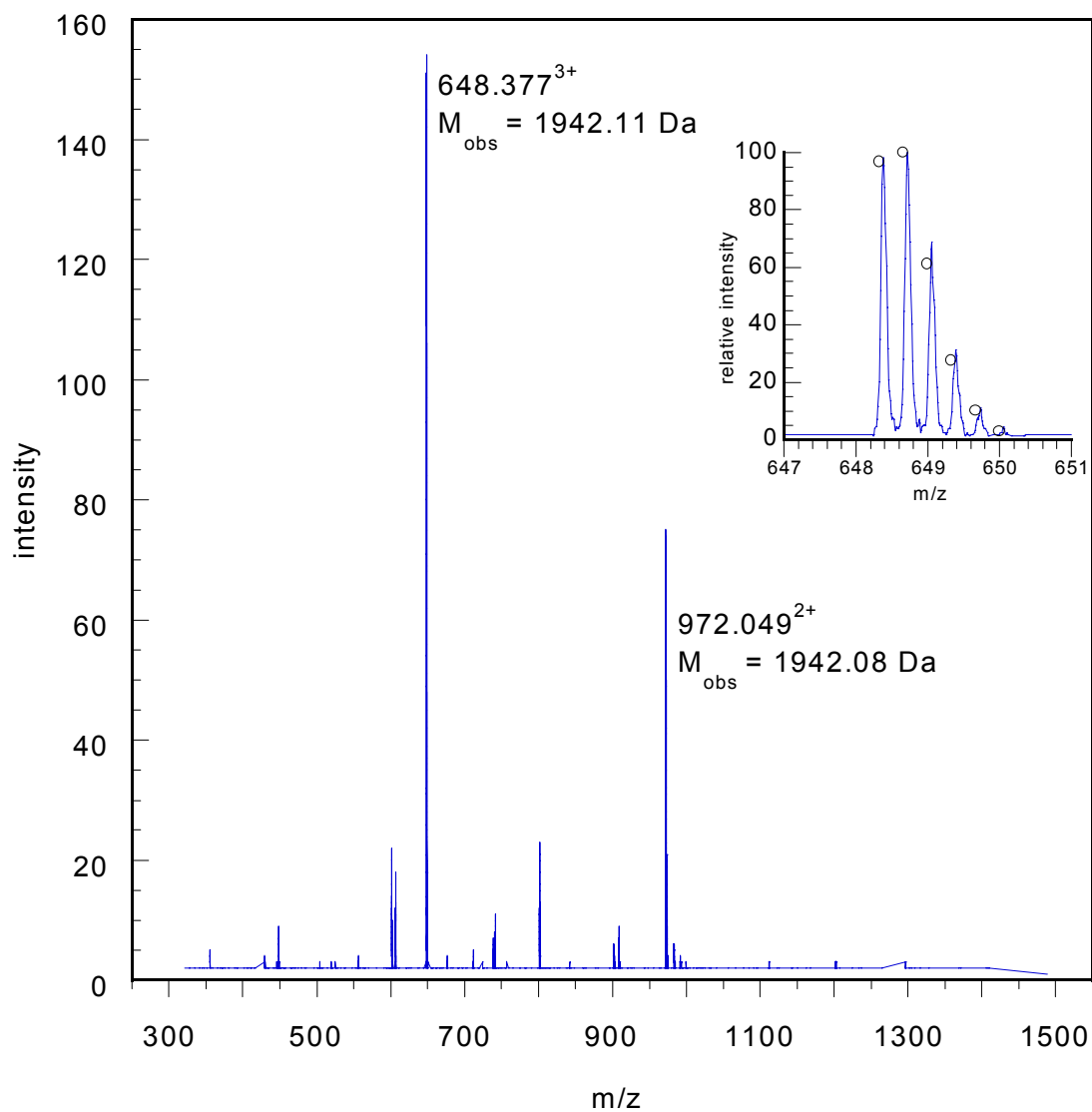


Figure 3.11. Mass spectrum recorded at 33.5 minutes during LC-MS run (peak starred in Figure 3.10). The two labelled peaks represent the doubly- and triply-charged ions of a peptide with $M_{\text{obs}} = 1942.15 \text{ Da}$. The inset shows the isotopic cluster for the 3^+ ion. The predicted isotopic distribution calculated for the structure shown in Figure 3.12A is shown by the small circles.

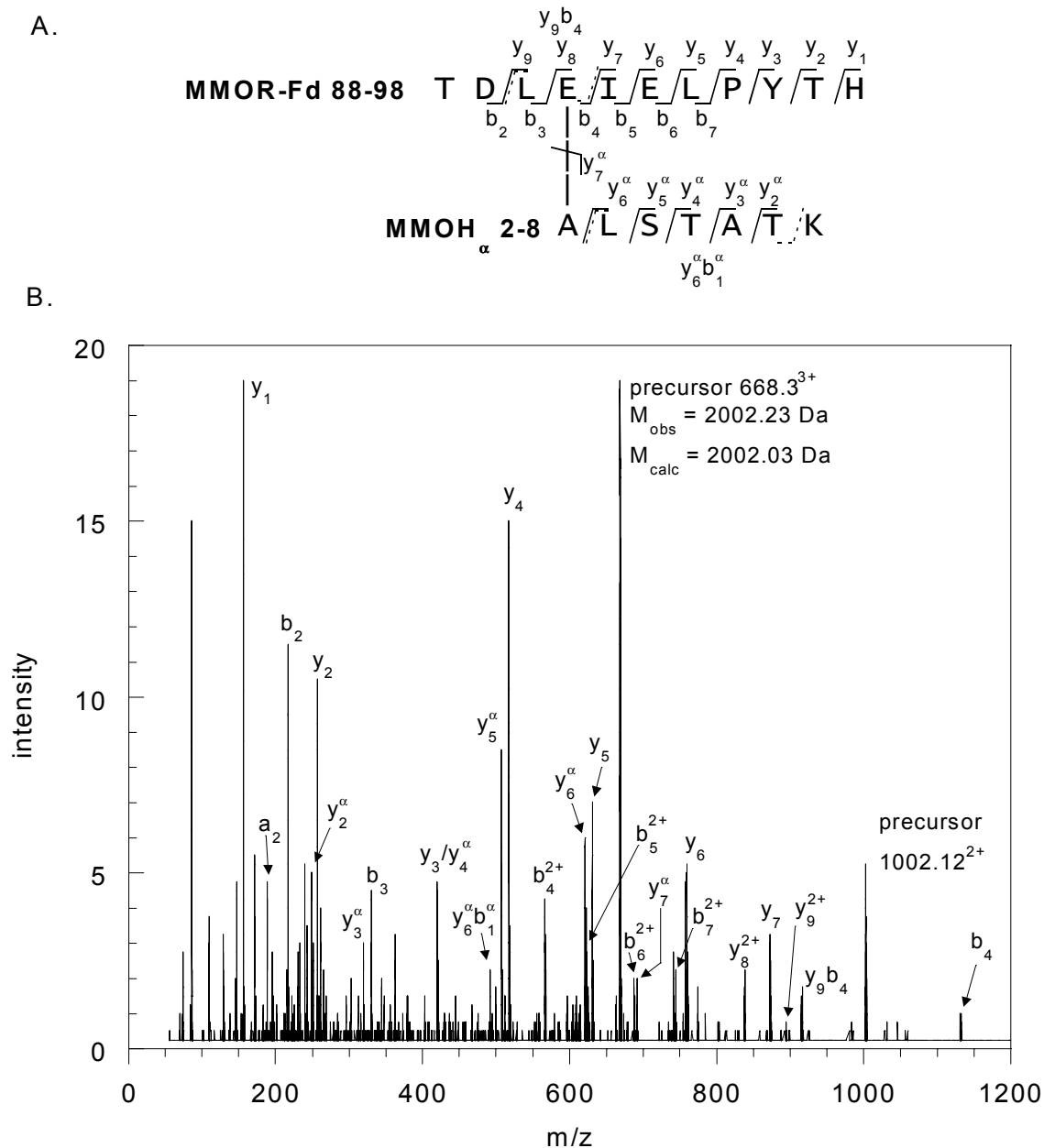
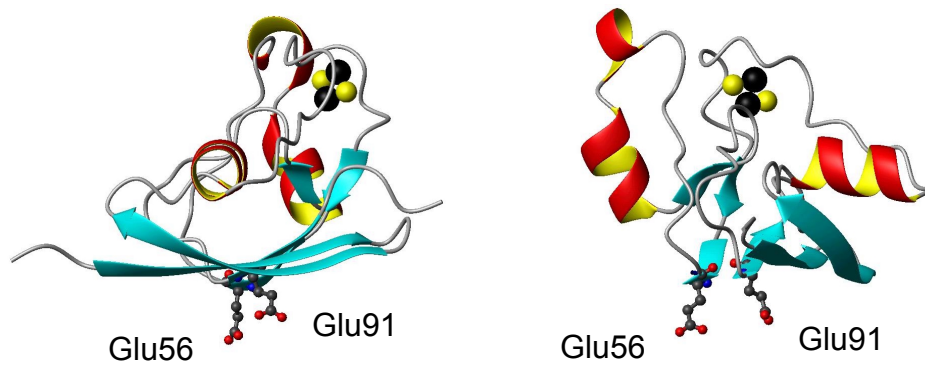


Figure 3.13. Cross-link between MMOH_α N-terminus and MMOR-Fd Glu91. (A) Structure of cross-link, indicating fragments observed in the tandem mass spectrum. Fragments are named according to Figure 3.9, with the α superscript indicating numbering with respect to the portion of the peptide derived from MMOH_α. (B) Tandem mass spectrum recorded upon fragmentation of precursor ions 668.3³⁺ and 1002.12²⁺.

A.



B.

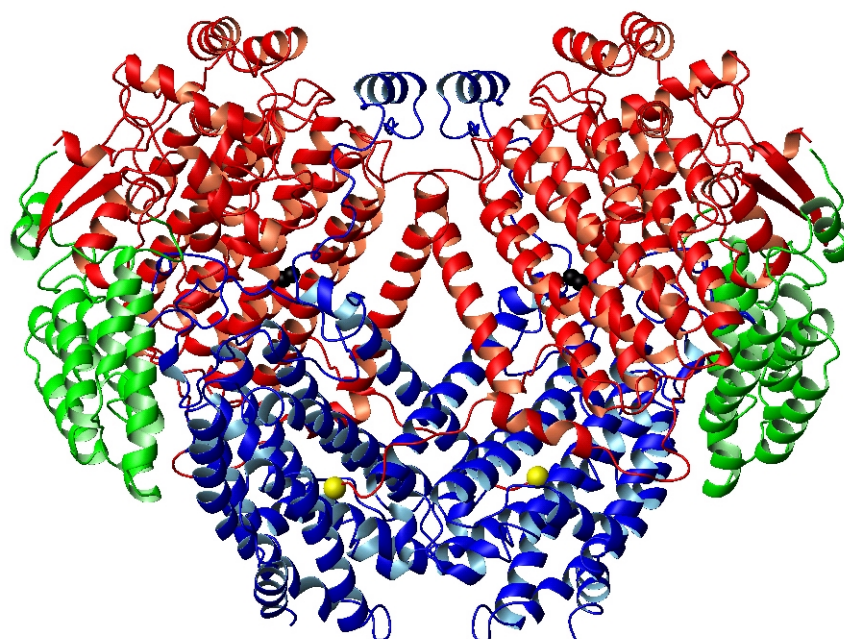


Figure 3.14. Locations of cross-linking residues. (A) Two views of MMOR-Fd, with Glu56 and Glu91 shown in ball-and-stick. (B) MMOH, with MMOH $_{\alpha}$ Ala15 alpha carbon depicted as a yellow sphere.

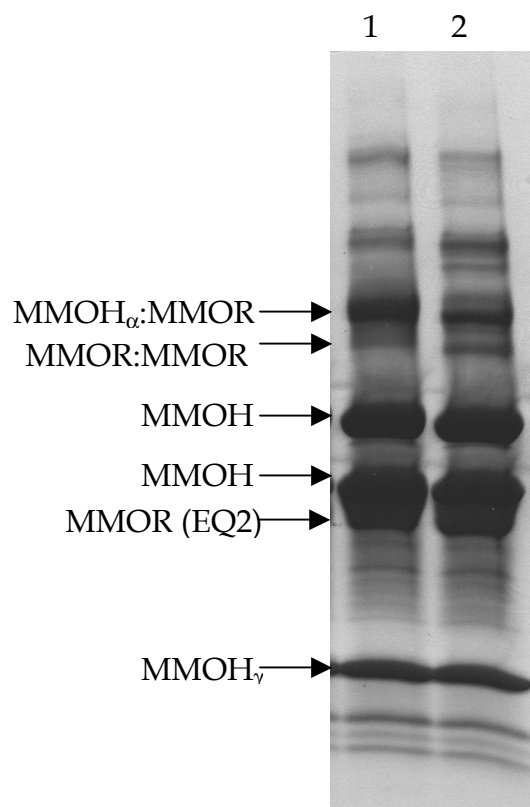


Figure 3.15. EDC cross-linking of MMOH to MMOR or MMOR EQ2. Lane 1, MMOH and MMOR cross-linking. Lane 2, MMOH and MMOR EQ2 cross-linking.

Chapter Four:

Cationic Species Can Be Produced in Soluble Methane Monooxygenase-Catalyzed Hydroxylation Reactions; Radical Intermediates Are Not Formed

Introduction^{1,2}

Soluble methane monooxygenase (MMO) systems from methanotrophic bacteria contain hydroxylase enzymes (MMOH) that have a diiron moiety at the active site. The MMOH enzymes efficiently oxidize methane to methanol, one of the more remarkable reactions in nature. Several intermediates in the catalytic cycle of MMOH accumulate and have been characterized spectroscopically.³ The mechanisms of catalytic hydroxylation of unactivated C-H bonds by these enzymes are not fully understood, however, and remain a subject of considerable research effort. The MMO hydroxylation reactions could be related to hydroxylations by cytochrome P450 enzymes.⁴

Various mechanistic probes have been employed in studies of the two well-characterized MMO systems, those from *Methylococcus capsulatus* (Bath) and *Methylosinus trichosporium* OB3b. The results from oxidations of chiral (by virtue of isotopic substitution) alkanes^{5,6} and hypersensitive cyclopropane-based probes^{7,8} are in general agreement that the "lifetimes" of putative radicals in MMO hydroxylation are too short for true intermediates and thus implicate insertion reactions. In a study reported by our groups in 1996, the regiochemistry of reactions of methylcubane with the tert-butoxyl radical, a cytochrome P450 enzyme, and the sMMO system from *M. capsulatus* (Bath) were compared.⁹ We reported that, whereas P450 oxidized all C-H positions to give four alcohol products, the MMO oxidation gave only cubylmethanol, and we proposed an insertion mechanism for this oxidation. Recently, it was reported¹⁰ that the *M.*

trichosporium OB3b sMMO system oxidized methylcubane at all positions and that the major alcohol product derived from rearrangement of the cubylcarbiny radical, thus implicating a radical-based mechanism.

We have now reinvestigated methylcubane oxidation by both sMMO systems. All positions of this substrate are indeed functionalized by both sMMOs, and the observed¹⁰ rearranged alcohol is produced in both cases. That rearranged product, however, is shown here to be the known compound 1-homocubanol, which derives not from a radical intermediate but from a cationic rearrangement process. In addition, a hypersensitive cyclopropane-based mechanistic probe designed to distinguish between "radical" and "cationic" species was successfully oxidized by the *M. capsulatus* (Bath) MMOH, and a cationic rearrangement product was detected as a minor product. The results clearly implicate a "cationic" component in MMO hydroxylation reactions as previously suggested,¹¹ and they support the conclusion that more than one species can effect oxidation in sMMO systems.³

Experimental Section

Protein Purification. MMOH from both *M. capsulatus* (Bath) and *M. trichosporium* OB3b was prepared from cell paste of the respective bacteria as described. *M. capsulatus* (Bath) MMOR and MMOB were purified from recombinant systems, whereas *M. trichosporium* OB3b MMOR and MMOB were purified from the native organism, following literature procedures.^{12,13}

Preparation of Substrates and Authentic Product Standards. Methylcubane (**1**) and its hydroxylation products (**2-4**) were prepared according to literature methods.^{9,14} Probe **5** and its products **6-8** were prepared using methods analogous to those used in preparation of the t-butoxyl analog of **5**.⁸

Substrate Hydroxylation and Product Analysis. MMOH, MMOB, and MMOR were combined in a 1:2:0.25 μ M ratio in 25 mM MOPS at pH 7.0. A volume of substrate was added to make a saturated solution. NADH was added to a final concentration of 1 mM to initiate the reaction, and the hydroxylation was allowed to proceed 10-20 min at 45 °C. Reactions were quenched by addition of methylene chloride. Hydroxylation products were extracted three times, and the organic layers combined and concentrated. GC and GC-MS analysis was performed by using a 30 m carbowax column with a Hewlett-Packard 5980 gas chromatograph with either flame ionization or mass spectrometric detection.

Results and Discussion

Oxidations of methylcubane (**1**) were performed with the MMO systems from *M. capsulatus* (Bath) and *M. trichosporium* OB3b.^{13,15,16} GC and GC-MS analyses of the product mixtures revealed the presence of five alcohol products from the *M. c.* (Bath) MMO oxidation (Figures 4.1 and 4.2). The same products were formed in lower yields in the *M. t.* OB3b MMO oxidation, although the GC traces from these reactions were complicated by the presence of traces of compounds from the enzyme mixture. Oxidation of methylcubane by the purified

cytochrome P450 isozyme CYP2B18 in a control experiment gave a clean product sample containing four of the five alcohol products. Cubylmethanol (**2**) was identified by comparison of the GC retention time and mass spectral fragmentation pattern to those of the known compound.¹⁷ The three methylcubanol products (**3**) were identified by their mass spectral fragmentation patterns.¹⁰

The fifth alcohol product from MMO oxidations, the major product, was not formed in detectable amounts in the P450-catalyzed oxidation. This product is the rearranged compound 1-homocubanol (**4**) as determined by comparison of its GC retention time and mass spectral fragmentation pattern (Figure 4.3) to those of an authentic sample.¹⁴ The mass spectrum of **4** is the same as that shown for the major product of methylcubane hydroxylation by *M. trichosporium* OB3b sMMO, and there is little doubt that this product is the one ascribed to a radical rearrangement.¹⁰ A control experiment showed that alcohol **2** does not convert to **4** during steady-state hydroxylation of acetonitrile, a good substrate for MMO.¹⁸ To confirm product identities, a mixture of products from *M. c.* (Bath) was treated with acetic anhydride and pyridine to give acetates that were characterized by GC and GC-MS. We found five acetates with GC retention times and MS fragmentation patterns matching those of the known^{9,19} acetates from products **2** and **3** and the acetate prepared from **4**. An authentic sample was prepared reaction of **4** with acetic anhydride and pyridine as described.⁹

The production of 1-homocubanol in the MMO oxidations is inconsistent with formation of a radical intermediate. The cubylcarbinyl radical ring opens by

a series of bond cleavage reactions that destroy the cube skeleton.^{17,20} Ring expansion of the cubylmethyl system to the homocubyl system is only known for cationic rearrangements.^{14,17,21}

In a typical experiment, the GC (flame-ionization) peak areas of the alcohols obtained from the *M. c.* (Bath) MMO oxidation of methylcubane were in the ratio 2:3:5 (**2**, **3**, **4**), and product **4** was the major one with *M. t.* OB3b as previously reported (Figure 4.2).¹⁰ The methylcubanol and 1-homocubanol are unstable compounds, however, and a control reaction containing a small amount of cubylmethanol (**2**) showed that this compound was consumed by MMO. The product instabilities might account for the differences in the present results from those we previously found with *M. c.* (Bath).⁹ These instabilities require that the product ratios be considered as qualitative rather than quantitative measures.

An alternative molecular architecture that can distinguish between radical and cationic intermediates is afforded by the hypersensitive cyclopropane-based probe **5** (Figure 4.4). The cyclopropylcarbonyl radical from **5** rearranges to give products derived from a benzylic radical, but the cyclopropylcarbonyl cation ring opens to the methoxy-substituted cation (an oxonium ion).^{22,23} In the context of hydroxylation reactions, alcohol **7** is produced from radicals, whereas aldehyde **8** is formed from cations via hydrolysis of the initially formed hemiacetal and isomerization of the β,γ -unsaturated aldehyde in buffer. We attempted to oxidize the tert-butoxy analogue of probe **5** with the *M. c.* (Bath) sMMO system, but that compound was an inhibitor and not a substrate.⁸ Probe **5** is a substrate, albeit a

relatively poor one, for the sMMO from *M. c.* (Bath). Oxidations of **5** gave the un-rearranged alcohol **6** as the major product and both radical-derived (**7**) and cation-derived (**8**) rearrangement products. Two diastereomers of **7** are possible, but only one was detected. The product alcohols from the MMO oxidation were identified by comparisons of GC retention times and mass spectral fragmentation patterns to those of authentic samples.²⁴ The yields of alcohols were small, rendering quantitation difficult, but the product ratios from four oxidations of **5** were 80:14:6 for **6**, **7**, and **8**, respectively.

The accumulated results of probe studies of MMO hydroxylations permit the firm conclusion that no radical intermediates are formed. No radical rearrangement products are found from methylcubane. From the product ratio and rate constant for ring opening of the cyclopropylcarbinyl radical derived from probe **5**,²³ the "radical" lifetime was computed to be 250 fs, corresponding to a capture rate constant of $4 \times 10^{12} \text{ s}^{-1}$. The small amounts of inversion found in MMO hydroxylations of chiral ethane^{5,6} and butane⁶ require that the lifetimes of the "radicals" be on the order of 100-200 fs. A variety of hypersensitive cyclopropane-based radical probes that cannot distinguish between radical and cationic rearrangements previously gave little or no rearrangement products^{3,7} requiring that the "radical" lifetimes be 250 fs or less. The lifetimes being measured are those of transition states.

In contrast to the firm conclusion regarding the absence of radical intermediates, the detection of cationic rearrangement products from both methylcu-

bane and probe **5** permits only qualitative statements. The lifetimes, and even the identities, of these species cannot be determined. A similar conclusion resulted from *M. t.* OB3b sMMO oxidation of 1,1-dimethylcyclopropane which gave some 1-methylcyclobutanol product.¹¹ Candidates for the cationic species are protonated alcohols.

The oxidations catalyzed by the sMMO and cytochrome P450 enzyme systems have been compared;⁴ the intermediate oxidants inferred for P450²⁴⁻²⁶ may be related to the spectroscopically observed intermediates found for MMO (Figure 4.5). Two electrophilic oxidant forms, presumed to be the hydroperoxo-iron complex and the iron-oxo, are implicated in the P450 reactions.²⁵ The hydroperoxo-iron species apparently hydroxylates by inserting "OH⁺" into C-H bonds to give protonated alcohols, whereas the iron-oxo inserts an oxygen atom.²⁴ Single turnover experiments with MMOH from *M. c.* (Bath) indicate that either H_{peroxo} or, more likely, a hydroperoxo species derived therefrom by protonation is an active oxidant that can epoxidize propene. This oxidant did not hydroxylate saturated hydrocarbons methane, ethane, or propane, however.³ If the hydroperoxo species in MMOH were able to hydroxylate the substrates studied here, then, by analogy to P450, the first-formed products would be the protonated alcohols **9** and **10** produced by insertion of "OH⁺" into C-H bonds (Figure 4.6).

Conclusion

In summary, the rearrangement product from sMMO-catalyzed hydroxylation of methylcubane is 1-homocubanol, formed via a cationic rearrangement, and production of a cationic species was also demonstrated in sMMO hydroxylation of probe **5**. Mechanistic studies of sMMO hydroxylations involving chiral alkanes,^{5,6} hypersensitive cyclopropane-based probes,^{7,8} methylcubane, and probe **5** provide compelling evidence that true radical intermediates are not produced in these reactions. The implication of a cationic component in MMO hydroxylations complicates the mechanistic picture, but it reinforces some similarities between P450 and MMO hydroxylation reactions.⁴ Future mechanistic studies of MMO hydroxylations of alkanes will focus on further assessment of the oxidizing properties of the H_{peroxo} and Q intermediates, both of which can be observed.

References

- 1) This work was previously published in a slightly different form. See reference 2.
- 2) Choi, S. Y.; Eaton, P. E.; Kopp, D. A.; Lippard, S. J.; Newcomb, M.; Shen, R. *N. J. Am. Chem. Soc.* **1999**, *121*, 12198-12199.
- 3) Valentine, A. M.; Stahl, S. S.; Lippard, S. J. *J. Am. Chem. Soc.* **1999**, *121*, 3876-3887.
- 4) Stahl, S. S.; Lippard, S. J. ; Ferreira, G. C., Moura, J. J. G. and Franco, R., Ed.; Wiley-VCH: Weinheim, 1999, pp 303-321.
- 5) Priestley, N. D.; Floss, H. G.; Froland, W. A.; Lipscomb, J. D.; Williams, P. G.; Morimoto, H. *J. Am. Chem. Soc.* **1992**, *114*, 7561-7562.
- 6) Valentine, A. M.; Wilkinson, B.; Liu, K. E.; KomarPanicucci, S.; Priestley, N. D.; Williams, P. G.; Morimoto, H.; Floss, H. G.; Lippard, S. J. *J. Am. Chem. Soc.* **1997**, *119*, 1818-1827.
- 7) Liu, K. E.; Johnson, C. C.; Newcomb, M.; Lippard, S. J. *J. Am. Chem. Soc.* **1993**, *115*, 939-947.
- 8) Valentine, A. M.; LeTadic-Biadatti, M. H.; Toy, P. H.; Newcomb, M.; Lippard, S. J. *J. Biol. Chem.* **1999**, *274*, 10771-10776.
- 9) Choi, S. Y.; Eaton, P. E.; Hollenberg, P. F.; Liu, K. E.; Lippard, S. J.; Newcomb, M.; Putt, D. A.; Upadhyaya, S. P.; Xiong, Y. S. *J. Am. Chem. Soc.* **1996**, *118*, 6547-6555.
- 10) Jin, Y.; Lipscomb, J. D. *Biochemistry* **1999**, *38*, 6178-6186.

- 11) Ruzicka, F.; Huang, D. S.; Donnelly, M. I.; Frey, P. A. *Biochemistry* **1990**, *29*, 1696-1700.
- 12) Gassner, G. T.; Lippard, S. J. *Biochemistry* **1999**, *38*, 12768-12785.
- 13) Fox, B. G.; Froland, W. A.; Jollie, D. R.; Lipscomb, J. D. *Methods Enzymol.* **1990**, *188*, 191-202.
- 14) Della, E. W.; Janowski, W. K. *J. Org. Chem.* **1995**, *60*, 7756-7759.
- 15) Pilkington, S. J.; Dalton, H. *Methods Enzymol.* **1990**, *188*, 181-190.
- 16) Willems, J. P.; Valentine, A. M.; Gurbiel, R.; Lippard, S. J.; Hoffman, B. M. *J. Am. Chem. Soc.* **1998**, *120*, 9410-9416.
- 17) Eaton, P. E.; Yip, Y. C. *J. Am. Chem. Soc.* **1991**, *113*, 7692-7697.
- 18) Stahl, S. S.; Francisco, W. A.; Merckx, M.; Klinman, J. P.; Lippard, S. J. *J. Biol. Chem.* **2001**, *276*, 4549-4553.
- 19) Eaton, P. E.; Yang, C. X.; Xiong, Y. S. *J. Am. Chem. Soc.* **1990**, *112*, 3225-3226.
- 20) Choi, S. Y.; Eaton, P. E.; Newcomb, M.; Yip, Y. C. *J. Am. Chem. Soc.* **1992**, *114*, 6326-6329.
- 21) Eaton, P. E. *Angew. Chem. Int. Ed.* **1992**, *31*, 1421-1436.
- 22) Newcomb, M.; Chestney, D. L. *J. Am. Chem. Soc.* **1994**, *116*, 9753-9754.
- 23) Le Tadic-Biadatti, M. H.; Newcomb, M. *J. Chem. Soc., Perkin Trans. 2* **1996**, 1467-1473.
- 24) Newcomb, M.; Shen, R.; Choi, S. Y.; Toy, P. H.; Hollenberg, P. F.; Vaz, A. D. N.; Coon, M. J. *J. Am. Chem. Soc.* **2000**, *122*, 2677-2686.

- 25) Vaz, A. D. N.; McGinnity, D. F.; Coon, M. J. *Proc. Natl. Acad. Sci. USA* **1998**, *95*, 3555-3560.
- 26) Toy, P. H.; Newcomb, M.; Coon, M. J.; Vaz, A. D. N. *J. Am. Chem. Soc.* **1998**, *120*, 9718-9719.

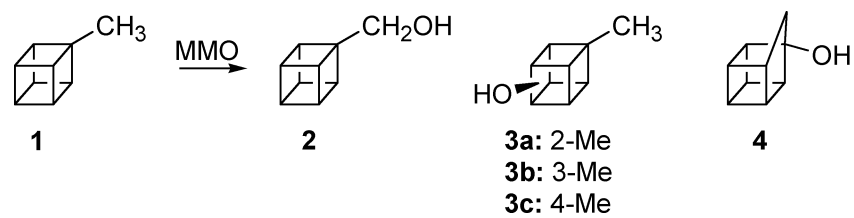


Figure 4.1. Hydroxylation of methylcubane (1) by MMO affords products 2-4.

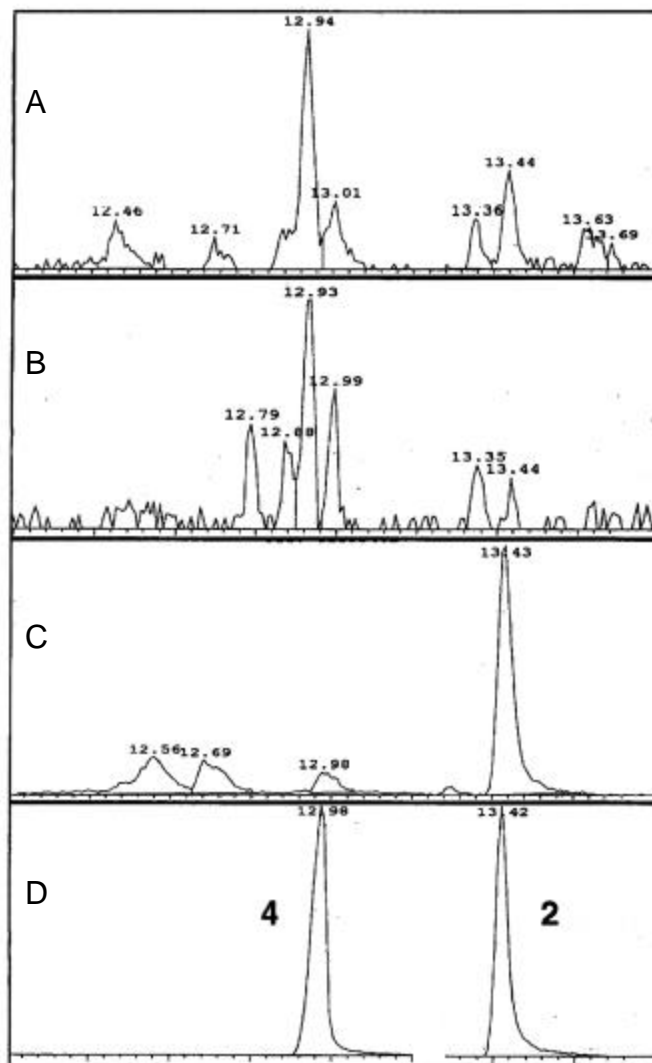


Figure 4.2. GC (FID) traces of products from reactions of methylcubane with (A) the MMO system from *M. capsulatus* (Bath), (B) the MMO system from *M. trichosporium* OB3b, and (C) the cytochrome P450 isozyme CYP2B1. (D) A composite of GC traces from authentic cubylmethanol (**2**) and authentic 1-homocubanol (**4**). Peaks corresponding to the three methylcubanol peaks (**3**) products elute at 12.5, 12.7 and 13.0 minutes; although these peaks are virtually absent in the trace from the *M. t.* OB3b product mixture, they were observed at higher sensitivity.

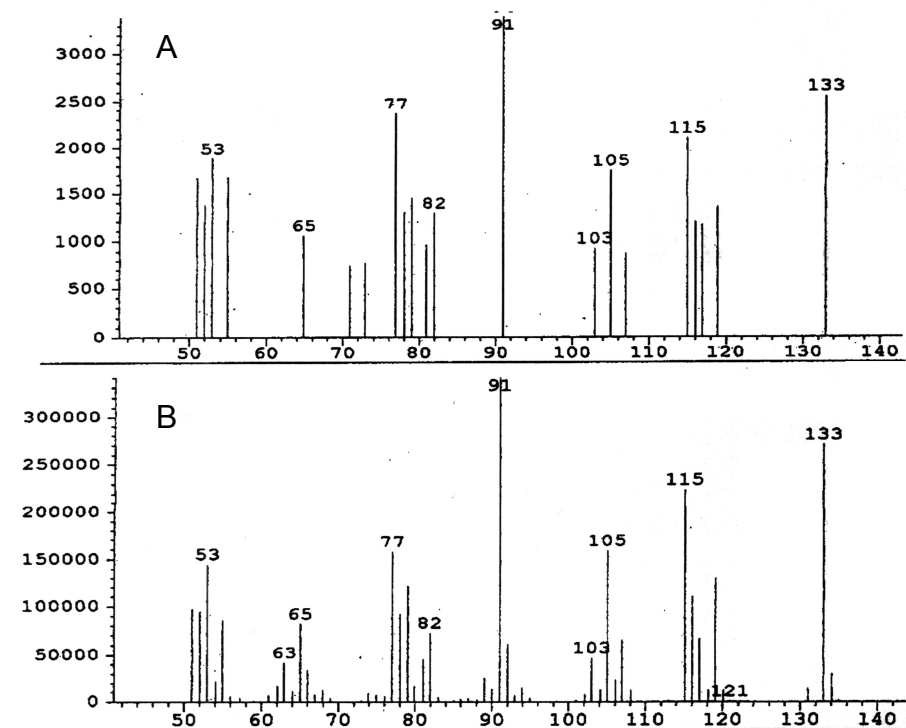


Figure 4.3. (A) Mass spectral fragmentation pattern of the major product from the oxidation of methylcubane by the MMO system from *M. capsulatus* (Bath). (B) Fragmentation pattern from authentic 1-homocubanol (**4**). The absence of some small peaks in the pattern from the enzyme product mixture results from the fact that the concentration of **4** in the authentic samples was about 100 times greater than that in the enzyme product mixture.

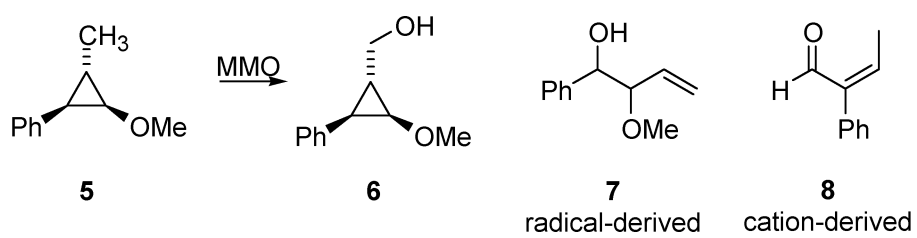


Figure 4.4. Hydroxylation of radical probe substrate **5** by MMO affords products **6-8**.

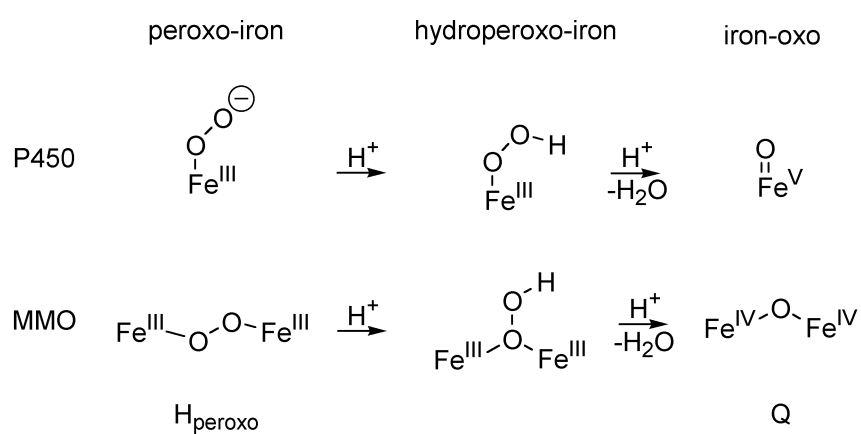


Figure 4.5. Possible analogous intermediates produced in cytochrome P450- and MMOH-catalyzed oxidations. The porphyrin ring of P450 and the surrounding protein of MMO have been removed. The intermediates for P450 and the hydroperoxo complex for MMO are putative. The structures shown are speculative.

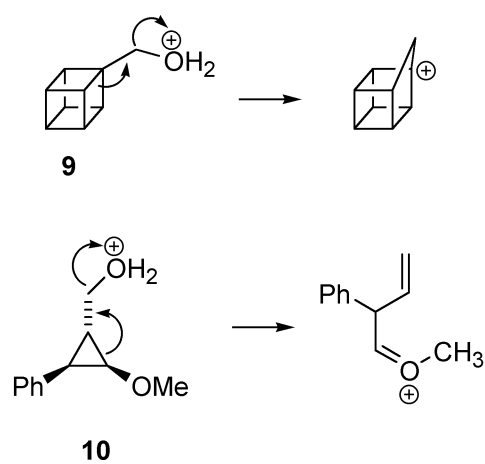


Figure 4.6. Cation-derived products may form by loss of water with coupled cationic rearrangement from protonated alcohols **9** and **10**.

Chapter Five:

Evaluation of Norcarane as a Probe for Radicals in Cytochrome P450- and Soluble Methane Monooxygenase-Catalyzed Hydroxylation Reactions

Introduction^{1,2}

The mechanistic details of enzyme-catalyzed hydroxylation reactions have intrigued chemists and biochemists for decades. Alkane hydroxylations are readily achieved at ambient temperature by the cytochrome P450 enzymes (P450),³ and methane monooxygenase (MMO) enzymes can accomplish the remarkably difficult hydroxylation of methane with ease.⁴ Simple chemical analogies of these reactions are not available, although some complex model systems behave in a biomimetic manner. Increasingly sophisticated instrumental techniques⁵⁻⁷ and high-level computational studies⁸⁻¹¹ undoubtedly provide important details about the mechanisms of the hydroxylation reactions, but much information currently available comes from probe studies that seek evidence for transients formed in the reactions.

Mechanistic probe substrates for oxidations are straightforward in concept, although interpreting the implications of their application can sometimes be difficult. One identifies a characteristic process of a transient of interest, such as a cation or radical, and then employs a substrate that might be used to detect the formation of the transient. For example, oxidation of a chiral compound at the asymmetric center might occur with racemization if a long-lived radical or cation formed in the reaction but with retention or possibly inversion if a concerted process occurred. Alternatively, a strained cyclopropyl substrate could ring open if a radical or cation were produced at the cyclopropylcarbinyl position but not

in a concerted process. Both chiral substrates and substituted cyclopropanes have been employed as probes of enzyme-catalyzed hydroxylation reactions.

One mechanistic probe that has been employed in studies of enzyme-catalyzed hydroxylations is bicyclo[4.1.0]heptane (norcarane). In principle, norcarane is a highly advanced probe because the radical and cation produced at C2, the cyclopropylcarbonyl position, react differently. The norcaran-2-yl radical ring opens predominantly (ca. 50:1) to the (2-cyclohexenyl)methyl radical,¹² and the rate constant for this ring opening reaction, $2 \times 10^8 \text{ s}^{-1}$, can be estimated from the results of tin hydride trapping studies¹² and the rate constant for reaction of a radical with tin hydride.¹³ C2 cationic species from norcarane react mainly by cleavage of the bridge bond to give ring-expanded products derived from 3-cycloheptanol, but cleavage of an exocyclic cyclopropyl bond to give products from (2-cyclohexenyl)methanol also occurs.¹⁴ The formation of the latter products from cationic reactions of 2-norcaranol appears to have been overlooked in previous studies that employed norcarane as a mechanistic probe. In addition, the cationic manifold is biased against ring cleavage in solvolytic reactions; for example, solvolyses of 2-norcaranol 3,5-dinitrobenzoate esters afforded mainly mixtures of endo- and exo-2-norcaranol.¹⁵

Norcarane was employed in mechanistic studies with cytochrome P450 by White et al.,¹⁶ but no rearranged alcohol products were detected. More recently, Austin et al. used norcarane in a study of hydroxylation by the AlkB hydroxylase

enzyme from *Pseudomonas oleovorans*.¹⁷ Consistent with earlier probe results that implicated a relatively long-lived radical intermediate in hydroxylations by this enzyme,¹⁸ they observed partial rearrangement in the alcohol products that led to an estimated radical lifetime in the oxidation reaction of about 1 ns.¹⁷ Quite recently, while the present work was in its final stages, Brazeau et al. reported a study of norcarane oxidation by the soluble methane monooxygenase (sMMO) from *Methylosinus trichosporium* (*Ms. trichosporium*) OB3b wherein small amounts of rearrangement products were found; the authors concluded that both a cationic species and a discrete radical intermediate were produced.¹⁹ Although evidence for cationic intermediates in sMMO hydroxylations had been reported previously,^{20,21} other probe studies of hydroxylation catalyzed by the sMMO of this species and by the related sMMO from *Methylococcus capsulatus* (*Mc. capsulatus*) (Bath) were consistent with reactions proceeding without formation of discrete radical intermediates.

The latter mechanistic inconsistency with norcarane is mirrored in oxidations that we have studied with both P450 and sMMO enzymes. We report here the results of hydroxylation of norcarane catalyzed by the sMMO enzyme from *Mc. capsulatus* (Bath). Norcarane hydroxylations by hepatic P450 enzymes were studied concurrently and in collaboration with Prof. Martin Newcomb and co-workers, and are included here for comparison. In all cases, small amounts of rearrangement products derived from putative cationic intermediates and radical intermediates were found, much like the recent results with *Ms. trichosporium*

OB3b. These results are in stark contrast to those obtained for the same enzymes with other probes. We conclude that mechanistic generalizations based on results with norcarane are unwarranted. The small amounts of rearrangement products likely result from multiple pathways in the enzyme-catalyzed hydroxylation reactions.

Experimental Section

Bicyclo[4.1.0]heptane²² (norcarane, **1**), 3-(hydroxymethyl)cyclohexene²³ (**2**), 3-cycloheptenol¹² (**3**), *endo*-bicyclo[4.1.0]heptan-2-ol²⁴ (*endo*-2-norcaranol, **4**), *endo*-bicyclo[4.1.0]heptan-3-ol²⁵ (*endo*-3-norcaranol, **6**), bicyclo[4.1.0]heptan-2-one²⁶ (2-norcaranone, **8**), and bicyclo[4.1.0]heptan-3-one²⁵ (3-norcaranone, **9**) were prepared by literature methods. *exo*-Bicyclo[4.1.0]heptan-2-ol (*exo*-2-norcaranol, **5**) was obtained as a mixture with **4** (70:30, 5:4) from LAH reduction of **8**,²⁶ and *exo*-bicyclo[4.1.0]heptan-3-ol (*exo*-3-norcaranol, **7**) was obtained as a mixture with **6** (13:87, 7:6) from LAH reduction of **9**.²⁵

Solvolysis Reactions. In a representative reaction, alcohol **4** (125 mg, 1.1 mmol) was added to a solution of freshly distilled MsCl (96 μ L, 1.21 mmol) and Et₃N (0.23 mL) in 10 mL of dry THF at -20 °C. After 1 h at -20 °C, the mixture was treated with 0.07 mL of water. The mixture was stirred at -20 °C for 1 h and at room temperature for 12 h. The reaction was quenched by addition of excess water, and products were isolated by an extractive workup (ether, acid). The ethereal solution was dried over MgSO₄ and analyzed by GC.

P450-Catalyzed Oxidations. The P450 enzymes were prepared as previously reported.²⁷⁻²⁹ In a typical reaction, a mixture of 1 nmol of P450 $\Delta 2B4$ and 2 nmol of P450 reductase was allowed to stand in an ice bath for 5 min. A mixture of 0.96 nmol of DLPC suspended in 20 mM potassium phosphate buffer (pH = 7.4), sonicated before use, was added to the enzyme mixture. The mixture was diluted to a volume of 2 mL with buffer. A solution of 10 μ L of **1** in MeOH (15 mg/mL) was added. The mixture was incubated at 37 °C for 5 min. The oxidation was initiated by the addition of NADPH buffer solution; the final concentration of NADPH was 1.2 mM. The mixture was gently shaken at 37 °C for 30 min and then extracted with CH_2Cl_2 (3×2 mL). The combined organic phase was dried (MgSO_4) and filtered. A solution of tridecane was added as an internal standard, and the solution was concentrated to ca. 0.05 mL by fractional distillation with a 60-70 °C oil bath.

The resulting mixture was analyzed by GC and GC-MS on 0.52 and 0.25 mm, respectively, Carbowax columns. Products **2** and **6** were not resolved and appeared as a merged peak. Whereas the MS of both **2** and **6** contained ions at $m/z = 79$, the MS of **2** had an ion at $m/z = 81$ that was not present in the MS of **6**. Using authentic samples of **2** and **6**, the relative intensities of the ions at $m/z = 79$ were determined as well as the relative intensities of the ions from **2** at $m/z = 79$ and $m/z = 81$. The ratio of **2:6** was then determined in the product samples from the GC-MS results and the measured ion ratios.

sMMO-Catalyzed Oxidations. The sMMO hydroxylase was purified from batch cultures of *Mc. capsulatus* (Bath) according to published procedures.³⁰ The reductase and coupling protein components of sMMO were purified from recombinant expression systems.^{30,31}

Norcarane hydroxylations with sMMO were carried out as follows. A 10 nmol portion of MMOH, 20 nmol of MMOB, and 5 nmol of MMOR were combined in a total volume of 400 μ L of 25 mM MOPS, pH 7.0, in a septum-capped vial. The enzyme was incubated for 1 min at 45 °C before addition of 8 μ L of norcarane (neat) was added by means of a gastight syringe. The reaction was initiated by addition of 1.6 μ mol of NADH and was incubated at 45 °C for 20 min with stirring. Addition of 2 mL of methylene chloride quenched the reaction by causing the proteins to precipitate. The organic layer was removed and the aqueous layer extracted twice more with 2 mL portions of methylene chloride each time. The organic layers were combined, dried with MgSO_4 , and filtered. The product mixture was concentrated by distillation, reducing the volume of the organic fraction from ~6 to ~0.5 mL. Concentrated extracts were analyzed by GC-MS as described above, and the yields are reported on the basis of the relative ionizations from each product.

Results

Enzyme-Catalyzed Oxidations. Norcarane (**1**) was oxidized with P450 enzymes that were overexpressed in *Escherichia coli* (*E. coli*) and purified. P450 2B4

is the phenobarbital-induced hepatic P450 from rabbit, and P450 Δ 2B4 is an expressed version of the same enzyme with a short deletion at the N-terminus. P450 Δ 2E1 is the truncated version of the ethanol-inducible hepatic P450 from rabbit, and P450 Δ 2E1 T303A is a mutant of this enzyme in which threonine in the active site was replaced with alanine. The preparations and purifications of these enzymes were reported previously.²⁷⁻²⁹ The reconstituted P450 enzyme preparations contained the purified P450 enzyme, 2 equiv of P450 reductase, and NADPH in DLPC liposomes in buffer solutions. The oxidation reactions were allowed to proceed for 30 min at 37 °C.

Norcarane also was oxidized with the sMMO system from *Mc. capsulatus* (Bath). In these reactions, the enzyme system was a 1:2:0.5 mixture of the hydroxylase, coupling protein, and reductase components. Reactions were conducted at 45 °C, the optimal growth temperature of the organism.

Following an extractive workup, products were identified by GC-mass spectral comparisons to authentic samples and quantitated by GC analysis. The products are shown in Figure 5.1. Oxidations at the 2- and 3-positions gave both *endo* and *exo* alcohols (**4-7**). Overoxidation of these alcohols gave the corresponding ketones **8** and **9** that were detected in low yields. In addition, small amounts of both possible rearranged products from oxidation of the C2 position, 3-(hydroxymethyl)cyclohexene (**2**) and 3-cycloheptenol (**3**), were detected in all cases. Table 5.1 lists the regioselectivity of the oxidations, the stereoselectivity in the alcohol products from oxidation at C2 and C3 of the substrate, and the per-

centages of rearrangement products **2** and **3** relative to the total amount of products from oxidation at C2.

The rearrangement products **2** and **3** are important with respect to mechanistic interpretations, and they were found in low yields. Various studies confirmed that these two products were formed in the oxidation reactions. In multiple run experiments, the deviations in yields of **2** and **3** were small. A product mixture from a P450 2B4 oxidation and one from an sMMO oxidation were analyzed in another laboratory using a different GC-MS protocol, and the results confirmed the presence of both **2** and **3**. [NOTE:GC-mass spectral analyses were conducted with a low-polarity column that gave a different order of product elution. We are grateful to Prof. J.T. Groves for providing us with these results.] In the case of P450 2B4, we determined the stability of **2** and **3**, as well as alcohol **4**, under enzyme-catalyzed hydroxylation conditions. In matched experiments, P450 2B4 oxidations were conducted with **1** and with mixtures of norcarane that contained products **2-4**. This type of control reaction provides realistic information about the stability of the products as they are being formed in the enzyme reactions because substrate **1** is always present in large excess during the reaction and might serve as a competitive inhibitor for oxidation of the small amounts of products. The results are listed in Table 5.2. Product **2** was slightly degraded in the control reaction, and product **3** was stable.

The major products were from oxidation of the C2 position of norcarane, consistent with the reduced C-H bond energy at a cyclopropylcarbonyl position

of about 3 kcal/mol.³² The relatively large differences in regioselectivity, stereoselectivity, and the amounts of rearrangement products formed between P450 Δ 2E1 and its T303A mutant are noteworthy because the mutation involves replacement of a highly conserved threonine that is thought to be involved in the protonation reactions in the evolution of the active oxidants. Similar differences in product distributions have been reported for this pair previously,^{29,33} and the T303A mutant gave larger amounts of cationic rearrangement products than the wild-type (wt) enzyme.³⁴ The near identity in the results for P450 2B4 and its expressed version containing an N-terminal deletion, P450 Δ 2B4, indicate that there is little difference in the reactions of the natural and truncated enzymes. The product distribution found in oxidation by the sMMO of *Mc. capsulatus* (Bath) is similar to that reported from oxidation by the sMMO of *Ms. trichosporium* OB3b.¹⁹

Solvolysis Studies. Previously reported solvolysis studies of the 3,5-dinitrobenzoate esters of 2-norcaranol conducted at 80 °C gave predominantly bicyclic alcohols.¹⁵ We briefly investigated reactions of 2-norcaranyl mesylates at lower temperatures. The mesylate from *endo*-2-norcaranol was prepared from reaction of the alcohol with methanesulfonyl chloride and Et₃N in tetrahydrofuran (THF) at -20 °C and allowed to stand at -20 °C for 1 h. Water was then added at -20 °C, and the mixture was stirred at room temperature for 12 h. Following an extractive workup procedure, GC analysis of the products showed a mixture of *endo*-2-norcaranol (**4**), *exo*-2-norcaranol (**5**), and 3-cycloheptenol (**3**) in a 67:28:5

ratio in approximately 50% yield. To the limit of detection (ca. 0.5%), no (2-cyclohexenyl)methanol (**2**) was formed. When the reaction sequence was repeated using a mixture of *endo*- and *exo*-2-norcaranol (30:70) for preparation of the mesylate, a similar mixture of products was obtained. The same product ratios were obtained when the reactions were repeated with the exception that the mesylates were prepared at room temperature.

The results of the mesylate solvolysis reactions are similar to those found in the solvolysis of the 3,5-dinitrobenzoate esters in aqueous acetone, where a 67:23:10 ratio of **4**, **5**, and **3** were found from both the *endo* and *exo* esters.¹⁵ The consistent ratio of products found from mesylates prepared from the *endo* alcohol and from the mixture of *endo* and *exo* alcohols shows that the mesylates were formed and reacted in solvolyses reactions in high yields.

Discussion

Mechanistic probe studies of enzyme-catalyzed oxidations have proven to be quite difficult to understand. Part of the confusion comes from probe studies that sought to test for a radical intermediate but employed probes that provided no method for differentiation between cationic and radical intermediates, and much of the mechanistic work reported for P450 and sMMO enzymes falls into this category. When no rearrangement or racemization of such a probe is observed, one can deduce that neither transient is produced with an appreciable lifetime, but a calculation of a radical lifetime from an observed product distribu-

tion is essentially meaningless if the probe gives the same products from a radical and a cationic intermediate. In addition, experimental results have been misinterpreted and products misidentified. Another layer of complexity arises from the possibility that more than one hydroxylation reaction pathway might exist for these enzymes.

Figure 5.2 displays the iron-oxygen species that form in the evolution of the oxidants in P450 and sMMO. In P450, the resting enzyme is reduced to an iron(II) species that can bind dioxygen. Further reduction gives a peroxo-iron species that converts to a hydroperoxy-iron unit upon protonation. A second protonation and loss of water give the ultimate oxidant, an iron-oxo species. Recent "cryoreduction" studies resulted in the EPR detection of the peroxo-iron and hydroperoxy-iron intermediates,^{5,35} but the iron-oxo species apparently is too short-lived to detect,⁵ despite its tentative identification in an earlier report.⁶ In sMMO, two iron atoms are reduced to the Fe(II) level, and dioxygen binding affords a species termed H_{peroxo} . H_{peroxo} converts to the ultimate oxidant, an oxo-bridged diiron(IV) species termed Q. For the *Ms. trichosporium* OB3b enzyme the H_{peroxo} to Q conversion apparently depends on protonation of H_{peroxo} ,³⁶ but this conversion is independent of pH for sMMO from *Mc. capsulatus* (Bath).³⁷ Unlike with P450, the H_{peroxo} and Q intermediates accumulate and are detectable during the reaction cycle of sMMO,³⁸ although the structures depicted in Figure 5.2 for these species are speculative.

Evidence has been reported that two electrophilic oxidants are formed in both P450 and sMMO oxidations. For P450, the evidence involves changes in regioselectivity in oxidations catalyzed by wild-type and mutant P450s,^{29,33} similar to the differences found here for P450 Δ 2E1 and its T303A mutant, and the finding that rearranged and unrearranged alcohols from oxidation of the methyl group in a methylcyclopropane mechanistic probe are formed with different Michaelis parameters, different kinetic isotope effects, and different solvent isotope effects.³⁹ The two oxidants are presumed to be the iron-oxo species and either the hydroperoxy-iron intermediate or iron-complexed hydrogen peroxide. For the sMMO from *Mc. capsulatus* (Bath), single-turnover studies revealed that H_{peroxo} or its immediate successor in the reaction cycle is capable of epoxidizing propene³⁷ and other substrates,⁴⁰ adding a second oxidizing species to Q, the active methane oxidant.

Computational studies of the iron-oxo species in P450 indicate that two reactive spin states are accessible, a low-spin ensemble that reacts by insertion and a high-spin ensemble that reacts by H-atom abstraction from substrate to afford a radical,⁸ and multiple spin state reactions of iron-oxo in P450 are supported by recent experimental results.³⁹ Theoretical analysis of sMMO hydroxylation of ethane⁴¹ indicates that the transition state can evolve into alcohol through both concerted and bound radical pathways. These pathways do not

represent "fundamentally different reaction mechanisms," as sometimes stated,¹⁹ but rather reflect the character of a late transition state.

The experimental and computational evidence for multiple reactive species and multiple reaction channels in hydroxylations catalyzed by P450 and sMMO enzymes indicates the difficulty one has in interpreting the results from any mechanistic probe in isolation. With that caution, we evaluate the results with norcarane in the context of other experimental and theoretical results. The mechanistic issues involve whether one can implicate discrete cationic and radical intermediates.

Cationic Rearrangement Product. The implication of a cationic intermediate in norcarane oxidation is consistent with previous mechanistic studies employing probes that give unique rearrangements upon formation of a cation (Figure 5.3). In the case of P450, the methylcyclopropane substrates **10** and methylcubane (**11**) afforded some cation-derived rearrangement products with several hepatic P450s, including the P450 enzymes studied in this work.^{34,42} For sMMO, evidence for production of cationic transients comes from oxidation studies with 1,1-dimethylcyclopropane²¹ (**12**), probe **10a**,²⁰ and methylcubane (**11**).^{20,43} In all of these studies, cation-derived products were obtained, but one cannot estimate the extent of cation formation because the rates, partitioning, and even the identities of the cationic intermediates are unknown. The norcarane results provide this same type of evidence, namely, that a cationic species is implicated, but the extent of its occurrence cannot be determined.

It is important to note that the detection of cationic rearrangement products does not necessarily demand that a norcaranyl C2 carbocation was produced. There exist two reasonable routes to cationic species in the enzyme-catalyzed oxidations. One is formation of a radical that is subsequently oxidized to a cation, favored by Groves and coworkers for norcarane (Figure 5.1).⁴⁴ This route is unlikely in the case of the hypersensitive probes **10** because the cyclopropylcarbonyl radicals produced from such species ring open with rate constants of $(5-8) \times 10^{11} \text{ s}^{-1}$ to give benzylic radical products,⁴⁵ but benzyl-substituted products were not formed in substantial amounts in the enzyme-catalyzed oxidations of probes **10**.^{20,34,42}

A second route to cationic products involves insertion of the elements of "OH⁺", the expected reaction effected by the iron-hydroperoxy species in P450 or by a protonated form of H_{peroxo} in sMMO (Figure 5.1). Protonated alcohols thus formed could be deprotonated to give unrearranged product or react by loss of water with concomitant cationic rearrangement. We have previously argued the logic of this route to cationic products.^{20,34,42} In their recent study of norcarane oxidation by the sMMO from *Ms. trichosporium* OB3b, Brazeau et al. attempted to detect reactions of H_{peroxo} (or its immediate successor) by stopped-flow kinetics methods but found no kinetic effect to suggest that norcarane was oxidized by these species.¹⁹ The authors assumed that the amount of cationic intermediate formed in the sMMO reaction with norcarane was significantly greater than the amount of cationic rearrangement product **3** they detected in the products.¹⁹ If,

however, the ca. 1.2% of 3 they report¹⁹ represents most of the norcarane that reacted by the cationic pathway in steady-state turnover, then perhaps no deviation in the observed single-turnover stopped-flow kinetics would be detectable (see also Appendix).

We therefore conclude that the detection of cationic rearrangement products from norcarane provides supporting evidence for cationic intermediates similar to that found in previous studies with probes that distinguish between cationic and radical intermediates.^{20,21,34} Given the high reactivity of cations and the small amounts of cationic products from all probes, it is likely that "cationic" reaction pathways are minor in both P450 and sMMO.

Radical Rearrangement Product. Although there is now general agreement for both P450 and sMMO hydroxylation reactions that the transition state for C-H bond activation has radical character, the key question is whether there is evidence for discrete radical intermediates. That is, does a radical species "live" significantly longer than the transition-state lifetime of the reaction, which is about 0.2 ps at ambient temperatures? Despite long histories of this claim for both types of enzymes, most of the evidence for discrete radicals was circumstantial. With little exception,²¹ early mechanistic work involved the use of probes that gave the same rearrangement product from radicals and cations, and the formation of rearranged products was assumed to involve radicals. Now that one has strong evidence that some type(s) of cationic species is (are) formed in

P450 and sMMO-catalyzed hydroxylations, that assumption is seen to be without foundation.

The detection of radical-derived rearrangement product **2** from the P450 enzymes, the sMMO enzyme from *Mc. capsulatus* (Bath) studied in this work, and the sMMO from *Ms. trichosporium* OB3b,¹⁹ is, therefore, apparently spectacular. It is seemingly unequivocal evidence for production of discrete radical intermediates by these enzymes, and it can lead to a mechanistic conclusion regarding discrete radical intermediates that is diametrically opposed to that deduced from studies with other probes that permit "radical lifetime" estimates.

Mechanistic probes that do not permit differentiation between a radical and a cationic intermediate provide equivocal information about the lifetime of a radical when rearrangement products are observed. The absence of any rearrangement products from such a probe is not equivocal because it eliminates the possibility of any intermediate with a lifetime adequate for formation of detectable amounts of rearranged product. For P450 enzymes, hydroxylations of several probes gave only unrearranged alcohol products to the limits of detection, which were typically less than 1% relative yield. These include methylcyclopropane,^{46,47} dimethylcyclopropanes,⁴⁷ and isopropylcyclopropane,⁴⁷ each of which is a potential precursor to a cyclopropylcarbinyl radical that ring opens with a rate constant similar to that of the norcaran-2-yl radical, on the order of $1 \times 10^8 \text{ s}^{-1}$. Interestingly, even norcarane was reported to be hydroxylated by P450 without formation of any rearrangement products,¹⁶ but the result probably reflects low

analytical sensitivity in that study because the enzyme employed was P450 2B4, the same enzyme used here in a reconstituted system. The observation of radical-derived product **2** from P450-catalyzed hydroxylation of norcarane in the present work is in marked contrast to other results.

In the case of sMMO-catalyzed hydroxylations, the dichotomy is more apparent. No rearranged products were detected from the *Mc. capsulatus* (Bath) sMMO oxidations⁴⁸ of trans-1,2-dimethylcyclopropane and bicyclo[2.1.0]pentane, radicals from which ring opening rate constants are 2×10^8 and 2×10^9 s⁻¹, respectively.^{49,50} Nor was any rearrangement found in the *Mc. capsulatus* (Bath) hydroxylations of "hypersensitive" radical probes, the radicals from which rate constants for radical ring openings exceed 1×10^{11} s⁻¹.^{48,51} The detection of product **2** in norcarane hydroxylation catalyzed by this MMO is clearly out of character.

Although equivocal concerning the origins of the rearranged products, the product ratios when rearrangement is found from probes that do not differentiate between cations and radicals can be used to establish upper limits on the lifetimes of a putative radical. The general trend in P450 mechanistic studies has been that smaller upper limits for radical lifetimes occur as the rate constants for the radical rearrangements increase. That is, the relative amounts of rearranged products change little, and the upper limits on the radical lifetimes are calculated to be smaller when the rate constants for the radical rearrangements are greater. For example, the limit for a radical lifetime from hydroxylation of bicy-

clo[2.1.0]pentane^{46,47} (k for the radical of $2 \times 10^9 \text{ s}^{-1}$)^{49,50} is 100 ps, the limit from hydroxylation of hexamethylcyclopropane⁴⁷ (k for the radical of $5 \times 10^9 \text{ s}^{-1}$ at 37 °C)⁴⁹ is 4 ps, and the limit from hydroxylation of several aryl-substituted methylcyclopropanes^{47,52-54} (k for the radicals in the range of $(1-5) \times 10^{11} \text{ s}^{-1}$) is about 0.3 ps. These values are limits to a radical lifetime. Direct calculations of radical lifetimes in P450 hydroxylations, however, are available from results with probes **10** that differentiate between radicals and cations; those results give radical lifetimes in the range of 0.08-0.2 ps,^{34,42} or about the lifetime of a transition state.

Radical lifetimes for the sMMO hydroxylations also are on the order of the lifetime of a transition state. Very short upper limits are calculated from the partial racemizations observed in hydroxylation of chiral (by virtue of isotopic substitution) ethane by the sMMO from *Ms. trichosporium* OB3b⁵⁵ and of chiral ethane and chiral butane by the sMMO from *Mc. capsulatus* (Bath).⁵⁶ Assuming that fast rotation of the alkyl radical ($k = 5 \times 10^{12} \text{ s}^{-1}$)⁵⁷ is the limiting process for racemization, one calculates an upper limit on the radical lifetime of less than 0.2 ps from the chiral alkane oxidations. As discussed elsewhere,⁴¹ the rotation of a bound radical must be accompanied by recoil from the hydroxylating OH group, but even with inclusion of this vibrational component the bound radical lifetime is only 0.3 ps. The radical lifetime upper limit calculated from the oxidation of an aryl-substituted methylcyclopropane by the sMMO from *Ms. trichosporium* OB3b

was less than 0.2 ps.^{43,48} In the hydroxylation of probe **10b** by the sMMO from *Mc. capsulatus* (Bath), the calculated radical lifetime was 0.25 ps.²⁰

Thus, radical lifetimes for P450 and sMMO oxidation reactions obtained from studies with probes that can differentiate between radicals and cations are 0.25 ps or less. In many cases, results from studies with probes that cannot differentiate between radicals and cations give upper limits on the radical lifetimes of 0.3 ps or less. Much larger upper limits for the radical lifetimes can be calculated from studies with some probes that do not differentiate between radicals and cations, but to do so is pointless because they are, after all, only limits. The preponderance of probe-derived evidence, then, is that the radical has a lifetime on the order of that of a transition state or about 0.2 ps.

In comparison to the above, the present results with norcarane suggest that radical intermediates are formed with relatively long lifetimes if one pathway gives alcohols **2**, **4**, and **5**. A rate constant of $2 \times 10^8 \text{ s}^{-1}$ for the norcaran-2-yl radical ring opening was previously estimated¹⁷ from product distribution results in tin hydride trapping reactions.¹² Using that value, one calculates apparent radical lifetimes in the P450-catalyzed oxidations of norcarane of 15-160 ps. For the oxidation of norcarane by the sMMO from *Mc. capsulatus* (Bath), one calculates an apparent radical lifetime of 150 ps, and, using the results for norcarane oxidation by the sMMO of *Ms. trichosporium* OB3b,¹⁹ one calculates an apparent radical lifetime in the range 20-150 ps. Although these are short lifetimes, they are 2-3 orders of magnitude greater than those determined previously.

The calculation of radical lifetimes from the norcarane results requires the assumption of a single pathway giving rearranged alcohol **2** and unrearranged alcohols **4** and **5**. If that condition is assumed, as it was by Brazeau et al.,¹⁹ then the conclusion that hydroxylation proceeds through a radical intermediate is predetermined.

We reject the assumption of a single reaction pathway on the basis of the preponderance of experimental and computational evidence that multiple oxidants and multiple pathways exist for both P450 and sMMO. It seems likely that the amounts of rearranged alcohol **2** from norcarane oxidations are not reporting on the lifetimes of radical intermediates at all but instead reflect the amounts of substrate that react by different channels, one involving an insertion process and the other involving a bound radical. For both P450 and sMMO, computational work indicates that such reaction channels are available.

In the case of P450, a two-state model for reaction of the iron-oxo species was presented and has been further refined by Shaik and co-workers.^{8,58} Both low-spin and high-spin reaction ensembles are found computationally for iron-oxo plus substrate. The low-spin reaction pathway resembles a hydrogen-abstraction reaction, but collapse of the nascent radical with oxygen is barrier-free, resulting in an insertion reaction. The high-spin reaction pathway gives a radical from substrate because a barrier to collapse exists.⁵⁸ Recent computational work by Yoshizawa et al. suggests that a barrier should exist on both the low-spin and high-spin surfaces, but limited dynamic simulations suggest a

short (ca. 200 fs) radical lifetime.¹⁰ Nonetheless, the Shaik two-state mechanism was invoked as an explanation for norcarane oxidation results similar to those described here.⁴⁴

The barriers for iron-oxo oxidation of methane on the two spin surfaces are computed to be similar,^{10,58} but the transition states for the reactions have different degrees of polarization with the low-spin TS being more highly polarized.⁵⁸ An increase in the donor properties of the substrate will favor reaction on the low-spin surface. This property seems to be an especially attractive explanation for why evidence for a discrete radical can be found for norcarane but not with probes **10**. Alkyl substitution and the cyclopropane ring in norcarane will increase the donor character of this substrate relative to methane, but the aryl and alkoxy groups in substrates **10** undoubtedly increase the donor character even more and would further favor reaction on the low-spin surface. Recent experimental results provided evidence that supports the two-state model for reactions of iron-oxo in P450, and the probe in that study was a methylcyclopropane that should have donor character similar to that of norcarane.³⁹

Computations of hydroxylation by sMMO^{11,41} by density functional and dynamics calculations find two approximately isoenergetic channels evolving from a common transition state in the reaction of Q with methane or ethane. One channel can be considered a bound radical recoil/rebound pathway; the other, a nonsynchronous concerted reaction.¹¹ Varying distribution into these channels

by different probe substrates may be responsible for the lack of correlation between k_r and the amount of rearranged product, although a more detailed description will have to await the completion of computations for these larger hydrocarbons. Molecular dynamics calculations of the activation of ethane by Q, however, does indicate that the partition ratio between bound radical recoil/rebound and concerted mechanisms is influenced by the mass of the substrate.⁴¹ As the mass of the substrate is increased, the insertion reaction becomes more highly favored.

For both enzyme types, the computations offer one possible rationale for the small amount of norcarane that appears to be processed by a radical channel. For P450, perhaps the spin state is important. For sMMO, a radical must somehow escape the bound radical state, perhaps because its secondary carbon atom cannot approach the bridging oxygen atom in Q as closely as the primary carbon atoms in the more massive substrates **10**. It appears reasonable that the radical channels might be insignificant for the latter substrates.

Although one can rationalize the results with norcarane in the context of minor hydroxylation pathways proceeding through a radical, they are so novel that one should use caution in drawing such a conclusion. Moreover, there exists a particularly worrisome aspect of the cation chemistry of norcarane that might be important in evaluating its reliability as a mechanistic probe. The premise that alcohol product **2** was formed by a radical reaction pathway is based on the assumption that the norcaran-2-yl cation does not react to give products derived

from the (2-cyclohexenyl)methyl cation, but that is not correct. Acid-catalyzed acetolysis of 2-norcaranol was found to give predominantly the acetate from alcohol **3**, but the acetate from alcohol **2** also was formed as a minor product.^{14,59} The solvolysis results previously reported for the 3,5-dinitrobenzoate esters of 2-norcaranol¹⁵ and found here for the corresponding mesylates show that alcohol **2** is not formed in measurable amounts in these reactions. The solvolysis products are skewed heavily toward the cyclic system, 2-norcaranol, and the results are similar to those found in many reactions that involve putative cyclopropylcarbinyl cations that are trapped to give predominantly cyclopropylmethanol derivatives.⁶⁰ Thus, it would seem logical to anticipate that alcohol products **2** and **3** would be minor products from a cationic reaction in the enzyme-catalyzed oxidations, but, then, they were minor products in the reactions we studied. A better understanding of the norcaranyl cation chemistry would therefore appear to be important for interpreting the results of norcarane probe studies of P450 and sMMO.

Conclusion

Small amounts of cation- and putative radical-derived rearrangement products are found in P450 and sMMO enzyme-catalyzed hydroxylations of norcarane. Formation of the cationic rearrangement product is consistent with the growing consensus that some type of cation-forming reaction is possible with these enzymes, perhaps involving reactions of predecessors of the ultimate oxi-

dants that insert OH^+ into a C-H bond of substrate. Formation of small amounts of the radical rearrangement product might indicate the extent of radical formation by minor pathways of the ultimate oxidants in the enzymes and is not necessarily a measure of the radical lifetimes in a single reaction pathway. It is also possible that the production of the radical-derived product is artifactual and reflects an unappreciated aspect of norcaranyl cation chemistry. One is well-advised not to formulate generalizations about P450- and sMMO-catalyzed hydroxylation pathways from the unexpected findings with norcarane.

References

- 1) This work was previously published in a slightly different form. See reference 2.
- 2) Newcomb, M.; Shen, R. N.; Lu, Y.; Coon, M. J.; Hollenberg, P. F.; Kopp, D. A.; Lippard, S. J. *J. Am. Chem. Soc.* **2002**, *124*, 6879-6886.
- 3) Ortiz de Montellano, P. R. ; 2nd ed.; Ortiz de Montellano, P. R., Ed.; Plenum Press: New York, 1995, pp 245-303.
- 4) Lippard, S. J. *Angew. Chem., Int. Ed. Engl.* **1988**, *27*, 344-361.
- 5) Davydov, R.; Makris, T. M.; Kofman, V.; Werst, D. E.; Sligar, S. G.; Hoffman, B. M. *J. Am. Chem. Soc.* **2001**, *123*, 1403-1415.
- 6) Schlichting, I.; Berendzen, J.; Chu, K.; Stock, A. M.; Maves, S. A.; Benson, D. E.; Sweet, B. M.; Ringe, D.; Petsko, G. A.; Sligar, S. G. *Science* **2000**, *287*, 1615-1622.
- 7) Merkx, M.; Kopp, D. A.; Sazinsky, M. H.; Blazyk, J. L.; Muller, J.; Lippard, S. J. *Angew. Chem., Int. Ed.* **2001**, *40*, 2782-2807.
- 8) Shaik, S.; Filatov, M.; Schroder, D.; Schwarz, H. *Chem. Eur. J.* **1998**, *4*, 193-199.
- 9) Filatov, M.; Harris, N.; Shaik, S. *Angew. Chem., Int. Ed.* **1999**, *38*, 3510-3512.
- 10) Yoshizawa, K.; Kamachi, T.; Shiota, Y. *J. Am. Chem. Soc.* **2001**, *123*, 9806-9816.
- 11) Gherman, B. F.; Dunitz, B. D.; Whittington, D. A.; Lippard, S. J.; Friesner, R. A. *J. Am. Chem. Soc.* **2001**, *123*, 3836-3837.

- 12) Friedrich, E. C.; Holmstead, R. L. *J. Org. Chem.* **1972**, *37*, 2546-50.
- 13) Chatgililoglu, C.; Newcomb, M. *Adv. Organomet. Chem.* **1999**, *44*, 67-112.
- 14) Friedrich, E. C.; Jassawalla, J. D. C. *Tetrahedron Lett* **1978**, 953-956.
- 15) Friedrich, E. C.; Jassawalla, J. D. C. *J. Org. Chem.* **1979**, *44*, 4224-4229.
- 16) White, R. E.; Groves, J. T.; McClusky, G. A. *Acta Biol. Med. Ger.* **1979**, *38*, 475-482.
- 17) Austin, R. N.; Chang, H.-K.; Zylstra, G. J.; Groves, J. T. *J. Am. Chem. Soc.* **2000**, *122*, 11747-11748.
- 18) Fu, H.; Newcomb, M.; Wong, C. H. *J. Am. Chem. Soc.* **1991**, *113*, 5878-80.
- 19) Brazeau, B. J.; Austin, R. N.; Tarr, C.; Groves, J. T.; Lipscomb, J. D. *J. Am. Chem. Soc.* **2001**, *123*, 11831-11837.
- 20) Choi, S. Y.; Eaton, P. E.; Kopp, D. A.; Lippard, S. J.; Newcomb, M.; Shen, R. N. *J. Am. Chem. Soc.* **1999**, *121*, 12198-12199.
- 21) Ruzicka, F.; Huang, D. S.; Donnelly, M. I.; Frey, P. A. *Biochemistry* **1990**, *29*, 1696-1700.
- 22) Kawabata, N.; Naka, M.; Yamashita, S. *J. Am. Chem. Soc.* **1976**, *98*, 2676-2677.
- 23) Chini, M.; Crotti, P.; Flippin, L. A.; Gardelli, C.; Macchia, F. *J. Org. Chem.* **1992**, *57*, 1713-1718.
- 24) Denmark, S. E.; Edwards, J. P. *J. Org. Chem.* **1991**, *56*, 6974-6981.
- 25) Chan, J. H. H.; Rickborn, B. *J. Am. Chem. Soc.* **1968**, *90*, 6406-11.
- 26) Dauben, W. G.; Berezin, G. H. *J. Am. Chem. Soc.* **1963**, *85*, 468-72.

- 27) Coon, M. J.; Van der Hoeven, T. A.; Dahl, S. B.; Haugen, D. A. *Methods Enzymol.* **1978**, *52*, 109-17.
- 28) Vaz, A. D.; Pernecky, S. J.; Raner, G. M.; Coon, M. J. *Proc. Natl. Acad. Sci. USA* **1996**, *93*, 4644-8.
- 29) Vaz, A. D. N.; McGinnity, D. F.; Coon, M. J. *Proc. Natl. Acad. Sci. USA* **1998**, *95*, 3555-3560.
- 30) Gassner, G. T.; Lippard, S. J. *Biochemistry* **1999**, *38*, 12768-12785.
- 31) Kopp, D. A.; Gassner, G. T.; Blazyk, J. L.; Lippard, S. J. *Biochemistry* **2001**, *40*, 14932-14941.
- 32) Halgren, T. A.; Roberts, J. D.; Horner, J. H.; Martinez, F. N.; Tronche, C.; Newcombe, M. *J. Am. Chem. Soc.* **2000**, *122*, 2988-2994.
- 33) Toy, P. H.; Newcomb, M.; Coon, M. J.; Vaz, A. D. N. *J. Am. Chem. Soc.* **1998**, *120*, 9718-9719.
- 34) Newcomb, M.; Shen, R.; Choi, S. Y.; Toy, P. H.; Hollenberg, P. F.; Vaz, A. D. N.; Coon, M. J. *J. Am. Chem. Soc.* **2000**, *122*, 2677-2686.
- 35) Davydov, R.; Macdonald, I. D. G.; Makris, T. M.; Sligar, S. G.; Hoffman, B. *J. Am. Chem. Soc.* **1999**, *121*, 10654-10655.
- 36) Lee, S. Y.; Lipscomb, J. D. *Biochemistry* **1999**, *38*, 4423-4432.
- 37) Valentine, A. M.; Stahl, S. S.; Lippard, S. J. *J. Am. Chem. Soc.* **1999**, *121*, 3876-3887.
- 38) Stahl, S. S.; Lippard, S. J.; Ferreira, G. C., Moura, J. J. G. and Franco, R., Ed.; Wiley-VCH: Weinheim, 1999, pp 303-321.

- 39) Newcomb, M.; Shen, R.; Aebischer, D. A.; Coon, M. J.; Hollenberg, P. F. **2002**, Submitted for publication.
- 40) Bautista, J.; Lippard, S. J. **2002**, Unpublished results.
- 41) Guallar, V.; Gherman, B. F.; Miller, W. H.; Lippard, S. J.; Friesner, R. A. *J. Am. Chem. Soc.* **2002**, *124*, 3377-3384.
- 42) Newcomb, M.; Le Tadic-Biadatti, F. H.; Chestney, D. L.; Roberts, E. S.; Hollenberg, P. F. *J. Am. Chem. Soc.* **1995**, *117*, 12085-12091.
- 43) Jin, Y.; Lipscomb, J. D. *Biochim. Biophys. Acta-Protein Struct. Molec. Enzym.* **2000**, *1543*, 47-59.
- 44) Auclair, K.; Hu, Z. B.; Little, D. M.; Ortiz de Montellano, P. R.; Groves, J. T. *J. Am. Chem. Soc.* **2002**, *124*, 6020-6027.
- 45) Le Tadic-Biadatti, M. H.; Newcomb, M. *J. Chem. Soc.-Perkin Trans. 2* **1996**, 1467-1473.
- 46) Ortiz de Montellano, P. R.; Stearns, R. A. *J. Am. Chem. Soc.* **1987**, *109*, 3415-3420.
- 47) Atkinson, J. K.; Ingold, K. U. *Biochemistry* **1993**, *32*, 9209-9214.
- 48) Liu, K. E.; Johnson, C. C.; Newcomb, M.; Lippard, S. J. *J. Am. Chem. Soc.* **1993**, *115*, 939-947.
- 49) Bowry, V. W.; Luszyk, J.; Ingold, K. U. *J. Am. Chem. Soc.* **1991**, *113*, 5687-5698.
- 50) Newcomb, M.; Manek, M. B.; Glenn, A. G. *J. Am. Chem. Soc.* **1991**, *113*, 949-958.

- 51) Valentine, A. M.; LeTadic-Biadatti, M. H.; Toy, P. H.; Newcomb, M.; Lippard, S. J. *J. Biol. Chem.* **1999**, *274*, 10771-10776.
- 52) Newcomb, M.; Le Tadic, M. H.; Putt, D. A.; Hollenberg, P. F. *J. Am. Chem. Soc.* **1995**, *117*, 3312-3313.
- 53) Toy, P. H.; Newcomb, M.; Hollenberg, P. F. *J. Am. Chem. Soc.* **1998**, *120*, 7719-7729.
- 54) Toy, P. H.; Dhanabalasingam, B.; Newcomb, M.; Hanna, I. H.; Hollenberg, P. F. *J. Org. Chem.* **1997**, *62*, 9114-9122.
- 55) Priestley, N. D.; Floss, H. G.; Froland, W. A.; Lipscomb, J. D.; Williams, P. G.; Morimoto, H. *J. Am. Chem. Soc.* **1992**, *114*, 7561-7562.
- 56) Valentine, A. M.; Wilkinson, B.; Liu, K. E.; Komar-Panicucci, S.; Priestley, N. D.; Williams, P. G.; Morimoto, H.; Floss, H. G.; Lippard, S. J. *J. Am. Chem. Soc.* **1997**, *119*, 1818-1827.
- 57) Sears, T. J.; Johnson, P. M.; Jin, P.; Oatis, S. *J. Chem. Phys.* **1996**, *104*, 781-792.
- 58) Ogliaro, F.; Harris, N.; Cohen, S.; Filatov, M.; de Visser, S. P.; Shaik, S. *J. Am. Chem. Soc.* **2000**, *122*, 8977-8989.
- 59) Newcomb, M.; Aebischer, D. A. **2002**, unpublished results.
- 60) Wiberg, K. B.; Hess, B. A., Jr.; Ashe, A. J. ; Olah, G. A. and Schleyer, P. v. R., Ed.; Wiley-Interscience: New York, 1972; Vol. III, pp 1295-1345.

Table 5.1. Results of Enzyme-Catalyzed Oxidations of Norcarane.

Enzyme ^a	Regio ^b	Stereo		% 2 ^e	% 3 ^e
		(C2) ^c	(C3) ^d		
2B4	91:9	76:24	49:51	0.31 ± 0.06	0.4 ± 0.1
Δ2B4	92:8	78:22	53:47	0.4	0.5
Δ2E1	94:6	27:73	62:38	0.5 ± 0.1	0.16 ± 0.01
<i>Mc. capsulatus</i> (Bath)	89:11	65:35		3	2
<i>Ms. trichosporium</i> OB3b ^f	91:9	63:37		1.5	1.2

^aThe first four enzymes listed are cytochromes P450. The last two enzymes are sMMOs. ^bRegioselectivity: ratio of products from oxidation of norcarane at C2 and C3; standard deviations from multiple run experiments are <1. ^cStereoselectivity at C2: ratio of *endo/exo* alcohols (**4:5**). ^dStereoselectivity at C3: ratio of *endo/exo* alcohols (**6:7**). ^ePercentage of products **2** and **3** relative to all products from oxidation at C2; standard deviations are given for multiple runs. ^fResults from ref ¹⁹.

Table 5.2. Results of Stability Control Studies.^a

Product	nmol added ^b	nmol found ^c
2	0	3.1
	10	9.7
3	0	0.7
	15	16.7
4	0	190
	200	380

^aReactions conducted with 1 nmol of P450 2B4. ^bAmount of product added before oxidation reaction. ^cYield of product in nmol.

Table 5.3. Products from Enzyme-Catalyzed Oxidations of Norcarane.

Enzyme	nmol ^b	2	3	4	5	6	7	8	9
2B4	2	1.1	1.3	337	102.5	5.7	17	20.3	3.1
2B4	2	1.8	2.5	356.6	107.8	9.2	18.8	20.3	4.1
2B4	2	1.4	2.1	344.8	113.8	8	25.2	22.8	7.1
Δ2B4	4	0.9	1.2	168	46.3	4.5	9.7	8.6	2
Δ2E1	2	0.5	0.14	21.6	57.1	2	3.4	1.6	0.3
Δ2E1	4	0.7	0.25	41.2	108.4	3.1	4.9	3.7	0.7
Δ2E1 T303A	2	1.2	0.32	19.5	15.6	0.45	5.4	1	1.5
Δ2E1 T303A	2	1.6	0.13	21.8	22.7	0.82	6.8	2.3	1.3
sMMO ^c	10	3	2	53	28	3	4	7	<1
sMMO ^c	10	3	2	53	29	3	3	6	<1
sMMO ^c	10	3	3	52	29	3	3	6	<1

^aNanomoles of products obtained in P450 oxidations are listed. ^bNanomoles of enzyme used in the oxidation reaction. ^cYields in nmol of products were not determined for sMMO reactions; the numbers listed are percentages of products.

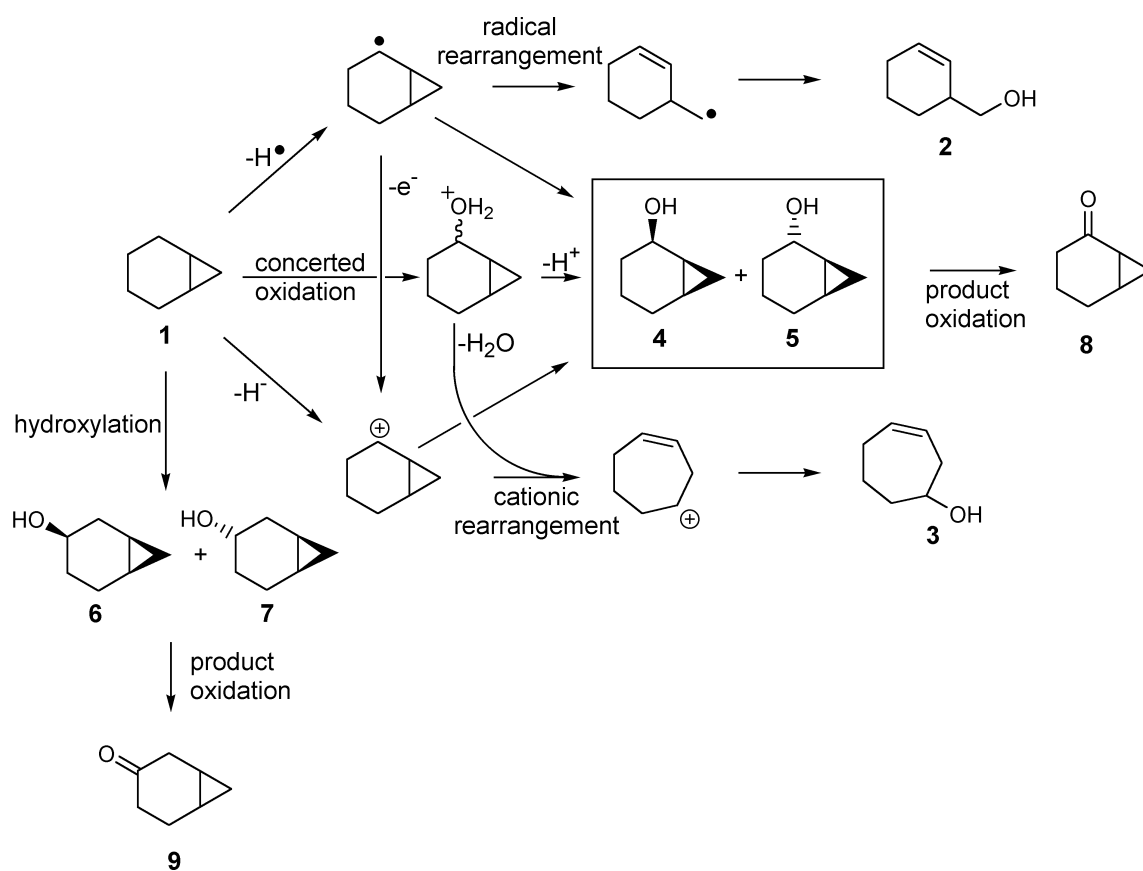


Figure 5.1. Norcarane (**1**) and products observed from its enzyme-catalyzed hydroxylation reactions. Major products **4** and **5** are boxed. Only products **2** and **3** are informative regarding hydroxylation mechanism.

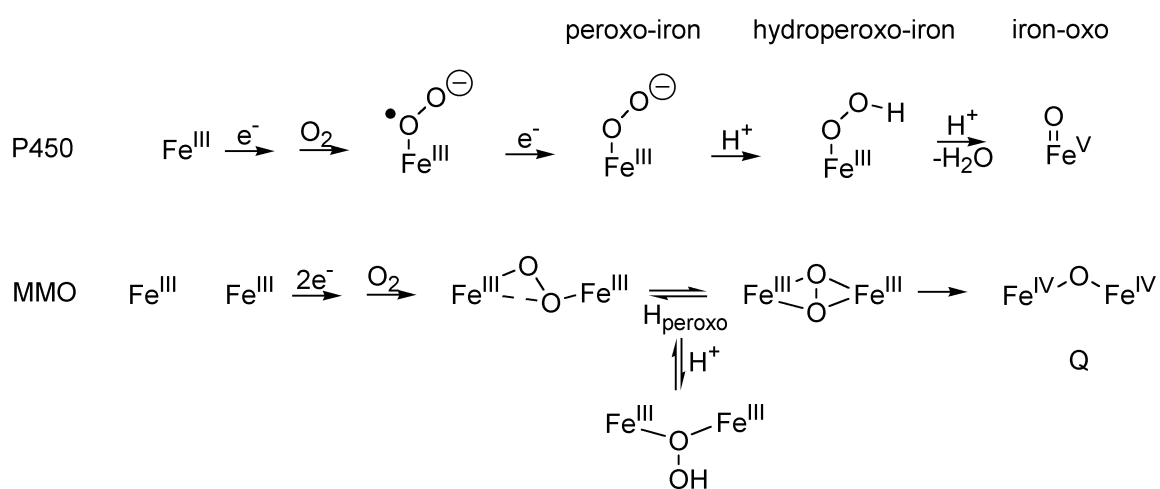


Figure 5.2. Iron-oxygen intermediates produced in P450 and sMMO oxidations.^{3,7}

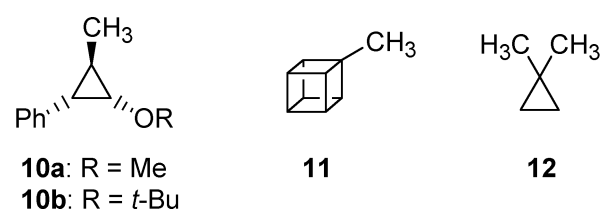


Figure 5.3. Other probe substrates that can distinguish between radical and cationic rearrangements.

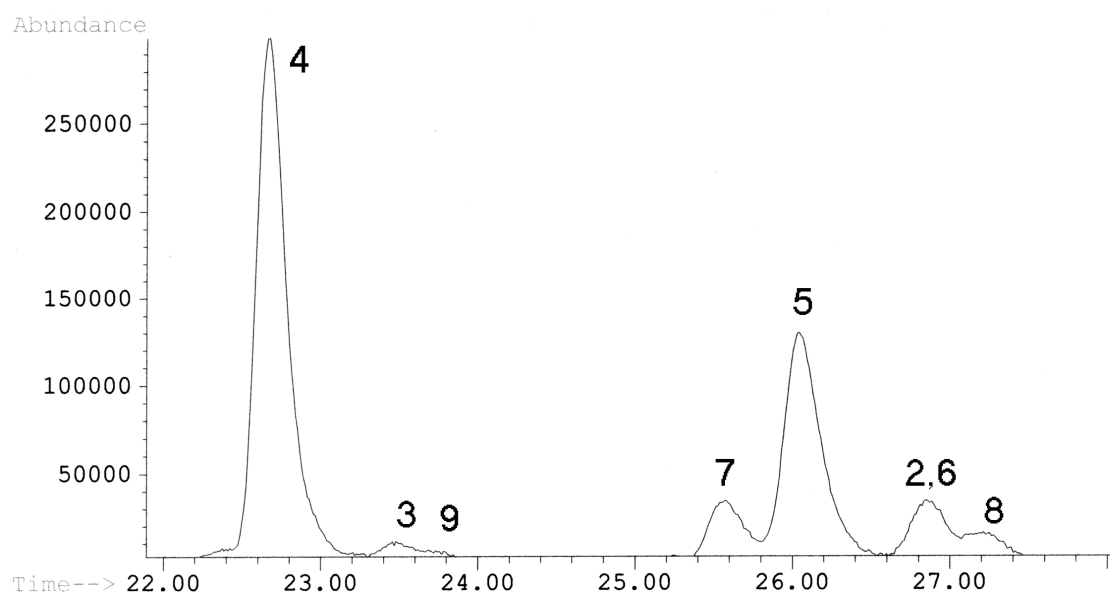


Figure 5.4. Representative GC-MS trace from oxidation of norcarane by sMMO.

Products are identified by their compound numbers.

Chapter Six:

**Product Binding to the Diiron(III) and Mixed-Valence Diiron Centers of
Methane Monooxygenase Hydroxylase Studied by ^1H and ^{19}F ENDOR Spec-
troscopy**

Introduction^{1,2}

The oxidation of methane to methanol catalyzed by the soluble methane monooxygenase (sMMO) enzyme systems of *Methylococcus capsulatus* (Bath) and *Methylosinus trichosporium* OB3b has been studied extensively.³⁻⁵ Interest in these systems remains high to obtain a better understanding of the dioxygen and C-H bond activation steps and to provide an efficient low-temperature conversion of methane to methanol on an industrial scale.⁶

Methane monooxygenase catalyzes the first step in the metabolic pathway of methanotrophic bacteria, according to eq 1. sMMO from *M. capsulatus* (Bath)



has three protein components required for activity, a 251 kDa hydroxylase, a 38.5 kDa reductase, and a 15.9 kDa coupling protein. The hydroxylase component, an $\alpha_2\beta_2\gamma_2$ dimer, contains a non-heme dinuclear iron center in each of its α subunits. The reduced diiron(II) form of the enzyme reacts with dioxygen to produce a high-valent iron intermediate that reacts with methane and a variety of other substrates, including alkanes up to C8, alkenes, aromatics, and haloalkanes.⁷⁻¹⁰

Structural studies of the hydroxylase component by X-ray crystallography have revealed the geometry of the active site in both the resting diiron(III) and diiron(II) states, as well as the mixed-valent Fe(II)Fe(III) state.¹¹⁻¹⁴ Kinetic and spectroscopic measurements have elucidated the nature of intermediates in the

reaction of MMOH with dioxygen.¹⁵⁻¹⁸ Electron-nuclear double resonance (ENDOR) spectroscopy serves as an important complement to X-ray crystallographic techniques in the study of metalloenzymes.¹⁹ Its use in the study of sMMO has primarily been to investigate the binding of exogenous ligands to the available sites of the diiron center, Figure 6.1. Early studies established the presence of a hydroxo bridge and characterized the binding of DMSO in the paramagnetic, mixed-valence, Fe(II)Fe(III) state of the cluster,²⁰ denoted H_{mv} , in which $S = 2$ and $S = 5/2$ centers couple antiferromagnetically to give a ground-state spin of $1/2$.

Knowledge of the substrate- or product-bound states of the enzyme provides valuable clues for unraveling details of the MMOH catalytic mechanism. A previous ENDOR study revealed that methanol coordinates to chemically prepared H_{mv} .²¹ The only spectroscopic evidence for the binding of this product alcohol to the oxidized diiron(III) center came through examination²² of samples of the frozen methanol and phenol complexes of the EPR-silent diiron(III) form (H_{ox}) that had been radiolytically cryoreduced.²³ This technique yields an EPR-visible mixed-valence state, denoted $(H_{ox})_{mv}$, that maintains the geometry of the precursor diferric cluster. When H_{ox} binds an alcohol or other small molecule, the cryoreduced state is designated $(H_{ox} + alcohol)_{mv}$. Dramatic differences between the EPR spectra of $(H_{ox} + methanol)_{mv}$ and of $(H_{ox})_{mv}$ disclosed ligation of the alcohol to the diiron(III) active site.²²

In the present work we have investigated the interactions of ethanol and 1,1,1-trifluoroethanol (TFE) with both the H_{mv} and H_{ox} forms of sMMO in solution by Q-band (35 GHz) CW and pulsed ENDOR spectroscopy of 1H , 2H , and ^{19}F nuclei. As part of this study we introduce ^{19}F , in this case from bound TFE, as a new probe for the binding of small molecules to a metalloenzyme active site. This approach is most favorably applied when the ENDOR measurements are made at 35 GHz or higher frequency. These measurements have been carried out in parallel with, and are discussed in terms of, the crystallographic studies of H_{mv} ¹⁴ and of alcohol binding to H_{ox} .²⁴ The crystal structures have led us to reinvestigate the ENDOR signals from the exchangeable protons of water bound to the mixed-valence diiron center both in the presence and absence of bound alcohol. The combined results suggest that alcohols bind differently to H_{ox} than to H_{mv} , permit a unified model for product binding to the enzyme, and confirm that the structures of the enzyme with product alcohols introduced by diffusion into preformed crystals are consistent with the structures in solution.

Experimental Section

Protein Purification and Sample Preparation. MMOH was purified from *M. capsulatus* (Bath) with the iron content and activity as reported previously.²⁵ Chemical reduction to the H_{mv} state was accomplished as described elsewhere.²¹ In brief, the protein was concentrated to ~ 1 mM by ultrafiltration, mixed with an equimolar amount of electron-transfer mediators (phenazine methosulfate, po-

tassium indigo tetrasulfonate, and methylene blue), and reduced with sodium dithionite. Small molecules were added prior to reduction to a final concentration of ~ 1 M. At 1 M concentration, ethanol is almost certain to inhibit activity, since it is a product and binds to the active site. A crystal structure of MMOH determined following a 1 M ethanol soak²⁴ reveals that the native structure is unperturbed, other than alcohol binding to the active site. Ethanol is also a substrate of the sMMO system, yielding acetaldehyde. Samples were allowed to equilibrate with the mediator solution for 1 h before being loaded in Q-band sample tubes and frozen. Samples of H_{ox} were similarly concentrated, mixed with small molecule, loaded in an EPR tube, and frozen prior to cryoreduction. Cryoreduction by γ -irradiation at 77 K to form EPR-visible $(H_{ox})_{mv}$ states was performed as described.²² Samples were prepared in the equilibrium mixed-valence H_{mv} form either by equilibration of $(H_{ox})_{mv}$ at ambient temperature²² or by chemical reduction. The two kinds of preparations yielded equivalent ENDOR signals. Most data displayed were collected by the former method, which afforded 2-3 times greater EPR, and therefore ENDOR, intensities.

ENDOR Spectroscopy. Previously described 35 GHz continuous wave (CW)²⁶ and pulsed²⁷ ENDOR instrumentation and procedures were applied. CW 100 kHz, rapid passage absorption spectra were recorded at 2 K. All ENDOR signals displayed here arise from nuclei with Larmor frequencies $\nu > A/2$, which in a single-crystal spectrum consists of a doublet centered at the Larmor fre-

quency and split by the hyperfine interaction, A . ^2H signal peaks are further split or broadened by the nuclear quadrupole interaction.

The Mims three-pulse^{28,29} and Re-Mims four-pulse³⁰ techniques were used to collect pulsed ENDOR spectra. The Mims technique utilizes a three-pulse electron spin-echo sequence ($t_p - \tau - t_p - T - t_p - \tau - \text{echo}$) and the Re-Mims sequence utilizes a four-pulse sequence ($t_p - \tau_1 - t_p - T - t_p - \tau_2 - 2t_p - (\tau_1 + \tau_2) - \text{echo}$), where t_p is the microwave pulse width. The Rf pulse is inserted during the interval T . For a signal characterized by a hyperfine constant, A , the Mims and Re-Mims pulsed ENDOR techniques have a response R that depends on the product, $A\tau$ ($A\tau_1$ for Re-Mims), according to eq 2. This function has zeroes (hyperfine

$$R \propto (1 - \cos(2\pi A\tau)) \quad (2)$$

"suppression holes") at $A\tau = n$; $n = 0, 1, \dots$, and maxima at $A = (2n + 1)/2$; $n = 0, 1, \dots$. Such hyperfine selectivity is very useful in cases when signals from different nuclear species overlap. Here, we have used this property to help distinguish between ^{19}F and ^1H signals. On the 35 GHz pulsed ENDOR instrument, however, cavity ringdown limited experiments to ones with $\tau > 300\text{-}350$ ns; where shorter values of τ were necessary, the Re-Mims sequence was used. The Re-Mims gives results equivalent to those of the Mims sequence, but it is independent of instrumental deadtime limitations.

For a nucleus (n) of a ligand coordinated terminally to one iron (i) of an exchange-coupled diiron center ($i = 1, 2$), the hyperfine tensor arising from dipolar coupling to the mixed-valence cluster with modest g -anisotropy has the sim-

ple axial form shown by a nucleus bound to a mononuclear site, where the unique axis for the tensor \mathbf{A} lies along the vector between the nucleus (n) and the

$$\mathbf{A}_i^{(n)} = \mathbf{T}_i^{(n)} [-1, -1, 2] \quad (3)$$

$$\mathbf{T}_i^{(n)} = K_i^{(n)} \times \frac{t^{(n)}}{r_i^{(n)3}}$$

Fe to which it is bound. The scale factor, $T_i^{(n)}$, is the product of three factors: one is the inverse cube of the Fe- n distance (r_i); the second, $t(n)$ is a product of fundamental constants and is specific to each nucleus; the third is a vector-coupling coefficient for Fe $_i$, K_i , which is determined by the spin-coupling scheme for the cluster. For convenience we list the $t(n)$ constants for several nuclei of interest in a spin-coupled cluster with total spin $S = 1/2$, comprising an Fe $^{3+}$ ($S = 5/2$) anti-ferromagnetically coupled to an Fe $^{2+}$ ($S = 2$).

$$\begin{aligned} t(^1\text{H}) &= 80 \text{ MHz} \cdot \text{\AA}^3; t(^2\text{H}) = 12.29 \text{ MHz} \cdot \text{\AA}^3 \\ t(^{13}\text{C}) &= 20 \text{ MHz} \cdot \text{\AA}^3; t(^{19}\text{F}) = 75.30 \text{ MHz} \cdot \text{\AA}^3 \\ |K| &= 7/3 \text{ for Fe}^{3+} (S = 5/2); 4/3 \text{ for Fe}^{2+} (S = 2) \end{aligned} \quad (4)$$

When the nucleus interacts with both Fe ions, as it would in a bridging or semi-bridging position, the dipolar interaction depends on the distances to both Fe ions and both K_i in a more complicated, but well-defined fashion.^{20,31-34} ENDOR simulations were performed following the algorithms described.¹⁹

To interpret the ^{19}F hyperfine couplings for a bound TFE and ^1H couplings for bound water, a search of the Cambridge Structural Database was performed to determine typical binding geometries. For TFE coordinated to iron (or

trifluoroacetic acid which has approximately the same size), sample Fe-F distances for the three fluorine atoms in a single structure range between 3.9 and 5.0 Å. For a TFE bound terminally to one iron ion of H_{mv} , these distances correspond to $T(^{19}F) \approx 5.4-2.5$ MHz if the atom is Fe^{3+} and $T(^{19}F) \approx 2.6-1.1$ MHz for Fe^{2+} . The Fe-O distances to the oxygens of water or hydroxide terminally coordinated to Fe^{3+} and Fe^{2+} are expected to be 1.9 and 2.1 Å, respectively; the Fe-O distances in an Fe-O-Fe bridge are $\sim 1.8-1.9$ Å. Assuming a tetrahedral O geometry, the corresponding Fe-H distances would be $\sim 2.5-2.6$ Å for a bridging hydroxide or water bound to the Fe^{3+} and $\sim 2.8-2.9$ Å for a water bound to Fe^{2+} .

Results and Discussion

EPR. Figure 6.2 presents the EPR spectra of H_{mv} ($g = 1.95(6), 1.86(8), \sim 1.76$) and H_{mv} to which were added methanol, ethanol, or TFE. As shown previously,²¹ coordination of methanol to H_{mv} changes the EPR spectrum ($g = 1.95(5), 1.85(5), 1.74$), shifting g_2 to a slightly lower value and making it broader at fields higher than g_2 . The $H_{mv} +$ ethanol and $H_{mv} +$ TFE samples have almost identical EPR spectra, $g = 1.94(2), 1.86(3), \sim 1.7$, and also differ from those of H_{mv} , though less than that of $H_{mv} +$ MeOH, suggesting that these alcohols, like methanol, may bind to the active site. Slight variations in the spectra of H_{mv} from different preparations have been observed, but the ENDOR spectra from all samples of a given state are the same.

The EPR spectra of $(\text{H}_{\text{ox}})_{\text{mv}}$ and $(\text{H}_{\text{ox}} + \text{MeOH})_{\text{mv}}$ have been reported previously.²² They are heterogeneous, showing the presence of multiple forms of H_{ox} , one class of which has a rather narrow g -spread ($g = 1.95, 1.85, \sim 1.75$) and the other a larger g -spread ($g = 1.94, 1.73, \sim 1.6$). The spectrum for $(\text{H}_{\text{ox}} + \text{EtOH})_{\text{mv}}$ is qualitatively similar to that of $(\text{H}_{\text{ox}} + \text{MeOH})_{\text{mv}}$; the one for $(\text{H}_{\text{ox}} + \text{EtOH})_{\text{mv}}$ is more homogeneous, comprising primarily a signal with smaller g -anisotropy ($g_2 = \sim 1.94, g_z = 1.79$), similar to that of *p*-nitrophenol and *p*-fluorophenol.²²

^{1,2}H ENDOR of Exchangeable Protons of H_{mv} . Figure 6.3 shows 35 GHz CW ¹H ENDOR spectra collected at g_2 for H_{mv} in H_2O and D_2O buffer, and for H_{mv} in H_2O to which the several alcohols of interest have been added. The contributions from exchangeable protons have been visualized both by comparison of the ¹H spectra of the mixed-valence center in H_2O and D_2O buffers and by direct detection in 35 GHz ²H pulsed ENDOR. Both modes are illustrated in Figure 6.3 for $\text{H}_{\text{mv}} + \text{TFE}$.

Our earliest investigation showed that the H_{mv} center exhibits ENDOR signals from the exchangeable proton of the hydroxo-bridge.³⁵ At g_2 this signal extends out to almost 30 MHz (not shown), but only a small fraction of the intensity of the exchangeable signals in the narrowed frequency range of Figure 6.3 arises from the bridge. As first found for H_{mv} and $\text{H}_{\text{mv}} + \text{MeOH}$,^{21,35} in each case the spectra show a strong signal from exchangeable proton(s) with splitting $A^{\text{H}} \approx 8$ MHz ($\nu_{+/-} = \nu_{\text{H}} \pm A/2$, where A is the hyperfine coupling), which is ascribed to terminally bound water.³⁵ Binding of methanol to H_{mv} does not displace this wa-

ter, as shown previously;²¹ Figure 6.3 shows that the same is true for the binding of ethanol and TFE. The ^1H $\text{H}_{\text{mv}} + \text{TFE}$ spectrum does show better resolution of some features with $A \approx 13$ MHz, an effect also observed upon the addition of DMSO,²⁰ but the features are present in the other spectra as well.

Our earlier discussions of this bound water were based on the simple assumption that a terminal water binds with an Fe-O distance of $r(\text{Fe-O}) \approx 2 \text{ \AA}$. In this case, the main intensity from exchangeable protons in the g_2 spectrum of H_{mv} and of $\text{H}_{\text{mv}} + \text{methanol}$, with $A \approx 8$ MHz, was best assigned to the "perpendicular" feature, with $A \approx T$ (eq 3), for a terminal water bound to Fe^{2+} .

The crystallographic investigation of H_{mv} carried out concurrently with the ENDOR studies¹⁴ confirms that H_{mv} indeed binds water but indicates that the hydroxo-bridged diiron site binds two H_2O ligands. These waters nominally bind to a single iron ion (Fe1),¹⁴ with this Fe being six-coordinate while the other iron (Fe2) can be three-, four-, or five-coordinate, varying with shifts of the carboxylate of Glu243 (Figure 6.1).¹⁴ For H_{mv} and for H_{mv} plus each of the alcohols, comparison of the CW ENDOR spectra taken in H_2O and D_2O at g_2 demonstrates that at least one, and probably both, of the water molecules remain coordinated to the center upon binding an alcohol.

It is intuitively appealing to assign the six-coordinate Fe seen in the structure as being the ferric ion. Normally $^1,^2\text{H}$ ENDOR is an ideal way to test this inference, through the dependence of the dipolar interaction parameter ($T_i^{(\text{H})}$) of

the water protons on the valence of the coordinating iron, eq 3. However, the crystal structure indicates that the waters are not 'simple' terminal ligands, but rather are 'semi-bridging' and do not have typical Fe-O distances. For example, the oxygen atom of one water in protomer 1 nominally occupies position 3 (Figure 6.1), but with an Fe1-O distance of 2.5 Å and an Fe2-O distance of 3.1 Å. Thus, the dipole interaction of the water protons with each Fe is less than for a typical distance. Indeed, a proton on an Fe³⁺-bound water located at the crystallographic $r(\text{Fe-O})$ distance would exhibit essentially the same T as would a proton on a water bound to Fe²⁺ at a typical distance. As a result, the expected ENDOR patterns for protons associated with the crystallographically characterized waters are not sensitive to the valence assignment as would be the case if the assumptions of terminal binding and typical Fe-O bond distances held.[NOTE:The crystal structure, at 2.07 Å resolution, of course does not visualize the protons and thus does not provide additional metrical parameters for analyzing the spectra.]

An attempt to analyze two-dimensional (2D), orientation-selective, field-frequency plots comprising numerous ²H Mims pulsed ENDOR spectra collected across the EPR envelope of H_{mv} (Figure 6.4) was thwarted by the task of locating the four water protons in each of the two nonidentical protomers, self-consistently and uniquely, along with the determination of the valency assignment.

$^{1,2}\text{H}$ ENDOR measurements on the alcohol-bound H_{mv} center showed that the patterns for the exchangeable protons are very similar to those for H_{mv} , and include contributions both from bound water and the OH bridge. Consideration of 2D ENDOR patterns (Figure 6.4) indicates that replacement of a water by a protonated bridging alcohol is unlikely but does not discriminate among other possibilities, such as replacement of terminal waters by an alcohol in the same position, or replacement of a water by a deprotonated bridging alcohol.

ENDOR of Nonexchangeable $^{1,2}\text{H}$ of Alcohols Bound to H_{mv} . To examine the binding of ethanol and TFE to H_{mv} , and if possible to determine the binding site, Fe(II) or Fe(III), and geometry (terminal, bridging), we performed Q-band Mims pulsed ^2H ENDOR measurements on $\text{H}_{\text{mv}} + \text{CD}_3\text{CD}_2\text{OH}$ and $\text{H}_{\text{mv}} + \text{CF}_3\text{CD}_2\text{OH}$, and compared them to similar results for $\text{H}_{\text{mv}} + \text{CD}_3\text{OH}$.²¹ As seen in Figure 6.5, $\text{H}_{\text{mv}} + \text{CD}_3\text{CD}_2\text{OH}$ shows a poorly resolved ^2H ENDOR doublet signal that is slightly more intense but of similar shape to that of the Fe(II)-bound CD_3OH of $\text{H}_{\text{mv}} + \text{CD}_3\text{OH}$ ($A(^2\text{H}) \approx 0.5$ MHz, corresponding to $A(^1\text{H}) \approx 3.3$ MHz).²¹ Moreover, the 2D pattern of field-dependent ^2H spectra for $\text{H}_{\text{mv}} + \text{CD}_3\text{CD}_2\text{OH}$ (Figure 6.6) is identical with that previously obtained for $\text{H}_{\text{mv}} + \text{CD}_3\text{OH}$.²¹ Therefore, the same analysis applies, and we conclude that ethanol, like methanol, coordinates through oxygen to an Fe atom of the H_{mv} diiron core. An assumption of normal Fe-O bond length leads to the suggestion that MeOH binds to the Fe(II), and the same argument would apply to ethanol. Although a semi-bridging structure with the alcohol closer to Fe(II), rather than Fe(III), can-

not be excluded, comparison between these results and those reported below for perdeuterated EtOH bound to H_{ox} support the assignment that CD_3CD_2OH is a terminal ligand to Fe^{2+} in H_{mv} . When the same measurements were made with $H_{mv} + CF_3CD_2OH$, a 2H doublet signal was observed (Figure 6.5), indicating that TFE also binds. The coupling is ~ 0.8 MHz.

DMSO coordinates to the Fe(III) iron of H_{mv} and changes its EPR spectrum without displacing bound methanol.²¹ Addition of DMSO to $H_{mv} +$ ethanol changed the EPR spectrum to that characteristic of $H_{mv} +$ DMSO, but similarly did not eliminate the 2H ENDOR signal from CD_3CD_2OH . Thus, as with methanol, ethanol can bind simultaneously to H_{mv} with DMSO.

ENDOR of Nonexchangeable $^{1,2}H$ of Alcohols Bound to $(H_{ox})_{mv}$. To examine the binding of ethanol and TFE to H_{ox} , we added the deuterated alcohols to the enzyme in H_2O buffer, cryoreduced the enzyme, and examined the resulting state by ENDOR spectroscopy. The samples $(H_{ox} + CD_3CD_2OH)_{mv}$ (data not shown) and $(H_{ox} + CF_3CD_2OH)_{mv}$ (Figure 6.5) both give well-resolved 2H ENDOR signals, clearly indicating that ethanol and TFE bind to H_{ox} . The hyperfine couplings are almost double those for $H_{mv} + CD_3OH$ and the $H_{mv} + CD_3CD_2OH$ complexes throughout a set of spectra at multiple fields (Figure 6.7). If we assume that the alcohols bind with comparable Fe-O bond lengths in both H_{mv} and H_{ox} , then according to eq 3, one may self-consistently conclude that the smaller couplings for the $H_{mv} +$ alcohol complexes reflect binding to the ferrous ion as suggested above, whereas the larger 2H couplings for the alcohol com-

plexes of the latter are compatible with alcohol binding to H_{ox} in the semi-bridging fashion (Position 3/4, Figure 6.1) found crystallographically for crystals prepared by diffusion of methanol or ethanol into crystalline H_{ox} .²⁴

¹⁹F ENDOR. ¹⁹F ENDOR of isotopically labeled TFE ($\text{CF}_3\text{CD}_2\text{OH}$) provides a new probe of the geometry of small-molecule binding to a metalloenzyme active site when the microwave frequency is sufficiently high. At X band the difference between the ¹⁹F and ¹H Larmor frequencies is very small, less than 1 MHz. As a result, the respective ¹⁹F and ¹H ENDOR signals would overlap completely for almost any protein sample. At 35 GHz, the difference between the ¹⁹F and ¹H Larmor frequencies is more than 3 MHz at $g = 2$, although in H_2O buffer, the signals are barely distinguishable from the baseline and often obscured by strongly coupled protons. It is possible, however, to resolve ¹⁹F signals from TFE in 35 GHz CW ENDOR spectra collected from a sample that is prepared in D_2O buffer and thus does not exhibit the broad ¹H ENDOR signals from the bound water shown in Figure 6.3. Far better results are obtained, however, through use of the Mims/Re-Mims Q-band pulsed ENDOR technique, and in this case it is not necessary to use D_2O buffers. A comparison of the ¹⁹F signal obtained in CW or pulsed ENDOR is presented in Figure 6.8. This pulsed-ENDOR approach allowed us to prepare a single sample with deuterated TFE ($\text{CF}_3\text{CD}_2\text{OH}$) in H_2O buffer, and to examine both its ¹⁹F and nonexchangeable ²H ENDOR responses. For ease of presentation, we first discuss results for $(H_{\text{ox}} + \text{CF}_3\text{CD}_2\text{OH})_{\text{mv}}$, then for $H_{\text{mv}} + \text{CF}_3\text{CD}_2\text{OH}$.

^{19}F ENDOR of $(\text{H}_{\text{ox}} + \text{TFE})_{\text{mv}}$. Figure 6.9 shows 35 GHz Mims pulsed ENDOR spectra of $(\text{H}_{\text{ox}} + \text{CF}_3\text{CD}_2\text{OH})_{\text{mv}}$ at several values of τ . The arrows in the figures indicate the Mims "suppression holes" in the spectra, the minima of the sinusoidal Mims response function, eq 2 [NOTE: An anonymous reviewer suggested that we show curves for both the proton and fluorine response functions superimposed on each spectrum; the approach we adopt keeps the spectra distinct and focuses attention to the points where one signal is absent and another one may be present.] In all cases, the highly visible ^1H signals that extend to $A(^1\text{H}) = 8\text{--}10$ MHz, in the CW spectra of Figure 6.2, are diminished in intensity relative to signals with smaller coupling by Mims suppression effects. The more strongly coupled ^1H signals are not gone, however. This is best seen in the portion of the $\tau = 228$ ns spectrum with $\nu > \nu_{\text{H}}$, which shows a low-intensity "scal-
loped" shape given by ^1H suppression holes in ^1H ENDOR signals from the bound water.

This Mims suppression of ^1H signals unmasks the ^{19}F signals, indicated in Figure 6.9, which are not mirrored to the high-frequency side of ν_{H} , as ^1H signals would be.³⁶ Figure 6.9 also contains a spectrum showing that the ^{19}F signal is unchanged by DMSO binding. The top two spectra in Figure 6.9 reveal how the appearance of the ^{19}F signals is sensitive to τ . With $\tau = 228$ ns, a ^{19}F doublet centered at ν_{F} and split by an apparent coupling of $A \approx 2$ MHz is clearly seen. In the spectrum with $\tau = 144$ ns, the $\nu_{+}(^{19}\text{F})$ branch is largely obscured by ^1H signals because the latter are not so fully suppressed, but one can see that the ^{19}F intensity actu-

ally spreads over a broader range of frequencies, corresponding to maximum couplings of $A(^{19}\text{F}) \approx 4\text{-}5$ MHz. In the $\tau = 228$ ns spectrum, the tails of the ^{19}F signals are suppressed.

^{19}F ENDOR spectra also were taken over a range of magnetic fields to produce a 2D field-frequency plot (Figure 6.10); they reveal splittings of the main ^{19}F intensities, similar to the ones shown in Figure 6.9. The expected "through-space" dipolar coupling for an Fe-F distance of 3.9-5.0 Å is 5.4-2.5 MHz if the Fe atom is Fe^{3+} and 2.6-1.1 MHz (1.6-0.4 MHz axial) for Fe^{2+} . The ^{19}F 2D-plot (Figure 6.10) reveals a moderate amount of anisotropy in the ^{19}F hyperfine coupling, but due to the presence of multiple Mims suppression holes and the partial overlap with the ^1H signal, it is not possible to determine unambiguously whether the ^{19}F hyperfine interaction contains a substantial isotropic component. Therefore, these data alone do not yield a structural model for the bound TFE. Because the data for $\text{H}_{\text{mv}} + \text{TFE}$ show much smaller ^{19}F couplings, however, we self-consistently interpret them with a model where TFE binds to the $(\text{H}_{\text{ox}} + \text{TFE})_{\text{mv}}$ at the Fe^{3+} ion, or in a bridging mode (see below).

^{19}F ENDOR of $\text{H}_{\text{mv}} + \text{TFE}$. Analogous ^{19}F ENDOR measurements were made with $\text{H}_{\text{mv}} + \text{CF}_3\text{CD}_2\text{OH}$, and Figure 6.11 shows ^{19}F Mims and Re-Mims pulsed ENDOR spectra collected at g_2 at several values of τ . As in Figure 6.9, the portion of the spectrum with $\nu > \nu_{\text{H}}$ shows a low-intensity "scallop" given by ^1H suppression holes in the ^1H ENDOR signals from the bound water. Again, the suppression of the water proton signal discloses a ^{19}F doublet centered around F,

with the suppression pattern confirming the assignment of this doublet to ^{19}F . In the top, Re-Mims, spectrum, with $\tau = 148$ ns, the short τ places the ^{19}F suppression holes well outside the ^{19}F intensity; the doublet splitting appears to be roughly $A \approx 1.3$ MHz, with the ν_+ peak being largely hidden under the proton signal intensity.

The $\tau = 400$ and 480 ns Mims ENDOR spectra respectively place a proton suppression hole at the ν_- and ν_+ peaks of the doublet assigned to ^{19}F . The fact that this doublet is not suppressed confirms that the intensity is indeed due to ^{19}F . From these two spectra we conclude that a somewhat better value for the ^{19}F hyperfine coupling is $A \approx 1$ MHz, roughly half that in $(\text{H}_{\text{ox}} + \text{TFE})_{\text{mv}}$, as is the case for the ^2H couplings. Thus, with the assumption of standard bond lengths, the ^{19}F ENDOR measurements of TFE are consistent with the $^1,^2\text{H}$ measurements of MeOH and EtOH. The alcohols bind terminally to the ferrous ion of H_{mv} , while binding in a bridging or semi-bridging fashion to H_{ox} , as found crystallographically for the MeOH complex of H_{ox} .²⁴[NOTE: If bond lengths vary appreciably, other options may become plausible.]

DMSO Binding to H_{mv} (+ Alcohols). The $\tau = 400$ spectrum in Figure 6.11 is overlaid with a trace from a H_{mv} sample that contains both DMSO and TFE, which has an EPR spectrum that is the same as that reported for $\text{H}_{\text{mv}} + \text{DMSO}$. The ^{19}F signal seen for $\text{H}_{\text{mv}} + \text{TFE}$ is eliminated, however, by the addition of DMSO, while the ^1H signals remain identical. Overlays of the ν_+ proton intensity over the ν_- peaks shows that some of the intensity left over in the region around F

is actually proton intensity, with less than 20% of it due to ^{19}F signals. Although the elimination of TFE is not complete, this result indicates that DMSO binding to the Fe(III) ion of H_{mv} prevents most of the TFE binding that occurs in the absence of DMSO. This competition between DMSO and TFE contrasts with the observation that DMSO binding to the Fe(III) of H_{mv} does not preclude methanol²¹ or ethanol binding to Fe(II).

Conclusion

The present study has combined $^{1,2}\text{H}$ and ^{19}F ENDOR measurements to examine ethanol and TFE bound to both the H_{ox} and H_{mv} diiron centers of solution MMOH and has compared these results to those from X-ray diffraction studies of preformed crystals into which alcohol had been diffused. In the process we have introduced ^{19}F ENDOR spectroscopy as a valuable complement to the use of $^{1,2}\text{H}$ ENDOR spectroscopy in probing the structure of substrates or products bound to catalytic metal centers in enzymes. The $^{1,2}\text{H}$ ENDOR spectra of d_5 -ethanol and of d_2 -TFE, and the ^{19}F ENDOR of TFE obtained for the alcohols bound to solution H_{ox} , as visualized by cryoreduction to $(\text{H}_{\text{ox}})_{\text{mv}}$, are compared with those for the alcohols as bound to H_{mv} prepared in solution. The results, as interpreted in terms of eq 3, indicate that the alcohols bind close to Fe(II) of the EPR-active, mixed-valence cluster of H_{mv} , either in a terminal or semi-bridging fashion, as previously suggested for MeOH.²¹ They bind to H_{ox} in a bridging, or semi-bridging fashion closer to the Fe^{3+} ion of $(\text{H}_{\text{ox}})_{\text{mv}}$, consistent with crystallo-

graphic structures for complexes prepared by diffusion of alcohols into preformed crystals of H_{ox} .²² The early proposal that alcohols bind to the diiron(III) state in a bridging mode and distal to the histidine ligands in the active-site cavity (positions 3 and 4, in Figure 6.1),¹¹ is thus strongly supported by the crystallographic result obtained from alcohol-treated H_{ox} crystals,²⁴ by the ENDOR studies on the enzyme in solution, and by recent density functional calculations³⁷ on the reaction of methane with intermediate Q. $^1,^2H$ ENDOR spectra of exchangeable protons further suggest that the ethanols, like methanol,²¹ bind to H_{mv} without replacing coordinated water. Detailed examination of the 2H ENDOR spectra of H_{mv} and H_{mv} + ethanol shows that the structural flexibility of the diiron centers (illustrated by differences in the crystal structure protomers) precludes an in-depth analysis, but the data are consistent with the crystallographic result^{14,24} that two waters bind weakly to one of the Fe ions of H_{mv} .

DMSO does not affect the binding of either of the ethanols or of methanol to H_{ox} , nor of ethanol or methanol to H_{mv} . It does, however, displace TFE from the diiron site in H_{mv} , a difference consistent with the weaker coordinating ability of this alcohol owing to the electron-withdrawing fluorine atoms.

References

- 1) This work was previously published in a slightly different form. See reference 2.
- 2) Smoukov, S. K.; Kopp, D. A.; Valentine, A. M.; Davydov, R.; Lippard, S. J.; Hoffman, B. M. *J. Am. Chem. Soc.* **2002**, *124*, 2657-2663.
- 3) Valentine, A. M.; Lippard, S. J. *J. Chem. Soc. Dalton* **1997**, 3925-3931.
- 4) Merkx, M.; Kopp, D. A.; Sazinsky, M. H.; Blazyk, J. L.; Muller, J.; Lippard, S. J. *Angew. Chem. Int. Edit.* **2001**, *40*, 2782-2807.
- 5) Wallar, B. J.; Lipscomb, J. D. *Chem. Rev.* **1996**, *96*, 2625-2657.
- 6) Furuto, T.; Takeguchi, M.; Okura, I. *J. Mol. Catal. A: Chem.* **1999**, *144*, 257-261.
- 7) Colby, J.; Stirling, D. I.; Dalton, H. *Biochem. J.* **1977**, *165*, 395-402.
- 8) Dalton, H.; Golding, B. T.; Waters, B. W.; Higgins, R.; Taylor, J. A. *J. Chem. Soc., Chem. Commun.* **1981**, 482-3.
- 9) Fox, B. G.; Froland, W. A.; Dege, J. E.; Lipscomb, J. D. *J. Biol. Chem.* **1989**, *264*, 10023-10033.
- 10) Liu, K. E.; Lippard, S. J.; Sykes, A. G., Ed.; Academic Press: San Diego, 1995; Vol. 42, pp 263-289.
- 11) Rosenzweig, A. C.; Frederick, C. A.; Lippard, S. J.; Nordlund, P. *Nature* **1993**, *366*, 537-543.
- 12) Rosenzweig, A. C.; Nordlund, P.; Takahara, P. M.; Frederick, C. A.; Lippard, S. J. *Chem. Biol.* **1995**, *2*, 409-418.

- 13) Rosenzweig, A. C.; Brandstetter, H.; Whittington, D. A.; Nordlund, P.; Lippard, S. J.; Frederick, C. A. *Proteins: Struct., Funct., Genet.* **1997**, *29*, 141-152.
- 14) Whittington, D. A.; Lippard, S. J. *J. Am. Chem. Soc.* **2001**, *123*, 827-838.
- 15) Lee, S. K.; Nesheim, J. C.; Lipscomb, J. D. *J. Biol. Chem.* **1993**, *268*, 21569-21577.
- 16) Liu, K. E.; Valentine, A. M.; Wang, D. L.; Huynh, B. H.; Edmondson, D. E.; Salifoglou, A.; Lippard, S. J. *J. Am. Chem. Soc.* **1995**, *117*, 10174-10185.
- 17) Valentine, A. M.; Stahl, S. S.; Lippard, S. J. *J. Am. Chem. Soc.* **1999**, *121*, 3876-3887.
- 18) Shu, L. J.; Nesheim, J. C.; Kauffmann, K.; Munck, E.; Lipscomb, J. D.; Que, L. *Science* **1997**, *275*, 515-518.
- 19) DeRose, V. J.; Hoffman, B. M. *Protein-Structure and Mechanism Studied by Electron-Nuclear Double-Resonance Spectroscopy*; Sauer, K., Ed.; Academic Press: New York, 1995; Vol. 246, pp 554-589.
- 20) DeRose, V. J.; Liu, K. E.; Lippard, S. J.; Hoffman, B. M. *J. Am. Chem. Soc.* **1996**, *118*, 121-134.
- 21) Willems, J.-P.; Valentine, A. M.; Gurbiel, R.; Lippard, S. J.; Hoffman, B. M. *J. Am. Chem. Soc.* **1998**, *120*, 9410-9416.
- 22) Davydov, R.; Valentine, A. M.; Komar-Panicucci, S.; Hoffman, B. M.; Lippard, S. J. *Biochemistry* **1999**, *38*, 4188-4197.
- 23) Davydov, R.; Kuprin, S.; Graslund, A.; Ehrenberg, A. *J. Am. Chem. Soc.* **1994**, *116*, 11120-11128.

- 24) Whittington, D. A.; Sazinsky, M. H.; Lippard, S. J. *J. Am. Chem. Soc.* **2001**, *123*, 1794-1795.
- 25) Gassner, G. T.; Lippard, S. J. *Biochemistry* **1999**, *38*, 12768-12785.
- 26) Werst, M. M.; Davoust, C. E.; Hoffman, B. M. *J. Am. Chem. Soc.* **1991**, *113*, 1533-1538.
- 27) Davoust, C. E.; Doan, P. E.; Hoffman, B. M. *J. Magn. Reson. Ser. A* **1996**, *119*, 38-44.
- 28) Mims, W. B. *Proc. Roy. Soc. (London)* **1965**, *283*, 452-7.
- 29) Gemperle, C.; Schweiger, A. *Chem. Rev.* **1991**, *91*, 1481-1505.
- 30) Doan, P. E.; Hoffman, B. M. *Chem. Phys. Lett.* **1997**, *269*, 208-214.
- 31) Willems, J.-P.; Lee, H. I.; Burdi, D.; Doan, P. E.; Stubbe, J.; Hoffman, B. M. *J. Am. Chem. Soc.* **1997**, *119*, 9816-9824.
- 32) Hendrich, M. P.; Fox, B. G.; Andersson, K. K.; Debrunner, P. G.; Lipscomb, J. D. *J. Biol. Chem.* **1992**, *267*, 261-269.
- 33) Fiege, R.; Zwegart, W.; Bittl, R.; Adir, N.; Renger, G.; Lubitz, W. *Photosynth. Res.* **1996**, *48*, 227-237.
- 34) Randall, D. W.; Gelasco, A.; Caudle, M. T.; Pecoraro, V. L.; Britt, R. D. *J. Am. Chem. Soc.* **1997**, *119*, 4481-4491.
- 35) DeRose, V. J.; Liu, K. E.; Kurtz, D. M.; Hoffman, B. M.; Lippard, S. J. *J. Am. Chem. Soc.* **1993**, *115*, 6440-6441.
- 36) A technical comment is in order regarding the spectrum-by-spectrum analysis of Mims pulsed ENDOR data in Figures 6.9 and 6.11. It might appear

that the simpler alternative for determining the line shape would be to use a "skyline" plot, where one overlays spectra with different t values. In such a plot one might anticipate that parts of the signal suppressed in one spectrum would be supplied by intensity not suppressed in another one, and that a "true" line shape would result. However, this approach is not useful for samples with substantial envelope modulation or with matrix ENDOR effects. The ESEEM effect produces a different echo height at different t values, and thus it is not possible to compare absolute intensities meaningfully. The line shape of the signal changes for longer t values, which enhance matrix/distant ENDOR signals which are centered at the Larmor frequency and which grow and can eventually swamp the local ENDOR signals as t increases [Astashkin, A. et al. *J. Magn. Res.* **1998**, *135*, 406-417]. Last we note that experiments at even higher microwave frequencies will further separate the proton and fluorine signals, likely making the use of fluorine as a probe even more convenient and useful.

37) Gherman, B. F.; Dunietz, B. D.; Whittington, D. A.; Lippard, S. J.; Friesner, R. A. *J. Am. Chem. Soc.* **2001**, *123*, 3836-3837.

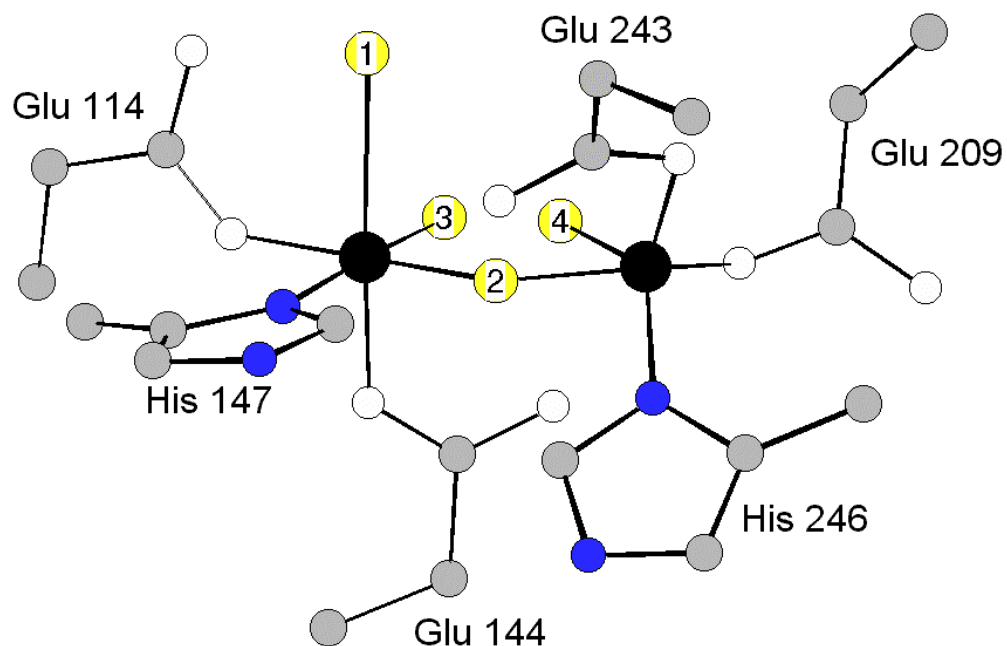


Figure 6.1. A representation of the MMOH active site based on the crystal structure of MMOH_{mv}; the actual cluster is highly flexible, adopting a variety of structures associated with shifts of the carboxylate of Glu243.¹⁴ Black spheres represent iron; light gray spheres, carbon; dark gray spheres, nitrogen; unfilled spheres, oxygen. Numbered positions represent known sites for binding exogenous ligands.

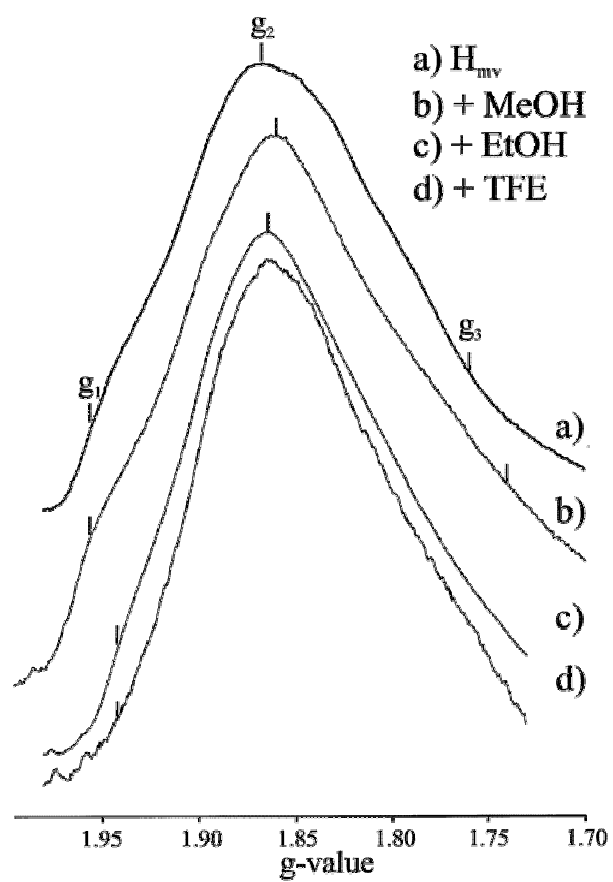


Figure 6.2. MMOH_{mv} EPR spectra in the presence and absence of substrates: 35.1 GHz MW frequency; modulation amplitude = 1.7 G; T = 2 K.

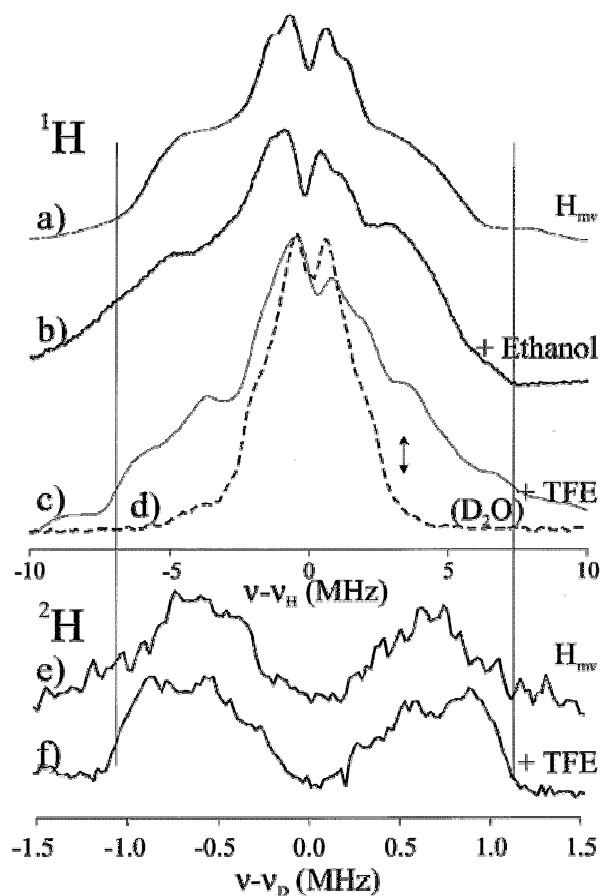


Figure 6.3. ^1H ENDOR spectra of H_{mv} , as well as H_{mv} in the presence of TFE, ethanol, or methanol. The spectrum of the sample exchanged in D_2O is representative of that of H_{mv} , as well as in the presence of the alcohols. (a) 35.02 GHz MW frequency, $g = 1.87$; negative scan direction; scan speed 1 MHz/s; 200 kHz (full width) broadening of rf excitation; modulation amplitude = 1.3 G. (b) As in (a) but 35.06 GHz, $g = 1.862$; modulation amplitude = 1.7 G; scan speed 1 MHz/s. (c) As in (a) but 35.105 GHz MW frequency, $g = 1.840$; negative scan direction; scan speed 2 MHz/s; modulation amplitude = 4.2 G. (d) As in (a) but 35.048 GHz MW frequency, $g = 1.841$; positive scan direction; scan speed 1 MHz/s; modulation amplitude = 1.7 G. (e) Re-Mims (four-pulse) sequence³⁰ with a $\pi/2$ microwave pulse = 32 ns, with 20 μs rf pulse and $\tau = 164$ ns; no rf excitation broadening; 34.836 GHz MW frequency, $g = 1.86$; pulse sequence repetition time = 20 ms; 30 averaged data shots per point; 40 scans. (f) As in (e) but 35.051 GHz MW frequency; pulse sequence repetition time 20 ms; 30 averaged data shots per point; 8 scans.

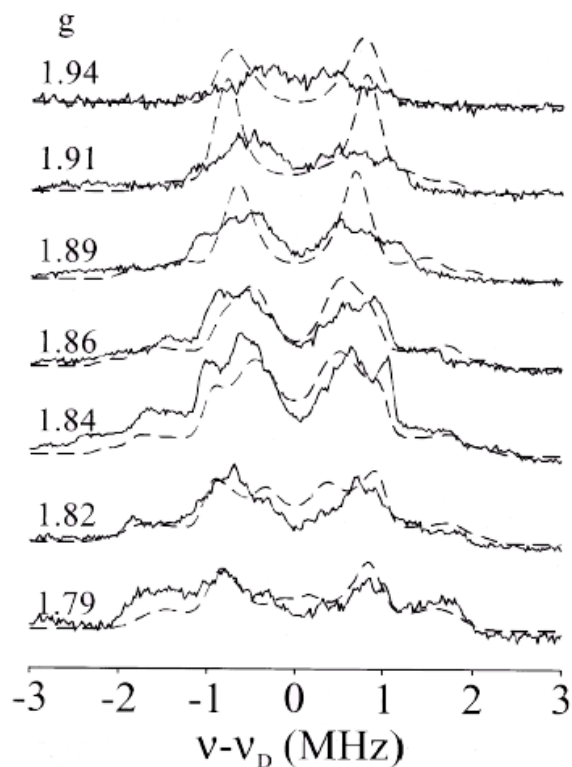


Figure 6.4. Re-Mims 2D Plot with Simulations. $H_{mv} + \text{TFE}/\text{D}_2\text{O}$ – field dependence of the ^2H 35 GHz ReMims pulsed ENDOR spectra overlaid with a simulation. ^2H Mims suppression holes are indicated by arrows. Spectra are identified by their g values. Re-Mims sequence with a $\pi/2$ microwave pulse = 32 ns, with 20 μs Rf pulse and $\tau = 164$ ns; no Rf excitation broadening; 35.051 GHz MW frequency, pulse sequence repetition time 20 ms; 30 averaged data shots per point. 6-17 scans recorded per spectrum.

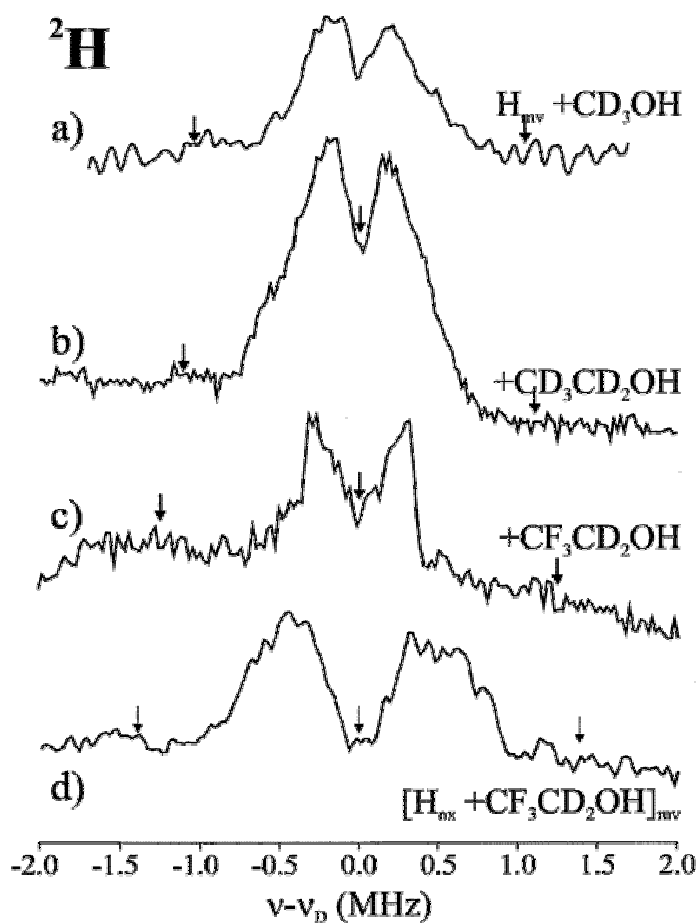


Figure 6.5. ^2H 35 GHz Mims ENDOR of H_{mv} , to which CD_3OH , or $\text{CD}_3\text{CD}_2\text{OH}$, or $\text{CF}_3\text{CD}_2\text{OH}$ have been added, and of $(\text{H}_{\text{ox}} + \text{CF}_3\text{CD}_2\text{OH})_{\text{mv}}$; ^2H Mims suppression holes are marked on each spectrum. (a) $\text{H}_{\text{mv}} + \text{CD}_3\text{OH}$ at $g_2 = 1.86$.²¹ (b) Mims sequence with a $\pi/2$ microwave pulse = 50–52 ns, with 60 μs rf pulse, $\tau = 452$ ns; 34.695 GHz MW frequency, $g = 1.864$; pulse sequence repetition time = 25 ms; 40 averaged data shots per point; 8 scans; the seventh proton harmonic at 8.09 MHz (-0.6 MHz in the figure) causes a slight asymmetry in this spectrum. ($\text{H}_{\text{VL}} = 56.62$ MHz). (c) As in (b) but $\tau = 400$ ns; no broadening of rf excitation; 34.594 GHz MW frequency, $g = 1.84$; pulse sequence repetition time = 20 ms; 30 averaged data shots per point; 10 scans. (d) As in (b) but Mims sequence with 60 μs rf pulse and $\tau = 360$ ns; 34.584 GHz MW frequency; pulse sequence repetition time = 20 ms; 11 scans.

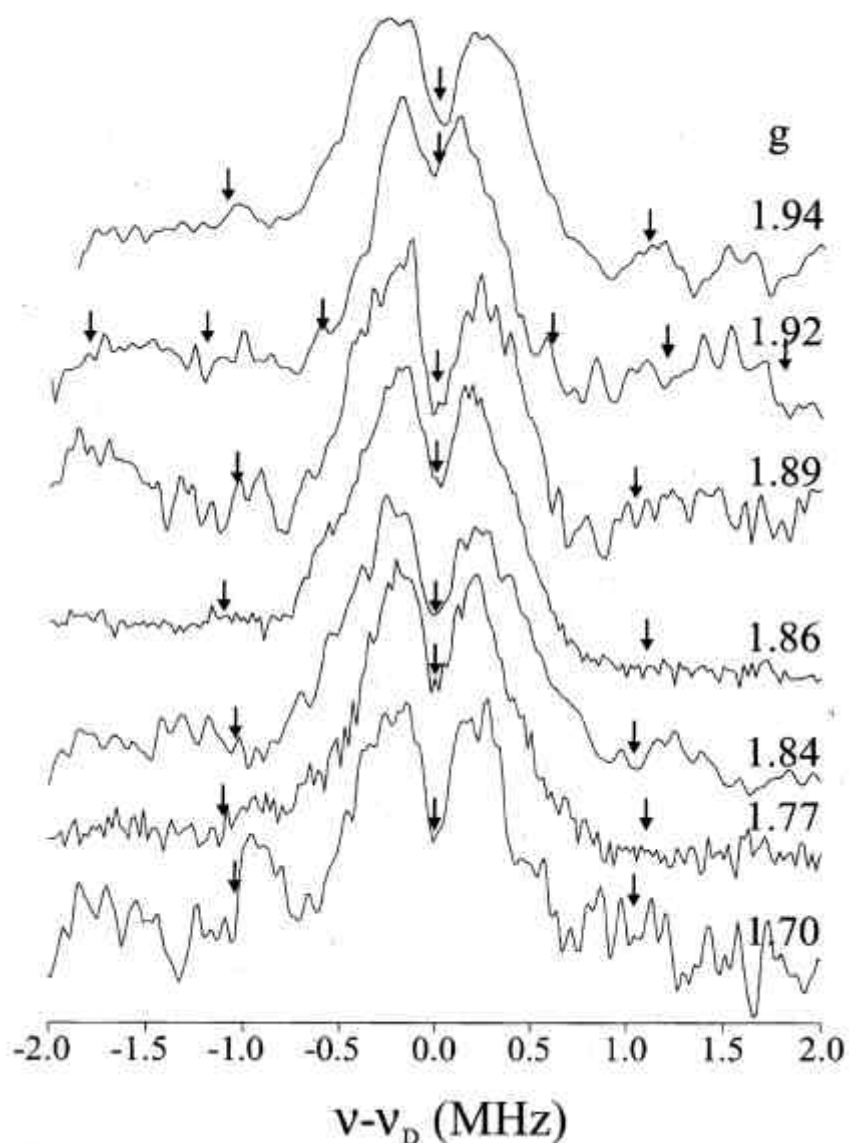


Figure 6.6. $H_{mv} + CD_3CD_2OH$ - field dependence of 2H 35 GHz Mims ENDOR spectra. 2H Mims suppression holes are indicated by arrows. The 7th proton harmonic at approximately -0.6 MHz from ν_D causes a slight asymmetry in these spectra. Mims sequence with a $\pi/2$ microwave pulse = 50-52 ns, with 100 μs Rf pulse and $\tau = 452$ ns; 40 kHz Rf excitation broadening; 34.695 GHz MW frequency. Spectra are designated by their g values.

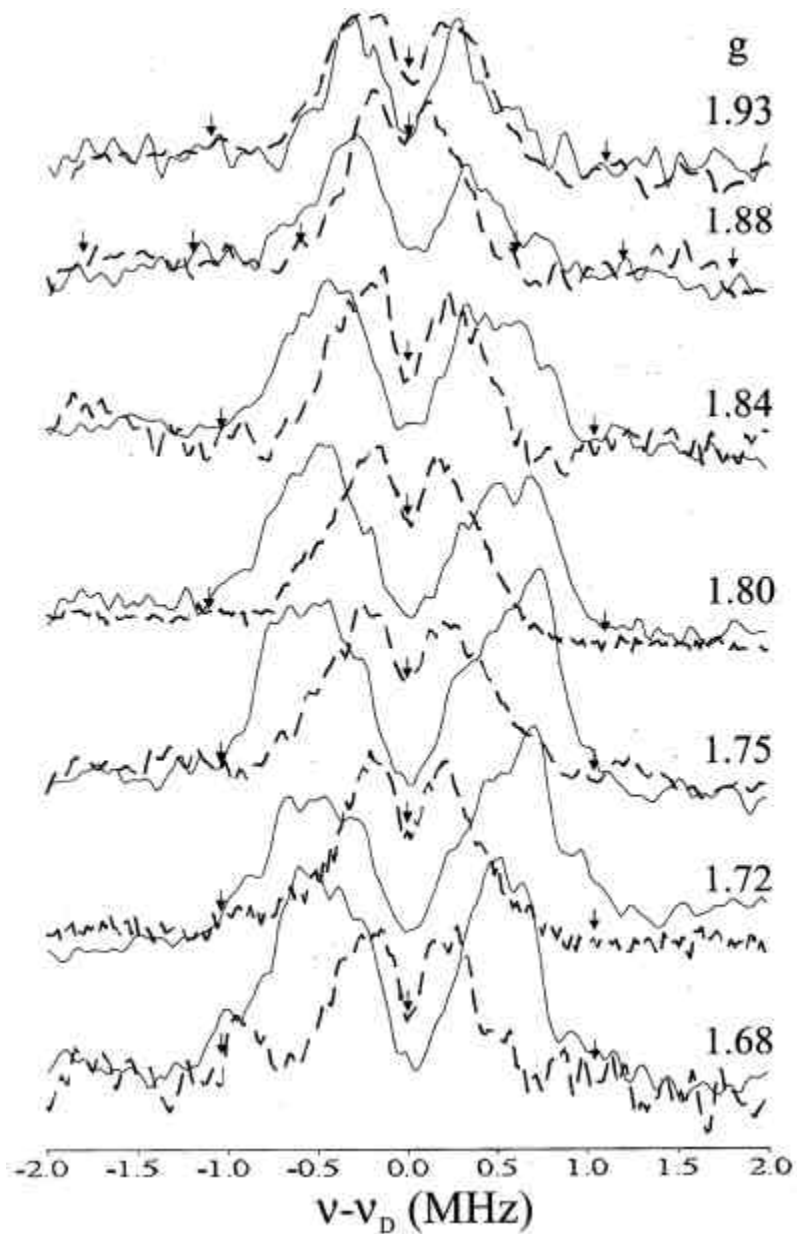


Figure 6.7. $(\text{H}_{\text{ox}} + \text{CF}_3\text{CD}_2\text{OH})_{\text{mv}}/\text{H}_2\text{O}$ - field dependence of the ^2H 35 GHz Mims pulsed ENDOR spectra. ^2H Mims suppression holes are indicated by arrows. Mims sequence with a $\pi/2$ microwave pulse = 50-52 ns, with 60 μs Rf pulse and τ = 360 ns; no Rf excitation broadening; 34.695 GHz MW frequency.

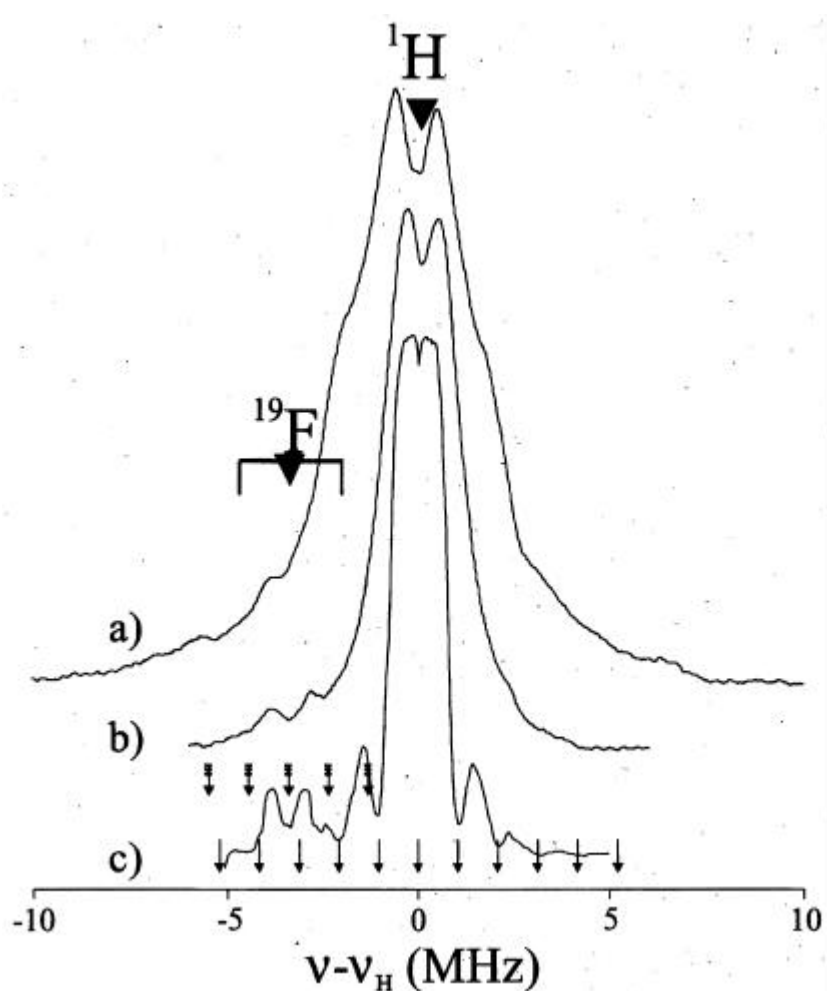


Figure 6.8. Typical CW vs. pulsed $^1\text{H}/^{19}\text{F}$ ENDOR of $\text{H}_{\text{mv}} + \text{TFE}$. ν_{F} at these frequencies is ~ -3.4 MHz relative to ν_{H} and is marked on the figure. (a) Typical CW ^{19}F signal sample in H_2O buffer, 34.84 GHz MW frequency, $g = 1.844$; 200 kHz Rf excitation broadening, modulation amplitude 5 G, 16 scans, time constant = 128 ms, gain = 320. (b) Best CW ^{19}F signal, sample in D_2O buffer, 35.05 GHz MW frequency, $g = 1.841$; 200 kHz Rf excitation broadening, modulation amplitude 0.5 G, 64 scans, time constant = 64 ms, gain = 1000. (c) Typical pulsed Mims ENDOR signal, sample in H_2O buffer. Mims sequence with a $\pi/2$ microwave pulse = 50-52 ns, with 20 μs Rf pulse and $\tau = 480$ ns; no Rf excitation broadening; 34.850 GHz MW frequency, $g = 1.838$, pulse sequence repetition time 15 ms, 60 averaged data shots per point, 6 scans.

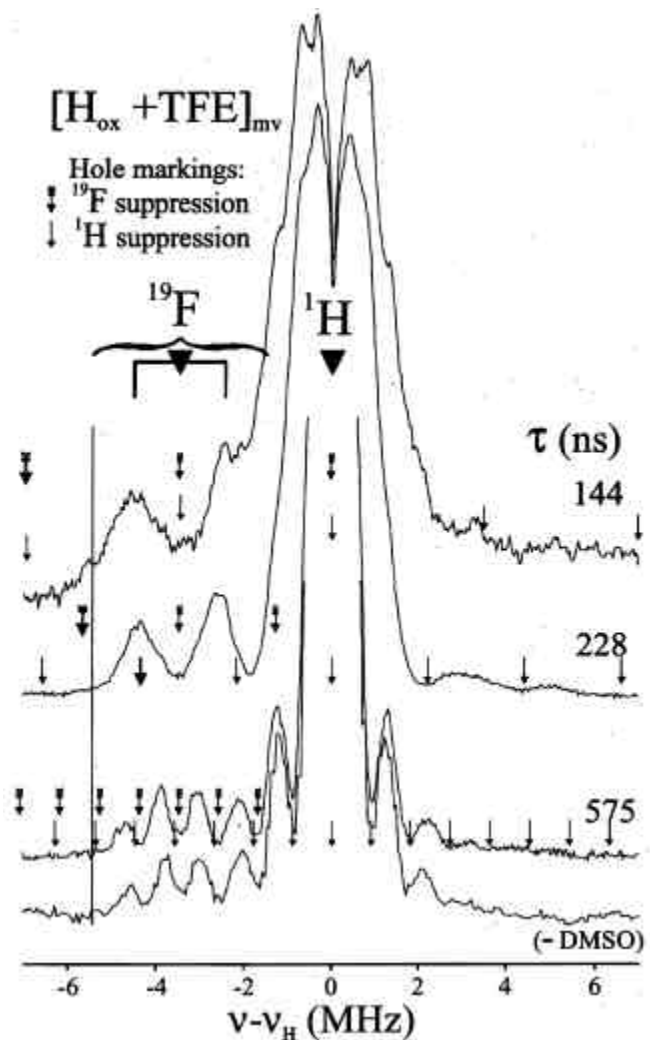


Figure 6.9. $(\text{H}_{\text{ox}} + \text{CF}_3\text{CD}_2\text{OH})_{\text{mv}}$ - τ -dependence of the $^1\text{H}/^{19}\text{F}$ ENDOR signal. All spectra taken on a sample containing DMSO, except as indicated for the last (bottom) spectrum (without DMSO). Arrows indicate Mims suppression holes, normal and feathered arrows refer to the proton and fluorine signals, respectively. Some arrows are addressed in the text and are printed in boldface for ease of finding them. The spectra are identified by τ : (144 ns) Re-Mims (four-pulse) sequence³⁰ with a $\pi/2$ microwave pulse = 32 ns, with 20 μs rf pulse, $\tau = 144$ ns; 34.720 GHz MW frequency, $g = 1.776$; pulse sequence repetition time = 5 ms; 200 averaged data shots per point; 10 scans. (228 ns) As in (144 ns) but $\tau = 228$ ns.

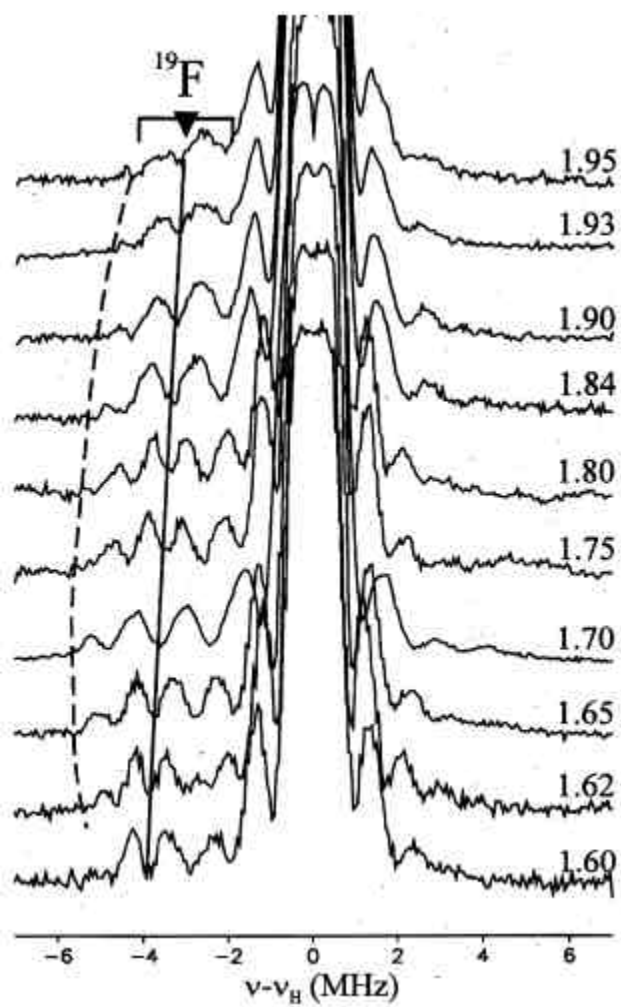


Figure 6.10. $(\text{H}_{\text{ox}} + \text{CF}_3\text{CD}_2\text{OH})_{\text{mv}}/\text{H}_2\text{O}$ - field dependence of the ^{19}F ENDOR signals.

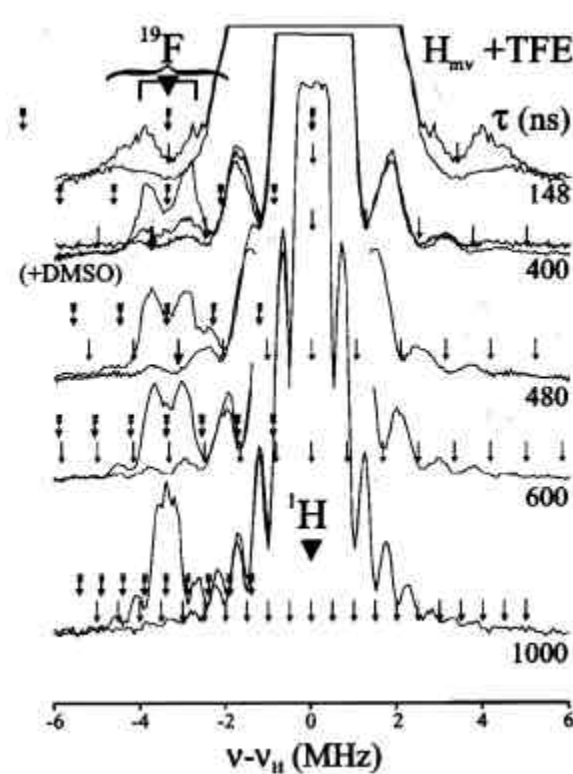


Figure 6.11. $H_{mv} + TFE$ - τ -dependence of the proton/fluorine spectra. All spectra were taken on a sample NOT containing DMSO except as indicated for one of the spectra with $\tau = 400$. (148 ns) Re-Mims (four-pulse) sequence³⁰ with a $\pi/2$ microwave pulse = 32 ns, with 20 μ s rf pulse, $\tau = 148$ ns; 34.638 GHz MW frequency, $g = 1.840$; pulse sequence repetition time = 25 ms; 40 averaged data shots per point; 20 scans. (400 ns) Mims sequence with a $\pi/2$ microwave pulse = 50-52 ns, with 20 μ s rf pulse, $\tau = 400$ ns; 34.596 GHz MW frequency, $g = 1.840$; pulse sequence repetition time = 25 ms; 40 averaged data shots per point; 3 scans. (400 ns + DMSO) As in (400 ns) but spectrum of $H_{mv} + TFE + DMSO$, $\tau = 412$ ns; 34.741 GHz MW frequency, pulse sequence repetition time = 30 ms; 30 averaged data shots per point; 2 scans; (overlaid with (400 ns) spectrum). (480 ns) As in (400 ns) but $\tau = 480$ ns; 1 scan; (600ns) As in (400 ns) but $\tau = 600$ ns; 2 scans; (1000 ns) As in (400 ns) but $\tau = 1000$ ns; 5 scans.

Appendix:

Single Turnover Hydroxylations of Norcarane

Introduction

The formation of both cation- and radical-type rearrangement products upon oxidation of norcarane was proposed to be a result of the action of multiple oxidant species.¹ Single turnover experiments are well suited to exploring the reactivity of the oxygen intermediates of sMMO. Due to their distinctive optical spectra, the time course for H_{peroxo} and Q formation and decay can be followed by stopped flow methods. Double mixing stopped-flow spectrophotometry is particularly useful because it can isolate the intermediates in time. Such experiments have provided evidence for the reaction of H_{peroxo} with substrates such as propylene² and acetonitrile.³ Both single and double mixing methods were used to investigate the reaction of norcarane with sMMO.

Experimental

MMO single turnover reactions were performed according to published procedures.² A solution of MMOH/2MMOB was combined with an equal amount of methyl viologen, degassed, and reduced with an excess of sodium dithionite. Dithionite and methyl viologen were removed from the protein solution by dialysis in an anaerobic glove box. All data were recorded with a Hi-Tech SF-61 DX2 instrument. In single mixing experiments, the $\text{MMOH}_{\text{red}}/2\text{MMOB}$ solution was rapidly mixed with a dioxygen-saturated solution containing either saturated norcarane or no substrate.

For double mixing experiments, $\text{MMOH}_{\text{red}}/2\text{MMOB}$ is mixed first with dioxygen-saturated buffer. After a delay designed to maximize the amount of either H_{peroxo} or Q formed, the protein is mixed with buffer that lacks substrate or is norcarane-saturated. The formation and decay of intermediates H_{peroxo} and Q were monitored at 725 and 420 nm, respectively. Data were fit either as a sum of exponential decays using the Hi-Tech KinetAsyst software, or by numerical simulation using DynaFit.⁴

Results

Single-Turnover Oxidation of Norcarane: Single Mixing. The reaction of norcarane with sMMO intermediates was measured by stopped-flow optical spectroscopy in two configurations, single mixing and double mixing. In the single mixing experiment, a solution of $\text{MMOH}_{\text{red}}/2\text{MMOB}$ is mixed with a buffer solution saturated with dioxygen containing either no substrate or saturated norcarane. Traces recorded at 420 and 725 nm are presented in Figure A1. A summary of rate constants determined from these data by fitting to a sum of three exponentials is shown in Table A1. This analysis indicates that addition of norcarane clearly accelerates the decay of Q , but the effect on decay of H_{peroxo} is less clear. The fitting routine returns a lower value for H_{peroxo} decay (monitored at 725 nm) upon addition of norcarane. If norcarane reacted only with Q , then there should be no effect on the H_{peroxo} to Q conversion rate constant. If, on the other

hand, norcarane reacts with both H_{peroxo} and Q , then the overall rate for decay of H_{peroxo} should increase.

Numerical simulations of the kinetic traces (Figures A2, A3, A4) improve our understanding of the changes that occur between reactions without substrate and with norcarane. In Figure A2, data recorded at two wavelengths in the absence of substrate are simulated by the mechanism $H_{\text{red}} \rightarrow H_{\text{peroxo}} \rightarrow Q \rightarrow \text{products}$. The rate constant for the conversion of H_{red} to H_{peroxo} was fixed at 19.0 s^{-1} , the value obtained by multiple-exponential fitting to 725 nm data. The other rate constants and extinction coefficients were allowed to float to find a best-fit value, with the constraint that a single set of rate constants must fit data recorded at both 420 and 725 nm. Figure A3 shows the results of a simulation of data recorded in the presence of norcarane, using the mechanism described above. In this case, the extinction coefficients were fixed to the values obtained from Figure A2. This mechanism provides a poor fit to the data. Figure A4 shows a simulation of the same data, but with a mechanism that allows conversion of $H_{\text{peroxo}} \rightarrow \text{products}$, representing the hydroxylation of substrate by H_{peroxo} . Again, the extinction coefficients were fixed to the values determined in the absence of substrate. The fit is much better than in Figure A3.

Single-Turnover Oxidation of Norcarane: Double Mixing. A double mixing experiment was also performed, in which $\text{MMOH}_{\text{red}}/2\text{MMOB}$ is mixed with dioxygen, allowed to age, and then mixed with buffer \pm norcarane. After the second mixing event, absorbance values at either 420 or 725 nm are recorded (Figure

A5). A summary of rate constants obtained by fitting the traces shown to a sum of two exponentials is presented in Table A2. The two rate constants determined from 725 nm data represent H_{peroxo} decay and Q decay; the two determined from 420 nm data represent two phases of Q decay. Decay rates of both H_{peroxo} and Q are accelerated by addition of norcarane.

Discussion

In order to address the question of multiple oxidants possibly reacting with norcarane, single turnover experiments were carried out where the kinetic behavior of H_{peroxo} and Q can be monitored spectroscopically in the presence or absence of norcarane. Extinction coefficients and rate constants in the absence of substrate determined by numerical simulation of single mixing stopped-flow data (Figures A1, A2) agree with those determined previously.² Addition of norcarane clearly accelerates Q decay, as expected (Figure A1).⁵ Numerical simulations are also clear in showing that a model that allows only changes in the rate constants of Q formation and decay is inadequate to model the reaction in the presence of norcarane (Figure A3). A model allowing reaction of both H_{peroxo} and Q with norcarane (Figure A4) fits well, but one cannot exclude other models on this basis alone.

Results of a double mixing experiment recapitulate those found in single mixing mode (Figure A5, Table A2). Q decay is accelerated, and H_{peroxo} decay is similarly accelerated. None of the preceding data, however, can rule out possi-

bilities that norcarane alters the kinetic behavior of the protein by, for instance, speeding up conversion of H_{peroxo} to Q , or changing the rate of autodecay.

Conclusion

The stopped-flow data are consistent with the conclusion that H_{peroxo} acts as an oxidant upon norcarane. Before such a statement can be made with great confidence, however, two more experiments should be performed. If H_{peroxo} does indeed react with norcarane, then the rate constant for H_{peroxo} decay should show a linear dependence on the concentration of norcarane. Such an analysis has helped confirm that H_{peroxo} can react with substrates such as propylene and acetonitrile.^{2,3} Rapid chemical quench experiments would allow the formation of hydroxylated products to be followed as a function of time after mixing, potentially providing further evidence that at early time points, only H_{peroxo} is kinetically competent to produce the products observed. This technique also has the advantage of allowing products to be identified, to answer the question of whether H_{peroxo} gives rise to a different product distribution than does Q .

References

- 1) Newcomb, M.; Shen, R. N.; Lu, Y.; Coon, M. J.; Hollenberg, P. F.; Kopp, D. A.; Lippard, S. J. *J. Am. Chem. Soc.* **2002**, *124*, 6879-6886.
- 2) Valentine, A. M.; Stahl, S. S.; Lippard, S. J. *J. Am. Chem. Soc.* **1999**, *121*, 3876-3887.
- 3) Bautista, J.; Lippard, S. J. **2002**, Unpublished results.
- 4) Kuzmic, P. *Anal. Biochem.* **1996**, *237*, 260-273.
- 5) Brazeau, B. J.; Austin, R. N.; Tarr, C.; Groves, J. T.; Lipscomb, J. D. *J. Am. Chem. Soc.* **2001**, *123*, 11831-11837.

Table A1. Rate Constants for Single Turnover of MMOH in the Presence or Absence of Norcarane, Measured by Single Mixing Stopped-Flow Spectroscopy.

Norcarane	rate constant (s ⁻¹)			
	-		+	
	420	725	420	725
wavelength (nm)				
H _{peroxo} formation	--	19 ± 3	--	64 ± 19
H _{peroxo} decay/Q formation	8.20 ± 0.03	9 ± 1	8.2 ± 0.17	6.0 ± 0.9
Q decay	0.31 ± 0.01	0.203 ± 0.003	0.48 ± 0.05	0.29 ± 0.05
Q decay (slow)	0.054 ± 0.003	--	0.58 ± 0.08	--

Table A2. Summary of Rate Constants Observed for Reaction of Norcarane with H_{peroxo} and Q Monitored by Double Mixing Stopped-Flow.

	sub- strate	k_1 (H_{peroxo} decay) (s^{-1})	k_2 (Q decay) (s^{-1})	k_3 (Q decay) (s^{-1})
725 nm	-	3.57 ± 0.09	0.32 ± 0.07	--
	+	7.63 ± 0.08	0.80 ± 0.07	--
420 nm	-	--	0.78 ± 0.10	0.15 ± 0.04
	+	--	1.25 ± 0.13	0.49 ± 0.06

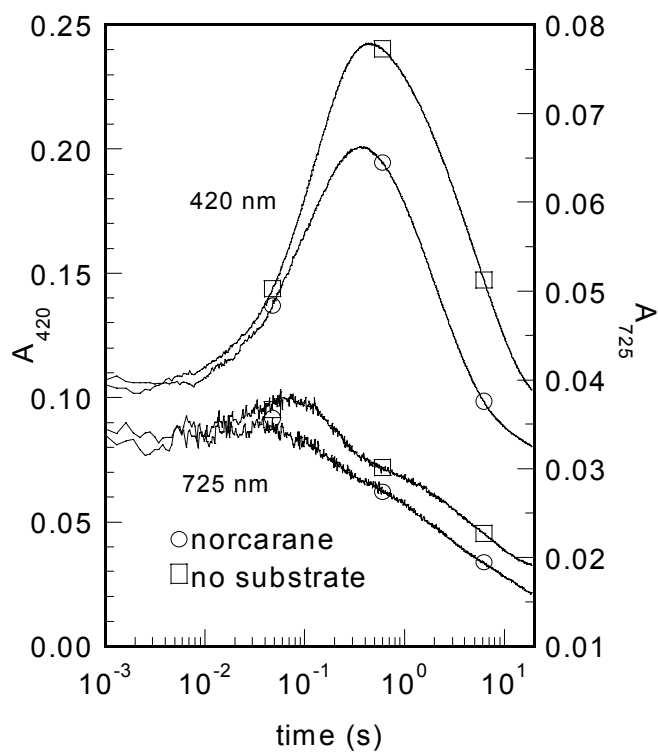


Figure A1. Single turnover reaction in single mixing mode of $\text{MMOH}_{\text{red}}/2\text{MMOB}$ with (circles) or without (squares) norcarane. Upper traces recorded at 420 nm, lower traces at 725 nm.

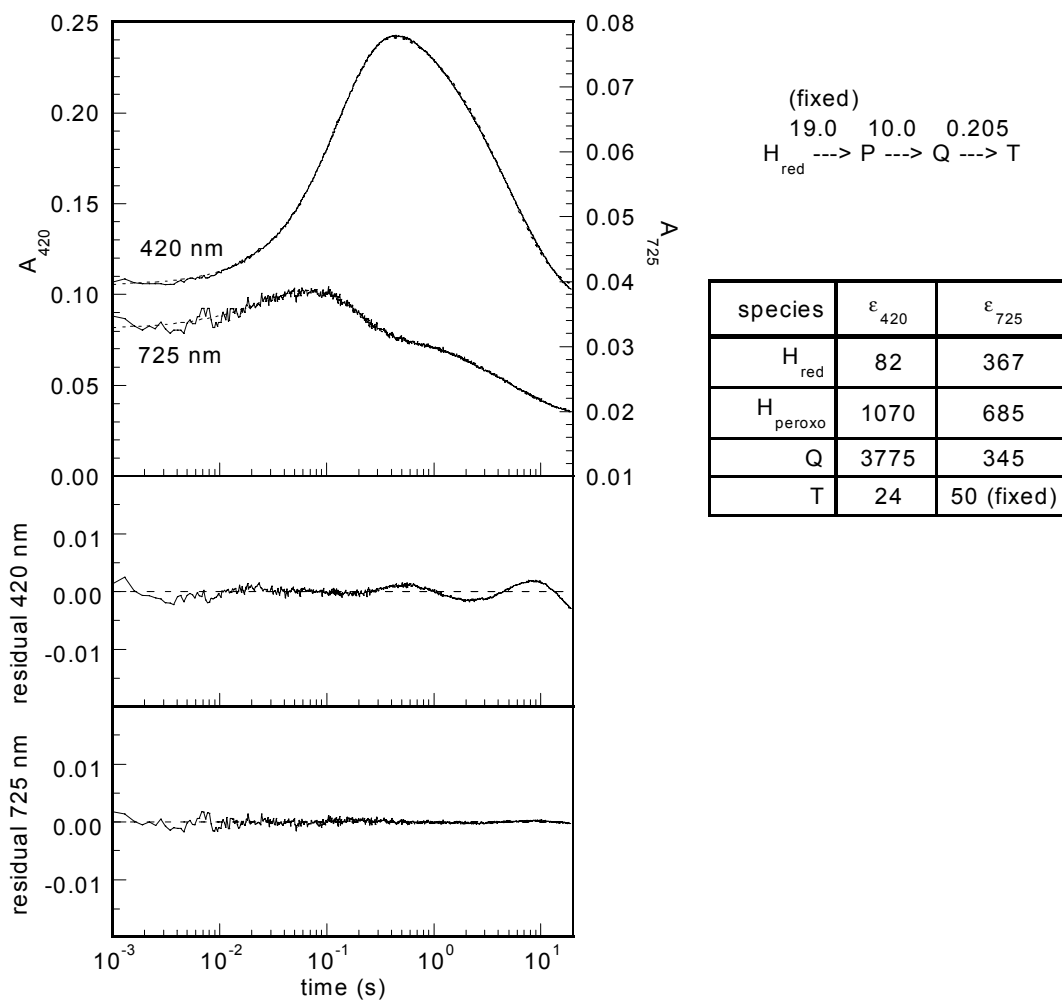


Figure A2. Simulation of single mixing data in the absence of substrate. Data with simulations are shown at left. Black dashed lines are simulations. Kinetic models are shown at right. All parameters were allowed to vary except where indicated.

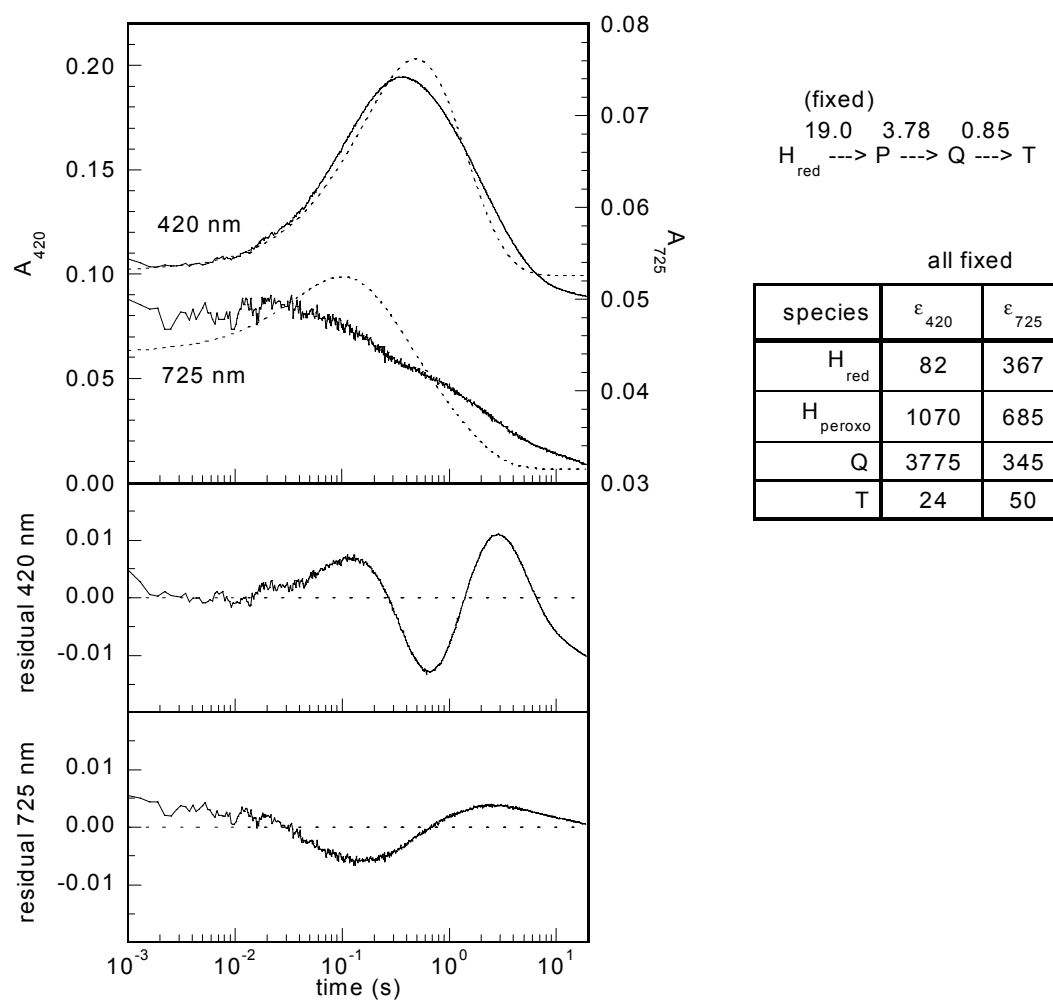


Figure A3. Simulation of single mixing reaction of $MMOH_{red}/2MMOB + O_2 +$ norcarane. Kinetic model does not include reaction of H_{peroxo} with norcarane.

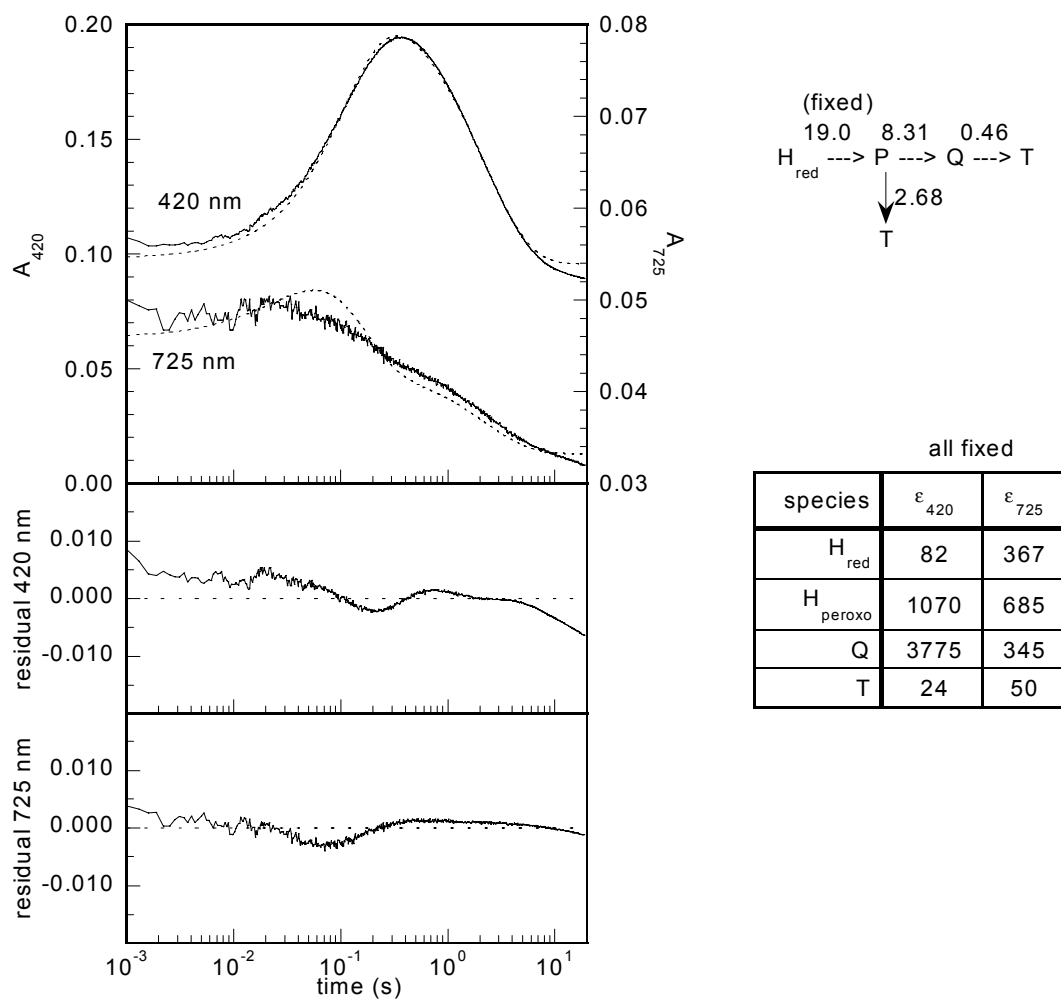


Figure A4. Simulation of single mixing reaction of $\text{MMOH}_{\text{red}}/2\text{MMOB} + \text{O}_2 +$ norcarane. Kinetic model includes reaction of H_{peroxo} with norcarane.

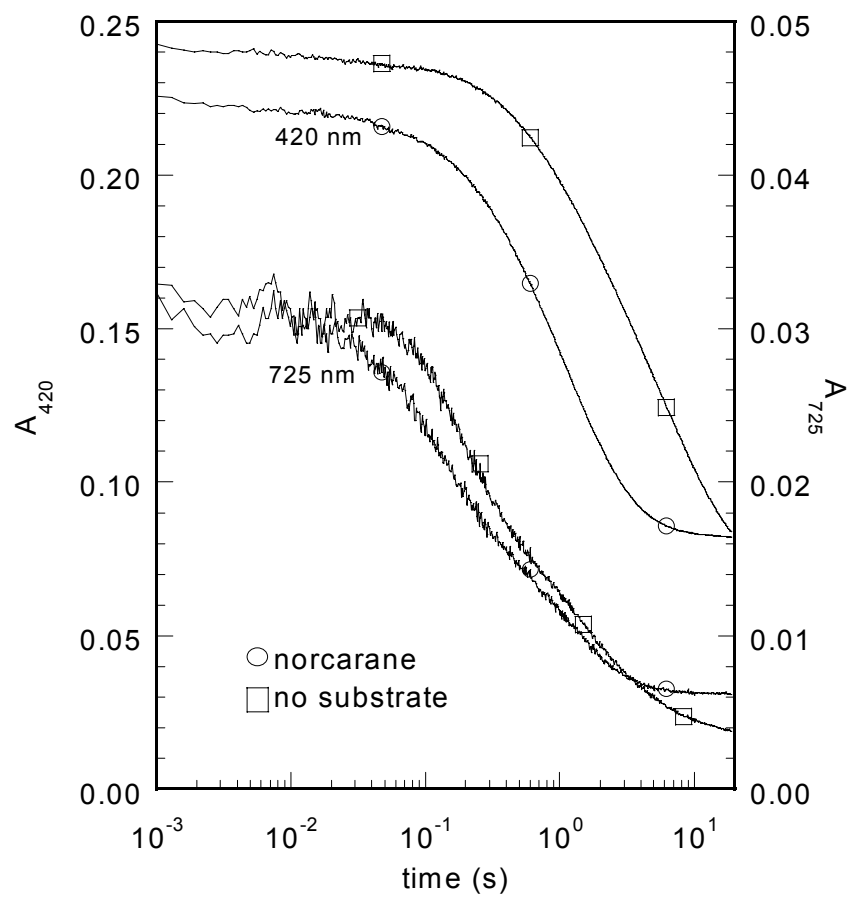


Figure A5. Double mixing stopped flow traces of the reaction of Q (420 nm) or H_{peroxo} (725 nm) with norcarane (circles) or no substrate (squares). Age times after the first mix were 400 ms (420 nm traces) or 55 ms (725 nm traces).

Biographical Note

The author was born on July 3, 1975 in Fairfax, Virginia to Jane and Harry Kopp, and was raised in Arlington, Virginia with his older sister Sarah. He lived in Brasilia, Brazil during 1982-1984. After graduating Yorktown High School in 1993, he attended the College of William & Mary in Williamsburg, VA. He earned a B.S. in Biology and Chemistry in 1997. Following his graduate studies at MIT, he plans to join the law firm of Fish & Richardson as a Technology Specialist in Washington, D.C.

Daniel A. Kopp

Education

Massachusetts Institute of Technology Cambridge, MA
Teaching Assistant, Research Assistant, and National Institutes of Health Biotechnology Predoctoral Trainee. Doctoral candidate in the department of Chemistry. Expected degree date: February 2003.

College of William and Mary Williamsburg, VA
B.S. with double majors in Chemistry and Biology, *magna cum laude*, 1997. Phi Beta Kappa. Awarded Highest Honors in Chemistry for thesis, "Solvent Effects on the Conformational Equilibria of Small Amides".

Awards

NIH Biotechnology Predoctoral Trainee 1999-2001. Phi Beta Kappa, 1997. Golden Key Honor Society, 1997. Merck Summer Research Fellow 1996; American Chemical Society Virginia Section Distinguished Achievement in Chemistry Award, 1997.

Research Experience

MIT Department of Chemistry, 1997-2002. Cambridge, MA
Advisor: Stephen J. Lippard

Investigated the mechanism and structure of soluble methane monooxygenase (sMMO). Electron transfer reactions involving NADH, FAD, and [2Fe-2S] were studied by stopped-flow UV-vis. Radical clock substrates were used to determine that activation of alkane C-H bonds by sMMO proceeds without free radical intermediates. In collaboration with Brian Hoffman at Northwestern University, EPR and ENDOR spectroscopies helped understand the nature of product binding to the dinuclear iron active site of sMMO. Structures of protein-protein complexes were probed by chemical cross-linking and mass spectrometry.

College of William and Mary, 1996-1997. Williamsburg, VA
Advisor: Kathleen M. Morgan

Investigated thermodynamics of interactions of cyclic and acyclic amides with solvents. Measured heats of vaporization and heats of solution of amides in a variety of protic, aprotic, and non-polar solvents. Electronic properties of amides were studied by *ab initio* calculational methods.

National Institutes of Health, 1992-1993. Bethesda, MD

Advisor: Alan R. Kimmel

Studied developmental genetics of the slime mold *Dictyostelium discoideum*. Performed Northern analysis of cAMP receptor mRNA expression as a function of developmental stage.

Teaching Experience

Research mentor to high school summer student, MIT, May-August 1999.

Teaching assistant, MIT, Chemistry 5.310 (lab for non-majors) August 1997-May 1998.

Presentations

Electron Transfer in Methane Monooxygenase. Invited talk at NIH Biotechnology Training Program Retreat, Dedham, MA. April 28, 2002.

Electron Transfer Reactions of Soluble Methane Monooxygenase Reductase. D.A. Kopp and S.J. Lippard. Poster, American Society of Biochemistry and Molecular Biology National Meeting, Boston, MA, June 4-8, 2000.

Solvent Effects on the Conformational Equilibria of Small Amides. D.A. Kopp and K.M. Morgan. Undergraduate Poster Session, American Chemical Society Virginia Section Meeting, Charlottesville, VA, April 18, 1997.

Publications

Structural Features of the MMOH/MMOR Complex as Revealed by Mass Spectrometric Analysis of Covalently Cross-linked Proteins. Kopp, D.A.; Berg, E.A.; Costello, C.E.; and Lippard, S.J. Manuscript in preparation.

Soluble Methane Monooxygenase: Activation of Dioxygen and Methane. Kopp, D.A. and Lippard, S.J. (2002) *Current Opinions in Chemical Biology* 6, 568-576.

Evaluation of Norcarane as a Probe for Radicals in Cytochrome P450- and Soluble Methane Monooxygenase-Catalyzed Hydroxylation Reactions. Newcomb, M.; Shen, R.; Lu, Y.; Coon, M.J.; Hollenberg, P.F.; Kopp, D.A.; Lippard, S.J. (2002) *Journal of the American*

Chemical Society 124, 6879-6886.

Product Binding to the Diiron(III) and Mixed-Valence Diiron Centers of Methane Monooxygenase Hydroxylase Studied by ^1H and ^{19}F ENDOR Spectroscopy. Smoukov, S.; Kopp, D.A.; Valentine, A.M.; Lippard, S.J.; Hoffman, B.M. (2002) *Journal of the American Chemical Society* 124, 2657-2663.

Electron-Transfer Reactions of the Reductase Component of Soluble Methane Monooxygenase from *Methylococcus capsulatus* (Bath). Kopp, D.A.; Gassner, G.T.; Blazyk, J.L.; Lippard, S.J. (2001) *Biochemistry* 40, 14932-14941.

Dioxygen Activation by Soluble Methane Monooxygenase: a Tale of Two Irons and Three Proteins. Merckx, M.; Kopp, D.A.; Sazinsky, M.H.; Blazyk, J.L.; Mueller, J.; Lippard, S.J. (2001) *Angewandte Chemie International Edition* 40, 2782-2807.

Cationic Species Can Be Produced in Soluble Methane Monooxygenase-Catalyzed Hydroxylation Reactions; Radical Intermediates Are Not Formed. Choi, S.-Y.; Eaton, P.E.; Kopp, D.A.; Lippard, S.J.; Newcomb, M.; Shen, R. (1999) *Journal of the American Chemical Society*. 121, 12198-12199.

Solvent effects on the stability of simple secondary amides. Morgan, K.M.; Kopp, D.A. (1998) *Journal of the Chemical Society, Perkin Transactions 2*, 2759-2763.